Design of a Macroencapsulation Device for Pancreatic Islets for Diabetes Therapy

Heller, Carolin

Awarding institution:
King's College London

Medizinische Klinik III, Inseltransplantation

Frau Prof. Dr. med. Barbara Ludwig

Design of a Macroencapsulation Device for Pancreatic Islets for Diabetes Therapy

D i s s e r t a t i o n s s c h r i f t

zur Erlangung des akademischen Grades

Dr. rer. medic.

vorgelegt

der Medizinischen Fakultät Carl Gustav Carus

der Technischen Universität Dresden

von

Carolin Heller, M. Sc.

aus Ostercappeln

Dresden 2021

1. Gutachter:

2. Gutachter:

Tag der mündlichen Prüfung: (Verteidigungstermin)

gez.: ----------
Vorsitzender der Promotionskommission

Anmerkung:

Die Eintragung der Gutachter und Tag der mündlichen Prüfung (Verteidigung) erfolgt nach Festlegung von Seiten der Medizinischen Fakultät Carl Gustav Carus der TU Dresden. Sie wird durch die Promovenden nach der Verteidigung zwecks Übergabe der fünf Pflichtexemplare an die Zweigbibliothek Medizin in gedruckter Form oder handschriftlich vorgenommen.

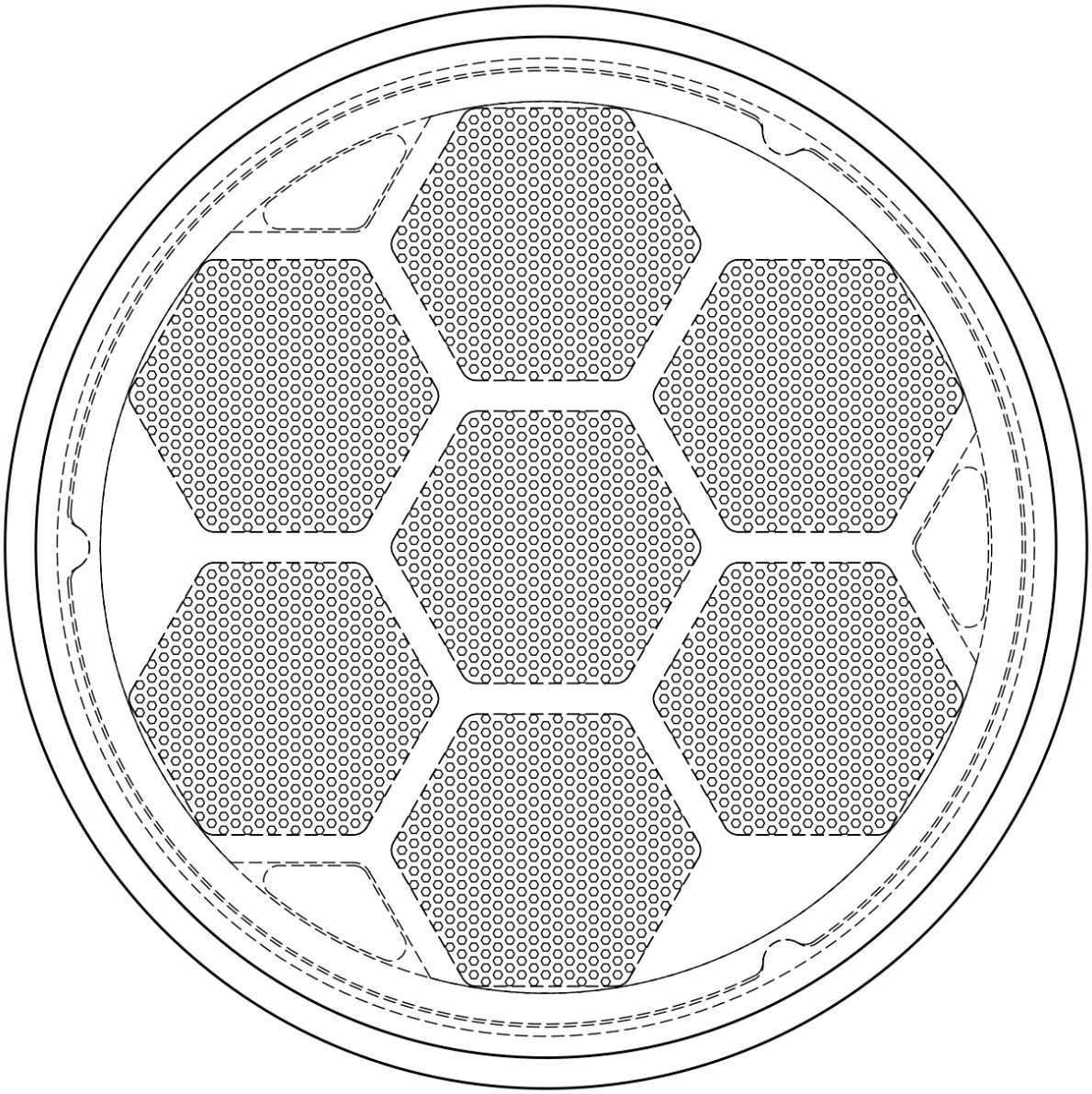

Design of a Macroencapsulation Device for Pancreatic Islets for Diabetes Therapy

Doctoral Thesis by Carolin Heller

Abstract

Cell macroencapsulation circumvents the host immune system response against foreign tissue, bearing enormous potential as a safeguard for cell-based therapies for diabetes treatment. With this technology, pancreatic islets can safely be transplanted without immunosuppression, facilitating islet survival and function by embedding these in a customised matrix. So far, no islet encapsulation device has been shown to be fully functional in a clinical trial. In this project, we aim to overcome the limitations of current approaches of cell encapsulation. By the application of advanced additive manufacturing technologies to the prototyping process, a modular encapsulation device has been designed. The design of this geometry focusses on sufficient oxygen availability and optimal diffusion characteristics to the islets in various means. The encapsulation device comprises three modules: a membrane holder, a skeleton and an islet housing module.

The membrane module carries a newly developed immunoisolating membrane with enhanced biocompatibility and vascularisation properties. To prevent immune-mediated rejection of the encapsulated cells, a composite membrane tuned to only allow passage of molecules smaller than 11.4 nm (exclusion of antibodies), while allowing diffusion of secreted hormones such as insulin. This composite membrane consists of modified polytetrafluoroethylene and a biohybrid heparin-starPEG hydrogel. The applied hydrogel can gradually bind and release growth factors and has previously been shown to mediate wound inflammation and stimulate angiogenesis. The skeleton module holds an oxygen-generating scaffold, which transiently provides endogenous oxygen inside the implant. During the initial post implantation period, it allows for adequate oxygen supply to the cell graft until vascularisation around the device has been sufficiently achieved. The distinguishing feature of the developed device geometry is the islet housing module comprising a microwell array, which separates single islets in a monolayer at defined distances and therefore is expected to create optimal diffusion characteristics for oxygen and effector hormones.

In summary, a novel macroencapsulation device for pancreatic islets down to the micro- and nanoscale has been designed covering the most critical aspects of immunoisolation, a clinically scalable device geometry, intrinsic oxygenation and a tailored matrix supporting long-term islet survival and function.

Zusammenfassung

Das grundlegende Prinzip von Systemen zur Zellverkapselung ist die Schaffung einer selektiven Barriere, wodurch eine immunologische Abschirmung eines Transplantats vom Empfängerorganismus geschaffen wird. Damit birgt die Zellverkapselung enormes Potential für zellbasierte Therapien in der Behandlung des Diabetes mellitus. Durch die immunologische Abschirmung können die Pankreasinseln ohne Einsatz von Immunsuppressiva transplantiert und deren Überleben und Funktion zusätzlich durch Einbettung in eine spezielle Mikroumgebung unterstützt werden. Bisher hat sich kein System zur Zellverkapselung im Rahmen klinischer Studien als vollständig funktionsfähig erwiesen. Mit dem hier vorgestellten Ansatz werden die identifizierten Limitationen der verfügbaren Verkapselungssysteme spezifisch adressiert. Durch die Anwendung innovativer generativer Fertigungsmethoden in der Prototypenherstellung ist es gelungen, ein modulares Kapselsystem zu entwickeln, dessen Aufbau in mehrfacher Hinsicht für eine suffiziente Sauerstoffversorgung und bestmögliche Diffusionscharakteristik optimiert ist. Das Verkapselungssystem besteht aus einem immunisolierenden Membranmodul, einem Korpusmodul mit initial intrinsischer Sauerstoffversorgung, sowie einem die Inseln enthaltenden Zellmodul.

Das Membranmodul besteht aus einer neuentwickelten immunisolierenden Membran mit erhöhter Biokompatibilität und verbessertem Vaskularisierungspotenzial. Um eine Interaktion der verkapselten Pankreasinseln mit dem Immunsystem des Empfängerorganismus zu verhindern wird mit Hilfe einer permselektiven Membran eine suffiziente immunologische Abschirmung geschaffen. Gleichzeitig ist die Diffusion von Molekülen wie Insulin, die kleiner als 11.4 nm sind, gewährleistet. Die immunisolierende Membran besteht aus modifizierten Polytetrafluorethylen und biohybridem Heparin-starPEG Hydrogel. Das imprägnierende Hydrogel kann Wachstumsfaktoren reversibel binden und freisetzen. Darüber hinaus hemmt es inflammatorische Reaktionen und stimuliert die Angiogenese. Im Korpusmodul ist ein sauerstoffproduzierendes Material enthalten, welches die Pankreasinseln in der Frühphase nach Transplantation transient mit Sauerstoff versorgt. Nach Etablierung eines suffizienten Gefäßnetzes im Umgebungsgewebe und der Oberfläche des Kapselsystems erfolgt die Oxygenierung der Inseln mit diffundierendem Sauerstoff über die Membran. Eine Besonderheit und Herzstück des neu entwickelten Kapselsystems ist das Zellmodul. Es besteht aus einem Microwell-Array, das die einzelnen Inselzellcluster in definierten Abständen in einer singulären Schicht separiert. Damit sind optimale Diffusionscharakteristika für Sauerstoff und Effektorhormone gewährleistet.

Zusammengefasst handelt es sich um eine neuartige, klinisch skalierbare Verkapselungstechnologie, die bis in die Mikro- und Nanodimension im Hinblick auf die kritischsten Aspekte der Immunisolierung entwickelt wurde: initiale intrinsische Oxygenierung, optimale Biokompatibilität, sowie eine maßgeschneiderte Matrix. Ziel ist es, damit ein langfristiges Überleben und die Funktionalität der Pankreasinseln sicherzustellen.

Acknowledgements

First and foremost I would like to express my sincere gratitude to my supervisors, Prof. Barbara Ludwig and Prof. Carsten Werner for their invaluable advice, continuous support and patience during my PhD study. I would also like to thank my academic advisor Dr. Petra Welzel for her expert advice and encouragement throughout this intense project. Their thoughtful comments and wise guidance pushed me to sharpen my thinking and were key in enhancing my research. For facilitating my stay at King's College, allowing me to conduct parts of my study in London, I am deeply grateful to Prof. Peter Jones. His wise guidance and insightful comments were crucial in shaping my understanding of islet physiology.

Special thanks to Susann Lehmann for her supportive laboratory work and above all her technical support with islet isolations. I would like to express my sincere thanks to Jana Scholze and Dzmitry Afanasenkau for their contribution towards the development of microwell arrays and Mirella Staecker for producing the first prototype of the novel encapsulation device in PEEK. I would like to thank my fellow colleagues in Dresden, both at Prof. Barbara Ludwig's research group at University Hospital Carl Gustav Carus and at Carsten Werner's research group at Leibniz Institute of Polymer Research, who helped me accomplish this study. I would like to extend my sincere thanks to Annika Möller, Takuya Miyagawa and Victoria Sarangova for their important groundwork and collaborative effort. Their continued enthusiasm for the project was instrumental for the completion of this dissertation. I would also like to acknowledge the financial support from the International Research Training Group 2251 - Immunological and Cellular Strategies in Metabolic Disease funded by the Deutsche Forschungsgemeinschaft.

Finally, I would like to express my gratitude to my family and friends. Without their tremendous understanding, encouragement and unconditional support over the past few years, it would have been impossible for me to finalise my PhD thesis.

Graphical Outline

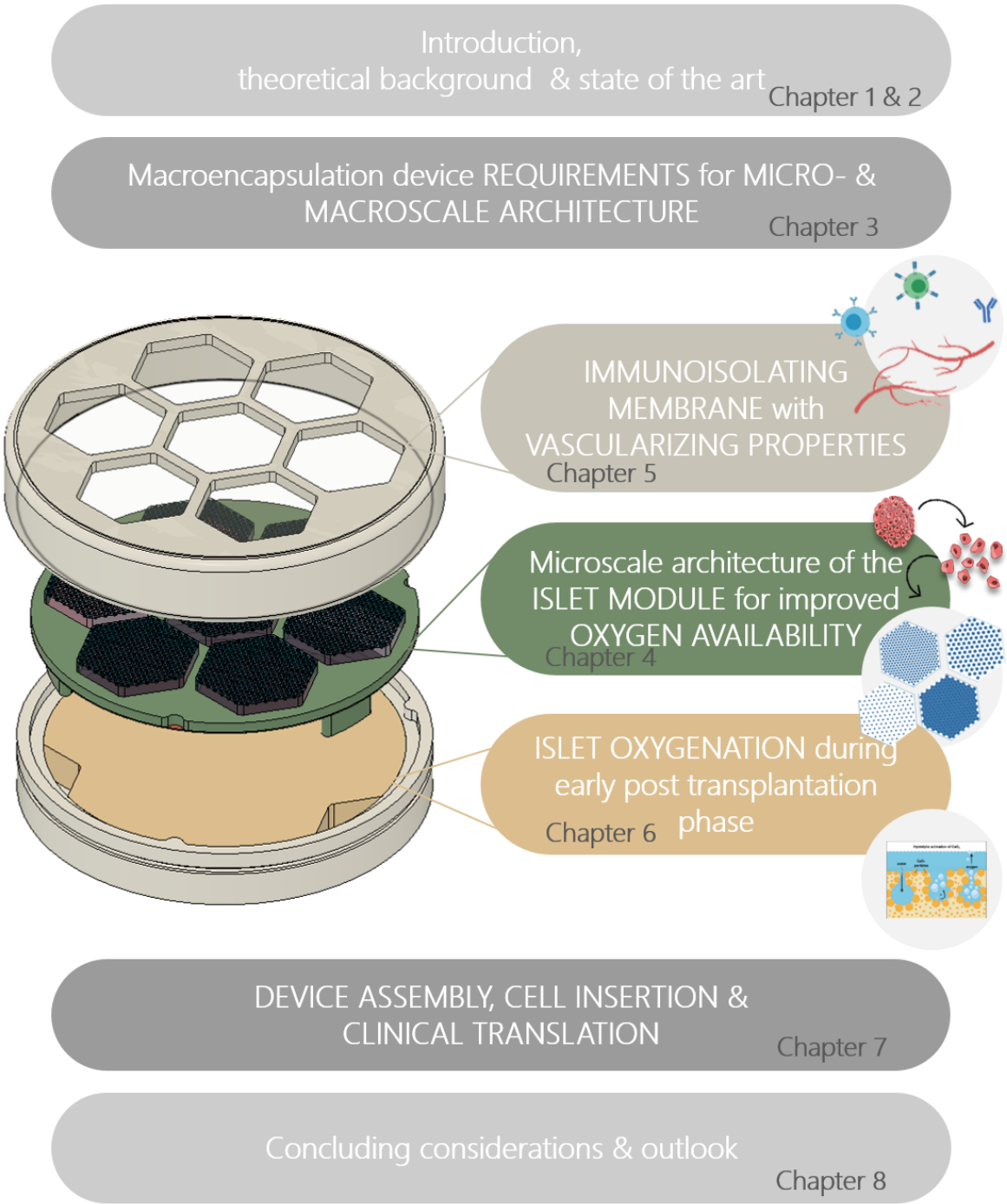

Table of contents

Abstract ..... **i**

Zusammenfassung ..... **ii**

Acknowledgements ..... **iii**

Graphical Outline ..... **v**

Table of contents ..... **vi**

List of Figures ..... **xi**

List of Tables ..... **xviii**

List of Abbreviations ..... **xix**

1 Introduction and aims **1**

2 Theoretical Background **4**

2.1 Diabetes mellitus 4

2.1.1 Pathophysiology of T1D and T2D 4

2.1.2 Epidemiology of diabetes 5

2.1.3 Physiologic glucose homeostasis 6

2.1.4 Islets of Langerhans 7

2.2 Treatment of Diabetes 8

2.2.1 Insulin therapy 8

2.2.2 Beta cell replacement strategies: pancreas and islet transplantation 10

2.3 Alternative insulin-secreting cell sources and therapeutic approaches 11

2.3.1 Stem cell derived beta-like cells 11

2.3.2 Xenogeneic islets 13

2.3.3 Pseudo islets 14

2.3.4 Islet encapsulation 15

2.4 State of the art: Macroencapsulation devices 17

2.4.1 MAILPAN® by Defymed 17

2.4.2 TheraCyte™ device by TheraCyte, Inc. 18

2.4.3 Encaptra and open device by ViaCyte Inc. 19

2.4.4 βAir device by BetaO_2 technologies 20

3 Macroencapsulation device requirements for micro- and macroscale architecture 21

3.1 Introduction 21

3.2 Fundamental requirements and general architecture of a macroencapsulation device 22

3.2.1 Macroencapulation device geometries 22

3.2.2 General basis of the design process 23

3.2.3 Preliminary Experiments: production and filling of a simple macro encapsulation device 23

3.2.4 Dimensional design criteria for development of a macroencapsulation device prototype 25

3.2.5 The distance between capillaries and encapsulated cells determines the diffusion pathway of macromolecules in the z-dimension 26

3.2.6 Oxygen available surface area per islet....28

3.2.7 Optimal islet arrangement derived from geometrical considerations....29

3.2.8 Oxygen provision in the post transplantation phase 30

3.3 Conceptual setup of prototype encapsulation device geometry and description of device modules....31

4 Microscale architecture of the islet module for improved oxygen availability 33

4.1 Introduction 33

4.1.1 Tailoring of the islets: Formation of pseudo islets in microwells....34

4.1.2 Available techniques for microwell production 35

4.1.3 Required properties of microwells for pseudo islet formation....37

4.1.4 Materials for pseudo islet microwell array....37

4.1.5 Oxygen distribution within islets 38

4.2 Methods 43

4.2.1 Microwell mould design and production by additive manufacturing....43

4.2.2 Microwell mould design and production by photo and soft lithography 43

4.2.3 Islet graft preparation: islet isolation and pseudo islet production 45

4.2.4 Scanning electron microscopy and light microscopy of microwells and islets ..46

4.3 Results....47

4.3.1 Production of a hydrogel array replica mould by additive manufacturing (direct production method) 47

4.3.2 Production of a microwell array replica platform for generation of microwell hydrogel arrays for *in vitro* cell culture and inside the encapsulation device 49

4.3.3 Production of microstructure scaffolds by additive manufacturing.....50

4.3.4 Production of microstructure scaffolds by photo and soft lithography techniques 51

4.3.5 Theoretical analysis of islet packaging density in microwell arrays based on an oxygen distribution model.....55

4.4 Discussion and outlook 60

4.5 Perspective on further experiments: optimal islet arrangement and size by design of experiment technique (DOE).....61

4.6 Acknowledgements 63

5 Immunoisolating membrane with vascularizing properties 64

5.1 Introduction 64

5.1.1 Immunologic reactions involved in the rejection of grafted tissue and material 65

5.1.2 Generation of a composite membrane with selective permeability.....66

5.1.3 ePTFE as reinforcing element of the composite membrane 66

5.1.4 Diffusion-based transport processes through a hydrogel network.....67

5.1.5 Relevant characteristics of molecules for designing the immunoisolating membrane.....68

5.1.6 Determination of the hydrogel network mesh size via rheology 71

5.1.7 Heparin-starPEG hydrogels as tuneable network of the composite membrane 71

5.1.8 Impact of heparin-starPEG hydrogels on wound healing and vascularisation..73

5.2 Methods 75

5.2.1 Preparation of heparin-starPEG hydrogels.....75

5.2.2 Mechanical characterisation of hydrogels.....76

5.2.3 Assessment of swelling properties of hydrogels 76

5.2.4 Preparation of the composite membrane.....77

5.2.5 Analysis of the composite membrane by SEM and EDX imaging 77

5.2.6 Assessment of permeability of the composite membrane 78
5.2.7 *In vitro* biocompatibility assessment by blood compatibility assays 80
5.3 Results 81
5.3.1 Mechanical and swelling properties of hydrogels 81
5.3.2 Microscopic analysis of the composite membrane by SEM imaging and EDX 83
5.3.3 Assessment of permeability of the composite membrane 85
5.3.4 *In vitro* biocompatibility of the composite membrane 88
5.4 Discussion and outlook 89
5.4.1 Concept for *in vivo* biocompatibility assessment and vascularisation properties of the composite membrane 91
5.5 Acknowledgements 94
6 Islet oxygenation during early post transplantation phase 95
6.1 Introduction 95
6.1.1 Oxygen provision by oxygen-generating materials 97
6.1.2 Carrier materials for oxygen-generating materials 98
6.2 Methods 100
6.2.1 Preparation of oxygen-generating disks fitted to device geometry 100
6.2.2 Measurement of released oxygen from oxygen-generating disks 101
6.3 Results 102
6.3.1 Release kinetics of oxygen disk in device prototype 102
6.4 Conclusion and outlook 104
6.5 Acknowledgements 105
7 Device assembly, cell insertion & clinical translation 106
7.1 Introduction 106
7.2 Prototyping of the encapsulation device design by additive manufacturing 107
7.3 Specification of detailed design features of the device geometry 108
7.4 Assembly process for modular macroencapsulation device 110
7.4.1 Membrane holder 111
7.4.2 Oxygen-generating disk and skeleton 112
7.4.3 Islet holder 113

7.4.4 Final assembly of the novel encapsulation device 116
7.5 Production techniques and materials for serial scale production....118
7.5.1 Available industrial methods for small and large scale production 118
7.5.2 Medical grade device materials and state for application....119
7.6 Scalability of the macroencapsulation device for clinical application 123
7.6.1 Scaling of dimensions 123
7.6.2 Estimation of islet loading capacity and optimal islet density 125
7.7 Concept for the preclinical evaluation of the implant....128
7.8 Discussion and outlook 131
8 Concluding considerations and outlook 133
9 References....137
10 Appendix....150
10.1 Microscale thermoresis 150
10.2 Sample size calculation of the response surface for parameter optimisation of the vascularizing hydrogel 150
10.3 Functional enhancement of pseudo islets by co-culture with MSCs....152
10.4 Attachments 1 & 2....157

List of Figures

Figure 1. Limitations of current macroencapsulation devices. 2
Figure 2. Pathophysiology of type 1 and type 2 diabetes. 5
Figure 3. Pancreatic Islets of Langerhans. A normal islet (left) and an islet affected by autoimmune destruction in type I diabetes (right). 8
Figure 4. Intrahepatic islets transplantation (Shapiro et al., 2000) 10
Figure 5. Nano-, micro- and macroencapsulation are based on the concept of placing a perm-selective barrier around the islets, allowing the diffusion of molecules like insulin, oxygen and nutrients, while preventing access of components of the immune system. While for nanoencapsulation single islets are shielded by a thin polymer layer, in microencapsulation one to a few islets are embedded in microscale capsules. For macroencapsulation the complete islet graft is placed into a single capsule. 16
Figure 6. MAILPAN® encapsulation device by Defymed (Strasbourg, France). The device is implanted for prevascularisation several weeks before insulin-secreting cells or islets are inserted via the two loading ports. 17
Figure 7. TheraCyte™ encapsulation device by TheraCyte Inc. a Cross-section of the device. The multi-layered membrane consists of (from the in to the out) of a 0.4 µm pore size PTFE membrane, a 5 µm pore size membrane and an outer woven polyester mesh. b Schematic of TheraCyte™ encapsulation device. c Variants of the device with different volume. 18
Figure 8. Cell encapsulation devices by ViaCyte Inc. (Strasbourg, France) a Schematic of Encaptra. b Cross section of the device. c Two device variants are available from ViaCyte Inc. Encaptra is an immunoisolating device, while the open device is a non-immunoisolating device accessible for transmembrane vascularisation. (Figure adapted from ViaCyte, 2021) 19
Figure 9. βAir device from BetaO_2 technologies consisting of a hard shell encapsulation chamber and two ports for oxygen tank refilling. 20
Figure 10. Planar and tubular macroencapsulation device designs (Figure edited from Giraldo et al., 2010) 22
Figure 11. Simple macroencapsulation device. Created by curing medical grade silicones in 3D printed injection moulds. a Technical drawing of injection mould for encapsulation device. b Fabricated simple macroencapsulation devices with filler port. 24
Figure 12. In vitro test of simple macroencapsulation device. a,b,c Implants filled with 500 rat islets alone a at day 0, b day 3 and, c FDA-PI staining at day. d,e,f Implants filled with 500 rat islets and heparin-starPEG hydrogels d at day 0, e day 3 and, f FDA-PI staining at day 3. ..25
Figure 13. Diffusion pathway of oxygen, nutrients and effector molecules in the z-dimension (capillaries to cells). 26
Figure 14. Oxygen diffusive surface area is dependent on the spacing of the islets in the x- and y-dimension. 28

Figure 15. Packing units of identical shape that can fill a plane. The highest packing density of circles is reached by hexagonal shape. 29
Figure 16. Microwell hexagons containing the islets arranged in larger hexagon units. 30
Figure 17. Conceptual setup of the prototype device geometry. a Closed device with hexagon structure for islet arrays. b Exploded view of the device representing the different modules for the immunoisolating membrane, the islets, the oxygen reservoir and the skeleton. 31
Figure 18. Large islets (>150 µm) develop a necrotic core, while small islets (<100 µm) stay viable without vascularisation as for example in an encapsulation setting. 34
Figure 19. Shapes of microwells. 35
Figure 20. Photo and soft lithography processes. 35
Figure 21 39
Figure 22 41
Figure 23. Production of rounded microwells by pressure skimming or deposition of PDMS droplets by printer. 44
Figure 24. Production of rounded microwells by dipping method. 44
Figure 25. Evaluation of micropillar structures produced by stereo lithography printing. a CAD drawing of designed structure. b Dimensions of pillars. c Detail of CAD structure. d Surface view of confocal light scattering analysis. e Measured width of printed pillars and designed pillars. f Measured height of printed pillars and designed pillars. 48
Figure 26. Schematic production of hydrogel array replica platform for framed (right) and unframed (left) microwell hydrogel arrays. Microstructure scaffolds (blue) are either printed inside the moulding platform directly or produced by photo and soft lithography techniques and placed manually into the printed moulding platforms. By moulding with PDMS hydrogel array replica platforms (yellow) are produced. These structures are used as negative moulds for repetitive production of microwell hydrogel arrays with agarose (pink). 49
Figure 27. Production of hydrogel array replica platform for framed microwell hydrogel arrays (photographs). 50
Figure 28. Scanning electron microscopy of stereo lithography printed microwells with 400 µm width. 50
Figure 29. Seeding of single islet cells into hydrogel microwell arrays with flat bottom, sharp rims and flat planes. a,b SEM of PDMS replica from wafer. c,d,e,f Microwell hydrogel arrays seeded with single islet cells. Microwells have a size of 200 µm and 200 µm distance between each other. Cells are falling into the microwells, but some cells keep lying at the planes and form large aggregates. 51
Figure 30. Replica platforms produced by repetitive moulding with intermediate steps of surface coating with SDS (surfactant) for the release of the next PDMS layer. Scale: left column 500 µm, centre and right column 100 µm. 52

Figure 31. Single islet cells seeded into microwell hydrogel arrays moulded from replica platforms depicted in Figure 28. 53
Figure 32. Microstructure scaffolds for production of replica platforms. 54
Figure 33. Microstructure scaffolds for microwell production. a Developed wafer with microstructures used for production of microstructure scaffolds. b Schematic of exemplarymicrowell arrangements of different width and distance. 55
Figure 34. Calculation of possible islet loading volume per scaffold. a Rat pseudo islet diameter relating to the seeded cell number b cIEQ (cell number based islet equivalents) per pseudo islet relating to the islet volume equivalent (IEQ) based on Buchwald et al. 2009. c Islet loading volume (cIEQ) of microwell hydrogel arrays. 58
Figure 35. Analysis of dimensional characteristics of microwells with varying distance and width. a Number of microwells per hexagon unit. These numbers are representing the maximal number of pseudo islets per hexagon hydrogel. b Distance from centre to centre of the microwell hexagons. c Spacing of pseudo islets of different sizes depicted as multiples of the islet size. Horizontal lines represent minimal required spacing of islets as modelled by Johnson et al. 2009. 58
Figure 36. Schematic presentation of the design for an experiment setup. a Variable microwell width, distance btw. microwells and cell number per well are representing the variables on a matrix to find the border conditions under which islets can maintain viability and function. b Example of a central composite design (CCD) to choose the factors tested in the experiment. 62
Figure 37. Experimental conditions for investigation of an optimal islet arrangement by application of ‘design of experiment’ method. a Table of conditions. b Graphical representation of conditions. The sphere’s size corresponds with the cell number to investigate in each condition. 63
Figure 38. Schematic drawing of the intertwined network of the composite membrane. 66
Figure 39. Size exclusion principle of the composite membrane. Large molecules of the immune system cannot pass the membrane (red), small molecules relevant for the metabolism can pass the membrane (green), cytokines are small and can pass the membrane, but there diffusion can partly be prevented by the electrochemical charge of the membrane. 69
Figure 40. Preparation of composite membranes via spin-coating process. 77
Figure 41. Side-by-side diffusion chamber used to assess the permeability characteristics of the membrane. 78
Figure 42. Blood incubation chamber for blood compatibility assessment. 80
Figure 43. Storage modulus G’ in Pa at different degrees of swelling of heparin-starPEG hydrogels with different solid content and crosslinking degree (y). 82

Figure 44. Swelling degree of heparin-starPEG hydrogels with different solid content and crosslinking degree (y). 83
Figure 45. SEM of native (A,B) and composite membrane (C,D). A, C: 10000x magnification (scale bar: 5 µm), B, D: 25000x magnification (scale bar: 2 µm).....84
Figure 46. Energy-dispersive X-ray spectroscopy (EDX) of a cross section of the membrane. Left SEM view. Middle Intensity distribution of fluor atoms abundant in PTFE. Right intensity distribution of sulphur atoms abundant in heparin.....85
Figure 47. Assessment of selectivity of the composite membrane. The diffusion of IgG over heparin-starPEG coated ePTFE membranes was investigated by creating a gradient of IgG over the membrane (n=6). a Total concentration of IgG in the compartments at the sink and the source site of the membrane with and without a gradient. b Percentage of penetration of IgG at the sink site of the membrane. 86
Figure 48. Fluorescence recovery after photobleaching (FRAP) of insulin-Dylight488 in solution or the composite membrane. a T-half (half maximal recovery time) of the regained fluorescence intensity. b Mobile fraction representing the fraction of the molecules that can freely diffuse (n=5-6). 87
Figure 49. In vitro biocompatibility of the composite membrane assessed by the activation of the complement system. a Deposition of complement factor 3 on the surface. b Levels of complement factor 5 in the blood.....88
Figure 50. Preparation of variants of the immunoisolating membrane for in vivo biocompatibility and vascularisation analysis. 93
Figure 51. Preparation of variants of the immunoisolating membrane for in vivo biocompatibility and vascularisation analysis in combination with mesenchymal stem cells.....94
Figure 52. Continuous oxygen supply to the encapsulated islets directly after implantation and during long-term engraftment of the implant. During the initial time of implantation, oxygen is provided from the oxygen module via a degradation process of the integrated calcium peroxide. After some time the implant surface is vascularised from the host tissue and oxygen is provided via diffusion from the capillary, when the oxygen reservoir from the oxygen module is exhausted.....96
Figure 53. Oxygen generation by CaO_2 embedded is silicone disks. Water can only slowly penetrate between the hydrophobic polymers and activate the degradation of CaO_2.....99
Figure 54. Oxygen measurement setup to quantify the released oxygen of oxygen-generating disks. 101
Figure 55. Oxygen release of oxygen-generating disk. Red dashed horizontal line: 6.7 mg/l oxygen ≙ 20,9 % oxygen saturation ≙ 149,30 mmHg (oxygen concentration in air). Orange horizontal line: 1.8 mg/l oxygen ≙ 5,6 % oxygen saturation ≙ 40 mmHg (physiologic tissue oxygen concentration). 103

Figure 56. Oxygen release of oxygen-generating disk in combination with a buffer layer of either silicone or agarose. Red dashed horizontal line: 6.7 mg/l oxygen ≙ 20,9 % oxygen saturation ≙ 149,30 mmHg (oxygen concentration in air). Orange horizontal line: 1.8 mg/l oxygen ≙ 5,6 % oxygen saturation ≙ 40 mmHg (physiologic tissue oxygen concentration). 104
Figure 57. Prototyping of encapsulation device components. a Insert for islet holder. b Islet holder. c Fitting of islet holder on insert to test tolerances. d Skeleton e Insert for membrane holder. f Membrane holder. g Membrane holder fitted with insert. h Assembly of whole setup with oxygen disk. 107
Figure 58. Detailed design features of the encapsulation device. a Alignment structures have been developed, which place the islets at the exact height under the membrane. b Technical drawing (top view) indicating the corner roundness for CNC milling. c Design variants of the device for different volumes of oxygen disks. d Cross section of the assembled device components indicating the position of the O-ring. e Cross section with aberrant oxygen-generating disk highlighting the requirement of the height positioning stands of the islet holder. 109
Figure 59. Overview of the post processing and assembly steps of the encapsulation device. 110
Figure 60. Post processing of the membrane holder. a A negative insert is placed behind the hexagon structure and glue is distributed by a spin coater. The negative is removed, the membrane is positioned on the hexagon struts and the left for curing. b A clean negative is placed behind the membrane and the hydrogel layer is distributed by a second spin coating step. After curing of the hydrogel the negative is removed and the complete membrane holder can be sterilised. 111
Figure 61. Production process of the oxygen module. The curing mould with triangular extrusions is filled with medical grade silicone premixed with CaO_2. After curing of the silicone, the oxygen-generating disk is removed and placed in the skeleton of the encapsulation device. 112
Figure 62. Photograph of the combined oxygen module. The skeleton (produced by CNC-drilling from PEEK) combined with an oxygen-generating disk and an O-ring.....113
Figure 63. Post processing and filling of the islet module. a A negative is placed in the islet holder and medical grade glue is distributed by a spin coating process. The negative is removed and an oxygen-permeable membrane to prevent the hydrogel arrays to fall through the islet holder is fixed on the bottom of the islet holder. b Microwell hydrogel arrays are produced and placed together with a funnel on the islet holder c, d The combined islet holder placed in cell culture dish and single islet cells are seeded on top and incubated for aggregation of the pseudo islets. e The funnel is removed from the islet holder with a removing. f Schematic

of complete islet holder with microwell hydrogel arrays. g Photograph of fully assembled islet holder with microwell hydrogel arrays. 114
Figure 64. Islet holder seeded with 400 INS-1 cells per microwell. Aggregated INS-1 clusters after one day of culture in hydrogel microwell arrays of 150 µm width and 150 µm distance or 150 µm width and 300 µm distance (upper and upper right hexagon). 115
Figure 65. Islet holder seeded with 400 INS-1 cells per microwell and stained for viability by fluorescein diacetate and propidium iodide. Aggregated INS-1 clusters after one day of culture in hydrogel microwell arrays of 150 µm width and 150 µm distance or 150 µm width and 300 µm distance (upper and upper right hexagon). a Seven hexagon islet holder. b Magnification of clusters. 116
Figure 66. Final assembly of the encapsulation device modules for implantation. a Exploded view of assembled device components. b Photograph of high fidelity prototype manufactured by CNC milling in PEEK. c Cross section of completely assembled device depicting the placement of the islets directly under the immunoisolating membrane. d Islet holder filled with hydrogel microwell arrays and funnel in 6-well plate to allow islet aggregation. e Single device modules before assembly. f Islet holder placed on skeleton. g Closing of device with membrane module. 117
Figure 67. Islet holder produced by additive manufacturing with glued membrane with silicone adhesives with different rheological properties. a Flowable / self levelling silicone adhesive pulls into the membrane and clocks the pores as indicated by arrows b Thixotropic / non-slump silicone adhesive stays at the supporting structures of the membrane holder and does not clock the membrane. 122
Figure 68. Scaling of the device by arrangement of repetitive hexagon units (microwell hydrogel arrays). a 1, b 3, c 7, d 19, e 37, f 61 hexagon units. Diameters in mm. 124
Figure 69. Relative surface area covered with islets (area of hydrogel microwell area/total surface area) for differently scaled devices produced by CNC milling. 126
Figure 70. Schematic cross sectional view of double-sided device design.....127
Figure 71. Properties of differently scaled single- and double-sided devices. a Islet capacity of differently sized encapsulation device sizes. b Theoretical weight of organism, which can be controlled by differently sized devices. 127
Figure 72. Hydrogel microwell array arrangements. For the preclinical evaluation of the encapsulation device the optimal pseudo islets density is investigated by placing microwell hydrogel scaffolds filled with pseudo islets of different size and distance into the encapsulation devices. Scale bar 100 µm. 128
Figure 73. Timeline for implantation of the novel encapsulation device for preclinical evaluation in a rat animal model. 129
Figure 74. Current and alternative filling strategy of the novel encapsulation device. 135

List of Tables

Table 1. Representative diffusion times of relevant molecules based on the approximation of the diffusion time by $t \sim x^2/2D$ with $D_{Insulin} = 1.5 * 10^{-7}$ cm^2/s, $D_{Glucose} = 5 * 10^{-6}$ cm^2/s and $D_{Oxygen} = 2.1 * 10^{-5}$ cm^2/s (Aso et al., 1998; PhysiologyWeb). 27
Table 2. Maximal packaging and pitch depending on islet size (rounded values). Data extracted from Johnson et al. 2009. 40
Table 3. Microwell arrangements theoretically supporting islet function and viability with highest islet packaging density (>450 IEQ/cm^2). 59
Table 4. Properties of molecules need to diffuse (green) or need to have restricted diffusion over the immunoisolating membrane (red), cytokines in the same size range as insulin, but that can potentially be bound by charge (orange). 70
Table 5. Components for the preparation of hydrogels for the composite membrane. The total volume of the mixture is 225 µl, which is sufficient for preparing 10 membranes. 76
Table 6. Materials applied in the high fidelity prototype of the proposed encapsulation device. 120
Table 7. Analysis of dimensions and islet loading capacity of differently scaled devices.....125

List of Abbreviations

BSA	Bovine serum albumin
C1q	Complement factor 1q
CAD	Computer-aided design
cIEQ	Cell number based islet equivalent
ECM	Extra cellular matrix
ePTFE	Expanded polytetrafluoroethylene
FDA	Fluorescein diacetate
GMP	Good manufacturing practice
HbA1c	Hemoglobin A1c
IEQ	Islet equivalent
IgG	Immunoglobulin G
IgM	Immunoglobulin M
ipGTT	Intraperitoneal glucose tolerance test
MEMS	Microelectromechanical systems
MHC	Major histocompatibility complex
OCR	Oxygen consumption rate
OGD	Oxygen generating disk
PBS	Phosphate buffered saline
PDMS	Polydimethylsiloxane
PEEK	Polyether ether ketone
PEG	Polyethylene glycol
PI	Propidium iodide
PTFE	Polytetrafluoroethylene
SDS	Sodium dodecyl sulphate
SLA	Stereo lithography
starPEG	4-arm polyethylene glycol
T1D	Type 1 diabetes
T2D	Type 2 diabetes
UV	Ultraviolet

1 Introduction and aims

Diabetes mellitus is a metabolic disease affecting millions of people worldwide. Estimates by the World Health Organisation and the International Diabetes Federation report about 463 million diabetic patients worldwide, corresponding to a prevalence of 7.3 % in the adult population. The number of diabetic patients is expected to rise to 700 million in 2045, an increase of 51 %. According to the information service of the German Diabetes Centre in Düsseldorf, the prevalence of diabetes in Germany in 2019 was 10.4 %, which is significantly higher than the international average. It is estimated that diabetes and its complications are responsible for 10 % of the global health expenditure (International Diabetes Foundation, 2019).

In the autoimmune disease diabetes type 1, a T-cell mediated immune reaction leads to a successive destruction of the beta cells causing a severe endogenous insulin deficiency. Before insulin was first isolated in 1921, type 1 diabetes (T1D) limited the life expectancy to only a few months. While this scientific breakthrough extended the lives of millions, it simultaneously created the medical challenge of long-term complications. A consequence thereof is a still significantly reduced life expectancy compared to the general population. In the century since its discovery, developments in insulin isolation and delivery as well as advances in glycaemic control technologies have significantly altered and improved T1D treatment. Yet despite this progress, a significant number of T1D patients nevertheless do not reach the glycaemic targets required to prevent or even slow diabetes complication progression. This continues to place high strains on those affected by T1D.

Currently, whole pancreas and islet transplantation are the only clinically available means of beta cell replacement. While pancreas transplantation is mainly performed simultaneously with a kidney transplantation in patients with T1D and end stage renal disease, the intraportal transplantation of isolated pancreatic islets is an established therapy for treatment of T1D patients with highly unstable metabolic control. Despite a steady improvement of graft survival and function in recent years, there are factors hampering a more widespread application of islet transplantation. The three most important and yet unresolved problems are insufficient oxygen supply to the isolated and transplanted islets, due to lack of revascularisation in the early post transplantation phase, permanent exposure to harmful allo- and autoimmunological and inflammatory processes, as well as lack of a sufficient number of donor organs for islet isolation.

A solution, eliminating transplant exposure to immunological processes, is the encapsulation of the islet graft prior to transplantation. This strategy creates an immunologically shielded

space, while the immunoisolating barrier allows interaction of donor and recipient tissue for glucose and insulin exchange, it prevents passage of immune system components. Furthermore, the encapsulation approach circumvents the shortage of donor organs as alternative cell sources, such as xenogeneic or stem cell derived insulin producing cells, could safely be transplanted. However, macroencapsulation poses the same even more enhanced problem of insufficient oxygenation.

For already existing encapsulation devices the following problems could be identified (Figure 1):

1. The oxygen and nutrient supply is hindered by the physical dimensions, which do not match the scale of diffusion. The distances from the capillaries at the outside of the device are too far for a sufficient supply of oxygen and nutrients.
2. The encapsulated islets themselves are too large for sufficient oxygenation in their core. Accordingly the central tissue dies and cannot contribute to the function of the islet anymore.
3. The islets inside the encapsulation devices are packed too dense and heterogeneously, that the availability and distribution of the sparse oxygen and nutrients is furthermore reduced for the single islet.
4. The surface of the encapsulation device has an insufficient biocompatibility. The surface material triggers fibrosis and does not sufficiently induce vascularisation for an exchange of nutrients and oxygen close to the membrane.

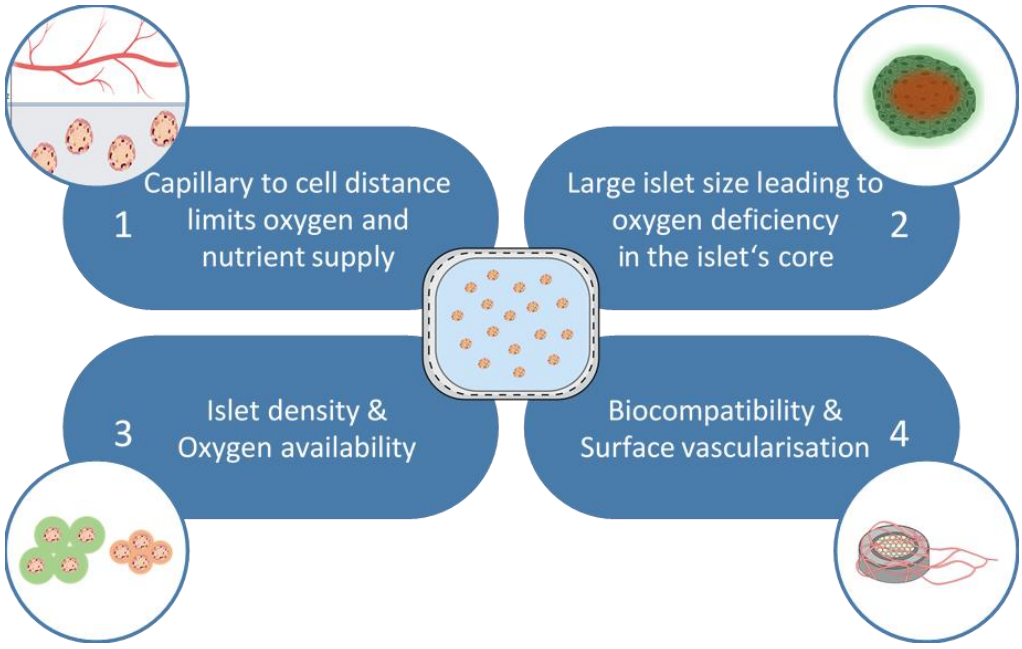

Figure 1. Limitations of current macroencapsulation devices.

To overcome these obstacles this thesis introduces the concept of a novel encapsulation device, designed from the ground up, starting at the microscale of the islet size. Furthermore, the methods to optimise this novel encapsulation device are introduced and discussed. Starting off with the dimensional requirements of an encapsulation device and continuing with the discussion of different functional modules in chapter 3. The microarchitecture of the islet arrangement and the concept to optimise this arrangement are discussed in chapter 4. Methods to create an immunoisolating barrier with a mesh size on the nanoscale and increase vascularisation are covered in chapter 5, while a material for the increased oxygenation in the early post transplantation period is subject of chapter 6. The final chapter 7 describes the assembly of the encapsulation device and discusses aspects of translation into clinical application.

2 Theoretical Background

2.1 Diabetes mellitus

Diabetes mellitus is a chronic metabolic disease resulting from an insufficient secretion of insulin by the pancreas or a resistance to insulin by the peripheral tissue. Both conditions are leading to an increased blood glucose level, causing many long-term complications if left untreated such as cardiovascular disease, neuropathy, nephropathy and retinopathy. Clinical symptoms are weight loss, polydipsia, polyuria and blurred vision, which are often present at clinical diagnosis. In an acute state diabetes can have fatal complications such as diabetic ketoacidosis, hyperosmolar hyperglycemic state, and death.

Diabetes is classified into the following general categories:

1. Type 1 diabetes or insulin dependent diabetes mellitus due to an autoimmune destruction of insulin-secreting β-cells,
2. Type 2 diabetes (T2D) or non-Insulin dependent diabetes due to a resistance to insulin of peripheral tissues the organism develops an progressive insulin secretory defect,
3. gestational diabetes, a type of diabetes mostly diagnosed in the second or third term of pregnancy,
4. other specific forms of diabetes arising from monogenetic defects of beta cell function or insulin action, diseases of the exocrine pancreas, endocrine disorders, drug-induced diabetes, infections, uncommon immunological forms, or other genetic syndromes.

2.1.1 Pathophysiology of T1D and T2D

T1D develops due to a loss of insulin-producing beta cells by a T-cell mediated immune attack (Figure 2) and is therefore also called immune-mediated diabetes. The progressive loss of beta cells leads to an irreversible failure of insulin secretion. The development of a metabolic phenotype occurs over a variable time (weeks to years) initially leading to impaired glucose tolerance and finally progressing into symptomatic hyperglycemia. The progression of the disease manifests itself in the development of beta cell specific antibodies such as antibodies to insulin (IAA), glutamic acid decarboxylase (GAA or GAD) and protein tyrosine phosphatase (IA2 or ICA512). Here, it is not the number of different antibodies, but the total amount of antibodies that allows a prediction on the progression to overt diabetes (Taplin and Barker, 2008). T1D is a multifactorial disease, which is triggered by a combination of genetic predisposition and environmental factors such as viruses, bacteria, diet, and unhealthy lifestyle. The most common genetic predisposition for development of T1D is associated with

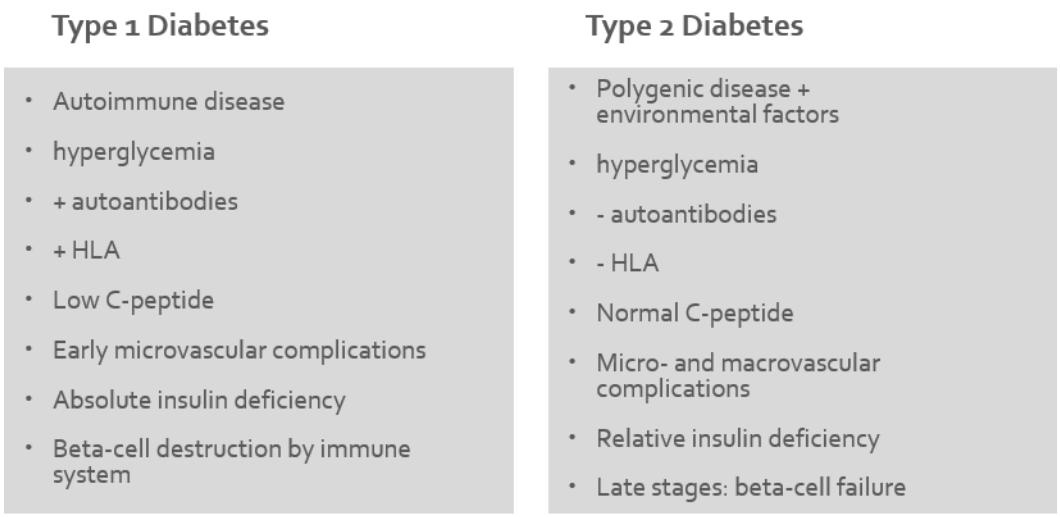

Figure 2. Pathophysiology of type 1 and type 2 diabetes.

the major histocompatibility complex (MHC), here the highest risk for beta cell autoimmunity is associated with the HLA-DR3/4 DQ8 genotype (Taplin and Barker, 2008). Furthermore, it is likely to appear in combination with other autoimmune diseases including Hashimoto's thyroiditis, Graves' disease, celiac disease, and autoimmune gastritis/pernicious anemia.

T2D originates from a reduction in peripheral insulin sensitivity leading to an impaired glucose uptake in skeletal muscle, liver and adipose tissue leading to an increased blood glucose concentration. Besides this, a reduced uptake of glucose in the periphery by an impaired glucose production can be present in the liver. To compensate for the resistance to insulin of peripheral tissues, the production of insulin by beta cells is upregulated. This excessive insulin production leads to a declining beta cell function over time. With the progression of the disease, insulin levels decrease and the patient becomes diabetic as the insulin production cannot compensate the insulin resistance. Beta cells are getting exhausted and are ultimately lost and the insulin secreting function cannot be regained, comparable to T1D.

T2D has a strong genetic component with environmental factors such as age, obesity, diet and lack of physical activity playing a role in disease development. Furthermore, T2D is a polygenic disease with no correlation to the development of the disease with single susceptibility genes.

2.1.2 Epidemiology of diabetes

A worldwide increase of the prevalence of diabetes is predicted. In 2019, 463 million people of the world's population have been diabetic and an increase of 51% to 700 million in 2045 is predicted (International Diabetes Foundation, 2019). Within the age group of 18 to 79 year-olds in Germany 7.2 % are diagnosed with diabetes based on health examination services and 9.9 % based on data provided by statutory health insurances (Rosenbauer et al., 2019). The largest proportion of diabetes cases are reported as T2D. 7.4 % of the male adult population

and 7.0 % of the female adult population are diagnosed with T2D (Rosenbauer et al., 2019). The prevalence of T1D in Germany has been estimated at 493.3 per 100 000 inhabitants in 2016; it is lower in women (455 reported cases in 100 000 inhabitants) than men (493 reported cases in 100 000 inhabitants) (Rosenbauer et al., 2019). The incidence of T1D has been reported to be 6.1 per 100 000 inhabitants in the years 2014-2016 (Rosenbauer et al., 2019). Recent calculations suggest an incidence increase for T2D-diagnosed patients from 10.7 million (+54 %) to 12.3 million (+77 %) between 2015 and 2040 in Germany. In contrast to earlier calculations, which only suggested an increase to 8.3 million (+21 %), these new calculations are taking into account temporal trends such as a decrease in mortality and changing incidence trends (Tönnies et al., 2019). The incidence rates for T1D in children has been rising worldwide over the past 60 years by about 3-5 % per year with an expected doubling of the incidence rate every 20 years (TEDDY Study Group, 2008). The life expectancy of patients with diabetes is lower than that of a comparable non-diabetic population. Men diagnosed with diabetes at the age of 40 to 59 have a 1.9-fold higher risk of death compared to the normal population, with an increase to a 2.6 times higher risk of death at the age of 55 to 74 (Meisinger et al., 2006). At the age of 20 patients with type 1 diabetes have a reduced life expectancy of approximately 11 years in male subjects and 13 year in female subjects, when compared with the general population (Livingstone et al., 2015).

2.1.3 Physiologic glucose homeostasis

Glucose is the most important energy source for many tissues and cells and irreplaceable for the brain. A continuous supply of glucose in the blood is inevitable, as there is no compartment in the brain to store glucose for more than a few minutes. The cell membranes of the brain continuously express GLUT-1 receptors, which are independent of insulin and can therefore continuously transport glucose to the brain.

Normal physiologic blood glucose homeostasis is maintained by a neuro-hormonal system, mainly under the control of the endocrine pancreas involving two main endocrine hormones, insulin and glucagon. Insulin release is stimulated by a high blood glucose concentration. The insulin acts on the peripheral tissues to mediate the uptake of glucose into the cells and the short-term storage of glucose in the form of glycogen (glycogenesis) in the liver, to lower the blood glucose concentration. In contrast, glucagon is released at low glucose blood levels and stimulates glycogenolysis (breakdown of glycogen into glucose) in the liver and gluconeogenesis (glucose production to raise blood glucose levels). Both hormones are constantly regulating the blood glucose homeostasis in a constant feedback loop. After the intake of a meal, the blood glucose levels rise and insulin is subsequently released to lower the blood glucose level. During exercise on the other hand, the body consumes glucose and the blood glucose level drops and glucagon is consequently secreted to raise the blood glucose

level again. In a ‘normal’ status the fasting blood glucose level is < 5.6 mM and <7.8 mM after an oral glucose tolerance test (Fischer et al., 2004).

2.1.4 Islets of Langerhans

The pancreatic islets secrete the endocrine hormones involved in the regulation of the blood glucose concentration. These were discovered by Paul Langerhans in 1869 and are therefore also called ‘islets of Langerhans’. The islets are distributed in between the exocrine tissue of the pancreas and make up 2 % of the whole pancreatic tissue, while 80 % of the tissue is exocrine tissue. The remaining 18 % of the pancreas are made up by blood vessels and ducts (Barrett KE, Boitano S, Barman SM, 2010). While the islets constitute a relatively small portion of the pancreas, they require 10 to 15 % of the pancreatic blood flow in rats (Henderson and Moss, 1985). Furthermore, islets have fenestrated capillaries, which make the exchange of oxygen and hormones in between the islets and the capillaries even faster, which further states their high oxygen demand.

Islets are clusters of multiple cells and come at various sizes in the range of 50 to 280 µm (In’t Veld and Marichal, 2010). For human islets, the average islet size is about 140 µm. The pancreatic islets consist of four major endocrine cell types, namely 30 % alpha cells (also referred to as A-cells), 60 % beta cells (also referred to as B-cells), with the remaining 10 % delta cells (also referred to as D-cells or A1 cells), PP-cells (pancreatic polypetide cells, also called F-cells or D1 cells), and epsilon cells (Figure 3). Each cell type secretes a unique endocrine hormone: Alpha cells are secreting glucagon, beta cells are secreting insulin, delta cells are secreting somatostatin, PP-cells secrete pancreatic polypeptide and epsilon cells secrete ghrelin. Next to endocrine cells, the pancreatic islets also consist of stromal cells, macrophages, neuronal elements, endothelial cells and pericytes. Surrounding the islet and in between the cells, the extracellular matrix contributes to the cellular communication. A peripheral capsule consisting of fibroblasts and collagen fibers is embedding the islets. It comprises two basement-membranes, one towards the exocrine epithelium and one towards the endocrine epithelium (Aamodt and Powers, 2017). These consist of different types of laminins, collagens and fibronectins. The extra cellular matrix is of great importance, as a lack of the basal membranes impairs beta cell proliferation and insulin gene expression. The interaction of integrin-α1β1 with collagen IV for example, regulates insulin secretion and beta cell differentiation (Bosco et al., 2000; Kaido et al., 2004).

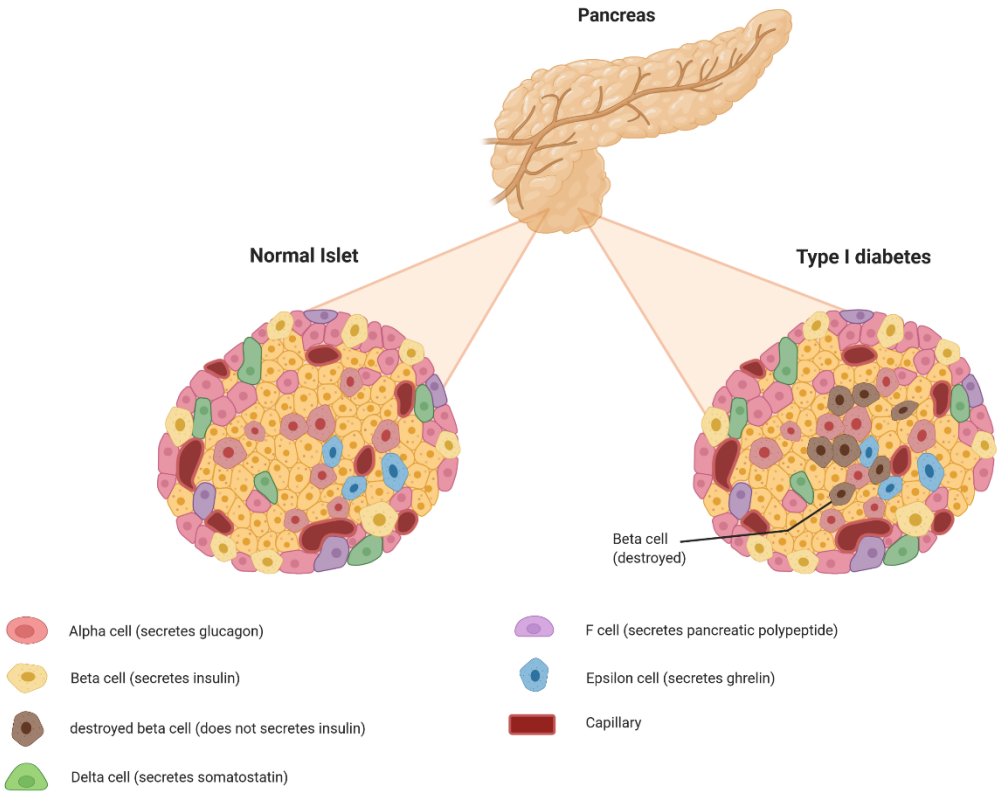

Figure 3. Pancreatic Islets of Langerhans. *A normal islet (left) and an islet affected by autoimmune destruction in type I diabetes (right).*

Together all these cell types make up complex aggregates acting like a mini organ with innervation and complex intercellular communication. The islets integrate many different types of signals from the blood stream, the innervation and the interstitial space in the form of nutrients, hormones and neurotransmitters to execute their endocrine function (Wassmer, Lebreton et al., 2020).

2.2 Treatment of Diabetes

2.2.1 Insulin therapy

Treatment of T1D is generally performed by frequent subcutaneous administration of insulin via manual injections (MDI-therapy) or a continuous infusing insulin pump (CSII) to regulate the blood glucose homeostasis.

In a healthy person, the pancreas secretes insulin when an increase of the blood glucose concentration due to carbohydrate intake is detected. Additionally, a basal rate of insulin is secreted to regulate metabolic processes. Insulin therapy is aimed to mimic these changes in requirement by differently acting insulin types with different effect duration and effect onset.

A reference point for treatment in the course of diabetes therapy is the hemoglobin A1c (HbA1c). It is a reference for the blood glucose level over the last two to three months. Based on the HbA1c a therapy aim is set according to the progression of the disease. For the therapy of diabetes, there are two main types of pharmacological insulin: human insulin and insulin analogues. Human insulin has the same molecular structure as insulin secreted by the beta cells. It is synthetically produced by yeast or bacteria. A subclass of human insulin is neutral protamine Hagedorn (NHP) insulin, which is supplemented with protamine to delay the onset of effects. Insulin analogues are synthetically produced insulins with small variations of amino acids. These modifications influence effect duration and effect onset. Extremely fast acting compounds used as bolus insulin, or insulin acting over long-term periods of 24 h used as basal insulin, can be produced (Deutsche Diabetes Gesellschaft, 2018).

Insulin therapy is individual for each patient and can generally be classified into either conventional or intensive insulin therapy. In conventional therapy patients receive a mixture of basal and bolus insulin at set times about twice a day. This therapy is only suitable for patients with a regular daily routine but carries a higher risk of hypoglycemia. Patients in intensive insulin therapy have one to two basal insulin injections and further bolus injections for meals. The injections can be performed with an insulin pen, syringe or pump. With the application of an insulin pump multiple injections of short acting insulin are dispensed. This therapy normally supports good glucose homeostasis. Regardless of the form of therapy, the blood glucose concentration must be checked regularly. The insulin requirement can change depending on the situation in life, as for example during pregnancy and lactation period, during infection or disease, or upon surgery. Insulin therapy in general is strongly dependent on the individual patient, the insulin requirement, capabilities and life situation (Deutsche Diabetes Gesellschaft, 2018).

T2D is prevented and treated by maintaining a normal body weight, physical exercise and, a healthy diet. If these actions cannot sufficiently lower the blood glucose concentration, antidiabetic medications must be added to prevent acute and long-term complications. The most commonly applied antidiabetic drugs are metformin (stimulating an increase in glucose uptake from the blood and a decrease of glucose production in the liver), sulfonylurea (which increases the glucose uptake into cells), dipeptityl peptidase-4 (DPP4) – inhibitors in the form of glucagon-like peptide-1 (GLP-1) - analogues (which increase the release of insulin and the glucose uptake of the cells), and sodium dependent glucose transporter 3 (SSGLT-2) - inhibitors (which reduce the reuptake of sugar in the kidney). If all these medications and their combinations are not sufficient to normalize glycemic control, insulin therapy is applied either as only basal, only bolus insulin or as an MDI-therapy concept.

In conclusion, matching the rapidly fluctuating insulin requirements is difficult and often causes diabetes-associated complications.

2.2.2 Beta cell replacement strategies: pancreas and islet transplantation

In contrast to insulin therapy, pancreas and islet transplantation are two ways to replace the immune destructed beta cell mass. Both have the ability to restore glucose homeostasis in a diabetic patient to an euglycemic state.

Whole pancreas transplantation was first performed in 1966 at the University of Minnesota by R. Lillehei and W. Kelly. It is a major surgical procedure, which is mostly reserved for patients with end-stage renal insufficiency. The pancreas is then transplanted in combination with the kidney as a simultaneous pancreas kidney transplantation (SPK). Since the procedure was first performed, success rates have increased with improved surgical techniques and immunosuppression, yet it still comes with a significant morbidity risk (Niclauss et al., 2016). This called for less invasive procedures, which promoted the development of islet transplantation in the 1970s, which is a procedure available for a larger cohort of patients. This minimally invasive procedure is aimed at nonuremic patients with severe hypoglycemia. With the development of the 'Edmonton' protocol, great improvements with good functional results were made (Shapiro et al., 2000) (Figure 4). Though the islet isolation and engraftment procedure contributes to a significant loss of cells due to isolation-related damage caused by a loss of vascularisation and extra cellular matrix (ECM), and the inflammatory microenvironment at the transplantation site. Therefore, long-term functional results are still unsatisfactory.

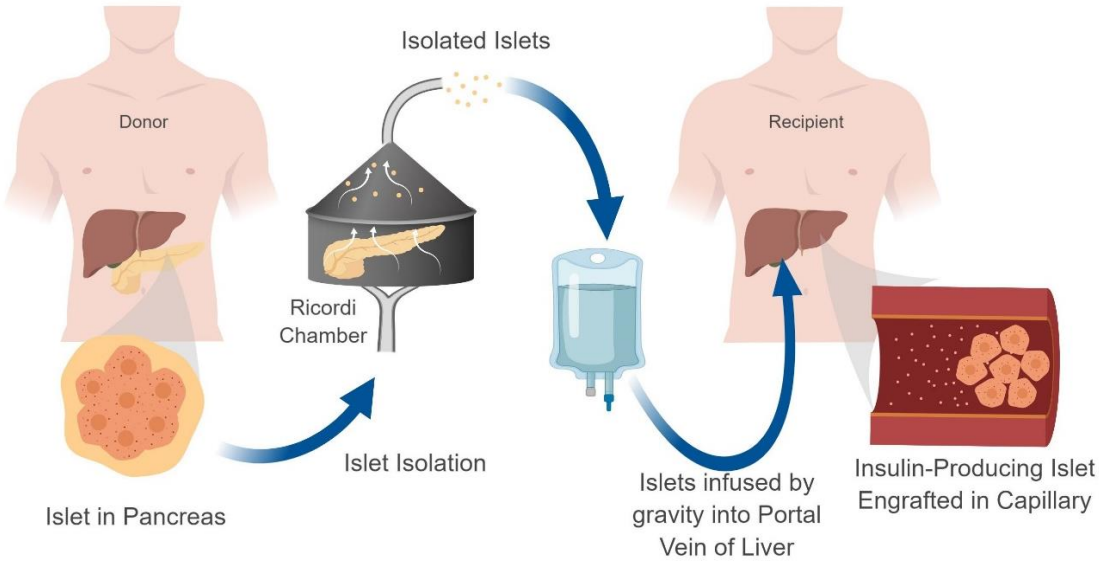

Figure 4. Intrahepatic islets transplantation (Shapiro et al., 2000).

While islet and whole organ pancreas transplantations potentially provide a functional cure of diabetes, the requirement for chronic immunosuppression and tissue availability limits the application of these options.

2.3 Alternative insulin-secreting cell sources and therapeutic approaches

A therapeutic approach to diabetes treatment is the restoration of the beta cell mass. Since human donor organs are scarce, alternative cell sources are investigated in the field of tissue and regenerative medicine. Approaches to obtain insulin-producing beta cells are for example the differentiation of beta cells from various types of stem cells, the replication of existing beta cells and the reprogramming of other cell types such as other pancreatic endocrine cells, acinar or duct cells from the pancreas. Further ideas are the engineering of non-beta cells that are able to produce insulin on a glucose stimulus or the construction of synthetic ‘cells’ (Nair et al., 2020). The transplantation of islets or beta cells from xenogeneic sources like pigs is a means to a less limited tissue source. Since the generation of beta cells from stem cells and xenogeneic sources are the most promising, these are discussed below.

2.3.1 Stem cell derived beta-like cells

For the differentiation of beta-like cells from stem cells in principle, three cell sources exist: human embryonic stem cells, adult stem cells and induced pluripotent stem cells. Embryonic stem cells (ESC) are pluripotent cells derived from the blastocyst of embryos and are self-renewing. These cells can theoretically generate any cell type in the body, while maintaining a normal karyotype. ESCs can furthermore be grown in culture for long periods. Their drawbacks are their development of antigenicity upon differentiation and they feature a low differentiation efficiency. Adult stem cells are self-renewing tissue specific to multipotent stem cells. These can be differentiated into a limited number of tissues and are mostly involved in repair processes of the human body. They have the great advantage of being the patient’s own cells and therefore do not provoke any immune rejection upon transplantation. Their drawbacks are their low abundancy *in vivo*, slow growth *in vitro* and limited regenerative capacity. Induced pluripotent cells (iPS) are reprogramed from somatic cells by a combination of reprogramming factors including Oct3/4, Sox2, Klf4, c-Myc, Lin28, Nanog and N-Myc. These cells have the advantage that they can be derived from the patient’s own cells and therefore do not provoke any immune response. They can be proliferated *in vitro* comparable to ESCs, but have the benefit over the latter ones in having less regulatory restrictions. However, the dangerousness of stem cells lies in their potency. In the same way as they can be differentiated into various somatic cells, they can just as well develop into cancerous tissue. The differentiation of stem

cells into endocrine beta-like cells follows the stages of differentiation during embryonic development of the beta cells. The development of the pancreas goes through several stages: From the blastocyst, where part of the tissue develops into definitive endoderm followed by differentiation into the foregut. From there the dorsal and ventral buds develop and fuse into the pancreatic endoderm. Finally, these cells evolve into the different cell types of the pancreas, including acinar cells, duct cells and endocrine precursors. Each stage of the development is marked by expression of different transcription factors. Though the final differentiation into fully glucose-responsive beta-like cells remains difficult *in vitro*. A first breakthrough in the *in vitro* differentiation of pancreatic cell lineages was the implantation of *in vitro* differentiated human pancreatic endoderm into mice, provoking the maturation of these cells into glucose-responsive insulin-secreting cells (Kroon et al., 2008). It took another six years until beta-like cells could be differentiated towards a final stage of mature beta-like cells by two independent research groups in 2014 (Pagliuca et al., 2014; Rezania et al., 2014). These cells were generated from a human embryonic stem cell line (hESC) HUES8 or two human induced pluripotent stem cell lines (hiPSC-1 and HiPSCs-2) and have been shown two resemble human islets in some characteristics as gene expression, glucose-responsive Ca^{2+} flux packaging of insulin into secretory granules and the secretion of insulin (Pagliuca et al., 2014). Comparable functionally mature beta-like cells were established by Rezania et al., (2014). These cells expressed markers of mature pancreatic beta cells and limited glucose stimulated insulin secretion. Furthermore, upon transplantation these cells matured as shown in previous experiments and could reverse a diabetic phenotype within 40 days. The developed differentiation protocols could then be applied to stem-cells derived from T1D patients to regenerate beta cells which were functional *in vitro* and *in vivo* (Millman et al., 2016). A major problem of the differentiation protocols into insulin-producing cells is to produce cells that only express one endocrine hormone rather than a combination (polyhormonal cells). Later studies recapitulated the clustering of endocrine cells as in mature islets. This greatly contributed to the maturation of the beta-like cells and further enrichment of beta-like cells could be achieved by cell sorting (Nair et al., 2019). Also, the involvement of extra cellular matrix factors could induce beta-like cells with a better function *in vitro* and *in vivo* (Hogrebe et al., 2020). In contrast to standard bioreactor culture, the cells were kept on plates coated with extracellular matrix factors for the final stages of differentiation. Here it could be shown that the cytoskeleton, interacting with the extracellular matrix, played a major role in the differentiation process.

The upscaling of these differentiation protocols to a clinical scale requires advanced cell culture setups such as multiplate culture incubators, roller bottle or wave bag cultures or a stirred suspension bioreactor culture (Nair et al., 2020). Though, for application in a patient it must be kept in mind that T1D is an immune system mediated disease. The replacement or regeneration of beta cells could reverse the diabetic phenotype, but the transplanted cells

would in turn be destroyed by the same autoimmune reaction initiating the disease in the first place.

2.3.2 Xenogeneic islets

Besides beta cells generated from stem cells, xenogeneic islets are another promising islet source. Xenotransplantation refers to transplantation of organs between different species. Islet from animals have fewer limitations to their availability over human islets and, in contrast to stem cells, are much easier to obtain and less cost intensive.

Pigs are the favored source for xenogeneic organ transplantation as they have physiologic similarities to humans, while having a low reproduction time and high progeny. Furthermore, porcine insulin only differs in one amino acid sequence from human insulin. Insulin isolated from pig pancreas has first been used as a drug in 1922 and animal insulin has been the standard way of care until the 1980s.

Similar to allogeneic transplantation, xenogeneic organs are rejected by the host immune system. The first major barrier is the instant blood mediated inflammatory reaction (IBMIR). Upon contact of the transplanted tissue with blood the coagulation and complement system are activated in combination with a platelet and leukocyte activation. Long-term function of transplanted xenogeneic islets has been proven difficult so far because of immune responses rejecting the tissue, but also by the detrimental effects of the required immunosuppression. Multiple preclinical trials have been executed with porcine islets in non-human primates, mostly with the application of monoclonal antibodies against CD154 or CD40, which could maintain the function of the xenogeneic islets for about two years (Shin et al., 2015; Min et al., 2018). Trials in humans have also been executed: In 1994 the first transplantation of neonatal porcine islets into humans took place. The graft was well tolerated by the patients and low levels of porcine C-peptide could be detected in the urine (Groth et al., 1994). Another study proved the survival of alginate encapsulated xenogeneic islets for 9.5 years in a diabetic patient (Elliott et al., 2007). The islets were laparoscopically retrieved and showed a low insulin secretion upon glucose stimulation.

With the genetic engineering tools available today the generation of genetically modified pigs has become possible. The modification of cell surface receptors can camouflage the cells to alleviate the ensuing immune rejection. A target are for example, carbohydrate epitopes which are differentially expressed and cause the response of human preformed antibodies in a hyperacute reaction (Cooper et al., 1993).

The major barriers of the graft rejection of xenogeneic tissue, IBMIR and T-cell mediated cell destruction, can be circumvented by the encapsulation of the xenogeneic islets. A risk of the

transplantation of xenogeneic tissue into humans is the transmission of animals´ diseases and viruses. To avoid such transmission, animals for the medical industry are farmed in a pathogen free environment. Furthermore, studies transplanting encapsulated porcine islets into non-human primates could prove that there is no risk of pathogen transmission (Ludwig et al., 2017).

2.3.3 Pseudo islets

Isolated pancreatic islets have various sizes ranging between 50 and 280 µm. After isolation, these are solely dependent on oxygen supply via diffusion, since the vasculature has been disrupted. The lack of oxygen in the inner core of the islets causes larger islets to develop a necrotic core during islet cell culture or upon transplantation (Komatsu et al., 2017). The restructuring of native islets into pseudo islets can be used to limit the islet cluster size to omit the development of a necrotic core.

The formation of pseudo islets is based on the principle of self-assembly (Achilli et al., 2012). After dissociation of the islets into single cells, the cells naturally reassemble into clusters. This can be attained by various methods, including culture in microfluidic chips, spontaneous self-aggregation in cell culture plates or rotational bioreactors, hanging drop culture, or microwell cell culture formats (Wassmer, Lebreton et al., 2020). In microfluidic chips single islet cells are clustered in droplets to obtain the desired islet size. These have the advantage that physiological perfusion results in optimal viability and function of the islet clusters. This format is optimal for drug screening, but only small amounts of organoids can be produced and the method is not upscalable. Spontaneous self-aggregation into non-uniform islets can be performed in non-adherent petri dishes or rotational bioreactors. Both have the advantage of easy application and a short handling time during setup of the culture, the cluster size however cannot be controlled, leading to the development of a necrotic core for larger islets and a higher risk of inflammation. The hanging drop technique is the oldest method to obtain clusters of uniform size. Droplets with single islet cells are placed on the lid of a petri dish and placed upside down to collect the cells by gravity at the lowest point of the droplet. This technique delivers homogenously sized and functional pseudo islets but is rather time consuming. The last method applies microwells in which the cells either settle down via gravity or by a centrifugation step. This technique also delivers islets of homogenous size and good functionality, with the drawback of possible dislodgement during medium replacement. When comparing the functionality and viability among different techniques of pseudo islet production, pseudo islets derived from hanging drop or microwell culture techniques have a higher stimulation index when functionally assessed in a glucose stimulated insulin release assay. Besides this, pseudo islets have a comparable arrangement of insulin-positive, glucagon-positive and somatostatin-positive cells to native islets (Wassmer, Bellofatto et al., 2020).

Pseudo islets can not only be produced from pancreatic islets, but can also be generated from other cell types, such as beta cell lines, human ESCs, iPS cells, pancreatic stem cells and other cell types (Wassmer, Lebreton et al., 2020). Biological self-assembly creates complex tissues during embryonic development. Extensive cell-cell contacts promote intracellular function. This easily explains why clustering and cluster size also seem to play an important role in beta cell differentiation (Nair et al., 2020).

2.3.4 Islet encapsulation

The major obstacles in islet transplantation are the dependence on rare organ donations for islet isolation, the destruction of the islet graft after transplantation due to inflammation and hypoxia of the transplanted tissue and the immunosuppression drug regime entailing strong comorbidities.

Islet encapsulation can overcome these drawbacks. The need for donor tissue has been made redundant by novel stem cell generated β-cells and the availability of xenogeneic graft tissue. When encapsulated, these tissues can be transplanted safely.

The application of advanced materials in the encapsulation process can overcome the second limitation. Novel materials which act as encapsulants can reduce the inflammation response and can camouflage the transplanted tissue from IBMIR. The drawback of the requirement for immunosuppressants can be made redundant by the encapsulation approach as well. Xenogeneic islet transplantation of encapsulated porcine islets into non-human primates has been performed without a need for immunosuppression.

The principle of encapsulation relies on a selective permeable barrier that allows free diffusion of oxygen, nutrients and effector molecules while preventing the migration of immune cells and cytotoxic molecules that can potentially harm the encapsulated cells. This barrier can be created at different scales: With the macroencapsulation approach, the complete islet graft is contained within a single capsule, while in microencapsulation only one or two islets are contained per microcapsule and in nanoencapsulation single islets are coated with a thin polymer layer (Figure 5).

Regarding the diffusion characteristics of oxygen and nutrients, nano- and microencapsulation approaches are superior to macroencapsulation as they boast the highest surface to islet ratio. However, macroencapsulation delivers great advantages when it comes to safety issues. The encapsulation of the total islet volume within one container permits the retrieval of the graft.

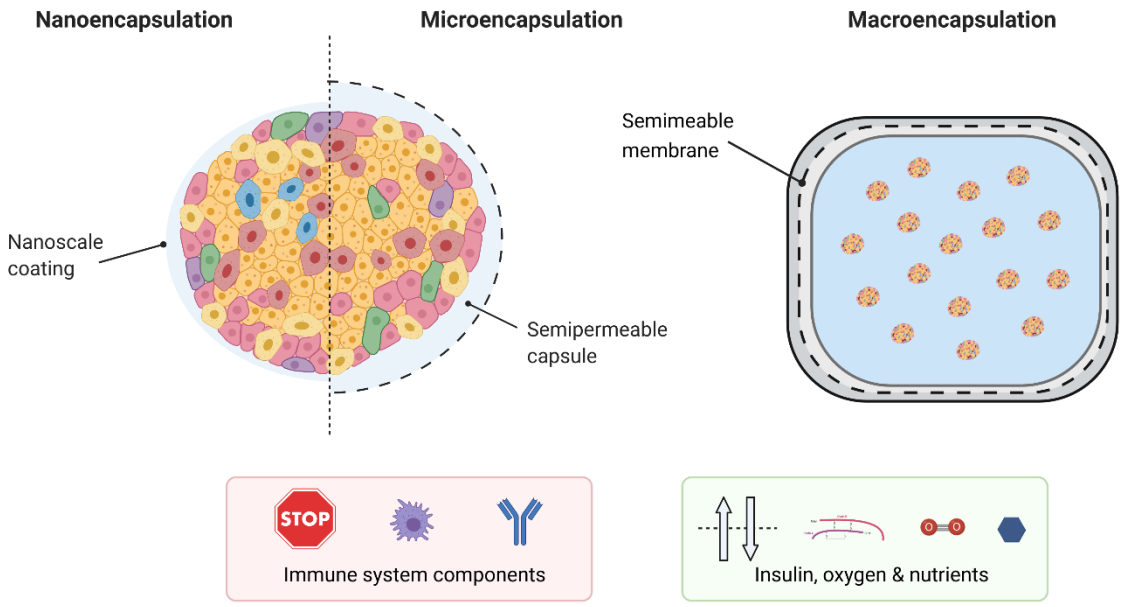

Figure 5. Nano-, micro- and macroencapsulation *are based on the concept of placing a perm-selective barrier around the islets, allowing the diffusion of molecules like insulin, oxygen and nutrients, while preventing access of components of the immune system. While for nanoencapsulation single islets are shielded by a thin polymer layer, in microencapsulation one to a few islets are embedded in microscale capsules. For macroencapsulation the complete islet graft is placed into a single capsule.*

The scale furthermore allows the application of more resistant membranes and materials which are less fracture-prone.

The compliance with the highest safety standards is the reason for the design choice of a macroencapsulation device in this thesis. The key aspects of this design are the materials and structure, the permeability and vascularisation properties of the immunoisolating membranes and the balance of the dimensions regarding a relevant transplanted islet mass, as well as clinical practicability and a sufficient supply of oxygen to the encapsulated tissue.

2.4 State of the art: Macroencapsulation devices

2.4.1 MAILPAN® by Defymed

The MAILPAN® device from Defymed (Strasbourg, France) is based on a dialysis membrane (AN69) consisting of a copolymer of acrylonitrile and sodium methallylsulfonate (Jesser et al., 1996; Thomas et al., 2011)(Figure 6). The empty device is implanted into the body for prevascularisation for several weeks, before filling the islets or islet-like clusters derived from stem cells into the device via the port system with an injection needle, avoiding the need for a second surgical intervention. This also allows for replacement of the cells at a later stage (Defymed, 2021). The patent of the MAILPAN device proposes an optimal size of the chamber between 8 and 14 cm with a volume of 15 to 50 ml to be able to load about 700 000 islet equivalents (IEQ) (Aoun et al., 2013). The membranes have a thickness between 45 µm to 200 µm. So far, no preclinical data has been published and a clinical trial has been withdrawn.

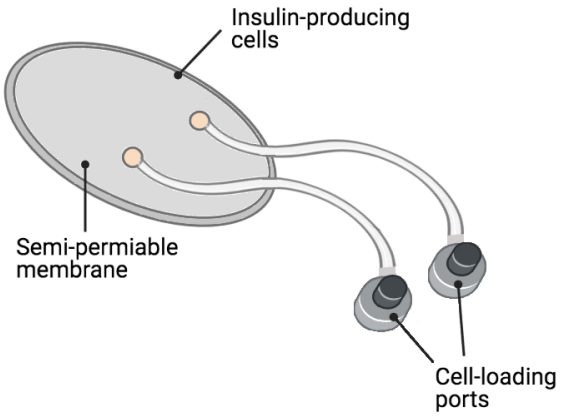

Figure 6. MAILPAN® encapsulation device by Defymed (Strasbourg, France). *The device is implanted for prevascularisation several weeks before insulin-secreting cells or islets are inserted via the two loading ports.*

2.4.2 TheraCyte™ device by TheraCyte, Inc.

The technology of the TheraCyte™ device has originally been developed by Baxter Healthcare (Round lake, IL) (Geller et al., 2006) and is manufactured by TheraCyte Inc. (San Clemente, CA). The membrane of the device is composed of multiple layers with increasing pore size (Figure 7). The innermost layer is a 0.4 µm pore size polytetrafluoroethylene (PTFE) membrane, the second layer a 5 µm pore size PTFE membrane and the outer layer a woven polyester mesh. The inner volume is created by a frame of polyester mesh insert. The membrane prevents the entry of host immune cells to protect the allograft. The differently sized devices have a total size of about 1.8 to 4.4 cm. The capsule is filled with the help of a tubing which allows insertion of 4.5 to 40 µl cell solution into the apparatus.

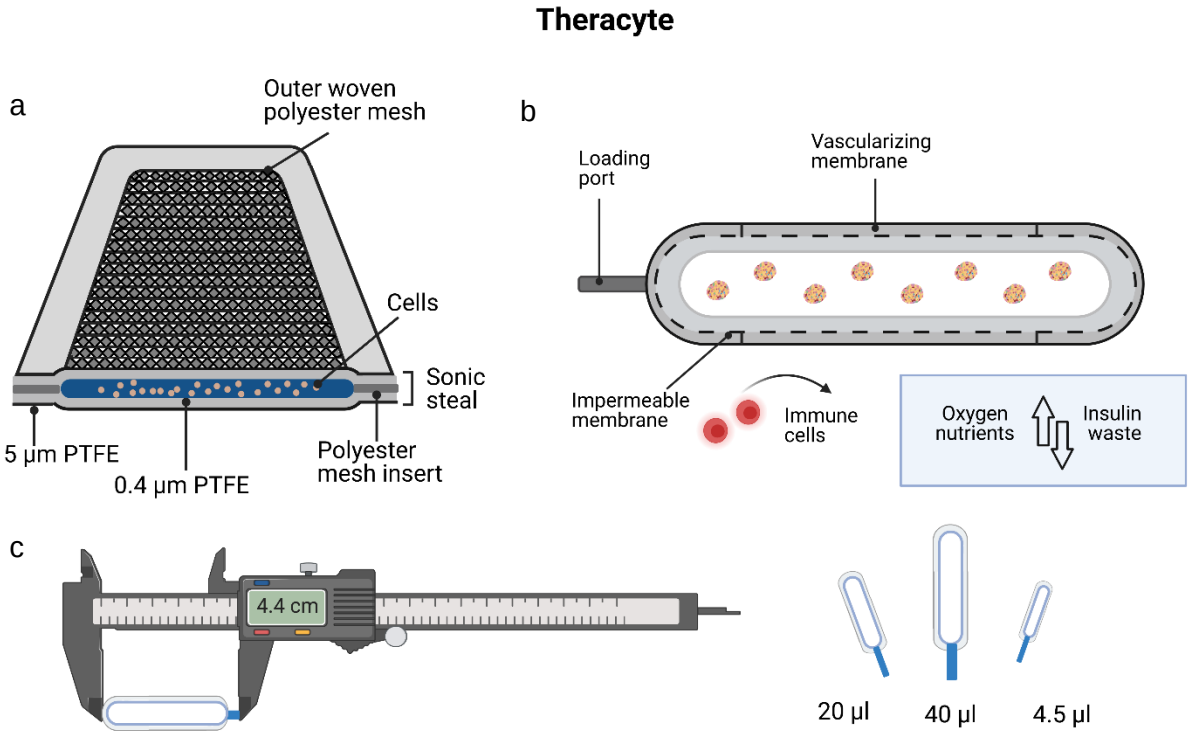

Figure 7. TheraCyte™ encapsulation device by TheraCyte Inc. a *Cross-section of the device. The multi-layered membrane consists of (from the in to the out) of a 0.4 µm pore size PTFE membrane, a 5 µm pore size membrane and an outer woven polyester mesh.* ***b*** *Schematic of TheraCyte™ encapsulation device.* ***c*** *Variants of the device with different volume.*

2.4.3 Encaptra and open device by ViaCyte Inc.

ViaCyte Inc. (Strasbourg, France) has developed two variants of an encapsulation pouch (ViaCyte, 2021). Some of these variants are in clinical trials and tested in combination with pancreatic endoderm cells differentiated from stem cells.

The devices are about 8.5 by 2.7 cm in size. Similarly to the TheraCyte™ apparatus, the PEC-Encap product (Encaptra) is a closed system based on a PTFE membrane, which immunoisolates the encapsulated cells. Meaning the encapsulated cells are only supplied via surface diffusion. This device is filled with pancreatic progenitor cells derived from stem cells, which are expected to mature into islet-like tissue when engrafted (clinical trial VC-02).

The second variant of the device is an open implant where the vasculature can grow through the membrane and is in direct contact with the encapsulated cells. This provides enhanced oxygenation of the contained cells, while on the other hand creating the need for

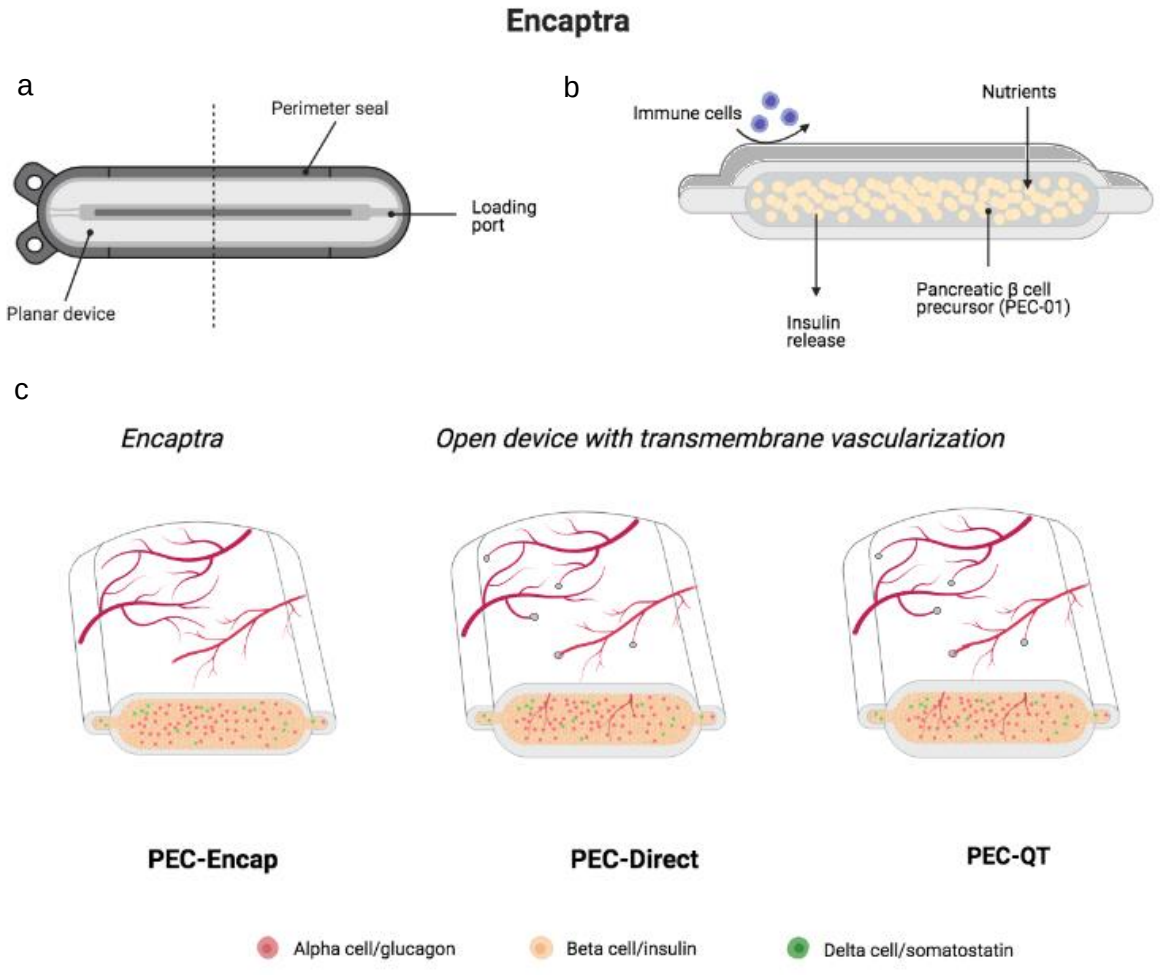

***Figure 8. Cell encapsulation devices by ViaCyte Inc. (Strasbourg, France) a** Schematic of Encaptra**. b** Cross section of the device**. c** Two device variants are available from ViaCyte Inc. Encaptra is an immunoisolating device, while the open device is a non-immunoisolating device accessible for transmembrane vascularisation. (Figure adapted from ViaCyte, 2021)*

immunosuppression for the patient. The open device is filled with pancreatic endoderm cells (clinical trial VC-01) or is intended to be used in combination with genetically engineered immune evasive pancreatic endoderm cells (PEC-QT) in order to dispense with the need for immunosuppressants (ViaCyte, 2021). There are several trials in the clinical evaluation phase, but no results have been published so far.

2.4.4 βAir device by BetaO_2 technologies

The βAir device developed by BetaO_2 Technologies comprises a composite membrane based on a PTFE membrane like the TheraCyte™ apparatus. It is composed of two 25 µm thin hydrophilised PTFE membranes with a pore size of 0.45 µm which are impregnated with high mannuronic (HM) acid alginate at 6% (w/v) under vacuum and crosslinked by 30mM $BrCl_2$ in saline. This membrane rejects the entry of host cells and is impermeable to viruses, complement factor 1q (C1q) and Immunoglobulin G (IgG), while allowing free transfer of glucose and insulin (Neufeld et al., 2013). The critical feature regarding the oxygen supply is the internal oxygen tank of this device (Barkai et al., 2013; Evron et al., 2018), which allows for the long-term survival of islets at high density in rat, minipig and primate models (Ludwig et al., 2010; Barkai et al., 2013; Neufeld et al., 2013) and in human trials (Ludwig et al., 2013; Carlsson et al., 2018). The device is about 6.8 cm in diameter and 1.8 cm thick. The islets inside the device are embedded in a 0.5 % high guluronic (HG) acid alginate slab of 500 µm thickness.

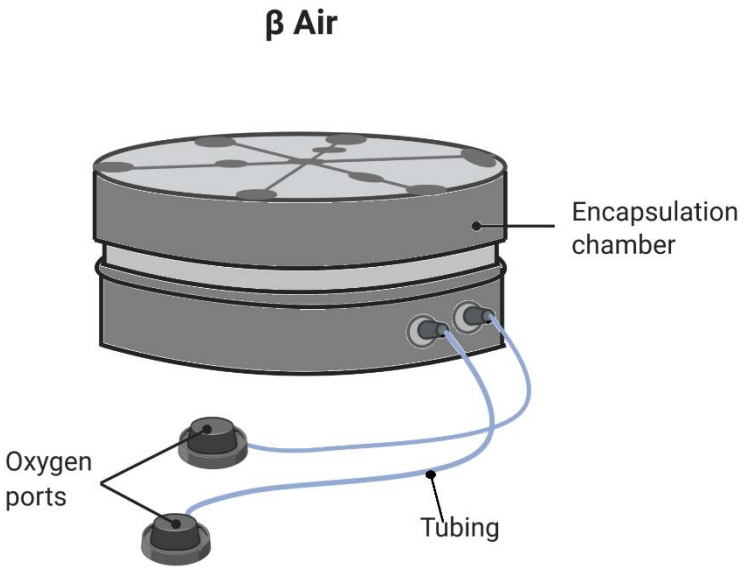

Figure 9. βAir device from BetaO_2 technologies *consisting of a hard shell encapsulation chamber and two ports for oxygen tank refilling.*

3 Macroencapsulation device requirements for micro- and macroscale architecture

3.1 Introduction

Oxygen supply is one of the main issues for viability and functionality of the encapsulated islets. In a macroencapsulation device, oxygen and other nutrients can only reach the encapsulated cells via diffusion since the inside is shielded from the outer environment by an immunoisolating membrane. The distances over which these molecules have to diffuse are determined by the arrangement and geometry of the encapsulation device and have to be kept at a minimum to ensure the sufficient supply of oxygen and nutrients to the cells.

This chapter outlines which dimensional requirements the structural and dimensional arrangement of a macroencapsulation device needs to fulfil. First, the limitation of the filling strategy of islets is recreated in a simple macroencapsulation device. Next, the design criteria for the proposed device on a micrometer scale are discussed and the modular setup of the proposed encapsulation device geometry is explained.

3.2 Fundamental requirements and general architecture of a macroencapsulation device

3.2.1 Macroencapulation device geometries

There are two main different design concepts of islet macroencapsulation devices in principle: A planar device geometry (designed as a planar diffusion chamber or simple slab) or a tubular hollow fibre membrane in which the islets are contained (Figure 10). In theory, a hollow fibre offers superior characteristics in terms of mass transfer across the membrane due to the high surface area, but is less feasible when it comes to practicability. A fibre containing sufficient islets (250 000 islet equivalents) would be approximately 1700 cm long, which is not suitable for transplantation (Colton, 2014). The most matured macroencapsulation device technologies are therefore of the planar geometry type.

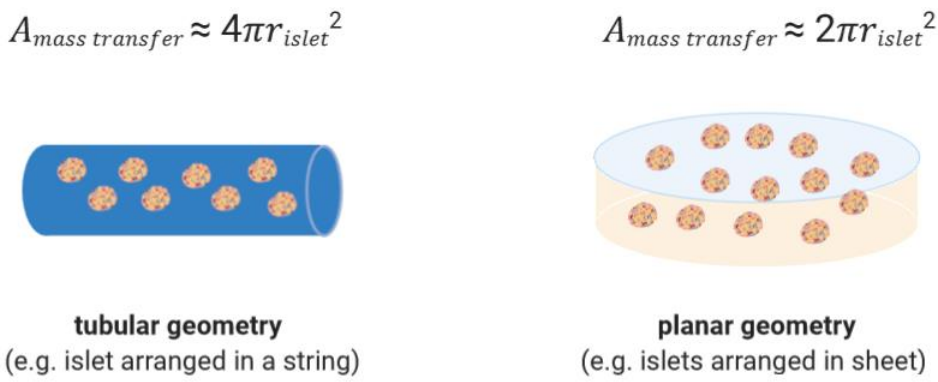

Figure 10. Planar and tubular macroencapsulation device designs *(Figure edited from Giraldo et al., 2010)*

For a functional bioartificial pancreas it is essential that the contained cells are supplied with sufficient oxygen and nutrients. The limitation of oxygen, which reaches the inside of the encapsulation device only by diffusion to the cells, is much more serious than a lack of nutrients. In contrast, very little is known about the extent to which limited transport across an immunoisolating membrane of macromolecules such as for example transferrin (carrying zinc required for insulin complexation) or the removal of waste products affects cell survival. The function of the islets is greatly reduced when the oxygen partial pressure drops, even if this has only a minor influence on the survival of the islets. For example, insulin secretion is reduced by 50% when the oxygen partial pressure drops to 27 mmHg (Dionne et al., 1993). A low oxygen concentration is therefore not able to maintain all required cell functions. Furthermore, after islet cell transplantation, about one third of the transplanted tissue is lost

due to an acute lack of oxygen. This acute oxygen deficiency cannot be reversed by revascularisation of the tissue. A macroencapsulation device must therefore serve the requirements of oxygen provision of the contained cells from the beginning on and be able to maintain a sufficient partial oxygen pressure on the long-term.

3.2.2 General basis of the design process

In this thesis, a new layout for a macroencapsulation device is going to be developed. The general approach of the technical development has been based on the proposed steps by Feldhusen and Grote (2013). This approach is generally used in the field of engineering and is structured into the following processes:

1. Specification of the needs (this chapter)
2. Creation of a functional structure and subdivision into sub-functions (last subsection of this chapter)
3. Formation, evaluation and selection of principle solution variants (conception) (Chapters 4, 5, and 6)
4. Formation, evaluation and selection of structurally concrete solution variants (implementation) (Chapters 4, 5, and 6)
5. Preparation of a final overall design of the preferred variant (chapter 7)

3.2.3 Preliminary Experiments: production and filling of a simple macro encapsulation device

One of the limitations of the previously studied islet macroencapsulation devices (chapter 2.4) is the scarcity of oxygen and nutrients, due the random arrangement of cells or islets of variable sizes in variable distance to the immunoisolating membrane. The encapsulated cells might lie in a non-suitable fashion too far away from the immunoisolating membrane. This further has an implication on the insulin response of the cells. The further the cells are away from the membrane, the longer it takes for the glucose to reach the encapsulated cells and trigger an insulin response. Likewise for the insulin secreted by the encapsulated cells, which has to diffuse out of the device and reach the capillaries. The longer the distance in between the encapsulated cells and the blood capillaries in the surrounding environment of the encapsulation device is, the longer it takes to trigger a response in the periphery.

Insertion of cells into a macroencapsulation device as described for the previously presented devices e.g. TheraCyte™, ViaCyte or Defymed (chapter 2.4) is carried out by an injection of the cells, clustered cells or islets via a filler port, which disperses the tissue randomly in

between the membrane layers. In contrast, the βAir device is filled differently as the cells are premixed with alginate and polymerised as a slab, which is then placed behind the membrane. The dispersion of the islets within the alginate hydrogel in this process is disordered as for the other encapsulation devices.

To test the feasibility of such a filling process via a port, a design of a device with a single filler port was created. Similar to the TheraCyte™ device, the device was produced by joining two layers of an expanded polytetrafluoroethylene (ePTFE) membrane around the edges by a perimeter sealing. Within the perimeter sealing ring there is an inlet port through which the islets can be injected (Figure 11).

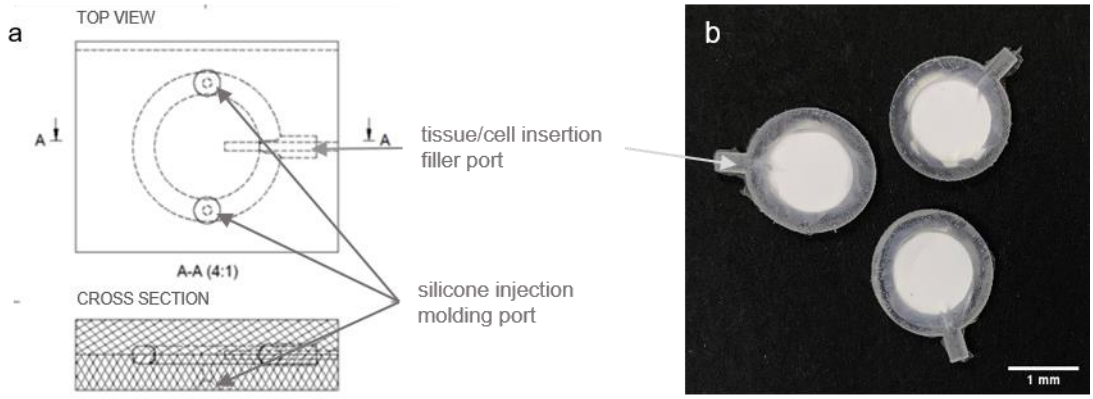

Figure 11. Simple macroencapsulation device. *Created by curing medical grade silicones in 3D printed injection moulds**. a** Technical drawing of injection mould for encapsulation device. **b** Fabricated simple macroencapsulation devices with filler port..*

In brief, the production process of the device has been performed as follows: a negative mould dividable into two components was designed by Computer-aided design (CAD) software and created by additive manufacturing techniques. In between the two mould components two membranes were fixed and a place holder was laid into the inlet port. The perimeter sealing of the two membranes was established by an injection of a medical grade silicone (MED4-4220, NuSil) via one of the two injection ports.

The injection of islets (500 rat islets) was carried out in one of two different ways: dispersed in a cell culture medium or in combination with *in situ* polymerising hydrogel precursor system. This hydrogel system consist of maleimide-functionalised heparin and thiol-terminated 4-arm polyethylene glycol (starPEG) (more details in chapter 5). The filled devices are then cultured *in vitro* for three days at 37°C in a 5% CO_2 humidified incubator. Islets encapsulated without a matrix inside the device clustered together after 3 days (Figure 12). In contrast, islets embedded in a hydrogel matrix inside the device, stayed apart from each other as their position

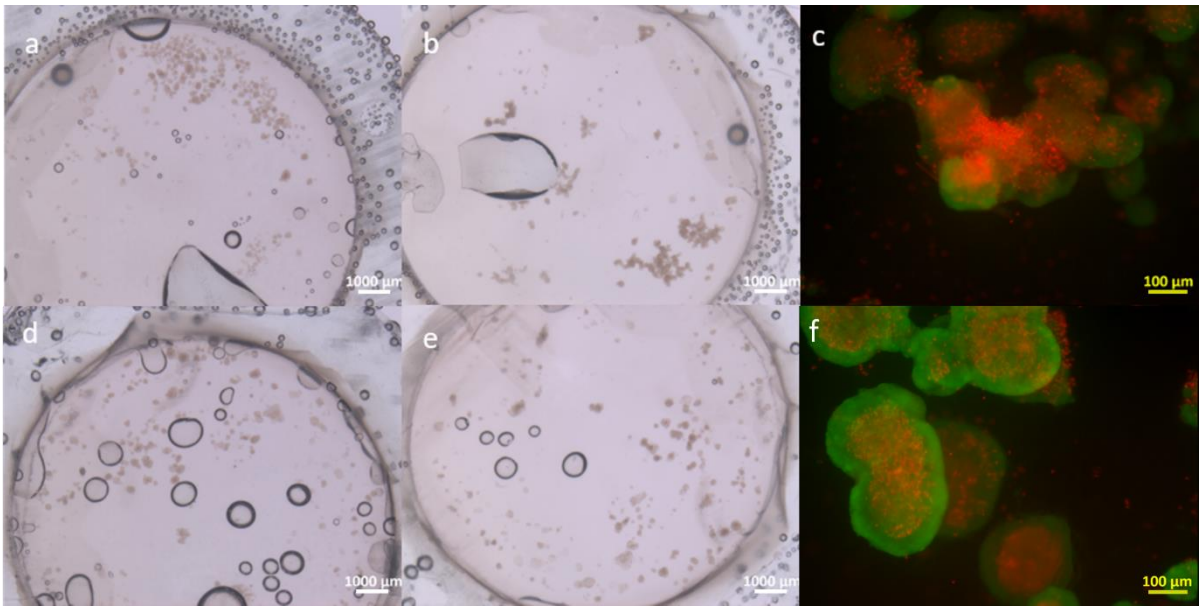

Figure 12. In vitro test of simple macroencapsulation device. a,b,c *Implants filled with 500 rat islets alone* ***a*** *at day 0,* ***b*** *day 3 and,* ***c*** *FDA-PI staining at day.* ***d,e,f*** *Implants filled with 500 rat islets and heparin-starPEG hydrogels* ***d*** *at day 0,* ***e*** *day 3 and,* ***f*** *FDA-PI staining at day 3.*

is fixed (Figure 12 d,e). A fluorescein diacetate (FDI) - propidium iodide (PI) staining, indicating the viability of the cells, showed a higher amount of dead cells within larger islet clusters.

With the aid of this simple experiment, it was possible to identify the disadvantages of a filler port design. The islets form clusters during distribution and access to the process is limited. As a result, individual islet clusters are conglomerating and forming large structures, which develop central necrosis due to limited oxygen diffusion into their core. This shows that with a filler port design it is impossible to place islets at a sufficient fixed distance from each other to prevent the formation of large islet clusters. Furthermore this experiment showed, that the fixation of the membrane around the edges only causes an unequal curvature of the membrane and places the islets at irregular distances to the membrane.

From this experiment it was concluded that the filling of a macroencapsulation device, which separates the islets from each other and arranges them into defined distances is essential for the function of the device.

3.2.4 Dimensional design criteria for development of a macroencapsulation device prototype

For the proposed design geometry in this thesis a focus has been laid onto the micro structural arrangement of islet clusters in three dimensions, which could not be achieved by the above described filling approach. This led to two design criteria: reducing the distance islets are placed apart from the next capillary in the z-dimension and finding an optimised arrangement of islets in the x- and y- dimension.

3.2.5 The distance between capillaries and encapsulated cells determines the diffusion pathway of macromolecules in the z-dimension

The distance of islets to the next blood capillary in the z-dimension determines the time signalling molecules need to be released from the implant and the availability of nutrients for the encapsulated cells. During the isolation process islets lose their vascularisation and are solely dependent on oxygen that reaches them by diffusion from the surrounding environment. Each type of encapsulation intensifies this effect, as the distance that the oxygen needs to diffuse towards the islets is increased with every layer around them. In more detail, the oxygen diffusion pathway in the setup of an encapsulation device is the following: The oxygen needs to pass from the hemoglobulin in the red blood cells through the capillary walls and the tissue in between capillary and membrane, through the immunoisolating membrane and finally through the matrix/lumen of the inside of the encapsulation device to the cells of the islets (Figure 13). The distance to be covered over all these compartments is crucial as it indicates the time the required molecules need to diffuse. Furthermore, the concentration gradient determines the local concentration at the site of the cells inside the device of the required nutrients. The higher the concentration at the outside the more nutrients reach the cells at the inside.

Diffusion is not a directed process, but depends on the random movement of molecules along a concentration gradient. The time of diffusion of a molecule grows exponentially with the

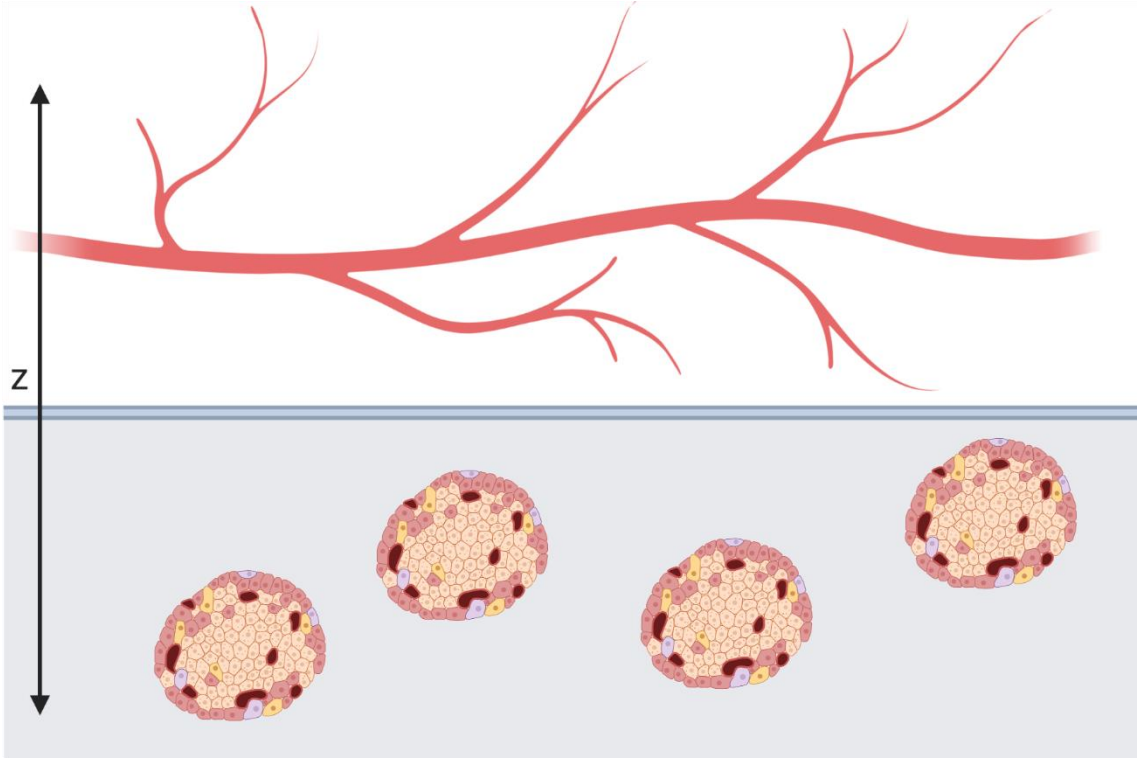

Figure 13. Diffusion pathway of oxygen, nutrients and effector molecules in the z-dimension (capillaries to cells).

distance it has to overcome. For example for 100 µm an oxygen molecule needs 2.38 s, for 200 µm an oxygen molecule already needs 9.52 s. For larger molecules like insulin this relationship is even more severe, for 100 µm an insulin molecule needs about 5.5 min, while it already takes 22.2 min to diffuse over a distance of 200 µm. A more detailed overview on diffusion times estimated from the diffusion coefficients D of relevant molecules is given in the Table 1.

Table 1. Representative diffusion times of relevant molecules based on the approximation of the diffusion time by $t \sim x^2/2D$ with $D_{Insulin} = 1.5 * 10^{-7}$ cm^2/s, $D_{Glucose} = 5 * 10^{-6}$ cm^2/s and $D_{Oxygen} = 2.1 * 10^{-5}$ cm^2/s (Aso et al., 1998; PhysiologyWeb).

	1 µm	**10 µm**	**50 µm**	**100 µm**	**150 µm**	**200 µm**	**300 µm**	**400 µm**	**500 µm**
insulin	0.033 s	3.33 s	1.38 min	5.55 min	12.5 min	22.2 min	50 min	1.48 hr	2.31 hr
glucose	0.001 s	0.1 s	2.5 s	10 s	22.5 s	40 s	1.5 min	2.67 min	4.16 min
oxygen	0.000238 s	0.0238 s	0.595 s	2.38 s	5.35 s	9.52 s	21.42 s	38.09 s	59.52 s

This requires to keep the distance a molecule has to diffuse to reach the encapsulated islets at a minimum. In healthy tissue the furthest distance of a cell towards the next capillary is about 150 – 200 µm (Barkai et al., 2016). The reduction of the diffusion distance has to be taken care of at both sides of the membrane: On the outside of the device capillaries have to develop in close proximity on the membrane with as little interfering tissue (prevention of fibrosis) as possible and on the inside of the encapsulating device the islets have to be as close to the membrane as possible.

When designing a macroencapsulation device the diffusion distance along the z-dimension needs to be reduced to a minimum. Meaning that the islets have to be in as close proximity as possible to the next blood vessels. In this way a carefully chosen design minimizing diffusion distances can support the survival of the encapsulated cells.

3.2.6 Oxygen available surface area per islet

For the geometrical design of an encapsulation device the aim is to have the smallest possible implant for the patient's comfort. When the distance of the islets towards the implant surface needs to be kept at a minimum, the islets need to be arranged in a monolayer.

In a monolayer arrangement, the mass transport of oxygen and nutrients towards the islets is only possible from the area above and/or below them. Theoretically, the oxygen can also diffuse towards the cells from the lateral dimension through the matrix, but in an encapsulation device of planar geometry there is no oxygen source in the lateral dimension. A gradient is generally established between a source and a sink. Here, the oxygen gradient therefore establishes from the implant surface, which is the oxygen source towards the oxygen consuming cells, which are the oxygen sink. The surface area above an islet therefore determines the area from which oxygen can diffuse towards the islet (oxygen diffusive area). Accordingly, the larger the distance in between two neighbouring islet is, the larger the area is from which oxygen and nutrients diffuse towards them without being consumed by the neighbouring islet. This can also be imagined as an expanding cone from the islet (Figure 14) indicating the open space for islet oxygenation above them. If the islets are placed too close to each other, this volume is decreased and the oxygen and nutrient availability is further limited by the islets next to them as these consume nutrients and oxygen as well. Therefore, for the encapsulation of islets in a monolayer in an encapsulation device that has a suitable size for implantation in humans, an optimum between minimum oxygen diffusive surface area and maximum islet number per area needs to be found.

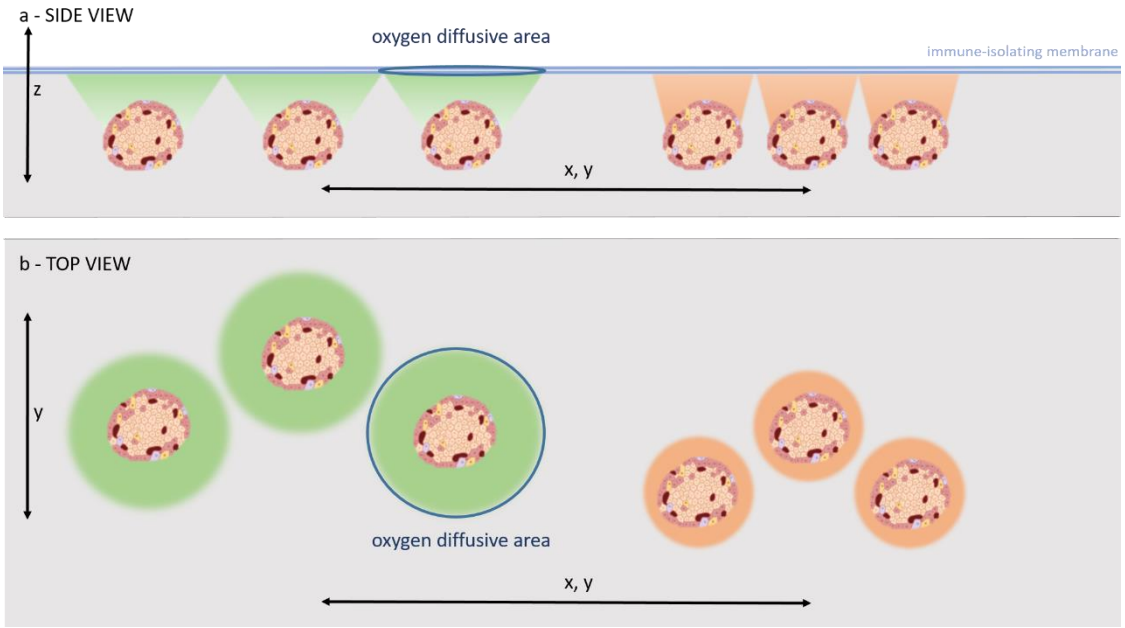

Figure 14. Oxygen diffusive surface area is dependent on the spacing of the islets in the x- and y-dimension.

3.2.7 Optimal islet arrangement derived from geometrical considerations

Insulin need depends on the size and weight of the particular organism. An encapsulation technique of cells should therefore be modular with regard to dimensions and the device surface under which the islets are placed therefore needs to be scalable.

An array of multiple repetitive units is a solution to this problem without having to adjust the single structures to each patient. The device thus needs to be planned from this single repetitive structure that can be scaled up to a higher number depending on the application.

When packing together units of identical shape and size to fill a plane, only three regular shapes can fulfil this criterion: equilateral triangles, squares and hexagons. Simplifying an islet as a sphere, the best fit of structure with the minimal empty surface area is a hexagon (Figure 15). Furthermore, from the centre of a hexagon the distance is most similar in all directions when compared to triangles or squares. This means that the deprivation from nutrients and oxygen taken from neighbouring cell clusters is the same in all directions.

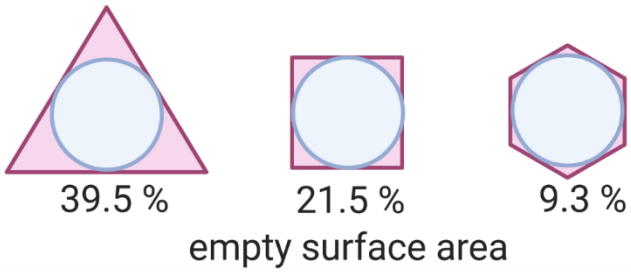

Figure 15. Packing units of identical shape that can fill a plane. *The highest packing density of circles is reached by hexagonal shape.*

For the proposed encapsulation device design, an array of hexagons was used to control the arrangement of the islets. Each islet is supposed to be placed in a microwell, which consequently defines the position of each islet. The positioning in microwells furthermore also allows arranging the islets into a monolayer. The design of this newly proposed device follows the shape of its smallest unit over multiple scales: For the next larger unit multiple hexagon microwells are framed in a larger hexagon (Figure 16). This larger hexagon unit can be repeated multiple times depending on the size of the organism. In this way, different device sizes of 2, 3, 4, 7 or more repetitive units can be designed.

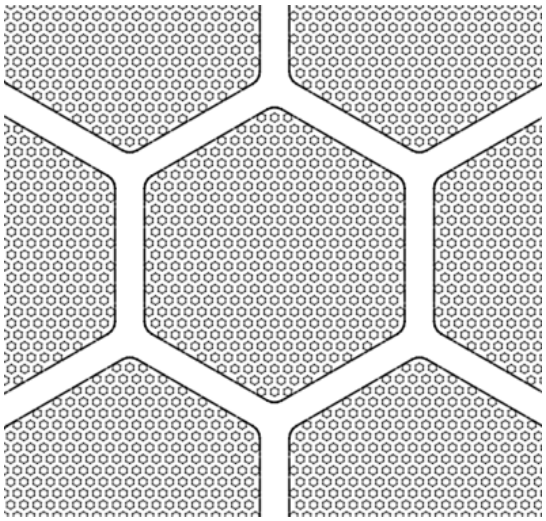

Figure 16. Microwell hexagons containing the islets arranged in larger hexagon units.

Here a design is proposed in which the islets are arranged in a regular fashion in microwells under a membrane. This gives the possibility to fix the position in a monolayer in a fixed distance to each other in the x- and y-dimension and in a fixed distance to the immunoisolating membrane, resulting in the most optimal diffusion parameters for oxygen and nutrient in the terms of the geometry. The aim is to reach a critical level of mass flow that allows the highest secretion of insulin to a given glucose stimulus per surface area.

3.2.8 Oxygen provision in the post transplantation phase

The supply of the encapsulated cells with oxygen and nutrients is strongly dependent on the availability of capillaries close to the membrane. For the creation of a device that does not need to be refilled with oxygen from external sources, the supply from the blood stream is crucial. Therefore capillaries need to grow in the close proximity of the implant. The biocompatibility of the material plays a major role here: An optimal biocompatible material has a surface that triggers the formation of capillaries and suppresses a fibrotic response.

The formation of capillaries takes a time course of several days to weeks until normoxic conditions are established in the tissue surrounding the implant. This poses a delay in oxygen provision to the encapsulated cells by the surrounding tissue. This issue of an initial lack of oxygen has been addressed in previous encapsulation approaches in different ways by e.g. a refillable oxygen tank (βAir device) or by different prevascularisation approaches (MAILPAN). Another option would be to incorporate a transient oxygen releasing material into the device that bridges the deprivation of oxygen in the tissue for the initial post implantation period (Coronel et al., 2019a). To bypass the initial lack of oxygen in this novel designed encapsulation device, the delayed vascularisation shall be bridged by an oxygen module to provide oxygen in the early post transplantation period (chapter 6).

3.3 Conceptual setup of prototype encapsulation device geometry and description of device modules

From the criteria described above four different modules were developed in this thesis, which fulfil different kind of functions and aim to arrange the islets in a suitable fashion (Figure 17).

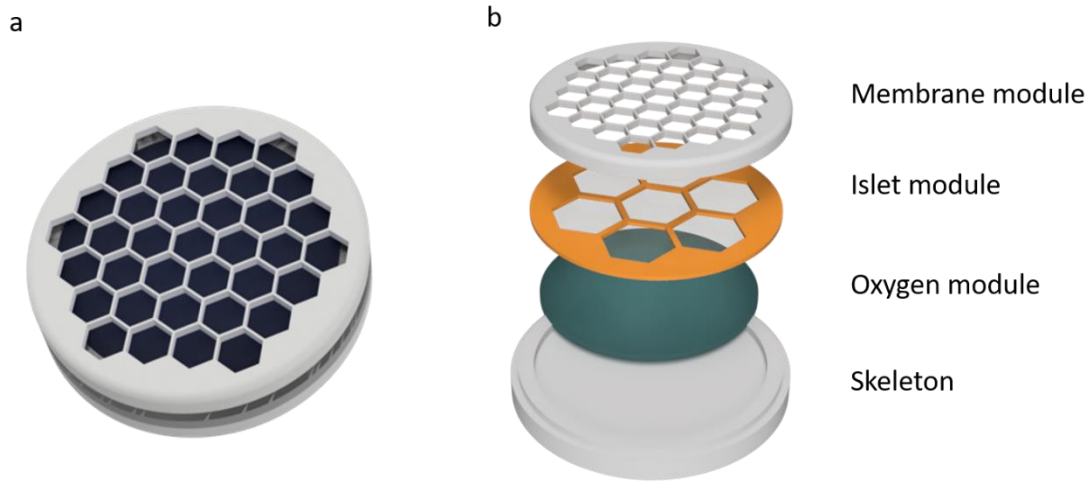

Figure 17. Conceptual setup of the prototype device geometry. a *Closed device with hexagon structure for islet arrays.* ***b*** *Exploded view of the device representing the different modules for the immunoisolating membrane, the islets, the oxygen reservoir and the skeleton.*

The first module is the skeleton giving stability to the structure. It acts as an outer housing, which connects the different functional parts of the device. Part of the skeleton functions as a holder for the second module. The membrane module as part of the rigid shell skeleton provides the stability for the 'fragile' membrane. The hard skeleton also circumvents mechanical stresses to the membrane from bending of the device during handling or after implantation.

The membrane itself, as the second module, acts as the immunoisolating barrier to the outer host tissue. In the same way as it protects the encapsulated tissue it is also the most exposed and vulnerable part of the device as it is the interface at which the islets encapsulated inside are 'connected' to the outside. For the supply of nutrients and oxygen of the cells at the inside, it is crucial that the membrane material does not trigger a strong immune response and fibrosis that blocks the membrane. Coating the membrane with different polymers and molecules can enhance biocompatibility and induce vascularisation in close proximity to the implant.

The inner core of the encapsulation device are the islets inside the islet module. This module aims to provide a comfortable environment to the islets. It mimics their physiologic environment in the pancreas. Each islets in here shall have its own diffusion open space from which it can get all nutrients and oxygen.

The last module is the oxygen module, which provides the cells/islets with oxygen right after the transplantation. In the initial phase after transplantation the outer surrounding has not yet established a passage with the surrounding tissue via blood vessels. The injured tissue, after the incision for the device has been made, is highly hypoxic and blood vessel formation has to be triggered. The healing of the resulting wound requires several days to weeks. For this period a temporally limited oxygen reservoir is the last module of the device. The oxygen in this reservoir though is not contained in a gaseous format but rather in a solid format and is hydrolysed via a reaction with water. Therefore it is important that the water can pass through the layers above or via an internal channel system in the skeleton.

The single modules are described in greater depth in the following chapters.

4 Microscale architecture of the islet module for improved oxygen availability

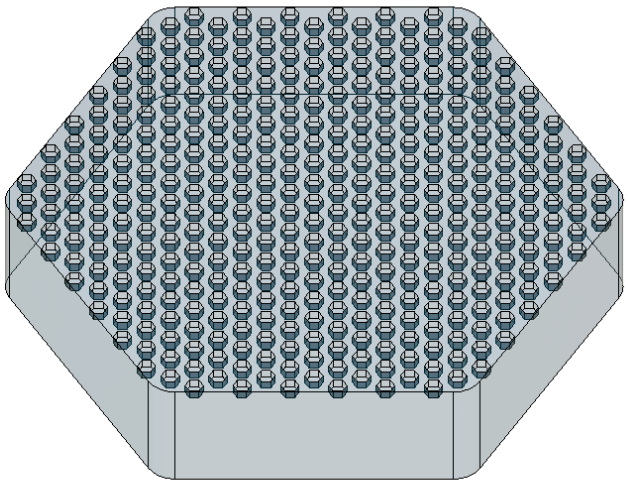

4.1 Introduction

As described above, a key requirement for a functional encapsulation device is a sufficient oxygen supply to the integrated cell graft. The structure and configuration of individual islet clusters as well as their arrangement within the islet module is thereby of crucial relevance. To support this structure and to allow a homogenous arrangement of the islets side by side in a monolayer, a hydrogel with and array of microwells plane is proposed to be used to place the islets inside the novel encapsulation device.

In this chapter a replica platform to cast microwell hydrogel arrays is created. Different methods are investigated to yield proper surface characteristics and microwell format suitable for seeding of pseudo islets. Next, data modelled on the oxygen distribution within an array of islets is extracted from literature and transferred onto potential microwell designs to give a prediction on which ones can potentially be used for tailoring the individual islet cluster and the optimal islet arrangement within the device. Finally, an experiment is proposed that investigates the optimal islet distribution and size at an oxygen pressure mimicking the *in vivo* transplant environment.

4.1.1 Tailoring of the islets: Formation of pseudo islets in microwells

The usage of intact islet clusters with minimal size distribution and high purity is of outmost importance in a macroencapsulation setting. This reduces hypoxia-mediated cell death and lowers the release of antigens that could provoke an inflammatory reaction. Especially suited to achieving optimal diffusion characteristics are smaller pancreatic islets which, due to their reduced susceptibility to ischaemia, have benefits in terms of survival and insulin secretion (Lehmann et al., 2007a; Suszynski et al., 2014; Hilderink et al., 2015). This is true across multiple species and when modelled a diameter of 100 µm was found to be optimal, based on nutrient diffusion throughout the islets and oxygen consumption rate (Figure 18). The need for oxygen is even more pronounced in macroencapsulation settings as the islet cores are at greater distances from the nearest blood vessel due to the presence of the immunoisolating membrane. Nonfunctional necrotic cells however, are unwelcome as they trigger an unwanted immune response. As further substantiated by Shizuru et al. (1985) seems to be diminished in reaggregated islet clusters.

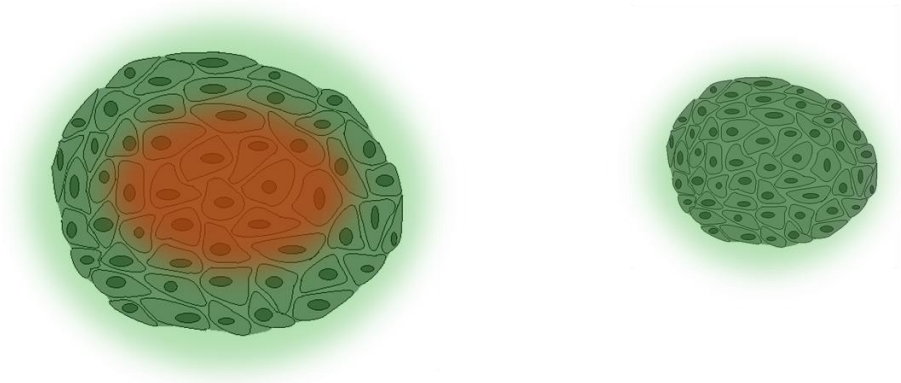

Figure 18. Large islets (>150 µm) develop a necrotic core, while small islets (<100 µm) stay viable without vascularisation as for example in an encapsulation setting.

The size of an islet can be controlled by first dissociating and then reclustering the islets as pseudo islets with a defined cell number. The successful formation of pseudo islets has been shown by different research groups before (Jun et al., 2014; Hilderink et al., 2015; Ichihara et al., 2016). The process for the generation of pseudo islets is the following: The islets are dissociated by a dissociation reagent and mechanical forces into single cells, which are then reseeded. The size of the islets can be controlled for example by seeding the cells at a certain density over a plane with microwells. Microwells are cavities in the micrometer range and can

have different shapes such as pyramidal, round bottom, or flat with sharp rim (Figure 19). The gravitational force causes the cells to fall into the microwells where the cells aggregate.

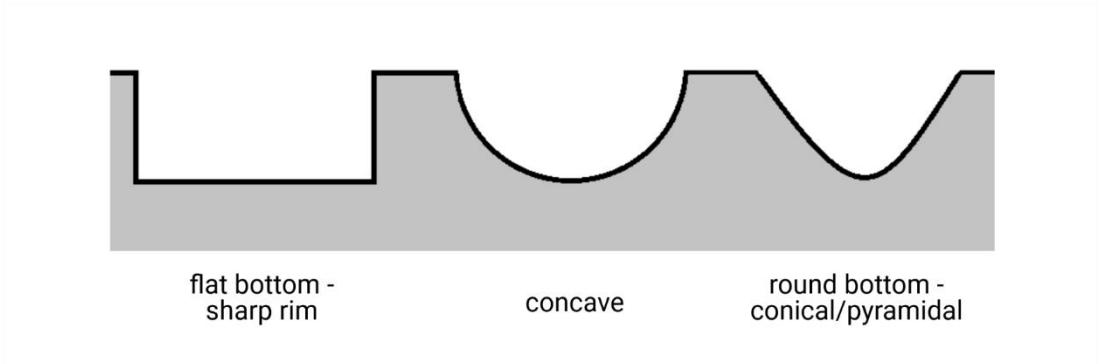

Figure 19. Shapes of microwells.

4.1.2 Available techniques for microwell production

An array of microwells is designed to place pseudo islets in arranged in a monolayer into the novel encapsulation device. For the fabrication of microwells different techniques from photo and soft lithography are available. These enable the production of high-resolution structures in large quantities. To create three-dimensional microstructures, replica moulding, embossing and solvent-assisted micromoulding techniques can be used (Qin et al., 2010).

For these techniques a pattern is created using computer aided design (CAD) software and printed as a mask (Figure 20). The pattern of the mask is projected by exposure to ultraviolet

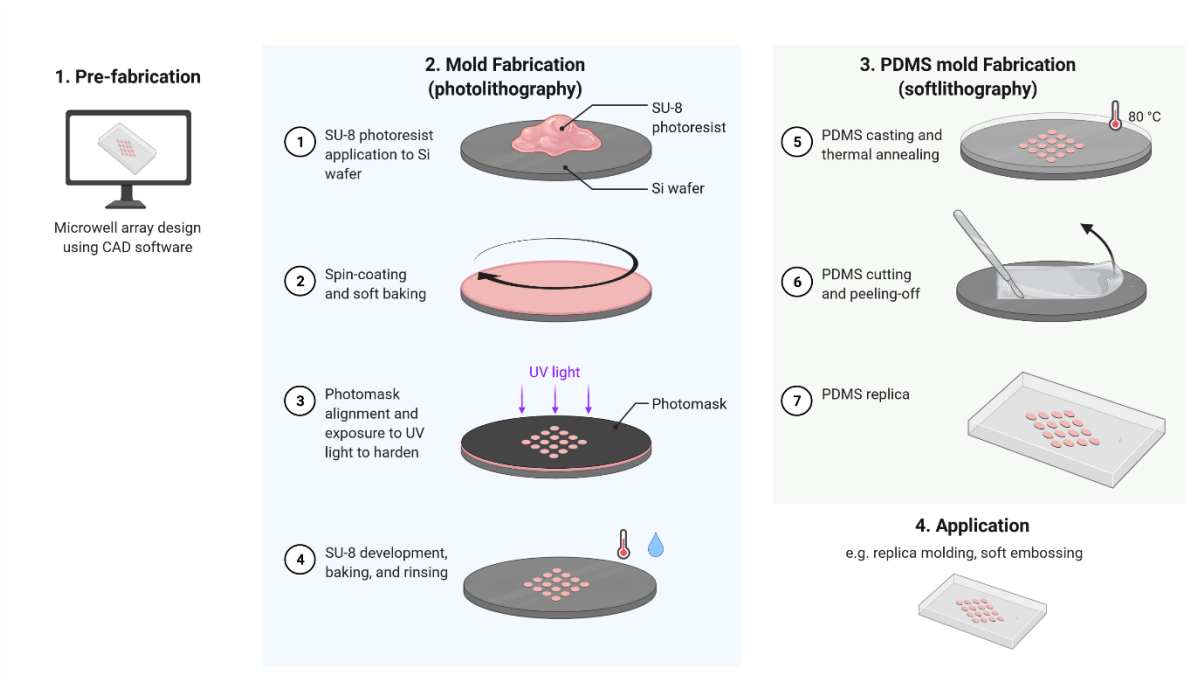

Figure 20. Photo and soft lithography processes.

(UV) light onto a wafer with a photoresist and imprinted. This master structure can then be further casted with an elastomer, usually polydimethylsiloxane (PDMS), yielding a negative structure, a process also called replica moulding. These casted PDMS structures have been used for example for soft embossing. In more detail, a substrate is filled with a hydrogel precursor solution and the pattern is embossed during the formation of the hydrogel (Kobel et al., 2009).

Another method to cast micropatterned hydrogels is solvent-assisted micromoulding. Here, a sacrificial stamp is produced from the master and a hydrogel is casted on the structure. After the gel is polymerised the stamp is dissolved from the structure (Müller et al., 2017). The advantage of this technique is that the replica can be released without any damage.

For pseudo islet formation a round bottom curvature is hypothesised to support the formation of pseudo islets the most and enhance their long-term function due to improved structural support. With the so far introduced photo- and soft lithography methods, flat bottom structures with a sharp rim can be produced easily, but creating round structures with photo lithography techniques is more challenging. Methods to produce round structures at microscale resolution are processes like deep reactive ion etching, nickel electroforming and sputtering (Park and Park, 2019). The methods are generally referred to as microelectromechanical Systems (MEMS) lithography, but unfortunately require advanced equipment and are relatively cumbersome.

Alternative methods to prepare arrays of rounded microwells by soft lithography techniques have been developed. For example, after casting a microwell structure, PDMS was given into the wells and raked out from the wells again (Lee et al., 2016). Another soft lithography method to produce round structures has been developed by the application of a vacuum pump (Jun et al., 2014). Here, an array of concave microwells was produced by pulling a foil through the holes of a sieve-like structure and casting a layer of PDMS on top of it.

A straight forward approach of creating microstructures is using additive manufacturing techniques as for example stereo lithography (SLA) printing. Various 3D printers exist on the market with high resolution options of a few µm per pixel. 3D structures are produced by exposing a photo-crosslinkable resin to different projected patterns in thin layers which are deposited on top of each other. This method is simple in its application and used to produce structures of nearly any design.

4.1.3 Required properties of microwells for pseudo islet formation

Different factors must be taken into account for the application of microwells within an encapsulation device.

- The method of microwell array production must be scalable up to the clinical needs. The production method therefore needs to be fast and reproducible and the material must be easily available in large quantities.
- The structures must be sterilisable during the production process.
- For application in the proposed modular encapsulation device, the material needs to be water permeable as the oxygen module below the islet module requires water for oxygen production.
- The material used must be non-toxic to the cells, durable, favourably be soft and of low swelling characteristics to avoid a change of dimensions of the wells.

4.1.4 Materials for pseudo islet microwell array

In their physiologic niche islets are embedded within an ECM providing the cells with structural, physical and chemical cues. In the field of tissue engineering this ECM is often mimicked by hydrogels. They consist of a network of polymers with hydrophilic functional groups, which can absorb large amounts of water, while the interchain crosslinks resist dissolution. The absorbed water allows free diffusion of solute molecules within the network and the polymers provide a three-dimensional matrix giving structural support for the integrity of cell clusters. Thus, a hydrogel matrix within the encapsulation device could provide a comfortable environment for functional long-term survival of the islets.

As hydrogels are able to take up water due to their hydrophilic nature, this consequentially has the effect that hydrogels have the property to swell. The degree of swelling is dependent on different factors such as the crosslinking degree, charge of the polymers, and the efficiency of the crosslinking reaction. For the application within an encapsulation device though, it is important to have a matrix, which is fixed in its geometry as the space is restricted by the skeleton of the device and the microwell size and distance is optimised to support sufficient diffusion of oxygen to the cells.

Commercially manufactured microwell-culture plates are available, though the problem of these is that the geometry is fixed and they are not designed to be placed inside an encapsulation device. These have a low packaging density of islets with wells of about 400 to 500 µm as for example Sphericalplate 5D® (Kugelmeiers Ltd., Switzerland) or AggreWell™ Microwell Plates (STEMCELL Technologies™, Canada).

Further materials have been used for the creation of microwells. For example polyethylene glycol (PEG) has been crosslinked on PDMS stamps to produce 75 µm small microwells for retinal organoid culture. The relatively high shear modulus G' of ~ 20 kPa for hydrogels with a solid content of 7.5 % (v/w) allowed to remove the stamp without damage to the microwells (Decembrini et al., 2020). For extra small sized wells of 3 µm, biohybrid glycosaminoglycan (GAG)-PEG hydrogels have been imprinted by a polystyrene stamp, which has been dissolved after the embossing step (Müller et al., 2017). Furthermore, a commonly used material for pseudo islet formation is agarose. It has the advantage, that it is a soft material and relatively easily cross linkable: agarose can be dissolved in a buffer by a short heating process in a microwave oven and forms a gel when cooled down again. For the moulding of microwells it can be poured on a mould and after cooling down for a few minutes it can be removed and a patterned gel can be yielded (Hilderink et al., 2015; Mirab et al., 2019). Also PDMS has been used as a basis for microwell culture. For example, Jun et al., (2014) cultured pseudo islets on concave PDMS microwells or Rojas-Canales et al., (2018) used a microwell based platform fabricated from PDMS for shipment of islets.

In conclusion, various materials have been used for the fabrication of microwells including glas, polystyrene culture plates, PDMS, PEG and, biohybrid PEG hydrogels, agarose and many more. For the following investigations a focus is put on agarose and PDMS as these are fulfilling the requirements of being clinically scalable, sterilisable and additionally have advanced properties due to their simplicity of their crosslinking and low swelling characteristics.

4.1.5 Oxygen distribution within islets

Komatsu et al. (2017) investigated the viability of islets in regard to size and oxygen tension in culture media. Therefore, they cultured human islets at 100, 160, 270 and 360 mm Hg oxygen tension (10, 21, 35, and 50 % oxygen environment, respectively) and analysed for viability. The *in vitro* data showed that smaller islets have a smaller area of dead cells in the centre compared to larger ones and the extent of cell death is directly related to the oxygenation status Based upon these findings, the authors developed a model to predict the oxygen concentration within an islet according to the cell number and the oxygen consumption rate (OCR) of a single cell.

Johnson et al. (2009) created a model of encapsulated islets in alginate spheres and slabs, which was utilised to determine the effect of the islet distribution, different islet sizes, and total amount of islets equivalents on oxygenation. Permeability of the encapsulation material for oxygen and the oxygen consumption rate of the islet tissue was taken into account. The model describes the gradient of partial oxygen pressure inside the islets and the surrounding matrix in a 500 µm thick alginate slab whereat a physiological tissue oxygen pressure of 40 mm Hg

was set at the outside of the encapsulating matrix (Figure 21). Furthermore, the model includes an estimation of the fractional insulin secretion rate and islet/tissue viability in dependence of the partial oxygen pressure. The fractional viability of the tissue is defined as:

$$\text{Fractional viability} = \frac{V_{\text{viable}}}{V_{\text{tissue}}}$$

Where the volume of viable tissue (V_{viable}) is the tissue fraction where the partial oxygen pressure (pO_2) is > 0.1 mm Hg and V_{tissue} is the total encapsulated tissue volume. The fraction (F_1) of normal second-phase insulin secretion rate is

$$F_1 = \frac{pO_2}{5.1} \quad \text{for } pO_2 < 5.1 \text{ mmHg}$$

and

$$F_1 = 1 \quad \text{for } pO_2 \geq 5.1 \text{ mmHg}$$

Along the cross-sectional area a decrease of partial oxygen pressure (pO_2) in dependence of the islets size and distance of the islets to the surface can be seen (Figure 21). For the planar slab configuration in which islets are positioned in the middle of a 500 µm thick slab at a density of 500 IEQ/cm^2 (Figure 21 A), the model predicts a lower oxygen availability at the centre of the spheres, which becomes more severe with increasing tissue size. At higher density of 2000 IEQ/cm^2 the single tissue units are packed closer together, which increases the hypoxic region

Figure 21

Please refer this figure from the original publication:

Amy S. Johnson, Robert J. Fisher, Gordon C. Weir, Clark K. Colton,

Oxygen consumption and diffusion in assemblages of respiring spheres: Performance enhancement of a bioartificial pancreas,

Chemical Engineering Science,

Volume 64, Issue 22, **Figure 8,**

2009,

Pages 4470-4487,

ISSN 0009-2509,

https://doi.org/10.1016/j.ces.2009.06.028.

in the centre of the islets (Figure 21 B). Furthermore, estimations of the fractional viability and fraction of normal insulin secretion rate can be made for different islet configurations in a slab of 500 µm thickness. For smaller spheres of 50 µm in a monolayer, the maximum packaging density is limited to 1400 IEQ/cm^2 while for larger 150 µm sized spheres packed side by side, the maximum is 4400 IEQ/cm^2. The model predicts that for a 150 µm, 125 µm, 100 µm and 75 µm islet sphere the whole islet is viable until about 500 IEQ/cm^2, 1200 IEQ/cm^2, 1500 IEQ/cm^2 and 1800 IEQ/cm^2, respectively. The fraction of normal insulin secretion is not reached for 150 µm islets or until 500 IEQ/cm^2, 1000 IEQ/cm^2 and 1300 IEQ/cm^2 for the other islet sizes respectively. Related to centre to centre spacing of the islets the fractional viability of 100 % is possible until 3 times, 2 times, 1.4 times, and 1 time the islet size (Figure 22, Table 2).

Table 2. Maximal packaging and pitch depending on islet size (rounded values). Data extracted from Johnson et al. 2009.

Islet size	***50 µm***	***75 µm***	***100 µm***	***125 µm***	***150 µm***
Maximum possible packaging density (IEQ/cm^2)	1400	2100	2800	3500	4400
100% viability till packaging density of … IEQ/cm^2	1400	1900	1500	1000	300
100% fractional insulin secretion till packaging density of … IEQ/cm^2	1400	1200	1000	500	not reached
Centre to centre spacing (pitch) of islets at 100% fractional insulin secretion	1	1.3	1.7	2.7	Not reached

Figure 22

Please refer this figure from the original publication:

Amy S. Johnson, Robert J. Fisher, Gordon C. Weir, Clark K. Colton,

Oxygen consumption and diffusion in assemblages of respiring spheres: Performance enhancement of a bioartificial pancreas,

Chemical Engineering Science,

Volume 64, Issue 22, **Figure 11,**

2009,

Pages 4470-4487,

ISSN 0009-2509,

https://doi.org/10.1016/j.ces.2009.06.028.

In conclusion, though smaller islets have a lower maximum packaging density (IEQ/cm^2) due to their smaller geometry, they have a higher viability and function at higher packaging densities than larger islets at the same packaging density. Similar results have been shown in the model for small islet spheres packed in multiple layers, which allow to reach even higher packing densities until about 3000 IEQ/cm^2. A further effect of smaller islets has been predicted: smaller spheres with a size of 37.5 µm at 1000 IEQ/cm^2 remain functional till a lowering of the surface oxygen to 17.5 mm Hg. Last but not least, Johnson et al. (2009) showed how the thickness of the slab relates to the function of the islets. A thinner slab thickness of 250 µm was able to keep 50 µm aggregates functional until a packing density of 4000 IEQ/cm^2.

The authors conclude that the oxygen availability to the islets is determined by the tissue sphere diameter, the distance in between the tissue spheres, and the encapsulant external surface oxygen concentration. When taking these model predictions into account for the encapsulation inside the proposed encapsulation device these parameters have the following implications for the design of the arrangement of islets in the islet module:

1. Preferably small pseudo islets clusters (50 µm and 75 µm) need to be chosen as these have the highest viability and function at the highest packaging density (Table 2, row 2 and 3)
2. The distance of the islets towards the membrane needs to be as small as possible as a thinner slab thickness allows higher packaging density of islets.
3. The centre to centre spacing of the islets and therefore the microwells gives a minimal required spacing of the microwells depending on the chosen islet size for the design of the islet array arrangement (Table 2, row 4).
4. The islet loading of the encapsulation device can further be increased by packaging multiple layers of smaller islets.

4.2 Methods

4.2.1 Microwell mould design and production by additive manufacturing

Microwell structures were designed by CAD software taking into account the resolution of the LED projector. The size of a single pixel is 27 x 27 μm^2. To yield the highest accuracy, pillars were designed in a way that they have a size and distance of multiple pixels. The files were exported in standard triangle language file format at a high resolution setting. Support structures were introduced by COMPOSER software and the designed structures were printed on an ASIGA MAX X27 stereo lithography printer with 385 nm LED (ASIGA, Australia). For printing of microstructures R11 resin (EnvisionTec, Germany) with the highest resolution of 10 µm in the z-axis was applied. For printing of moulds for the agarose replica platform, ClearImpact (Liqcreate, The Netherlands) was used with a slice thickness of 25 µm or 50 µm.

4.2.2 Microwell mould design and production by photo and soft lithography

The following protocol was developed in collaboration with the microstructure facility at the Center for Molecular and Cellular Bioengineering, TU Dresden, Dresden. A photomask was designed containing patters of hexagons with a width of 100 µm to 500 µm and 25 µm to 500 µm distance in between the hexagons. The pattern was developed by standard photo lithography techniques onto a wafer. A negative of the wafer was replicated with PDMS (Sylgard® 184, Dow Corning, USA) by mixing base and curing agent at a ratio of 10:1 creating microwells with planar bottom.

First, a modified protocol of Lee et al. (2016) was used to create structures with round bottom. was used (Figure 23). The microwells were either filled with PDMS and pressure skimmed or filled with the printer by dropping PDMS into the wells. To resolve this pattern into a hydrogel scaffold multiple further replica moulding steps were introduced. Between each moulding step with another layer of PDMS the negative structure was treated with plasma and incubated with 2 % sodium dodecyl sulphate (SDS) solution in MilliQ water for 30 minutes. Afterwards the surface was blow dried with pressured air and a thin layer of PDMS was added and degassed in vacuum to release gas bubbles trapped in the microstructures. After this step a thicker layer of PDMS was added and again degassed. The PDMS was polymerised for at least 1 hour at 120°C and separated from each other again resulting in a structure with pillars rounded at the top. To round off the planes a thin layer of PDMS was deposited again in between the pillars and polymerised as stated before.

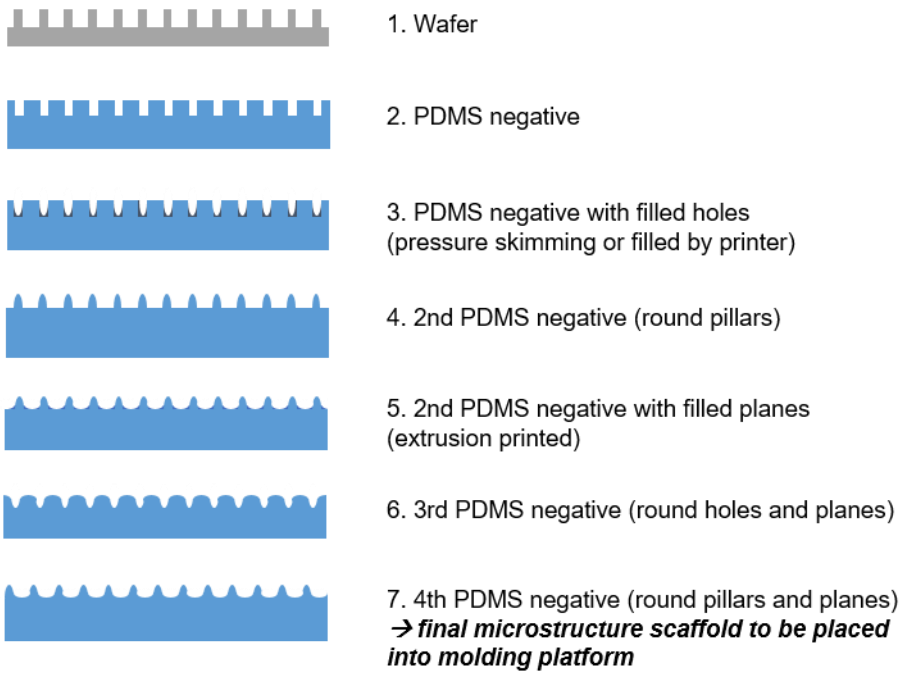

Figure 23. Production of rounded microwells by pressure skimming or deposition of PDMS droplets by printer.

The second method investigated was the dipping method: For this method the microwells are not filled, but replicated again. Instead of SDS for the release of PDMS from PDMS, the PDMS microwells were incubated in dish washing soap (1:28). The resulting positive with pillars was then dipped into a thin layer of PDMS to round of the planes and cured as described before (Figure 24).

The microstructures prepared by the above methods were then placed into a 3D printed mould (Figure 27) and replicated with PDMS again to yield a mould that creates walls around the plane. The final moulding step was done with ultra pure low melting agarose (Sigma-Aldrich,

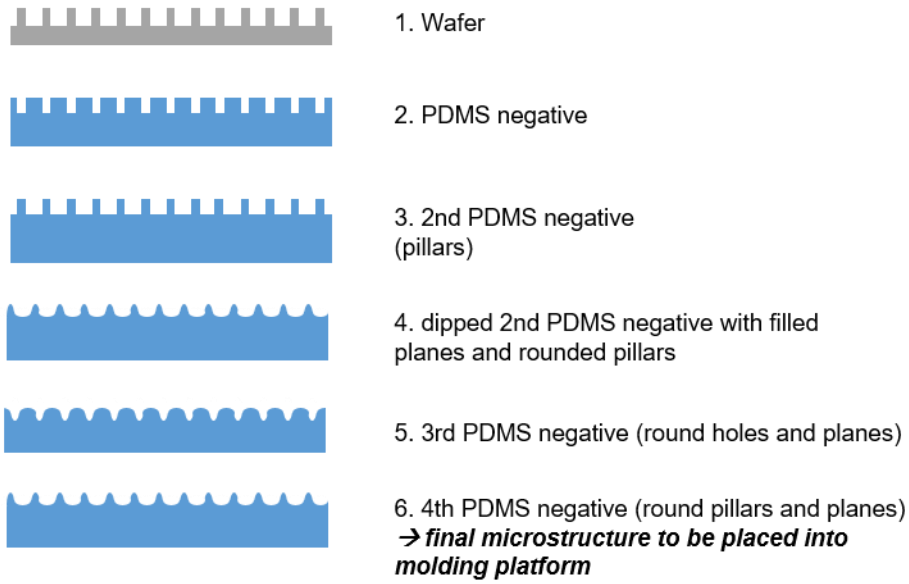

Figure 24. Production of rounded microwells by dipping method.

USA). 2 % agarose in phosphate buffered saline (PBS) was heated in the microwave at 700 W until all particles were dissolved, pipetted onto the PDMS mould and cooled down at 4°C. The agarose microwells were immersed in a thin layer of RPMI (Roswell Park Memorial Institute) 1640 cell culture medium in a cell culture dish and sterilised under a UV lamp for 30 min.

4.2.3 Islet graft preparation: islet isolation and pseudo islet production

Female Wistar rats (Charles River Laboratories, Germany) were sacrificed at 8 to 12 weeks of age. The abdomen of the rats was opened and 10 ml collagenase solution containing 1 mg/ml collagenase (Sigma-Aldrich, USA) and 1 µl DNase I (Sigma-Aldrich, USA; dissolved at 100 mg/ml) per ml in RPMI 1640 w/o glucose (Gibco, Thermo Fisher Scientific, USA) per rat was infused into the pancreas. The pancreas was taken out and digested by the infused collagenase at 37 °C for 12 minutes. The digestion was stopped with islet washing buffer (RPMI 1640, 5.5 mM, 10 % fetal bovine serum (FBS)). After the digestion, the tissue was additionally homogenised by pipetting up and down with a serological pipet and by passing the tissue through a sieve. The digested pancreata were spinned down by centrifugation for 1 minute at 277 x g and the supernatant was discarded. The pellet was resuspended in washing buffer and the washing step was repeated another time. To purify the islets, the pellet was mixed with Ficoll (Sigma-Aldrich, USA) dissolved in Euro Collins Glucose solution (Corning) with a density of 1.125 g/cm^3 and overlaid with Ficoll of the densities 1.096 g/cm^3, 1.08 g/cm^3 and 1.069 g/cm^3 and centrifuged at 4°C for 15 minutes at 1590 x g with reduced acceleration and deceleration. The islets concentrated in between the layers of different densities were collected. The Ficoll was removed with two additional washing steps and the islets were cultured overnight in islet medium (RPMI 1640, 5.5 mM glucose, 10% FBS, 20 mM HEPES, 5% penicillin/streptomycin) before further processing.

Islets were centrifuged at 300 x g for 4 minutes, medium was removed and islets were resuspended in 50 ml PBS. Islets were centrifuged at 300 x g for 2 min for a second wash step with 15 ml PBS and spun down again at 300 x g for 2 min. PBS was exchanged by 1.5 ml cell dissociation solution non-enzymatic 1x (Sigma-Aldrich, USA) mixed 1:1 (v/v) with TripLE Express (Thermo Fisher Scientific, USA). The cell solution was incubated at 37°C and after 4 to 6 minutes islet cluster dissociation was supported by mechanical disruption via gentle pipetting. After 10 to 12 minutes, cell dissociation was stopped by dilution with 15 ml complete medium. Cell solution was spun down at 300 g for 2 minutes, decanted and replaced with fresh complete media. After a final centrifugation step the cells were resuspended in 1 ml and counted. The single cell solution was diluted to the required concentration and carefully given on the microwell scaffolds. Cells were allowed to settle on the microwell scaffold by gravity for

15 minutes and placed in a humidified incubator with 5% CO_2. The medium was exchanged every second day.

4.2.4 Scanning electron microscopy and light microscopy of microwells and islets

To visualise the hydrogel array replica platforms scanning electron microscopy (SEM) was executed. Samples were stuck onto SEM sample holders (PLANO GmbH, Germany) by conducting carbon pads (PLANO GmbH). The samples were sputter coated in a BAL-TEC sputter coater for 40 s at 40 mA to deposit a gold layer of about 10 nm and visualised by a Quattro S environmental scanning electron microscope (ESEM) (Thermo Fisher Scientific) with a secondary electron (SE) detector.

Microwell hydrogel arrays filled with islet cells were imaged by light microscopy with an Olympus IX73.

4.3 Results

To place the islets in an optimised oxygen diffusion arrangement inside the encapsulation device. Pseudo islets shall be seeded and aggregate in a microwell hydrogel array, which is placed directly into the encapsulation device within the islet holder.

This microwell hydrogel array needs to be produced multiple times for each encapsulation device. A favourable method to repeatedly obtain the same microstructure with little time consumption is replica moulding. The results section investigates first, how microstructure scaffolds with suitable surface characteristics can be produced and how a replica mould can be created from these. A wafer mask is designed to produce a set of microwell arrays of different width and distance, and an optimised oxygen diffusion arrangement is theoretically investigated.

4.3.1 Production of a hydrogel array replica mould by additive manufacturing (direct production method)

Additive manufacturing offers a fast way to produce microstructures. To assess whether structures printed by additive manufacturing techniques can be used as a hydrogel array, replica platform to mould microwell hydrogel arrays from agarose. Therefore negative structures of microwells (hence pillars) were printed.

The printer system ASIGA MAX 27 utilises a LED source and a DLP projector with a pixel size of 27 µm. This system can resolve features at the microscale at about four times the pixel size and the highest resolution can be reached, when the borders of the structure align with the pixel on the screen of the printer. Following these two design criteria to yield the highest resolution, micrometer-sized pillars were drawn by CAD at multiples of the pixel size of the printer (Figure 25 b) and aligned in such a way, that the borders of the structures matched the position of the pixels of the projector.

Confocal light scattering revealed the surface characteristics of the microstructures printed with R11 resin. Similar to the structure originally designed (Figure 25 a, c), pillars were defined as singular structures arising from the horizontal plane (Figure 25 d). Analysis of the profiles revealed that the width of the structure is 71.6 % to 85.6 % smaller than the original design. The pillar height was 93.5 % to 96.3 % of the original.

a

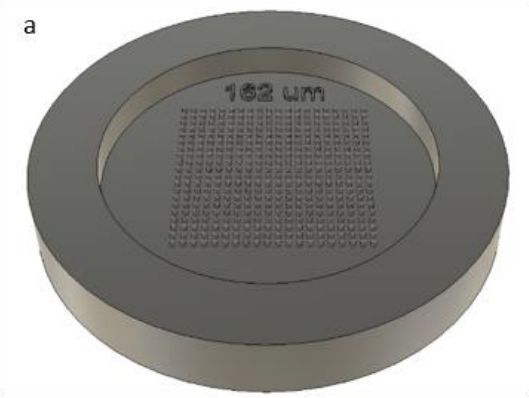

b

width in µm	width in pixels	height in µm
108	4	154
162	6	181
216	8	208

c

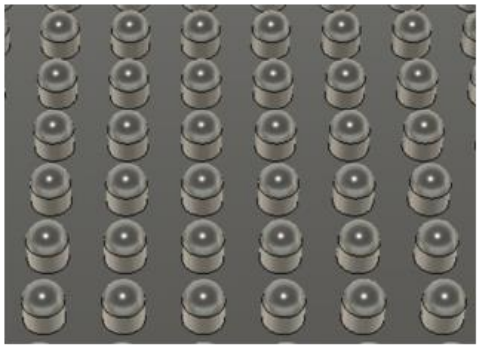

d

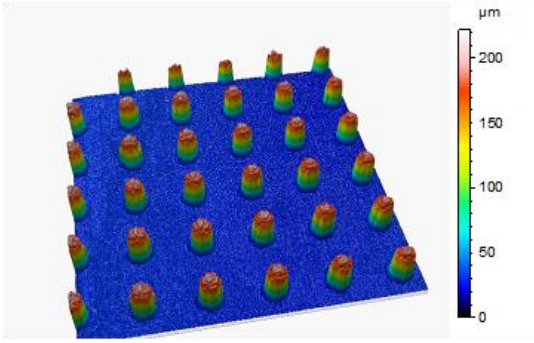

e

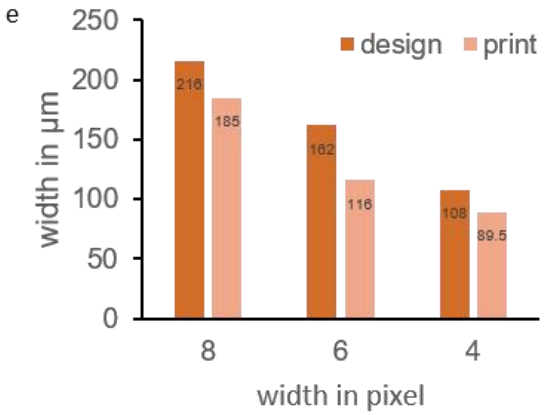

f

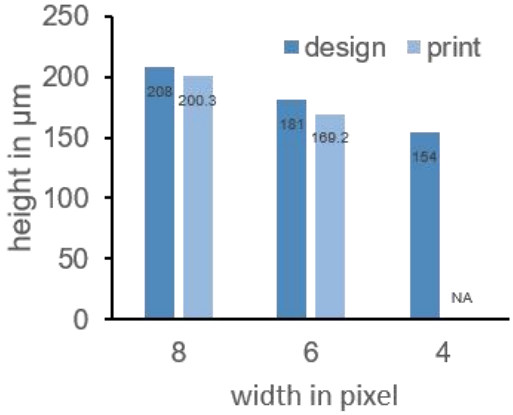

Figure 25. Evaluation of micropillar structures produced by stereo lithography printing. a *CAD drawing of designed structure.* ***b*** *Dimensions of pillars.* ***c*** *Detail of CAD structure.* ***d*** *Surface view of confocal light scattering analysis.* ***e*** *Measured width of printed pillars and designed pillars.* ***f*** *Measured height of printed pillars and designed pillars.*

Finally, the printed structures were used as a negative stamp to mould 2 % agarose hydrogels with microwells. Gel release from the printed structures was not possible without destroying the microscale structures. The gels stuck to the mould and had to be removed with a spatula which caused unwanted indentations on the hydrogel. From this experience a microwell hydrogel array replica platform, allowing the gels to be taken from the mould without additional tools, was developed. This is described in the following section.

4.3.2 Production of a microwell array replica platform for generation of microwell hydrogel arrays for *in vitro* cell culture and inside the encapsulation device

To circumvent the problem of the release of a soft material as mentioned in the section above, a hydrogel array replica platform is produced from PDMS, which can then be bent to release the microwell hydrogel array produced from agarose similar to MicroTissues® 3D Petri Dish® micromoulds (Sigma-Aldrich, USA).

For *in vitro* pseudo islets experiments and the later application within an encapsulation device, two different formats of agarose microwells are required. For *in vitro* cell culture it is handy to have a frame around the array of microwells, allowing to seed cells on top of the microwells and preventing cell suspension flowing off the structure. For loading the islets into the encapsulation device, the microwell hydrogel arrays shall be placed directly inside the encapsulation apparatus within the islet holder. There, a removable funnel acts as a frame to prevent cell suspension from flowing off the structure. For this application it is important to have a mould, tuneable in height, to achieve an exact cell placement in the z-dimension.

Two different structures were 3D printed in ClearImpact resin to create replica platforms for the production of framed and unframed hydrogel arrays (Figure 26 and Figure 27). In a second step these structures were cast with PDMS yielding a hydrogel array replica platform, from which even soft hydrogels can easily be removed by gently bending the PDMS and popping out the hydrogel. The indentations in the 3D printed structure (indicated by orange arrows) can

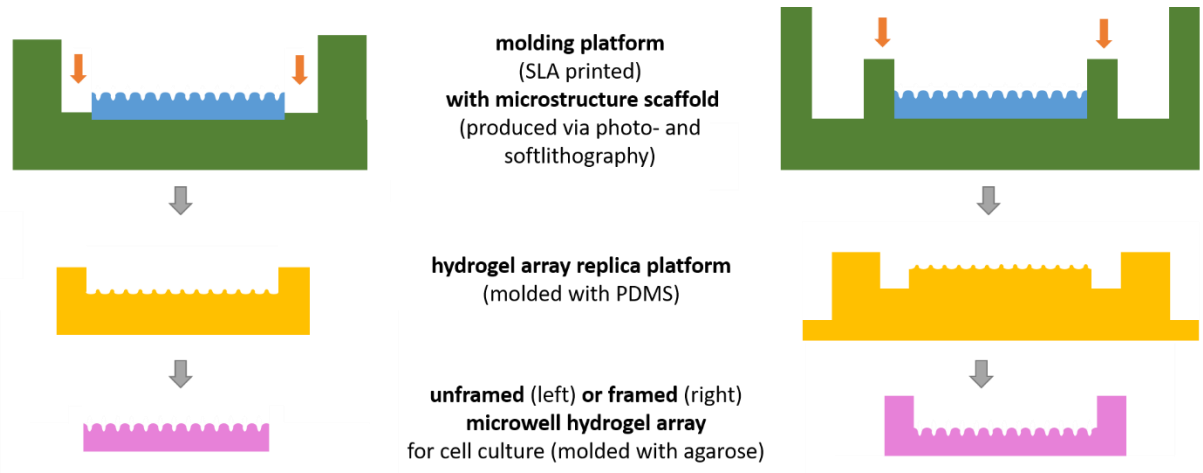

Figure 26. Schematic production of hydrogel array replica platform for framed (right) and unframed (left) microwell hydrogel arrays. *Microstructure scaffolds (blue) are either printed inside the moulding platform directly or produced by photo and soft lithography techniques and placed manually into the printed moulding platforms. By moulding with PDMS hydrogel array replica platforms (yellow) are produced. These structures are used as negative moulds for repetitive production of microwell hydrogel arrays with agarose (pink).*

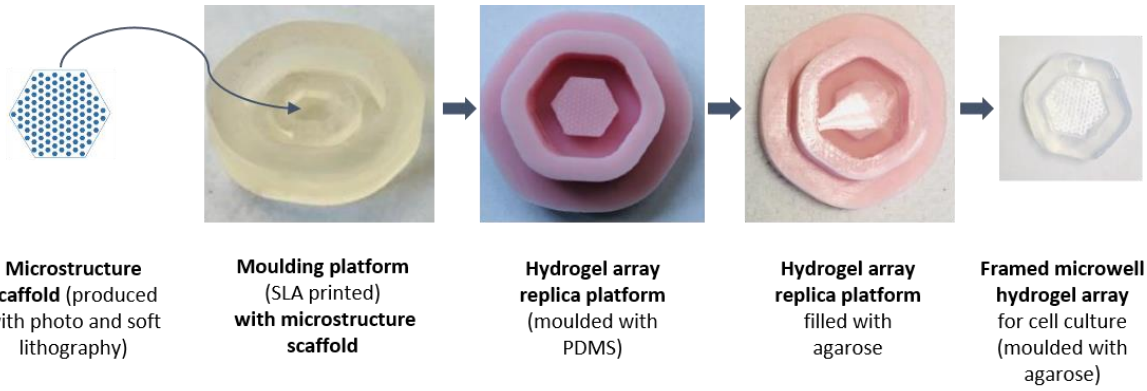

Figure 27. Production of hydrogel array replica platform for framed microwell hydrogel arrays (photographs).

easily be redesigned and reprinted to obtain an exact placement in the z-dimension inside the encapsulation device.

Different fabrication techniques were investigated for the microstructured region in the centre of the hydrogel array replica platform, which are described in the following sections. The microstructure scaffolds were either printed directly onto the moulding platform or produced by photo and soft lithography techniques and then placed manually into the moulding platform. These structured surfaces can then be placed inside the printed platform and replicated by PDMS. This way different array arrangements can be applied to the moulding process. The development process for these microstructures is explained in the following subsections.

4.3.3 Production of microstructure scaffolds by additive manufacturing

A microstructure scaffold with 400 µm sized microwells was designed by CAD software and 3D printed. Scanning electron microscopy revealed a layered and rough structure (Figure 28). The layers can be explained by the fabrication method of the 3D printer. This method includes the photocrosslinking of thin layers of resin on top of each other. The roughness corresponds to the 27 µm pixel size of the printer. The microwells did not appear to be smooth enough for

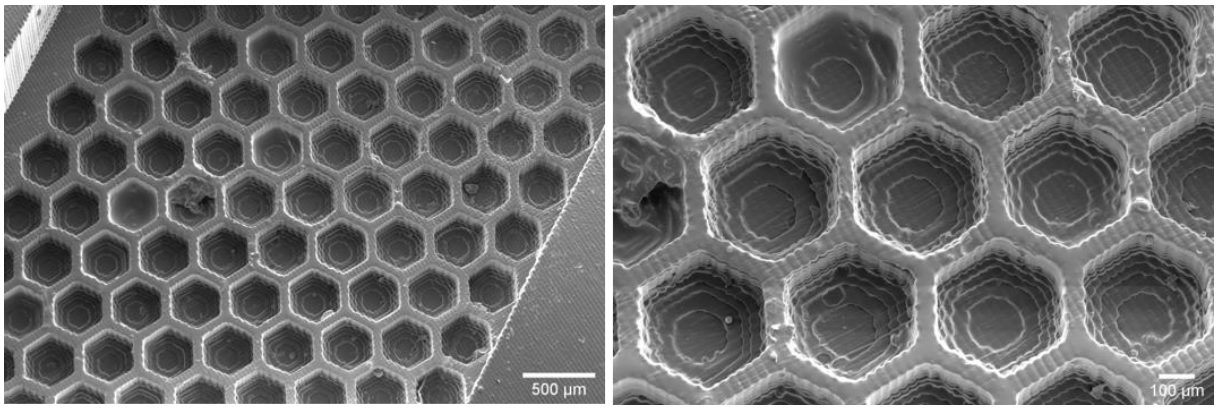

Figure 28. Scanning electron microscopy of stereo lithography printed microwells with 400 µm width.

further fabrication of cell culture microwell arrays and therefore this method was not further investigated.

4.3.4 Production of microstructure scaffolds by photo and soft lithography techniques

As an alternative method to additive manufacturing of microstructures, microstructure scaffolds for placement inside the printed moulding platform were produced by photo and soft lithography.

To investigate whether the simplest way to produce microwells is by moulding a PDMS replica (micro structure scaffold) from a microstructured wafer without any further modifications (Figure 29 a, b) and processing it by the methods described above into a microwell hydrogel array. This delivers microwells with flat bottom, sharp rims and flat planes in between the microwells. In an initial experiment, single islet cells were seeded on these microwell hydrogel arrays and left for aggregation. Some pseudo islets formed in the wells, but so did large

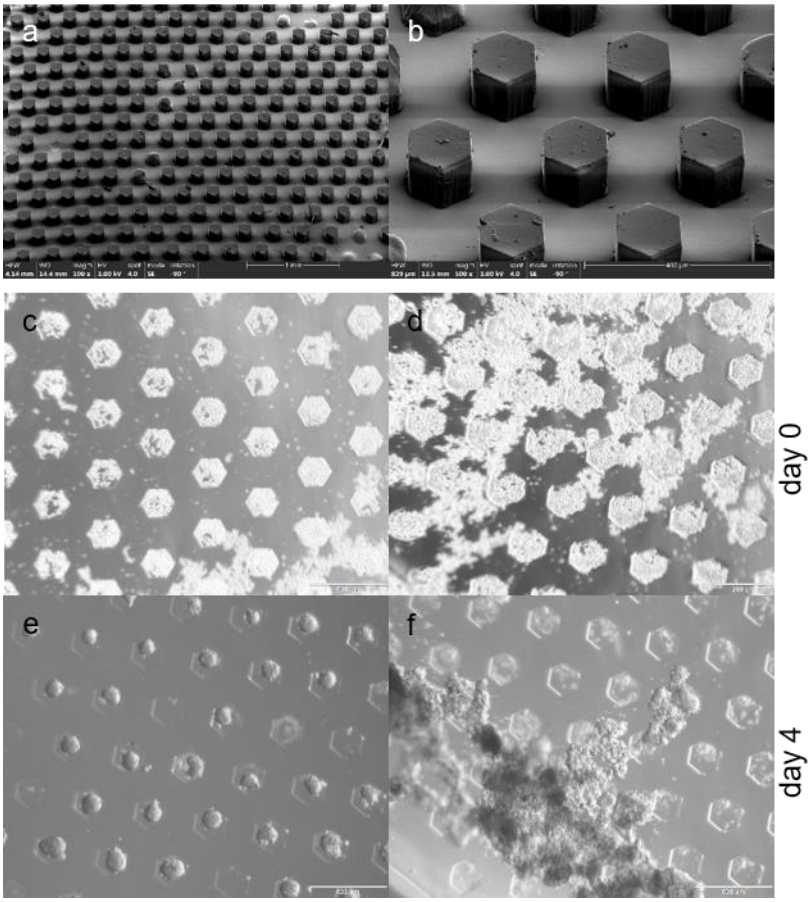

Figure 29. Seeding of single islet cells into hydrogel microwell arrays with flat bottom, sharp rims and flat planes. a,b *SEM of PDMS replica from wafer****. c,d,e,f*** *Microwell hydrogel arrays seeded with single islet cells. Microwells have a size of 200 µm and 200 µm distance between each other. Cells are falling into the microwells, but some cells keep lying at the planes and form large aggregates.*

aggregates formed on the planes in between the microwells (Figure 29 c-f). This might be due to the cells not falling into the microwells, as these planes do not have any curvature.

To create microwells with curvature, microstructure scaffolds were produced by repetitive moulding, with additional pressure skimming or dipping of the microstructures. In contrast to methods in literature investigated earlier, the applied methods do not require any specialised equipment. The additional moulding steps rounded off the sharp rims of the initial structure, but some surface roughness was introduced (Figure 30). In between the moulding steps the surfaces were coated with SDS for the release of the casted PDMS layer.

At a large scale the microwell stamps appeared to be homogenously spaced and rounded, with only a few pillars showing abbreviations (Figure 30, first column). At higher magnification though, the pillars exhibit some artefacts. These are presumably provoked by crystallised SDS particles remaining in the microwells after drying of the structures (Figure 30, centre and right column).

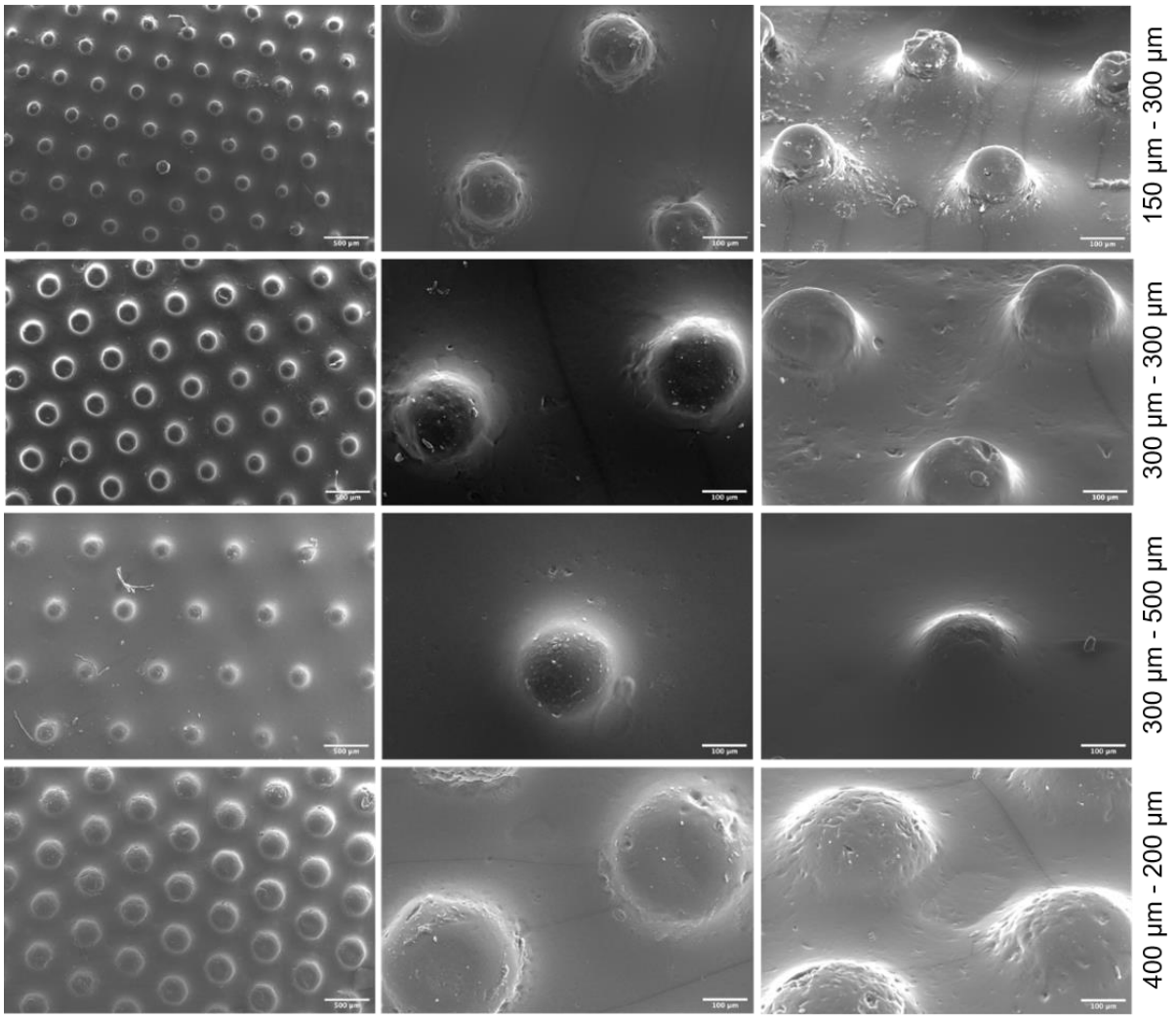

Figure 30. Replica platforms produced by repetitive moulding with intermediate steps of surface coating with SDS (surfactant) for the release of the next PDMS layer. Scale: left column 500 µm, centre and right column 100 µm.

Microwell hydrogel arrays of different microwell sizes and distances were moulded in agarose from the above depicted replica platforms and single islet cells were seeded on top to observe whether these support the formation of pseudo islets. After six days the single islet cells accumulated in the agarose microwells (Figure 31). For smaller microwells with a width of 150 µm the cells were more condensed, than for larger wells with a width of 300 µm or 400 µm. Some single cells were still lying at the struts between the microwells, though no large clusters of cells could be observed anymore, as for the flat bottom microwells with sharp rims and planes in between. Except for the smaller wells however, the single islet cells did not aggregate into pseudo islet clusters (Figure 31). The reason for this might lie in the surface roughness as revealed by SEM.

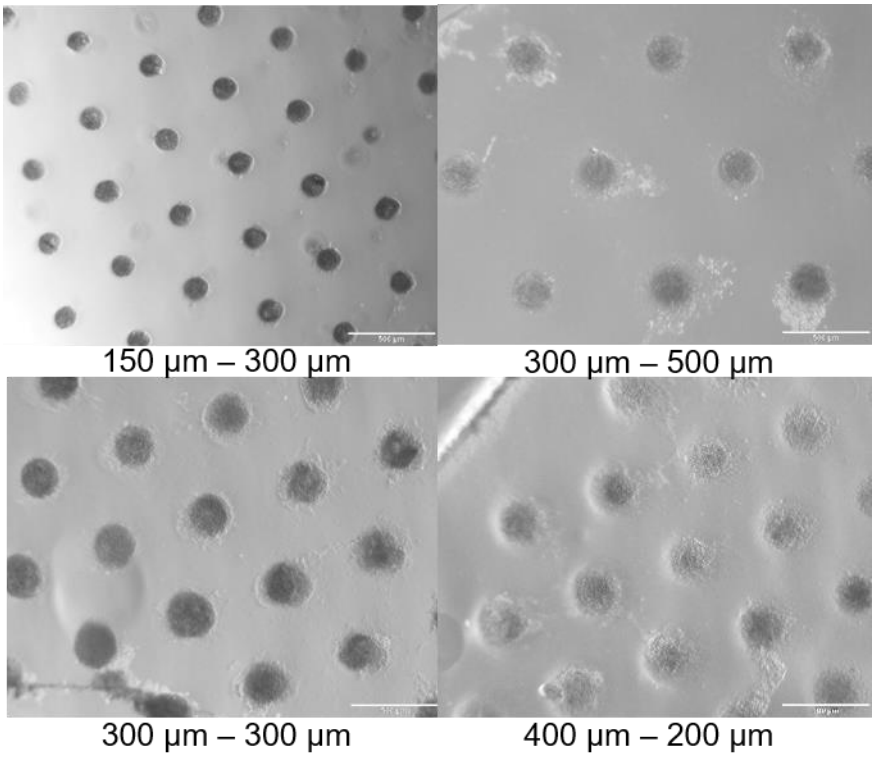

Figure 31. Single islet cells seeded into microwell hydrogel arrays moulded from replica platforms depicted in Figure 30.

Other releasing agents were tried to yield surface structures without artefacts. Dish washing soap turned out to be a suitable releasing agent that does not produce any crystals. Therefore, the method developed for rounding of the structures by pressure skimming and dipping, was utilised again in combination with the application of dish washing soap (Fit, Germany) diluted to 1:28 in MiliQ water. By this method microwell structure scaffolds without artefacts could be created (Figure 32). The depicted structures were finally converted into hydrogel microwell arrays and achieved a good aggregation of pseudo islet clusters in the microwells.

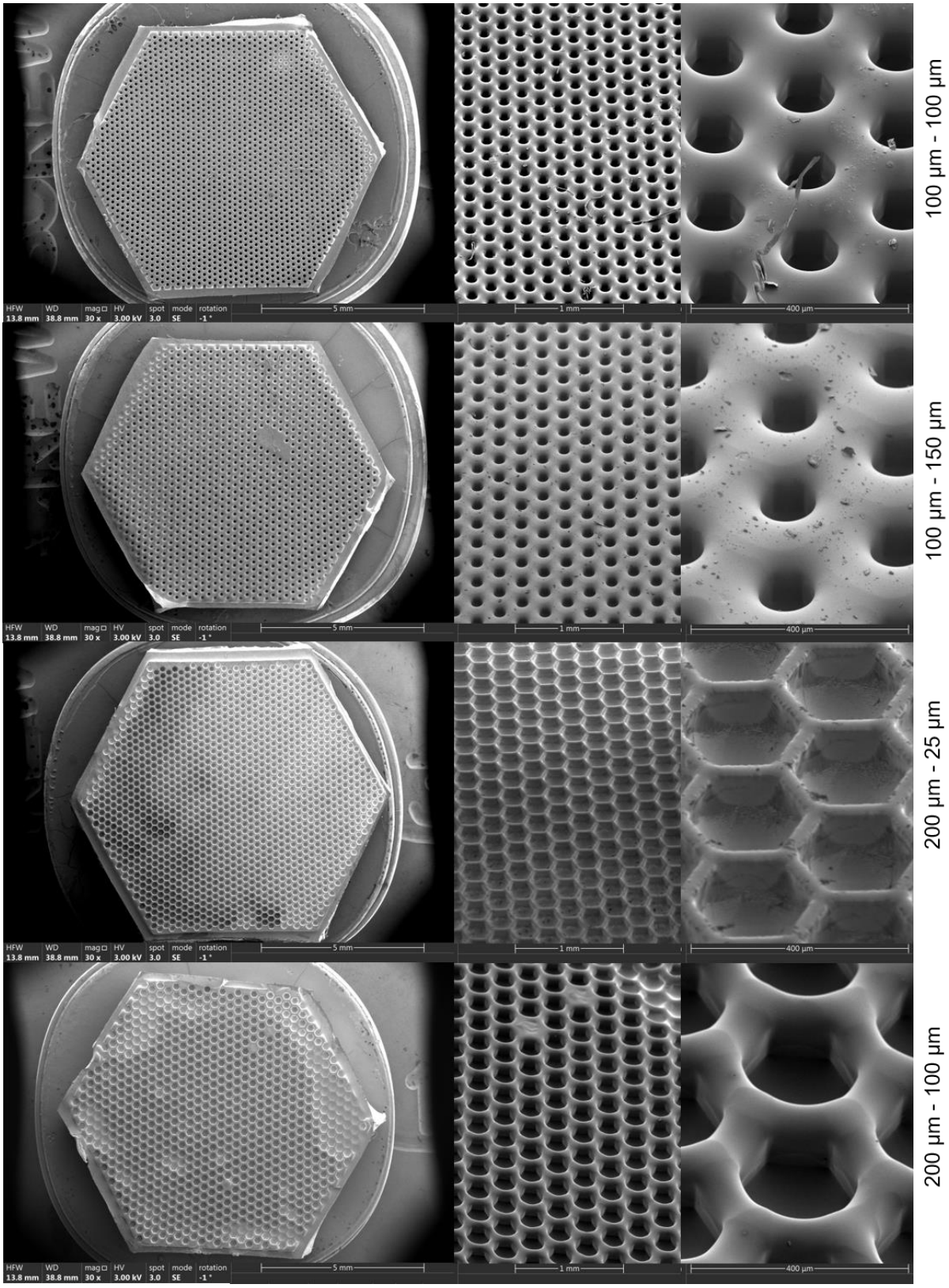

Figure 32. Microstructure scaffolds for production of replica platforms.

4.3.5 Theoretical analysis of islet packaging density in microwell arrays based on an oxygen distribution model

The formation of pseudo islets has been repeatedly proven to work in microwells, though no optimal microwell size and distance of islets have been identified yet.

While the curvature of the microwells allows the cells to slide into the well centre by gravitational force and thus might support the formation of pseudo islet clusters, the size of the microwells might have an effect on the integrity of the islet. A microwell with a size in the range of the pseudo islet could provide more structural support to the cells. In addition, a higher number of small microwells fits onto the same surface area in comparison to larger wells. The distance of the microwells (and thereby of the islets) has an effect on oxygen availability as described by the previously discussed model from Johnson et al. (2009), which is a major factor for islet functionality and viability. To reach the goal of achieving the highest insulin response per surface area of a microwell array possible, first the properties regarding the geometrical dimensions of the microwells were investigated theoretically and islet volume packaging densities calculated. Furthermore, a method based on the design of experiment techniques is proposed in this subsection to determine the best possible configuration of microwell size and distance.

For production of the microwells by photo and soft lithography techniques, a wafer has been designed covering multiple sizes of microwells (Figure 33). The microwell width was set to 100 µm, 125 µm, 150 µm, 200 µm, 300 µm, 400 µm and 500 µm and the distance in between the microwells to 25 µm, 50 µm, 100 µm, 150 µm, 200 µm, 300 µm, 400 µm and 500 µm. The combinations of microwell sizes of 400 µm or 500 µm with a distance of 400 µm and 500 µm were excluded from the design as the size of the wafer only fitted 60 combinations.

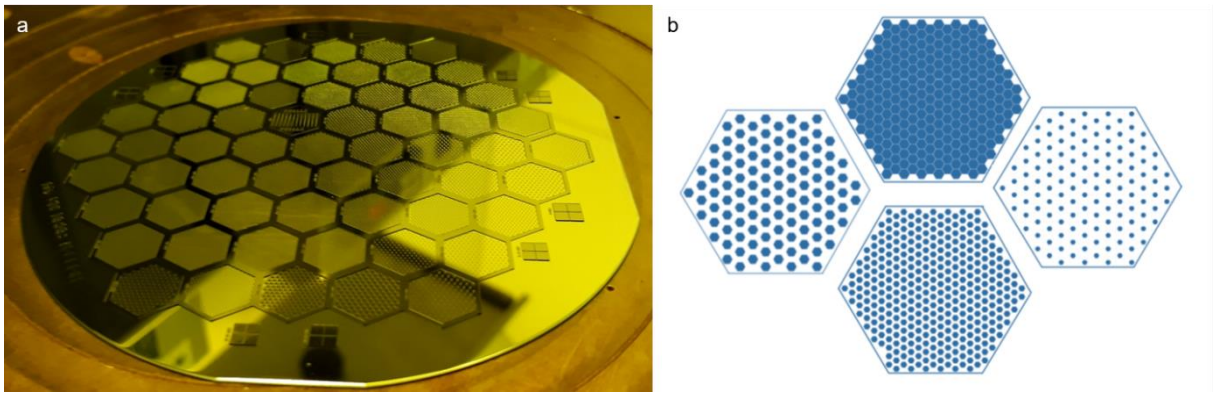

Figure 33. Microstructure scaffolds for microwell production. a *Developed wafer with microstructures used for production of microstructure scaffolds****. b*** *Schematic of exemplarymicrowell arrangements of different width and distance.*

Figure 35 a represents the number of microwell hexagons for each chosen size and distance of a microwell hydrogel array at the size of a ‘framing’ hexagon with an apothem (r) of 4.405 mm (Figure 16). The smaller the distance between the microwells, the more microwells fit on the array (Figure 35 a). Reducing the distance of 100 µm sized microwells by a factor of 20 from 500 µm to 25 µm, allows to place 22.8 times more microwells in the same area (4803 microwells instead of 210). For larger microwells of 500 µm, only 111 microwells can be placed at a distance of 300 µm, and 252 microwells at a distance of 25 µm, which is a reduction by a factor of 2.27, while the distance increased by a factor of 12 (Figure 35 a).

Johnson et al., (2009) showed in their model of assemblages of respiring spheres that the distance in between the clusters plays a major role for distribution and availability of oxygen in islets. Figure 35 b shows the pitch of the microwells from centre to centre. The pitch has the reverse distribution compared to the number of wells. Figure 35 c relates the pitch to the islet sizes of 75 µm, 100 µm, 125 µm, and 150 µm by how many multiples of the islet size the islets would be placed apart from each other. To refer to the predictions from the model of Johnson et al. (2009) (Table 2) the horizontal lines indicate which of the microwell array arrangements could theoretically support complete islet function and viability. The intersections of the diagonal and horizontal lines of the same color thus indicate at which microwell arrangements fulfill the criteria derived from the model (Figure 35 c).

The aim for housing the islets in an islet encapsulation device is to generate the maximum insulin response per surface area possible. Therefore, next to taking into account which arrangements can keep the clusters viable, the maximum packaging density per microwell hydrogel array has to be considered as well. The gold standard for estimating the transplanted islet volume is in islet equivalents (IEQ). An islet of 150 µm size is referred to as one unit. The creation of pseudo islets allows to have an exact estimate of the cell number an islet is composed of. Figure 34 a represents the cells seeded per microwell and their respective size for rat islets. From this data a continuous scale determining the IEQ was derived by relating the cell number for each islet size to the cell number of an islet of 150 µm corresponding to one islet equivalent (Figure 34 b). The original transformation factors proposed by Ricordi et al. (1990) and later on adapted by Buchwald et al. (2009) categorises islets into bins of 50 µm to 100µm, 101 µm to 150 µm, 151 µm to 200 µm and so on. Each category has a certain transformation factor with which the IEQ of an islet can be estimated (green line in Figure 34 b). The continuous scale derived from pseudo islet size data correlates well with the original categories developed by Buchwald et al. (2009).

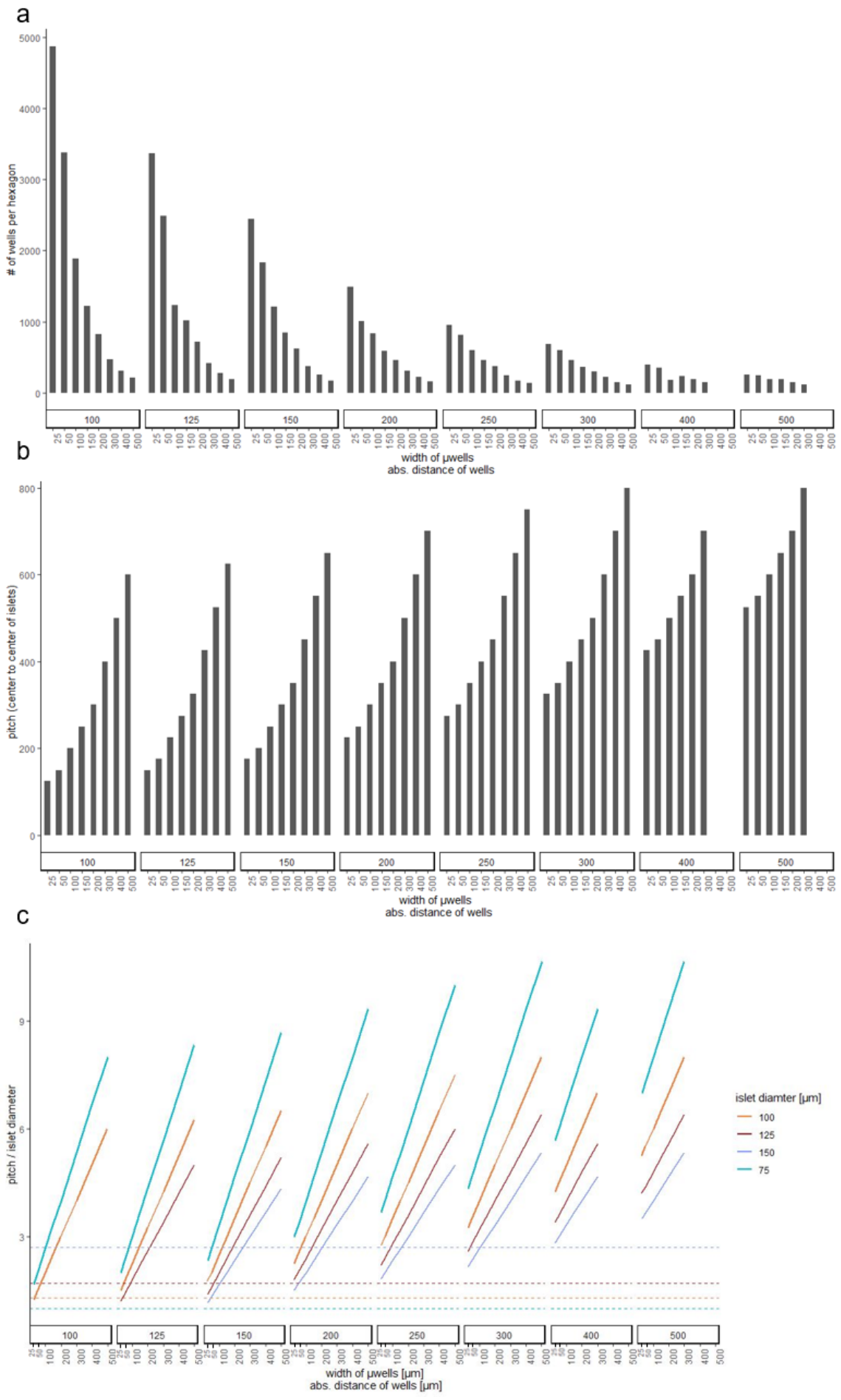
a
# of wells per hexagon
width of µwells
abs. distance of wells
b
pitch (center to center of islets)
width of µwells
abs. distance of wells
c
pitch / islet diameter
islet diamter [µm]
100
125
150
75
width of µwells [µm]
abs. distance of wells [µm]

Figure 35. Analysis of dimensional characteristics of microwells with varying distance and width. a *Number of microwells per hexagon unit. These numbers are representing the maximal number of pseudo islets per hexagon hydrogel.* ***b*** *Distance from centre to centre of the microwell hexagons.* ***c*** *Spacing of pseudo islets of different sizes depicted as multiples of the islet size. Horizontal lines represent minimal required spacing of islets as modelled by Johnson et al. 2009.*

Figure 34 c describes the estimated IEQ that can be loaded per islet scaffold related to different sizes of pseudo islets. Islets larger than 150 µm are thought to develop a necrotic core, therefore only islets of sizes 75 to 150 µm were considered for filling the microwell array and subsequently for the calculations described here.

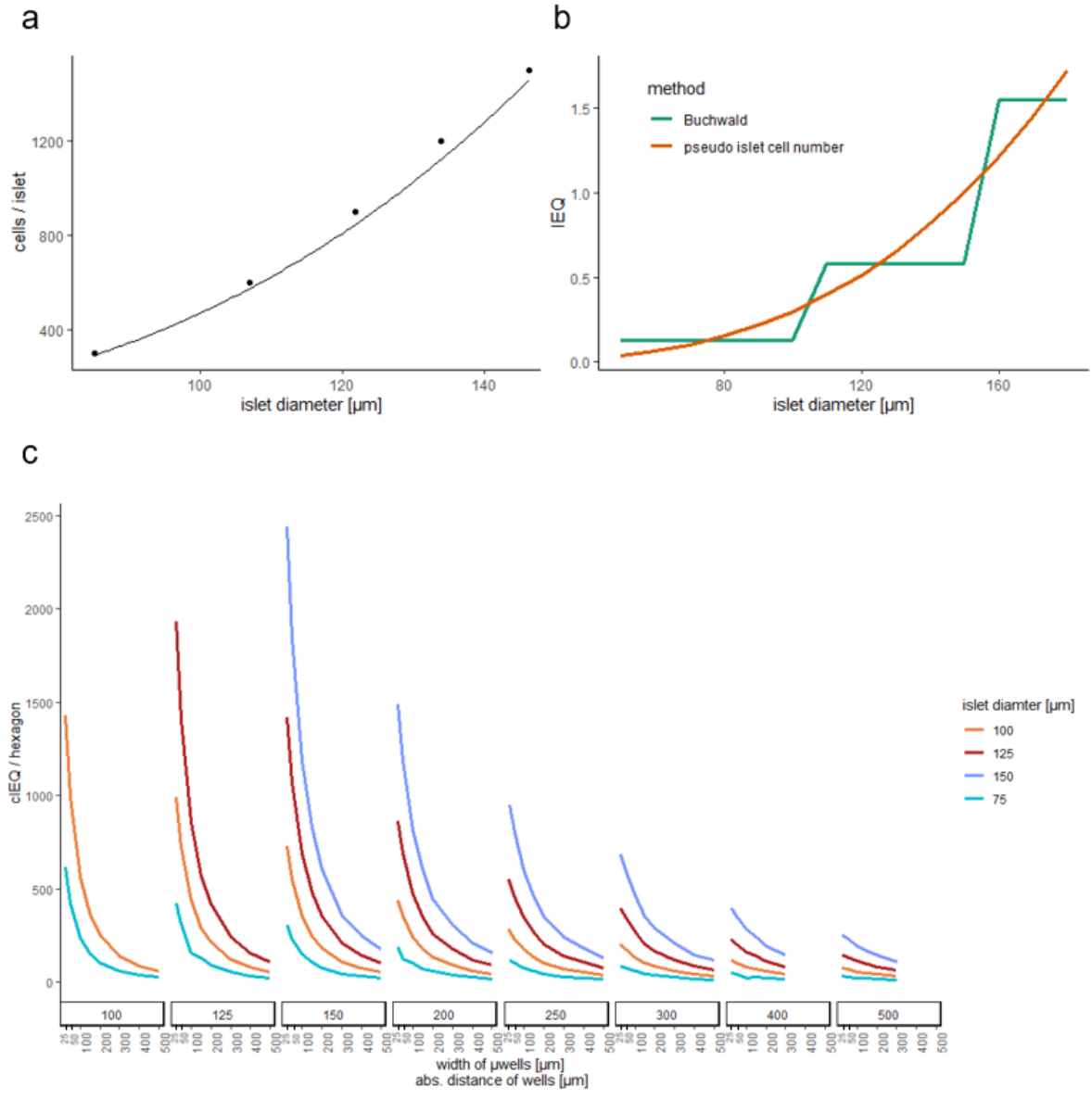

Figure 34. Calculation of possible islet loading volume per scaffold. a *Rat pseudo islet diameter relating to the seeded cell number* ***b*** *cIEQ (cell number based islet equivalents) per pseudo islet relating to the islet volume equivalent (IEQ) based on Buchwald et al. 2009.* ***c*** *Islet loading volume (cIEQ) of microwell hydrogel arrays.*

The highest loading of the scaffold taking into account the theoretical model of oxygen availability by Johnson et al., (2009) can be reached with a scaffold carrying hexagons with 100 µm width and 50 µm distance with an islet size of 100 µm. Packed in this way one large hexagon can carry 1007.5 cell number based islet equivalent (cIEQ). Table 3 gives an overview of the 14 most efficient arrangements of microwells.

Table 3. Microwell arrangements theoretically supporting islet function and viability with highest islet packaging density (>450 IEQ/cm^2).

microwell width	Distance of microwells	# of microwells	pitch [P]	cIEQ per hexagon	islet size [S]	multiples of islet size [M] (M = P/S)	Predicted minimum required pitch (Johnson et al. (2009)) (J)	M-J
100	50	3381	150	1007.5	100	1.50	1.4	0.20
125	25	3364	150	1002.4	100	1.50	1.4	0.20
125	50	2485	175	740.5	100	1.75	1.4	0.45
150	25	2446	175	728.9	100	1.75	1.4	0.45
150	100	1205	250	699.1	125	2.00	2	0.30
100	25	4876	125	615.4	75	1.67	1	0.67
125	150	1012	275	587.1	125	2.20	2	0.50
200	50	1005	250	583.1	125	2.00	2	0.30
100	100	1882	200	560.8	100	2.00	1.4	0.70
250	25	950	275	551.2	125	2.20	2	0.50
150	50	1833	200	546.2	100	2.00	1.4	0.60
150	150	845	300	490.3	125	2.40	2	0.70
200	100	834	300	483.9	125	2.40	2	0.70
250	50	812	300	471.1	125	2.40	2	0.70

4.4 Discussion and outlook

This chapter described how a method was developed for the creation of microwell hydrogel arrays for pseudo islet seeding with simple soft lithography methods in contrast to MEMS lithography processes, which require advanced equipment. A set of microwell moulds were designed to produce microwell hydrogel arrays with microwells of different width and distance to each other. These can be produced either in a framed format for *in vitro* optimisation processes or in an unframed format for placement within the islet holder of the encapsulation device. With this set of microwell hydrogel arrays an experiment has been designed to find an arrangement of islets with optimised oxygen distribution characteristics for good survival and function of the islets and the highest islet volume packaging density (in IEQ/cm²) to yield a maximal insulin response per surface area.

For optimisation of the islet distribution, data modelled by Johnson et al. (2009) was applied. This data provided a prediction at which sizes and distances between one another, the islets would still be viable and functional. However, it should not be forgotten that these assumptions are based on OCRs, which might not represent the actual oxygen consumption of the islets and might therefore not indicate the actual hypoxic regions of the encapsulated cells. OCR is depending on the actual metabolism and cell type, therefore it is crucial to evaluate the optimised islet arrangement with the proposed experiment *in vitro* and *in vivo*.

The availability of microwells of different arrangements makes it possible to optimise the arrangement easily for specific cell types. Islets of different species have different mean diameters. That way, microwells of different sizes could be used for different species or cell sources, such as xenogeneic pig islets, allogeneic human islets or islet-like clusters derived from stem cells. The pitch distance could also be reduced for the application of engineered cells, which are more resistant to hypoxic oxygen conditions.

Coatings of the wells with different molecules are another way to enhance islet function and viability. Hadavi et al. (2019) showed that surface functionalisation of microwells with different ECM molecules like laminin 111 and collagen IV could increase glucose secretion of the encapsulated islets. Similar methods could be applied to the microwells of the encapsulation device discussed in this thesis or with ECM containing hydrogels.

Molecules increasing oxygen diffusivity such as for example perfluorcarbons could further be used to enhance the oxygen supply of the cells in the microwells. In the model of Johnson et al. (2009) could show that alginate containing perfluorcarbons lowered the steepness of the oxygen gradient inside the device and increased the partial oxygen pressure at the islet site.

Finally yet importantly, by positioning the islets closer to the membrane not only the mount of oxygen available to the islets increases, but also the diffusion of any other molecule, mainly blood glucose and the respective insulin response, can be accelerated rapidly and in a shorter amount of time.

4.5 Perspective on further experiments: optimal islet arrangement and size by design of experiment technique (DOE)

A previous subsection (4.3) theoretically analysed the optimal arrangement and size of islets. Still this model might not reflect all the variables influencing the viability and function of the islets as they do occur in the *in vitro* or even *in vivo* setting.

The identified variables that can be controlled with the described microwell approach are microwell size, distance and number of cells per microwell/pseudo islet cluster. These variables open a matrix with the factor 8 (for the microwell width) times 8 (microwell distance) times a continuous variable (cell number), resulting in a complex optimisation problem with too many combinations that cannot be tested in a feasible number of experiments.

Design of experiments (DOE) techniques are a statistical approach to optimise a condition or process. In contrast to the traditional ‘one factor at a time’ it has many advantages as increased experimental efficiency and determination of individual and interactive effects of multiple variables that have an influence on the result. A response surface design is a DOE technique that helps to understand and optimise a response given by various input variables. The resulting response surface plot models, how changes of the variables affect a response of interest indicating which level of the variable results in the optimised response. The most common DOE design is the Central Composite design (CCD), a fractional or full factorial design with centre points, complemented by a group of axial points to estimate first and second order terms, suitable for the opposed optimisation problem (Figure 36).

As an input for the experimental design microwell designs were chosen which can house more than 400 IEQ as the size of the implant would be tremendously large with smaller islet loading. The variables chosen for the design are for the first variable the microwell width, for the second variable the microwell distance and for the third variable the cell number per well, bringing forward the following table of conditions to be tested (Figure 36 a, Figure 37).

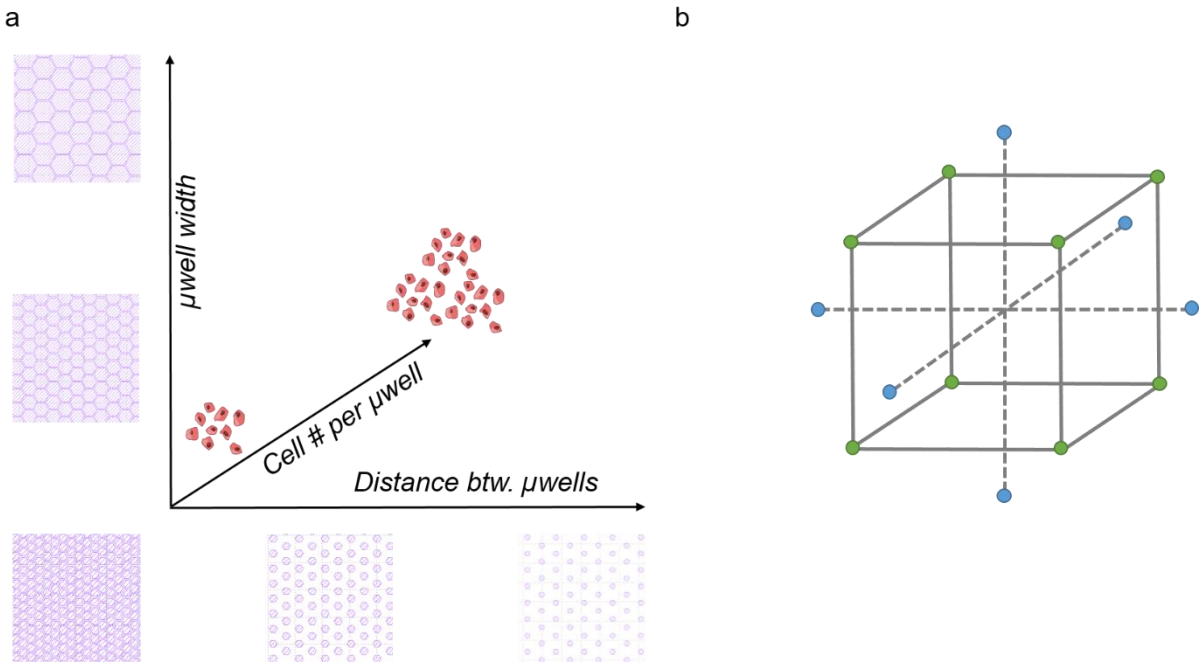

Figure 36. Schematic presentation of the design for an experiment setup. a *Variable microwell width, distance btw. microwells and cell number per well are representing the variables on a matrix to find the border conditions under which islets can maintain viability and function.* ***b*** *Example of a central composite design (CCD) to choose the factors tested in the experiment.*

With the well-established method for pseudo islet formation in our lab, these combinations of pseudo islet cluster arrays are going to be tested in different oxygen conditions. More specifically, after the formation of the pseudo islets these are placed at physiological oxygen concentration at 40 mm Hg, as reported for tissue. As a readout parameter the cell viability will be determined by live-dead staining alongside the measurement of glucose stimulated insulin secretion.

a

Width	Distance	Cell number
100	50	468
100	200	200
125	25	900
125	150	900
150	25	200
150	50	1600
150	100	830
150	150	1600
150	150	200
150	200	1600
200	200	760
250	25	1600
250	50	830
250	100	200
250	150	970
250	150	970
300	25	200
300	50	1250
300	200	1600
300	200	200

b

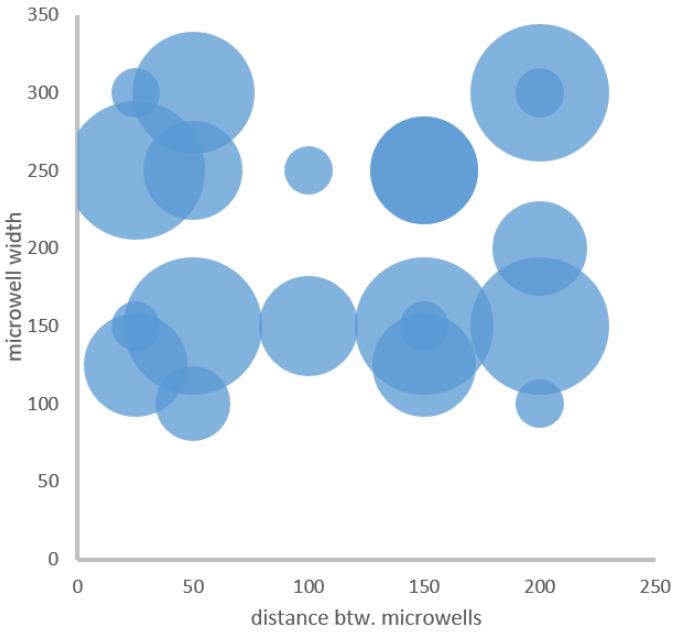

Figure 37. Experimental conditions for investigation of an optimal islet arrangement by application of 'design of experiment' method. a *Table of conditions.* ***b*** *Graphical representation of conditions. The sphere's size corresponds with the cell number to investigate in each condition.*

4.6 Acknowledgements

Microstructures were produced at the microstructure facility of the Center for Molecular and Cellular Bioengineering (CMCB), Dresden. Victoriya Sarangova (IPF Dresden) performed SEM. Undine Schubert (University Hospital Carl Gustav Carus, Dresden) kindly provided data on rat pseudo islet size and cell number.

5 Immunoisolating membrane with vascularizing properties

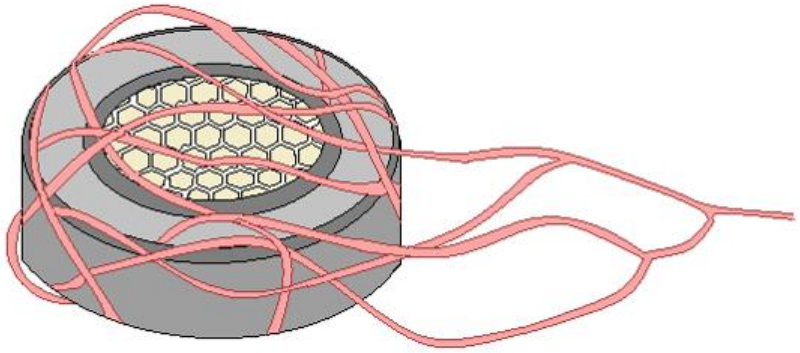

5.1 Introduction

The basic principle of an encapsulation device is to hide the transplanted cells from the host's immune system and thereby protect the encapsulated cells from immune-mediated destruction. In this immunoisolating capsule the membrane is the only area of passage where molecules can diffuse between the outside and the inside of the device. To meet the requirements of immunoisolation, the membrane needs to prohibit the passage of components of the immune system, while allowing the passage of certain molecules required or secreted by the encapsulated cells. Besides providing permselective properties, certain functional properties are required: the immunoisolating membrane needs to be stable, biocompatible, sterilizable and scalable in its production process.

This chapter explains how a selective permeability can be created by coating a tuneable hydrogel network into the pores of a polymer membrane and how this selectivity can be assessed *in vitro*. Furthermore, the wound healing and vascularisation supporting properties of the applied hydrogel system are discussed and how these can be optimised for improved vascularisation of the membrane surface in an *in vivo* setting.

5.1.1 Immunologic reactions involved in the rejection of grafted tissue and material

The immunologic response against foreign tissue or material can be subdivided into the cellular immune response, the humoral immune response and inflammation-type reactions. The cellular immune response results from a direct interaction of the cellular part of the immune system with the cells of the implanted tissue. This is mediated by interaction of the MHC class I receptor with cytotoxic T-cells. If a T-cell recognises a specific antigen presented by a foreign-tissue cell, the T-cell destroys the grafted cell. This cytotoxic reaction is prevented by placing an immunoisolating membrane that prohibits the direct contact between the grafted tissue and the host immune system physically.

The humoral immune response is mediated by an antibody-complement activation via IgG or immunoglobulin M (IgM). If an antibody detects a foreign cell, so called membrane attack complexes are established leading to necrosis of the attacked cell. These antibodies can either arise against the foreign tissue or are already present as in the case of T1D where autoantibodies against beta cells or components thereof have been developed by the immune system. A further component of the immune system endangering the transplanted tissue is C1q, a rate-limiting factor of the complement cascade. These molecules are relatively large and their passage over the immunoisolating membrane can partly be excluded via the size-exclusion principle of immunoisolating membranes.

Inflammation-type reactions are promoted during the implantation of the tissue or material graft. During surgery the tissue is disturbed and inflammatory reactions are induced. This is further enhanced by the foreign material placed inside the wounded tissue. Neutrophils, basophils and macrophages are activated and release cytotoxic cytokines and chemokines promoting the inflammation and leading to the destruction of the transplanted islets. This is the primary pathway of islet deterioration during transplantation of the islet graft and is the major reason for the loss of islets in the early transplantation phase.

It is therefore important that an immunoisolating membrane blocks the contact of the cellular arm of the immune system mediated by T-cells. Besides, passage of components of the immune system needs to be restricted. Here though, it has to be taken into account that certain nutrients, waste products and endocrine hormones such as insulin need to be able to pass the membrane. When preventing molecules from permeation over the membrane via a size exclusion principle, the size cut off has to be chosen above the size of the molecules that need to diffuse over the membrane.

5.1.2 Generation of a composite membrane with selective permeability

The immunoisolating barrier of the encapsulation device is based on a size exclusion principle. The size-restrictive barrier is created by combining two components with different functions and pore sizes: the mechanically strong basis (reinforcing element) of the composite membrane is provided by an ePTFE membrane, while the size selectivity restricting the diffusion of large molecules is given by the tuneable polymer network of a hydrogel.

The ePTFE used for this composite membrane is hydrophilised. In this way the pores can be filled up by an aqueous solution carrying the hydrophilic polymer precursors of the hydrogel, which then crosslink in between the pores of the ePTFE membrane. The two components of the composite membrane create a selectivity on different scales. The ePTFE material with a pore size of 400 nm hinders cells of the immune system to pass the membrane. The mesh size of the hydrogel network is tuneable between about 10 to 30 nm, which allows to additionally prohibit the diffusion of large molecules (Figure 38).

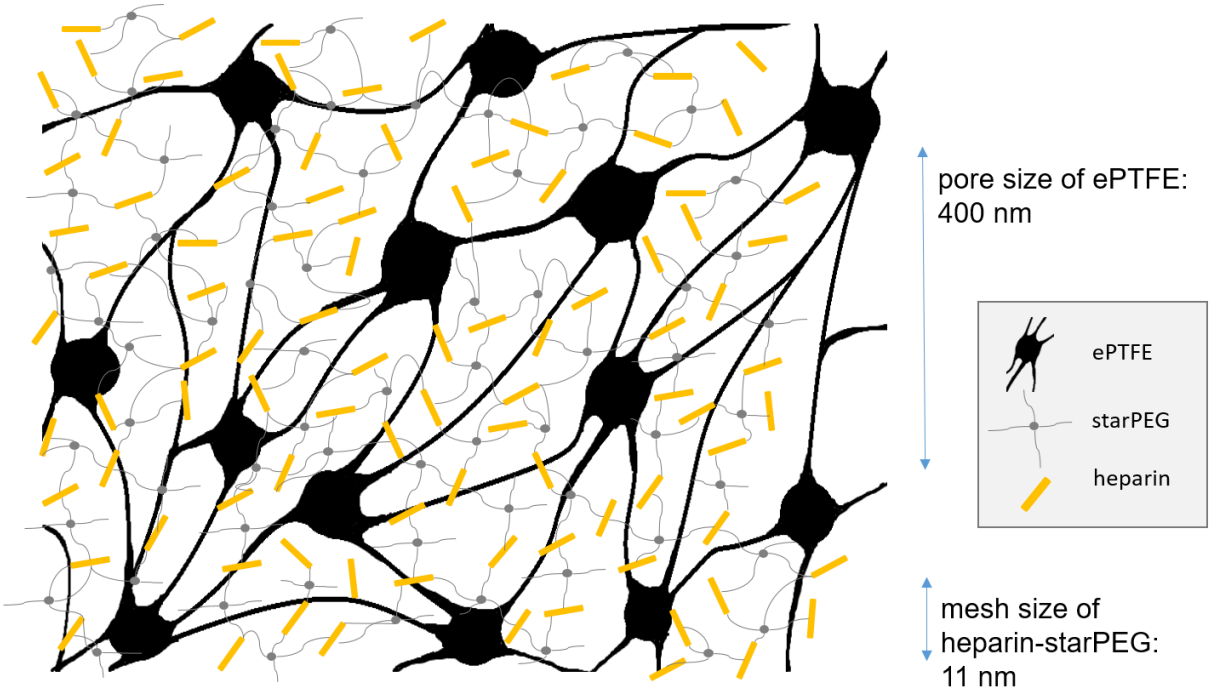

Figure 38. Schematic drawing of the intertwined network of the composite membrane.

5.1.3 ePTFE as reinforcing element of the composite membrane

The ePTFE membrane acts as a reinforcement element of the composite membrane. Polytetrafluorethylene (PTFE) is an unbranched polymer composed of fluor and carbon also known under the trade name Teflon™. It is an inert material with high resistance against chemical or thermal treatment. The ‘e’ of ePTFE stands for the ‘expansion’ of the material in the production process. This expansion contributes to the orientation of the molecular fibers

and the introduction of pores into the material. The expanded material has a higher tensile strength and mechanical resistance.

The ePTFE membrane applied for this novel encapsulation device furthermore is hydrophilised. The native PTFE has hydrophobic properties, though by a processing step, which is not revealed by the manufacturer, the polymer is modified to obtain hydrophilic properties. This allows water to easily penetrate through the pores of the membranes. With the water hydrogel precursor molecules can be brought into the membrane and crosslink into a hydrogel network intertwining with the porous structure of the PTFE membrane.

Furthermore, ePTFE is one of the thinnest membranes available on the market. ePTFE membranes are sold with a thickness of 40 µm. The thickness of the membrane is of great importance in this context as it determines the total distance molecules such as oxygen or other nutrients have to diffuse to reach the encapsulated islets (as described in chapter 3).

5.1.4 Diffusion-based transport processes through a hydrogel network

In the composite membrane the hydrogel is applied as an additional barrier, permselective at a smaller scale (molecule size) compared to the PTFE carrier membrane. The selectivity arises from the mesh size of the hydrogel network.

Hydrogels are composed of a hydrophilic polymer network which takes up lots of water molecules under swelling. When a hydrophilic network gets into contact with water, the polar groups are hydrated first. These first attached water molecules can be depicted as the bound fraction of the water. After the polar groups are saturated with water, the hydrophobic groups are exposed and interact with the water as so called secondary-bound water. Finally, when all groups are fully hydrated, the hydrogel can imbibe additional free water molecules (Hoffman, 2012).

On the sub-micrometer scale the dominant form of material transport is diffusion, where particles or molecules diffuse from a region of high concentration to a region of low concentration. The distribution of the particles is generally described by Fick's second law:

$$\frac{\partial c}{\partial t} = D \frac{\partial^2 c}{\partial x^2}$$

Here, the change of the concentration (c) of a solute over time (t) is dependent on the second derivative of concentration difference at the position (x) times the diffusion coefficient. In a viscous fluid the diffusion coefficient can be approximated by the Stokes-Einstein-equation:

$$D = \frac{kT}{6\pi\eta r}$$

where *k* is the Boltzmann constant, *T* is the absolute temperature, *η* is the dynamic viscosity, and *r* is the radius of the diffusing particle.

In a porous system though, the diffusion path of the molecules is hindered by the abundance of other molecules. The tortuosity describes the path a molecule has to diffuse through the network. It is dependent on different factors such as the average pore size, the pore size distribution and the pore interconnections. Accordingly, the effective diffusion path length across a porous barrier is dependent on the film thickness times the ratio of the pore volume fraction divided by the tortuosity (Hoffman, 2012).

Lustig and Peppas (1988) derived a scaling law to estimate the normalised diffusion coefficient of solutes in hydrogels, which applies for solutes smaller than the mesh size of the hydrogel network which is dependent on the composition and crosslinking density. It is valid only for nonporous gels and chemically inert solutes and gels:

$$D_{app} = D_o \left(1 - \frac{r_S}{\xi}\right) e^{\left(\frac{-Y}{Q-1}\right)}$$

with D_{app} being the solute diffusion coefficient in the gel, D_0 the diffusion coefficient in pure solvent, Q the swelling degree, Y the ratio of required critical volume for translation movement to available free volume per molecule (which is about 1), ξ the mesh size of the hydrogel, and r_s the radius of the volume of a sphere estimating the size of the solute. This formula shows that the apparent diffusion coefficient of insulin (D_{app}) is inversely related to the ratio of the solute radius over the mesh size of the hydrogel. Thus the larger the pores of the hydrogel the faster the insulin can penetrate through the composite membrane.

5.1.5 Relevant characteristics of molecules for designing the immunoisolating membrane

Next to the described hydrogel parameters, the permeation of a solute is dependent on the permeate itself. The solute size and shape, its charge and relative hydrophilic and hydrophobic character and the availability of free water molecules play a role (Hoffman, 2012). The hydrodynamic radius of the molecule describes the size of a protein or peptide in solution. It is the size of the molecule itself including the water molecules binding to the outer surface of the molecule. The charge of a diffusing molecule furthermore defines the interactions with the hydrogel. If the protein has a net charge opposite to the hydrogel, it gets electrostatically bound to the hydrogel. The actual charge of molecule is described by the isoelectric point (pI). If the

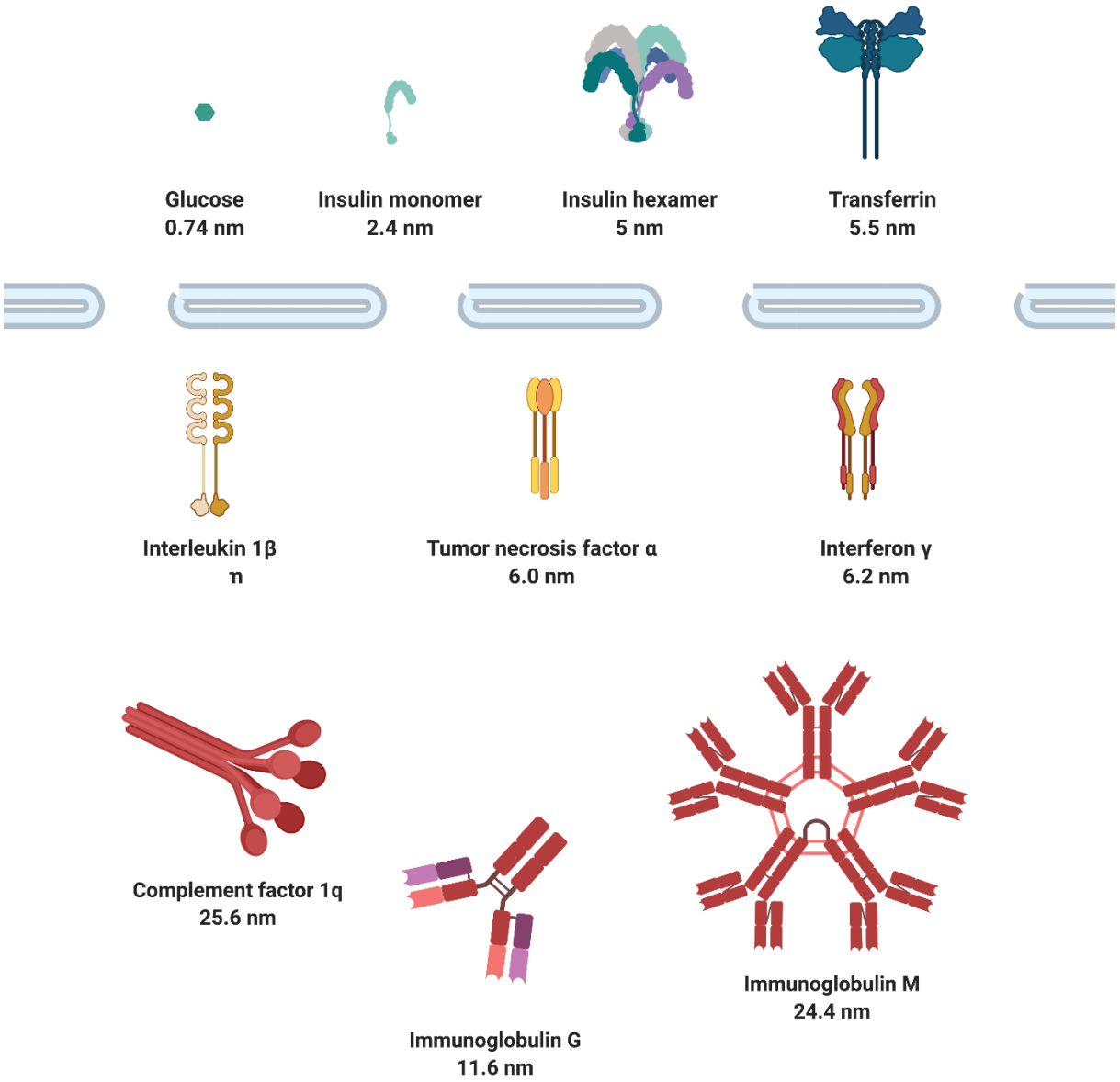

Figure 39. Size exclusion principle of the composite membrane. *Large molecules of the immune system cannot pass the membrane (red), small molecules relevant for the metabolism can pass the membrane (green), cytokines are small and can pass the membrane, but there diffusion can partly be prevented by the electrochemical charge of the membrane.*

pH of the solution is lower than the pI, the protein is positively charged. If the pH is higher than the pI the protein is negatively charged.

The principle of the immunoisolating membrane is based on the mechanism that excludes certain molecules of the immune system from the penetration into the encapsulation device while allowing passage of molecules required for the metabolism of the encapsulated cells such as glucose, transferrin, and secreted hormones of the cells such as insulin. The insulin monomer has a hydrodynamic diameter of 2.4 nm; in the hexameric form the hydrodynamic radius increases to 5.0 nm (Table 4, Figure 39). Components of the immune system, which shall not pass the membrane, e.g. IgM and C1q, have a hydrodynamic radius of about 25 nm

(Table 4, Figure 39). IgG that can specifically react against insulin or islets in autoimmune T1D has a hydrodynamic diameter of 11.8 nm (Table 4). However, molecules triggering an inflammatory reaction are much smaller and of the same size as the molecules that are required to pass the membrane. These are, for example, interleukin 1 beta, interferon gamma and tumor necrosis factor alpha (Table 4). Most cytokines have a positive charge at neutral pH in contrast to proteins required to pass the membrane such as insulin, which has a negative charge (Table 4).

Table 4. Properties of molecules need to diffuse (green) or need to have restricted diffusion over the immunoisolating membrane (red), cytokines in the same size range as insulin, but that can potentially be bound by charge (orange).

Molecule	Hydrodynamic diameter [nm]	Molecular weight [kDa]	Isoelectric point (pI)	Reference
Glucose	0.365 nm	0.18	-	(Bouchoux et al., 2005)
Insulin	3.0 nm	9.4	5.3 – 5.4	(Scott and Fisher, 1935; Artimo et al., 2012; Jensen et al., 2014)
Transferrin	3.7 nm	75.2	5.2 – 5.7	(Stibler and Jaeken, 1990; Artimo et al., 2012)
Interleukin 1 beta	2.2 nm	17.3	5.91	(Artimo et al., 2012; Barkai et al., 2016)
Interferon gamma	3.1 nm	16.2	9.52	(Artimo et al., 2012; Barkai et al., 2016)
Tumor necrosis factor alpha	3 nm	17.4	7.0	(Artimo et al., 2012; Barkai et al., 2016)
Immunoglobulin G	11.5 nm	150	7.0 – 9.9	(Prin et al., 1995; Charles A Janeway et al., 2001; Gagnon et al., 2015)
Immunoglobulin M	12.7 nm	950	5.8 – 8.5	(Rosén et al., 1979)
Complement 1q	12.8 nm	68.5	8.8 – 9.3	(Heinz, 1989; Artimo et al., 2012)

In conclusion, a size cut-off in the range of 3.7 nm to 11.5 nm could prevent a humoral response against the encapsulated islets graft. Importantly, the larger the pore size the faster small molecules can diffuse. An additional selection based on the charge of the proteins could furthermore prevent a penetration of most cytokines while allowing the passage of insulin, transferrin and glucose.

5.1.6 Determination of the hydrogel network mesh size via rheology

The average mesh size of a hydrogel network can be derived from its rheological properties. Rheology is the study of the deformation and flow of matter and can be used to determine the mechanical properties of a material.

The viscoelastic properties of hydrogels are described by the storage modulus G' and the loss modulus G''. The viscous properties of hydrogels are reflected by the loss modulus G''. These emerge from the liquid-state behavior, which is mostly represented by the water molecules in the sample. When energy is applied to the gel, part of the molecules undergoes internal friction and absorbs energy that cannot be retained by the material and thereby contributes to the loss of energy. The elastic properties are represented in the storage modulus G'. These properties are attributed to the solid-state behavior of the hydrogel, which is given by the polymer chains of the gel. The polymer chains can take up a part of the energy applied to the gel by internal stretching of the polymer structures. When this energy is released, the polymer chains release the stored energy and the hydrogel retains its original shape again.

The elastic properties of the hydrogel allow for the application of the rubber-elasticity theory. It relates the stiffness of the hydrogel measured by the storage modulus (G') to the average pore size of the polymer network (ξ):

$$\xi = \left(\frac{G' N_A}{RT}\right)^{-1/3}$$

Where G' is the storage modulus, N_A is the Avogadro constant, R is the molar gas constant, and T is the temperature. The function is based on the assumptions that all polymer chains retract in the same way after the application of a deformation force (affine deformation), while not taking into account the effect of non-crosslinked polymer ends and the entanglement of the polymers (Rubinstein and Colby, 2003; Freudenberg et al., 2009).

5.1.7 Heparin-starPEG hydrogels as tuneable network of the composite membrane

The immunoisolating function of the composite membrane is reached by creating a permselective barrier preventing the ingress of large components of the immune system by a

hydrogel network with pores on the nanoscale (meshes). Small molecules still need to be able to penetrate the network. To fulfill these requirements a network needs to be obtained, which can be tuned to a fitting pore (mesh) size cut-off.

Heparin-starPEG hydrogels are a well-studied system with tuneable network properties. These are consisting of two polymer components: an extracellular matrix (ECM) polymer, heparin, and a synthetic polymer, 4-arm polyethylene glycol (starPEG). Heparin is a glycosaminoglycan with a high anionic charge. It provides high biocompatibility as a natural occurring polymer and can modulate biomolecular cues to the cells in the matrix. starPEG has a high modularity in polymer length and end-functional groups making it an optimal crosslinker for a hydrogel network.

By crosslinking heparin and starPEG at different molar ratios, heparin-starPEG hydrogels have been shown to have a tuneable stiffness and therefore pore size. When increasing the molar ratio of the starPEG content to heparin, the crosslinking degree (y) of the gels is increased. With increasing y the storage modulus of the hydrogel increases (0.18 ± 0.01 kPa to 4.45 ± 0.62 kPa), while the swelling degree decreases (Freudenberg et al., 2009). The calculation of the theoretical pore size according to the rubber-elasticity theory revealed a mesh size range from 29 ± 2 nm to 10 ± 3 nm with increasing crosslinking degree. The theoretically evaluated mesh size was supported by investigating the penetration of the hydrogels by fluorescently labeled bovine serum albumin (BSA) and FGF-2 into the gels. BSA, which has a size of 14 x 4 nm, penetrated into the gels with 29 nm pore size within 24 h. The smaller fibroblast growth factor (FGF-2) with a size of 3 – 4 nm diffused into the hydrogel even faster within 1 min (Freudenberg et al., 2009). The variability in hydrogel stiffness was further investigated by Welzel et al. (2011), showing that heparin-starPEG hydrogels can be prepared to an even broader range of storage moduli by using starPEG and heparin polymers with a varied molecular weight and a higher range of molar ratios.

The degree of swelling is another parameter that needs to be considered in the context of the coating for an immunoisolating barrier. The swelling of the hydrogel can increase the absolute thickness of the membrane. However, for the dimensions of the encapsulation device it is critical to limit the distance over which molecules have to diffuse. Variations in the solid content of the hydrogel precursor solution have shown that the swelling degree is reduced with reduced solid content and increasing crosslinking degree (Atallah et al., 2018).

The diffusion of different molecules through heparin–starPEG hydrogels has been investigated by FRAP (fluorescent recovery after photobleaching). For this method an area of the hydrogel is bleached by a strong laser pulse and afterwards the time of diffusion of the fluorescently labeled molecules moving back into the bleached spot is observed. In heparin-starPEG hydrogels with 500 Pa, which have a theoretical mesh size of 20 ± 1.4 nm, 20 kDa FITC

(fluorescein isothiocyanate)-dextran with a hydrodynamic radius of 6.6 nm has a diffusion coefficient of 34 ± 1.5 $\mu m^2/s$ and a 100 % mobile fraction. A significantly larger 2000 kDa FITC-dextran with a hydrodynamic radius of ~54 nm had, in contrast, a much smaller diffusion coefficient of 1.45 ± 0.4 $\mu m^2/s$ with a mobile fraction of 36 % (Atallah et al., 2018).

A detailed investigation of the diffusion of molecules within heparin-starPEG hydrogels of different heparin content has been conducted by examining the diffusion constants of differently charged and sized growth factors (Limasale et al., 2020). Heparin itself has a highly negative charge and binds molecules with a positive charge. With increasing heparin content (0 to 1500 µM), stromal cell-derived factor 1 (SDF-1), a small and positively charged molecule, showed a reduction of the diffusion coefficient from 80 to 10 $\mu m^2/s$ as it is attracted stronger by the increase of negative charges of heparin. For a highly positively charged molecule such as vascular endothelial growth factor 165 (VEGF165), the diffusion was even more limited as indicated by the decrease of the diffusion coefficient from 18 to 10 $\mu m^2/s$. Here, the reduced diffusion due to ionic interactions with the heparin was added up to the low mobility of the large molecule within a network with a smaller average mesh size than the diameter of the molecule. In contrast, the increasing heparin concentration within the hydrogel did not have an effect on the diffusion of small negatively charged molecules such as epidermal growth factor (EGF, diffusion coefficient 60 - 70 $\mu m^2/s$). Additionally, there was no effect of the charge of heparin on negatively charged large molecules such as vascular endothelial growth factor 121 (VEGF121). Its low diffusion coefficient of 20 $\mu m^2/s$, therefore, can be explained solely by its size.

In conclusion, heparin-starPEG hydrogels can be tuned via the crosslinking degree and solid content to obtain a suitable range of stiffness and therefore network mesh sizes required for the application in an immunoisolating membrane. Insulin with its small size and negative charge, which are comparable to EGF (which has been investigated by Limasale et al. (2020) in heparin-starPEG hydrogels), is assumed to easily penetrate through a heparin-starPEG network. Larger components of the immune system are assumed having restricted diffusion similar to the introduced large molecules probed in the presented studies.

5.1.8 Impact of heparin-starPEG hydrogels on wound healing and vascularisation

Besides suitable perm-selectivity and diffusion characteristics, the membrane surface of the encapsulation device also needs to have a proper biocompatibility that reduces the inflammatory response towards the foreign-body material and directs neovascularisation towards the surface of the membrane.

A further feature of heparin-starPEG hydrogels is their ability to reversibly bind a wide range of biomolecules such as growth factors or cytokines. Heparin-starPEG hydrogels can be loaded with growth factors and release them over a prolonged period of time to orchestrate the cell-matrix interaction and increase phenotypic behavior of different cell types. As such they have been used as cell-instructive matrices for cultivation of multiple cell types, including vascular endothelial cells, tumor cells and neural cell types (Freudenberg et al., 2009; Chwalek et al., 2014; Bray et al., 2015).

The support of angiogenesis by heparin-starPEG hydrogels has been shown in multiple *in vitro* and *in vivo* applications. The anionic charge of the heparin component can electrostatically bind growth factors involved in the induction of vascularisation such as FGF-2 and VEGF and release them over a prolonged period of time (4 days). In combination with cell-attachment sites covalently attached to the heparin such as the integrin binding RGD (Arg-Gly-Asp) peptide motif, the hydrogels can, for example, support the growth of human umbilical cord vein endothelial cells (HUVECs) (Zieris et al., 2010). Furthermore in a chicken embryo chorioallantoic membrane assay, the hydrogel droplets loaded with growth factors induce increase of relative vascularisation of the membranes (Zieris et al., 2011). For use of heparin-starPEG hydrogels as three-dimensional cell culture matrices, peptide sequences, that are cleaved by the cell-secreted matrix metalloproteinases can be introduced between the crosslinks of the hydrogel network (Tsurkan et al., 2013). In another study loading of heparin-starPEG hydrogels with SDF-1α directed the migration of endothelial progenitor cells (EPCs) isolated from human peripheral blood. In more detail, the local established gradient within cell-cleavable heparin-starPEG hydrogels induced a migration of the cells *in vitro* of about 40 µm within 72 h. When transplanted under the skin in a mouse model, the growth factor loaded gels had a statistically significant higher count of EPCs than non-loaded transplanted hydrogels (Prokoph et al., 2012). It was further revealed that a syngeneic effect of growth factor by a loading of the hydrogels with VEGF, SDF-1 and FGF-2 in combination with the loading of the gels with mesenchymal stem cells (MSC) could induce an angiogenic phenotype in the form of tubular structures *in vitro* (Chwalek et al., 2014).

In vivo, heparin-starPEG hydrogels loaded with VEGF have been applied as a wound dressing for diabetic wounds in mice. Tissue samples showed an increase in granulation tissue and a larger area stained positive for CD31 (marker for endothelial cells) after an implantation period of 10 days (Freudenberg et al., 2015). Further *in vivo* studies could reveal that heparin-starPEG hydrogels can sequester inflammatory chemokines from wound tissue such as IL-8 (interleukin-8), MCP-1 (monocyte chemoattractant protein–1), MIP-1a (macrophage inflammatoryprotein–1a), and MIP-1b (macrophage inflammatory protein- 1b). These chemokines are small, but strongly charged biomolecules which electrostatically get bound by

the negatively charged groups of heparin. The removal the chemokines contributes to reduced inflammation, increased vessel formation and wound closure of chronic wounds (Lohmann et al., 2017). A recent study investigated the host response of heparin-starPEG hydrogels of different properties of the gel by varying degradability, stiffness and biofunctionality (growth-factor loading). They found that the optimal gel for enhanced vascularisation is MMP-cleavable heparin-starPEG gel with a medium stiffness of 1 to 2.5 kPa loaded with the growth factors VEGF, FGF-2 and SDF-1α.

In summary, heparin-starPEG gels have been shown to be beneficial for the induction of vascularisation by sustained release of growth factors. Moreover, heparin-starPEG gels can sequester harming cytokines from the wound environment and by that contribute to a relieve of the inflammatory response in the tissue preventing the excess formation of fibrotic tissue. Emerging from these findings is the insight that a proangiogenic response of the membrane with reduced inflammation can be induced by either loading of the immunoisolating memberane with growth factor or an additional layer of a cell-cleavable heparin-starPEG hydrogel loaded with growth factors and/ or MSCs can induce a proangiogenic response of the membrane with reduced inflammation.

5.2 Methods

5.2.1 Preparation of heparin-starPEG hydrogels

Heparin (from porcine intestinal mucosa; Merck, Germany), starPEG-NH_2 (4-armed polyethylenglycol-amine, JemKem Technology), EDC (1-ethyl-3-(3-dimethylamino-propyl)carbodiimid, Iris Biotech) and NHS (N-hydroxy-3-sulfosuccinimid, Acros Organics) were weighted in. During the preparation all components, solutions and MilliQ-water were stored on ice. For the preparation of hydrogels, heparin and starPEG-NH_2 were first dissolved in the calculated amount of MilliQ-water by vortexing. The starPEG solution was additionally homogenised by sonication in an ice-cooled ultrasound bath for 5 minutes. NHS and heparin were dissolved in the calculated amount of water. For the activation of the carboxyl groups of heparin, first the NHS-solution and directly afterwards the EDC-solution was added. After 10 minutes of activation time, the dissolved starPEG-NH_2 was added to the solution with the EDC-NHS-activated heparin and vortexed for 15 minutes. The weighted amounts of the components and volumes of the solutions are given in the following Table 5

Table 5. Components for the preparation of hydrogels for the composite membrane. *The total volume of the mixture is 225 µl, which is sufficient for preparing 10 membranes.*

Component	Batch number	Amount in mg	Volume of MilliQ-water in µl
Heparin	2972517	4.47	127
starPEG-NH_2	ZZ288 P162	9.59	75
NHS	BCBV5863	0.835	8.35
EDC	-	1.47	14.7

For investigation of rheological and stiffness properties, cylindrical hydrogels were produced by the following method. Six hydrogels were produced by pipetting 67 µl of the prepared hydrogel precursor solution onto sigma-coated (Sigmacote®, Sigma-Aldrich, USA) cover glasses (VWR Chemicals) with the diameter of 9 mm and an additional cover glass was placed on top. For polymerisation the gels were stored in a sealed petri dish with water-saturated air environment. The next day 3 hydrogels were incubated in PBS for swelling. The size of the non-swollen gels was measured by a fluorescence scanner and afterwards assessed by rheometry. After 24 hours the swollen gels from the PBS were measured in the same way.

5.2.2 Mechanical characterisation of hydrogels

The rheological properties of the hydrogels were measured by an Ares Rheometer (TA Instruments) via oscillatory shear rheology. The swollen and non-swollen gels were punched to a diameter of 8 mm to fit the plate geometry of the rheometer (8 mm plates) and placed on the lower plate of the rheometer. For a reproducible measurement of each gel the upper plate was moved down until the acceleration force F of 1 g and the distance between the plates was measured. Afterwards the plates were moved apart again and moved down again to 90 % of the gel height to have a matching contact pressure. The measurements were carried out via the TA orchestrator software. The storage modulus (G’ [kPa]) and the loss modulus (G’’ [kPa]) were measured at a range of frequencies from 1 to 100 rad/s and a strain of 3 %. The storage modulus indicates the hydrogel stiffness and can be used to calculate the average mesh pore size of the hydrogels.

5.2.3 Assessment of swelling properties of hydrogels

The swelling properties of the hydrogels were defined by measuring the size of the hydrogel disks before and after swelling in PBS. The gels were scanned by a fluorescence scanner and the diameter of the gels was calculated via 3-point determination with the software MultiGauge. The volume swelling degree was determined via the following equation:

$$Q = \left(\frac{d_{swollen}}{d_{non-swollen}}\right)^3$$

with Q as the swelling degree and $d_{swollen}$ as the diameter of the swollen hydrogel disk and $d_{non\text{-}swollen}$ as the diameter of the unswollen hydrogel disk. The formula relates the swollen volume to the non-swollen volume of the disk assuming that the degree of swelling is the same in all three dimensions. With these results further conclusions could be drawn on the distribution of the hydrogel in the composite membrane.

5.2.4 Preparation of the composite membrane

The composite membrane is prepared by filling an ePTFE with heparin-starPEG hydrogels crosslinked via EDC/NHS chemistry. The ePTFE membrane serves as a carrier providing stability to the heparin-starPEG hydrogel.

ePTFE membrane (Biopore Membrane Filter roll, hydrophilic PTFE; Merck, Germany) was punched into circles of 30 mm and clamped onto custom made polyether ether ketone (PEEK) holders (Figure 40). The hydrogel solution was prepared as described in the above. 20 µl hydrogel solution were pipetted on top of the membrane and distributed with a 39 cm disposable cell scratcher (Sarstedt, Germany) to yield a homogenous distribution. Superfluous material was removed by a spin-coating process for 3 s at 6000 rpm with an acceleration of 4000 rps^2. The short and fast spinning ensured that the wetted membranes did not dry out during the preparation process. Additionally a sigma-coted cover glass was laid on top of the membrane and the whole sandwich was stored in a sealed humidified petri dish over night for crosslinking at room temperature.

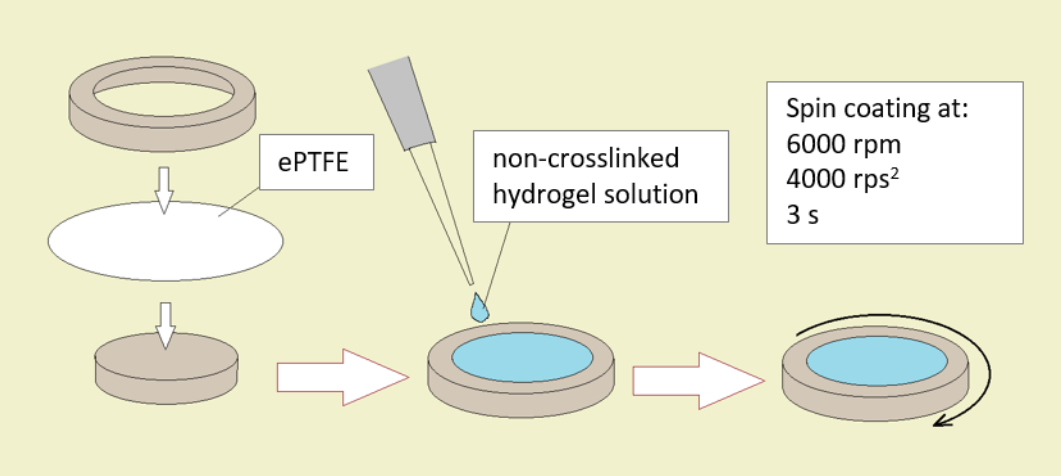

Figure 40. Preparation of composite membranes via spin-coating process.

5.2.5 Analysis of the composite membrane by SEM and EDX imaging

To visualise the composite membrane, scanning electron microscopy (SEM) and energy dispersive X-ray spectroscopy (EDX) was executed. Samples were punched out from the

produced composite membranes and sticked onto SEM sample holders (PLANO GmbH) by conducting carbon pads (PLANO GmbH). The samples were sputter coated with gold in a BAL-TEC *Sputter Coater* for 40 s at 40 mA and visualised by a XL30 Environmental scanning electron microscope (ESEM) with the secondary electron (SE) detector. The imaging was performed at a magnification of 10 000x and a voltage of 5 kV. As a control plain ePTFE membranes were used.

For EDX imaging the mode of the ESEM was switched to the EDX mode. For cross section views the composite membranes were embedded into agarose, cut with a vibratom (Leica VT 1200) and sticked onto profiled sample holders (PLANO GmbH).

5.2.6 Assessment of permeability of the composite membrane

The permeability of the composite membrane was assessed by a diffusion chamber. The diffusion chamber used for this setup is a side-by-side chamber system with an orifice of 11.28 mm diameter (PermeGear, SES-Analytical Systems, Germany). The double wall glass chamber system can be connected to a water circuit to pump water between the outer and the inner wall to keep the inner compartment at a constant temperature. The membrane is clamped between the two chambers, which are pressed together via a screw clamp. The solutions are constantly mixed by a Teflon stir bar laid into a small convexity at each side of the chamber. The volume contained in each side of the chamber is 2 ml and can be filled from the top via an inlet (Figure 41).

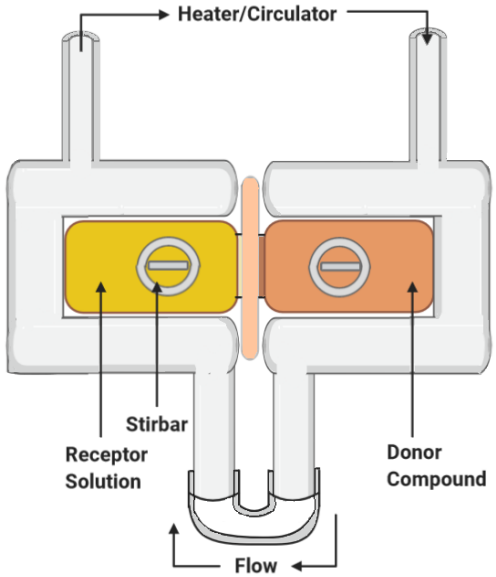

Figure 41. Side-by-side diffusion chamber used to assess the permeability characteristics of the membrane.

For each diffusion experiment diffusion buffer was freshly prepared by adding Kreb's Ringer Buffer (KRB; 136 mM NaCl, 5.9 mM KCl, 1.18 mM KH_2PO_4, 1.2 mM $MgSO_4 \cdot 7\ H_2O$, 3.3 mM $CaCl_2 \cdot 2\ H_2O$, 25 mM $NaHCO_3$), 0.2 % bovine serum albumin (BSA) and 2 mM HEPES. Before the start of each experiment, the chambers were cleaned by Ethanol and preincubated with diffusion buffer for 30 minutes to saturate the chamber walls with BSA and reduce absorption effects of Insulin with the chamber walls. After the washing and preincubation step, the chambers were emptied again and the membrane sample was clamped between the two sides of the chamber. The system was heated to 37 °C by the heating circuit and 2 ml diffusion buffer with a defined concentration of insulin or IgG was pipetted into each chamber. The volumes were stirred at 700 rpm for the whole duration of the experiment. The time was measured from the time point that the solution had been added to the chambers. At the defined time points, 5 µl samples were taken from each side of the chamber, diluted in 145 µl diffusion buffer and frozen at – 20 °C. The insulin concentrations of the samples were determined by a human Insulin ELISA kit (Mercodia, Sweden) according to the manufacturer's protocol.

Fluorescent recovery after photobleaching (FRAP) was applied to determine the diffusion coefficient and mobile fraction within heparin-starPEG coated membranes. Insulin (Insuman Infusat 100 IE/ml, Sanofi) was labeled by Dylight™ 488 NHS Ester (Thermo Fisher Scientific, USA). Briefly, Insulin buffer was transferred into bicarbonate buffer (100mM). Dylight™ 488 NHS Ester was added at 1.5 times molar excess and incubated for 2 h at room temperature. The labelled insulin was purified via a purification column (NanoTemper Technologies, Germany) and the insulin concentration was determined by nanodrop (Thermo Fisher Scientific, USA).

Heparin-starPEG impregnated membranes were produced as described above, though a heparin labeled with Atto647 was used to obtain a fluorescently labeled membrane. Protein solution was prepared containing KRB buffer with 0.2% BSA, 20 mM HEPES, and 2.5 uM insulin-Dylight 488. Membranes were punched to a diameter of 9mm and placed on a glass slide with an imaging spacer with 120µm thickness around them. 10 µl protein solution was added, a cover glass was placed on top and the samples were left to equilibrate for 1 hour. FRAP was performed by a Leica TCS SP5 confocal microscope (Leica) using a 10× magnification objective (HC PL Fluotar 0.30 NA) with FRAP Wizard software (Leica). A time-series of 20 pre-bleach frames was recorded every 141 ms (resolution of 256 x 256 pixels, attenuated argon laser beam with 80 % output and 4 % transmission. A spot with a radius of 20 µm was bleached with full laser intensity of the combined laser lines at 488, 576, and 495 nm for 5 frames (~600 ms). A post bleach image series was taken of 100 frames for 140 ms and additional 120 frames at 1 s intervals at low laser intensity of 4 %. T- half (half time until

full intensity is reached) and the mobile fraction were extracted as described by (Koulouras et al., 2018). The diffusion coefficient (D) was calculated according to the following formula

$$D = \frac{w^2}{T - half}$$

where D is the diffusion coefficient and w the radius of the bleached spot.

5.2.7 *In vitro* biocompatibility assessment by blood compatibility assays

Insights into the biocompatibility of the composite membrane were obtained by a blood-compatibility assay measuring the activation of the complement system. For this experiment the composite membranes were clamped into custom designed incubation chambers as depicted in the following Figure 42. Glass, Teflon and membranes coated with alginate were chosen as controls and clamped into additional chambers. Each condition was tested in triplicate. All components and membranes were sterilised by autoclaving before usage for the experiment. Fresh whole human blood was taken and mixed with 1.7 IU/ml heparin. 1.5 ml of this mixture was filled into each chamber. The chambers were rotated for three hours at 37°C to prevent coagulation. After the incubation period the blood was removed from the chambers and the activation of the complement system was assessed by determining two complement factors. The concentration of C5a was measured by a C5a ELISA (DRG International, Inc., USA) according to the instructions of use. C3b at the surface of the membranes was determined by a C3b surface ELISA. The membranes were washed subsequently with veronal buffer (Lonza, Basel) and distilled water and incubated with mouse anti-human C3c antibody

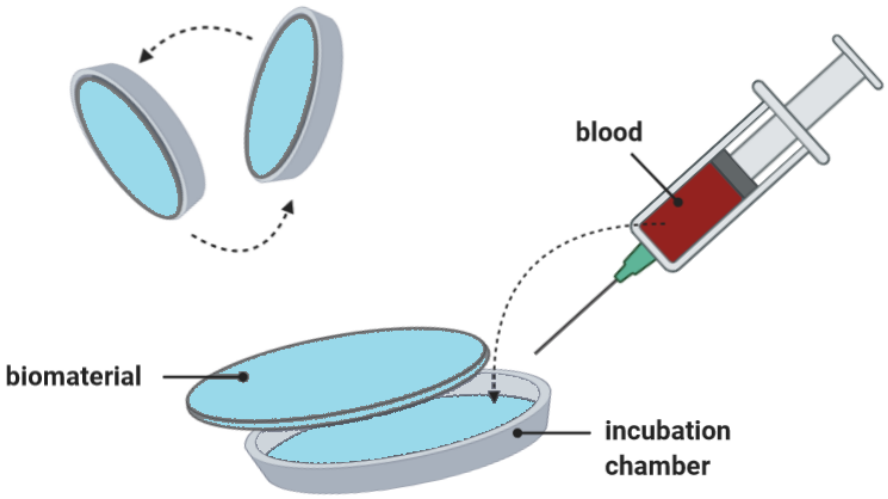

Figure 42. Blood incubation chamber for blood compatibility assessment.

conjugated with horse radish peroxidase (DakoCytomation, Golstrup, Denmark). After 60 minutes the surfaces were washed with phosphate buffered saline (Sigma-Aldrich, USA) with 0.1% Tween20 (Sigma-Aldrich, USA). Substrate buffer containing o-phenylenediamine dihydrochloride (Sigma-Aldrich, USA) 5 mg / 10 ml ureaperoxide buffer (Sigma-Aldrich, USA) was added on the surfaces as a substrate for the HRP. After 20 minutes the reaction was stopped by 1M HCl and the absorbance was read at 450 nm with a TECAN fluorescent multiplate reader.

5.3 Results

The foundation of an immunoisolating encapsulation device lies on the principle of preventing the contact of the host immune system with the transplanted tissue. In this novel cell encapsulation device, immunoisolation is established by a composite membrane with permselective properties. A set of requirements for the composite membrane have been defined: Selectivity and permeability, biocompatibility and angiogenesis-stimulating properties, stability, sterilisability, and applicability for clinical usage. In this thesis, a focus has been laid on an applicable and scalable manufacturing process, suitable selectivity and permeability parameters and an *in vitro* approach to assess the biocompatibility of the membrane. Furthermore, a protocol for the *in vivo* evaluation of biocompatibility and angiogenesis-stimulating properties is proposed and characteristics playing a role for stability, sterilisability, and applicability for clinical usage are discussed.

5.3.1 Mechanical and swelling properties of hydrogels

The immunoisolating properties of the composite membrane are established based on the principle of size exclusion. Molecules that are smaller than the mesh size between the polymers of the hydrogel can pass the membrane. The characteristics of relevant molecules are discussed in above. By assessing the rheological properties of the hydrogel component of the composite membrane, the theoretical pore size can be estimated.

Heparin-starPEG hydrogels were fabricated at different crosslinking degrees and solid content expected to reach a relevant stiffness based on lab internal data. The results of the executed experiments were in accordance with the general expectations about the hydrogel network. Hydrogels with the same solid content had a higher stiffness with increasing crosslinking degree as the networks were getting denser (Figure 43). Gels with the same crosslinking degree but lower solid content became softer as reactive groups are less concentrated during the reaction. The results presented in Figure 43 are a selection of a data set of hydrogels created with different crosslinking degrees and different solid content. Furthermore, these are the results with the lowest possible crosslinking degree for their respective solid content as

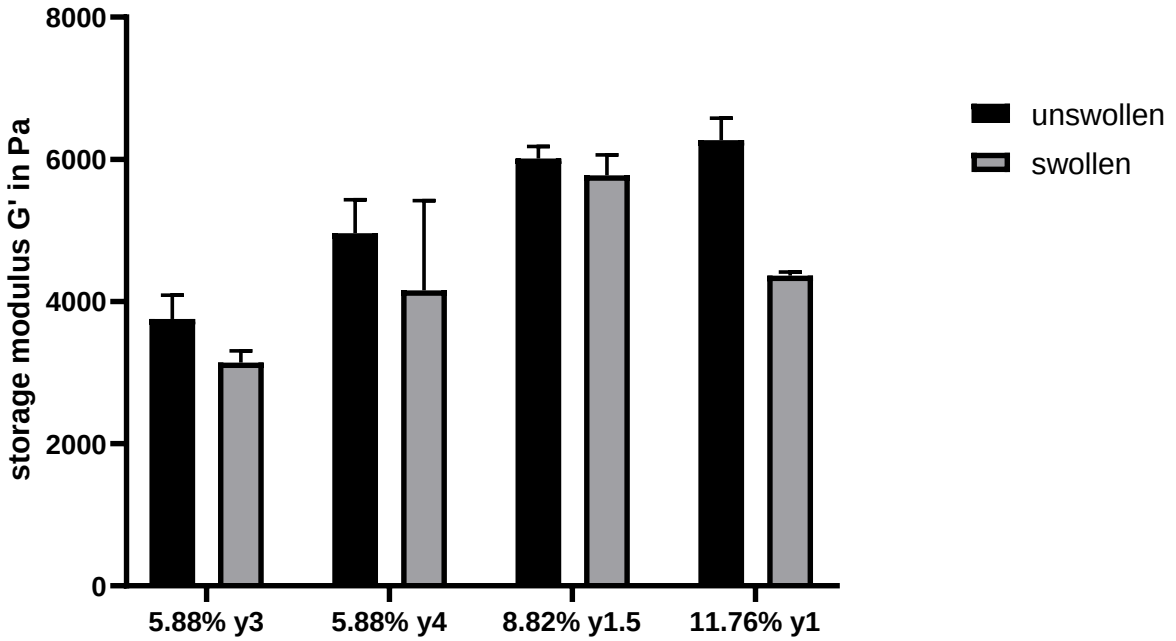

Figure 43. Storage modulus G' in Pa at different degrees of swelling of heparin-starPEG hydrogels with different solid content and crosslinking degree (y).

gels with a lower crosslinking degree did not crosslink. For gels with a higher solid content of 11.76 %, hydrogels with a crosslinking degree (γ) of 1 had a comparable storage modulus to gels with half the solid content of 5.88 % with a higher crosslinking degree.

The degree of swelling for the different hydrogel configurations is presented in Figure 44. As expected the swelling of gels with a lower solid content is much lower than for hydrogels with a higher solid content. The hydrogels with a lower solid content are more close to an equilibrium state than gels with a higher solid content and therefore take up less water in their hydrophilic polymer network chains.

Preliminary experiments showed that composite membranes with heparin-starPEG hydrogels with a lower solid content had a higher permeability for insulin than gels with a higher solid content. Therefore it was hypothesised that the swelling of the hydrogels in the pores is restricted due to the limited space within the pores and assumed that the hydrogels are equilibrating into a state between the swollen and the unswollen state as the polymer chains cannot move unrestrictedly. To estimate the range of the pore size of this semi-swollen state, the storage modulus of the unswollen state was measured as well (Figure 43).

The lowest storage modulus and swelling degree is reached by crosslinking heparin and starPEG at a crosslinking degree of 3 and a solid content of 5.88 %. In the unswollen state the gels had a storage modulus of 2440 ± 324 Pa, which results in a calculated pore size according to the rubber-elasticity theory between 11.4 and 12.4 nm. In the swollen state the storage modulus for these gels is 2120 ± 437 Pa resulting in pore size of 11.7 to 13.4 nm. When

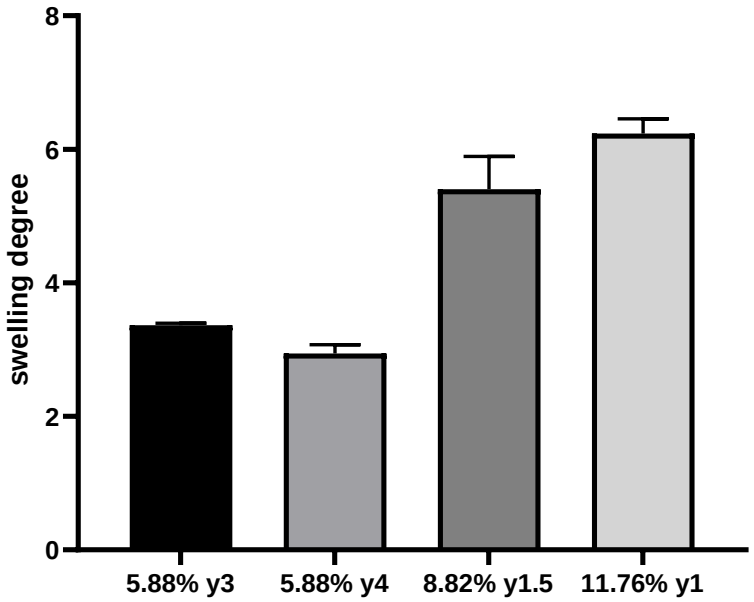

Figure 44. Swelling degree of heparin-starPEG hydrogels with different solid content and crosslinking degree (y).

infiltrated into the pores of the ePTFE membrane, the semi-swollen state can hypothetically reach a ‘mixed’ pore size of 11.4 to 13.4 nm.

5.3.2 Microscopic analysis of the composite membrane by SEM imaging and EDX

Heparin-starPEG hydrogels with a crosslinking degree of 3 and a solid content of 5.88% have been chosen for further investigations as these have the lowest swelling degree and a suitable network mesh size for the selective properties for an immunoisolating membrane. The composite membranes were produced by a spin-coating process. For this, the membranes were fixed into a circular frame and the hydrogel precursor solution was spread on top by a cell scraper. The membranes were spinned in a spin coater to remove excess material and distribute the material homogenously. The optimal settings of rotational speed and acceleration were constituted, that wetted the membranes completely though prohibited drying out of the membranes as described above.

The composite membranes, prepared from an ePTFE membrane coated with heparin-starPEG hydrogel, were imaged by SEM for a qualitative analysis of the impregnation method. The control image for a native ePTFE membrane revealed the structure of the membrane. Here, the expansion during the production process can be seen by the oriented fibril structures (Figure 45 a,b). The surface of the composite membrane has the same underlying structure, which is masked by the thin layer of heparin-starPEG hydrogel. The hydrogel fills up the pores between the struts of the pores. The cracks of the fibrils are likely to be artifacts from the applied electron beam during the imaging process, which creates tensions in the material. SEM

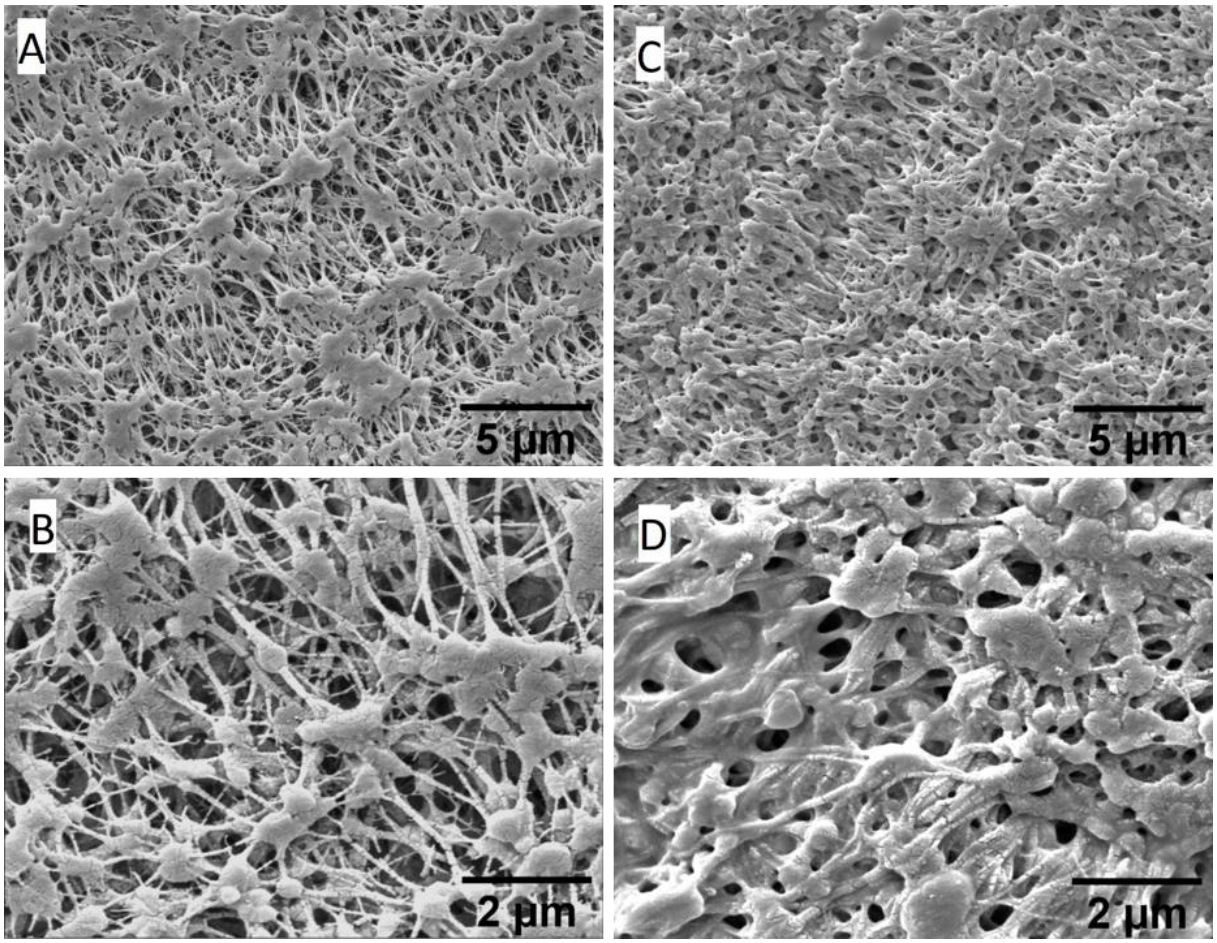

Figure 45. SEM of native (A,B) and composite membrane (C,D). A, C: *10000x magnification (scale bar: 5 µm),* ***B, D****: 25000x magnification (scale bar: 2 µm).*

is carried out within a vacuum, which requires the drying of the samples before imaging. The hydrogels are thus not in a swollen state during the imaging process, which does not represent the original state of the material. Pores that are not filled completely might be due to contraction of the hydrogel due to the drying process.

To further examine, whether and how consistently the polymer components penetrate into the pores of the membrane, cross sections of the membrane were analysed by energy-dispersive X-ray spectroscopy (EDX). EDX is an analytical technique to reveal the elemental composition of a sample. The two singular components of the membrane each have an atom, which is not abundant in the other component. For PTFE fluor is the characterizing primary atom that is not available in heparin and visible in the X-ray spectra. For heparin sulfur is the unique atom that is not present in PTFE. The surface analysis by EDX reveals that the polymer is penetrating throughout the whole membrane with a thicker layer at the outside of the membrane (Figure 46).

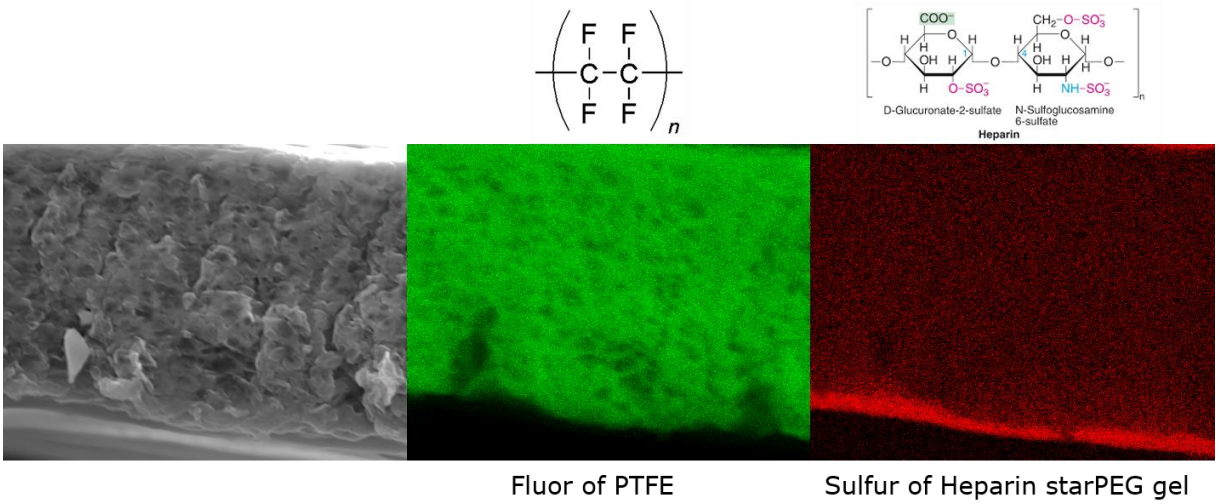

Figure 46. Energy-dispersive X-ray spectroscopy (EDX) of a cross section of the membrane. Left *SEM view.* ***Middle*** *Intensity distribution of fluor atoms abundant in PTFE.* ***Right*** *intensity distribution of sulphur atoms abundant in heparin.*

5.3.3 Assessment of permeability of the composite membrane

To proof the selectivity of the composite membrane, a diffusion assay of IgG over the membrane was established. A composite membrane was fixed between two glass chambers filled with a physiologic salt buffer. At one side of the membrane human plasma IgG was given to create a gradient over the membrane. To investigate other effects, e.g. adsorption to the membrane or glass that could influence the concentration of IgG, experiments without a gradient were carried out. For these IgG was given on both sites of the membrane. Over 24 hours samples were taken from both sides of the chamber to assess whether IgG was penetrating through the membrane.

In the first 6 hours of incubation, the IgG concentration was increasing in the gradient and non-gradient condition (Figure 47 a). After 6 hours the concentration stayed consistently high. This unexpected increase can be attributed to specific aggregation effects of IgGs. These tend to create aggregates, which are removed by a filtration step during the processing, though small aggregates still remain. During the storage these small aggregates act as seed aggregates for larger aggregates. When the large aggregates are disturbed due to the mechanical stirring by the stir bar during the experiment, these large aggregates are falling apart again and are contributing to the higher measured concentration of IgG.

The percentage of penetration of IgG through the composite membrane is depicted in Figure 47 b. At the first time point of 5 min, 1.3 % of the total IgG detected at the source site of the membrane was detected at the sink site of the membrane. At all later time points the detected percentage of IgG is less than 0.32 %.

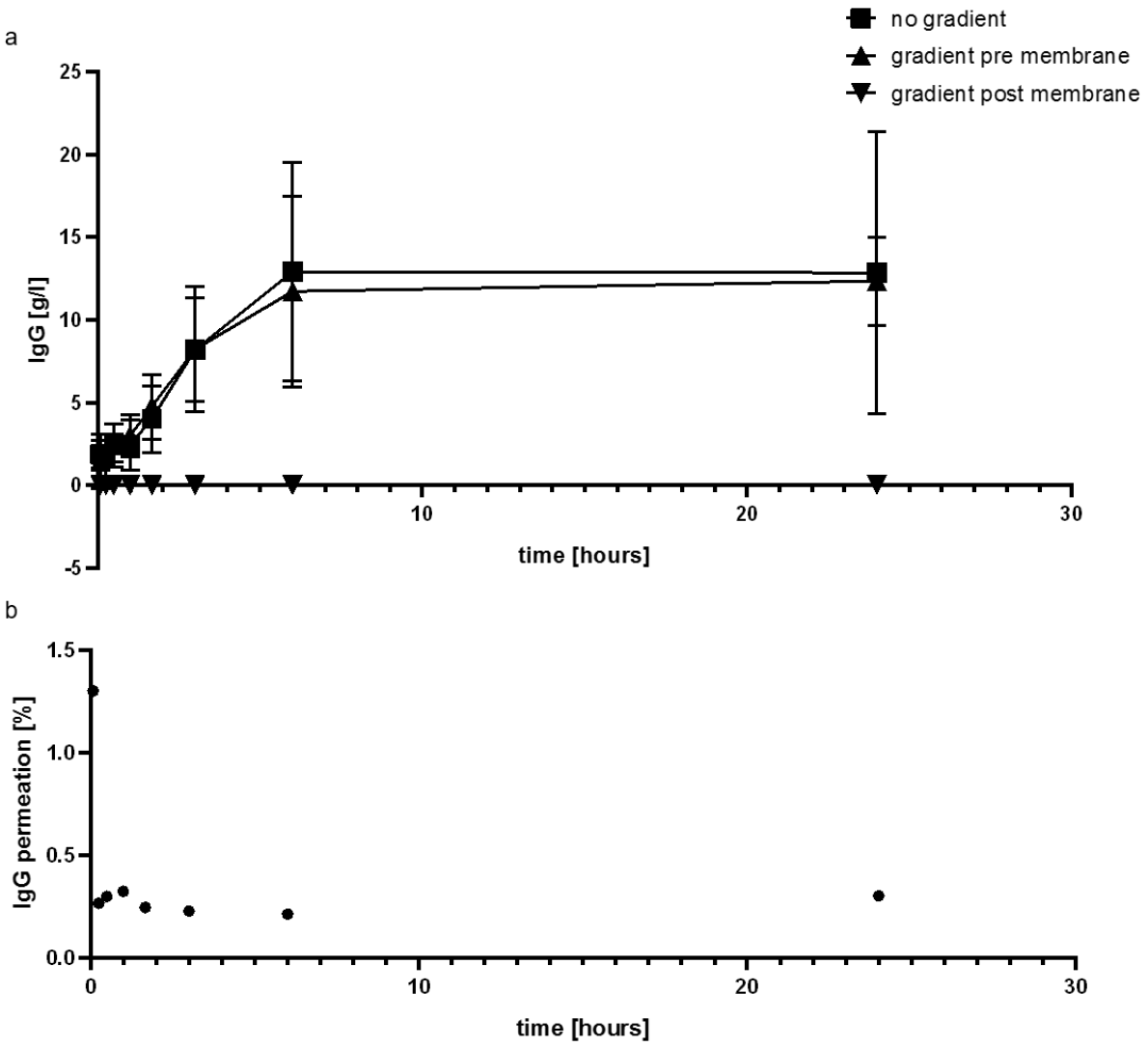

Figure 47. Assessment of selectivity of the composite membrane. *The diffusion of IgG over heparin-starPEG coated ePTFE membranes was investigated by creating a gradient of IgG over the membrane (n=6).* ***a*** *Total concentration of IgG in the compartments at the sink and the source site of the membrane with and without a gradient.* ***b*** *Percentage of penetration of IgG at the sink site of the membrane.*

To assess the diffusion of insulin over the membrane, FRAP was applied. For this technique Insulin was labeled with Dylight488 fluorescent dye and the diffusion of the fluorophores within the composite membrane was investigated. FRAP is based on the principle that after bleaching a spot of the sample, fluorescent molecules from the surrounding are diffusing into the spot. The migration of these molecules is observed by the fluorescence intensity, which is increasing over the time.

T-half, the time at which half of the intensity is regained in the bleached spot, is 1.392 s for insulin in solution labeled with a Dylight488 fluorophore (Figure 48). For insulin diffusing inside the composite membrane immersed with heparin-starPEG hydrogel with a crosslinking degree of 3 or 4, T-half is 1.998 s and 2.076 s, respectively. The derived diffusion coefficient (D) for insulin in solution is 287.35 $\mu m^2/s$, in composite membranes with a crosslinking degree of 3 D is 200.20 $\mu m^2/s$ and for composite membranes with a crosslinking degree of 4 D is 192.6782 $\mu m^2/s$. The mobile fraction represents the fraction of molecules, which can freely diffuse. The mobile fraction of insulin within the immunoisolating membrane is lower than in solution. Within heparin-starPEG hydrogels with a crosslinking degree of 3 or 4 the mobile fraction is drastically decreased to 0.53 and 0.47 ($p = 0.0001$ and $p < 0.0001$) when compared to insulin in free solution (mobile fraction = 0.96).

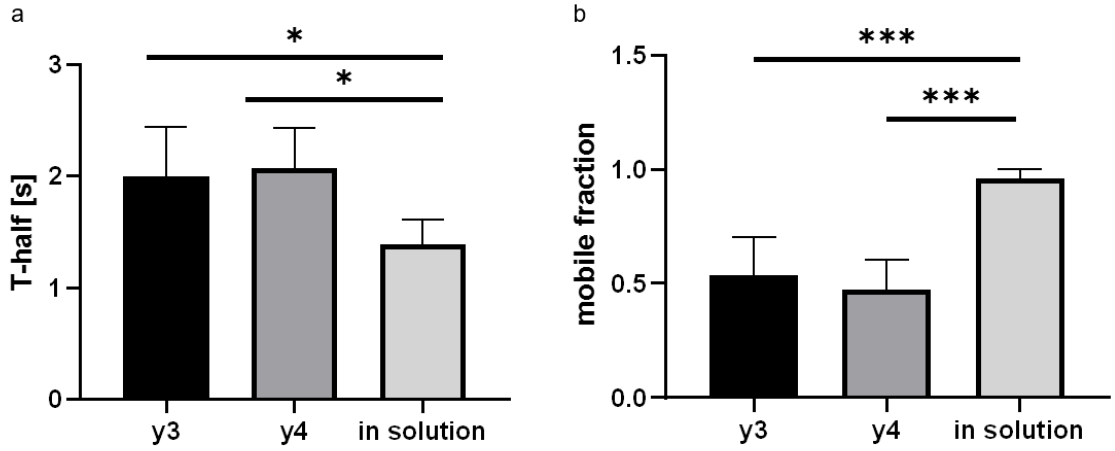

Figure 48. Fluorescence recovery after photobleaching (FRAP) of insulin-Dylight488 in solution or the composite membrane. a *T-half (half maximal recovery time) of the regained fluorescence intensity.* ***b*** *Mobile fraction representing the fraction of the molecules that can freely diffuse (n=5-6).*

Heparin is a molecule that transiently binds to many molecules. The comparably low mobile fraction of insulin might be explained by the interaction of insulin with heparin. To exclude such an effect between insulin and heparin, microscale thermoresis has been performed (Appendix 10.1). This method is based on the principle that molecules transiently interacting with each other move slower with solution. No effect on the mobility of insulin could be detected with increasing heparin concentration. Therefore the reduced mobility can only be explained by the obstructive diffusion pathway, rather than an interaction with the network polymers.

5.3.4 *In vitro* biocompatibility of the composite membrane

The foreign-body response in an implantation setting against the cell encapsulation device deposits a fibrotic layer on the outside of the capsule. This layer delays the diffusion of functional metabolites and nutrients between the outside and inside of the membrane. We modeled the initiation of this foreign body reaction in an *in vitro* setting by incubating the membrane with full human blood. The complement system is part of the innate immunity and rapidly activates upon contact with foreign material (Mödinger et al., 2018). After incubation of the membranes for 3 hours in whole blood, the activation of the complement cascade was assessed by measuring the concentration of complement factor 5 in the blood and the deposition of complement factor 3a on the surface. Both complement factor had similar levels of activation for the different applied surfaces (Figure 49). Native ePTFE membrane had the strongest activation of the complement cascade, while composite membranes (coated with heparin-starPEG) activated the membranes to a level comparable to the negative controls (Teflon AF and glass). To compare the heparin-starPEG hydrogel coating to other immunoisolating membranes previously applied for macroencapsulation devices, the complement activation of ePTFE membranes coated with alginate (as applied in the βAir device) was measured as well. These alginate-coated membranes activated the complement cascade comparably strong as the native PTFE.

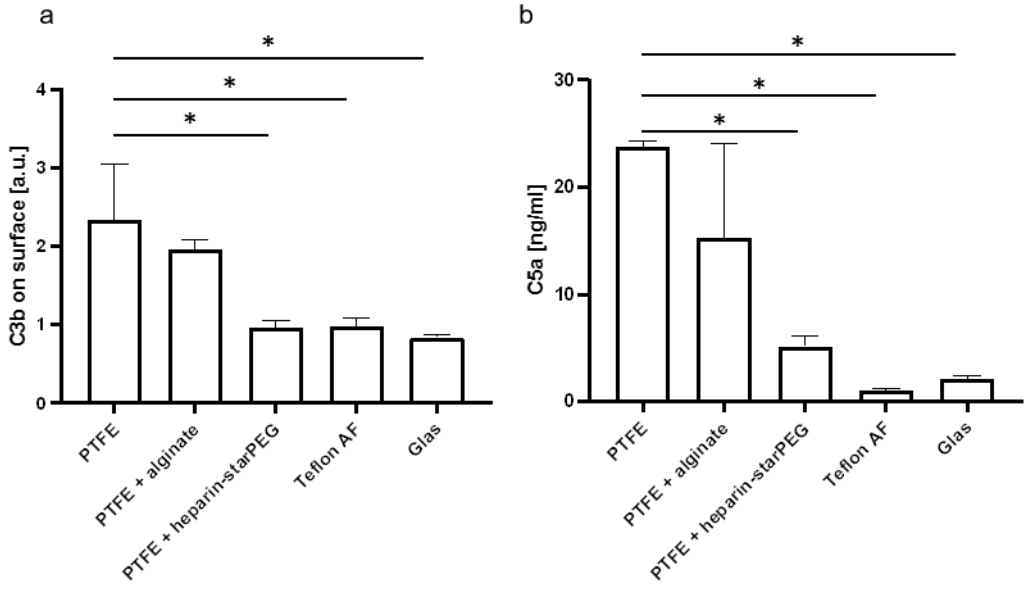

Figure 49. In vitro biocompatibility of the composite membrane assessed by the activation of the complement system. a *Deposition of complement factor 3 on the surface.* ***b*** *Levels of complement factor 5 in the blood.*

In conclusion, composite membranes coated with heparin-starPEG evoke lower levels of activation of the complement system compared to a previously applied alginate-coated membrane as used for the βAir encapsulation devices.

5.4 Discussion and outlook

In this chapter a concept of an immunoisolating membrane with tuneable permeability has been developed. For coating, the microporous polymer network a profound hydrogel system, consisting of the ECM-compound heparin in combination with the synthetic starPEG, was chosen. This hydrogel has advanced properties, which are of great advantage for the application in an immunoisolating membrane. The electrostatic charge of the heparin compound can bind inflammatory chemokines at the implantation site and can be loaded with vascularising and trophic growth factors stimulating vascularisation at the implantation scene. The mesh size of hydrogel polymer network can be determined by the stiffness. Therefore the stiffness (G') of heparin-starPEG hydrogels with varied crosslinking degrees and solid content was empirically investigated by rheology. For the application of the hydrogel on the membrane a method to homogenously coat an ePTFE membrane by a spin-coating process has been developed. Next, a set of methods has been developed to study further parameters of the membrane. Surface and cross-section analysis by SEM and EDX were used to study the morphology and showed complete filling of the pores of the ePTFE membrane by the hydrogel material. A first series of FRAP experiments has been performed to determine the diffusion coefficient of insulin within the composite membrane that defines permeability. The selectivity to prevent components of the immune system to pass the immunoisolating membrane has been investigated with the model protein IgG. The biocompatibility of the membrane has been investigated by a blood compatibility assay, which showed a reduced activation of the developed composite membrane for the complement system. Finally, an animal experiment has been proposed to study the optimal parameters for a proper vascularisation of the membrane, which is key to a sufficient supply of nutrients and oxygen to the encapsulated cells.

For the clinical application of the composite membrane next to the spin coating technique a spraying of the hydrogel precursor solution might be suitable. For this procedure quality controls need to be established. One would be visual: upon wetting the membrane its opacity changes to transparent. Furthermore, the permeability could be checked by exploiting the diffusion setup. Through testing the passage of the model proteins insulin and IgG, the function of the coating could be controlled.

Some of the experiments described above are not yet executed with the necessary repetitions required for a good scientific practice. Therefore the described methods are rather proof of principle developments and pave the way for final optimisation steps for the immunoisolating membrane.

Comparing the resulting diffusion coefficient D of insulin with values derived from literature (e.g. 150 $\mu m^2/s$ (Skrzypek et al., 2020), 116 $\mu m^2/s$ (Shorten et al., 2007)), a relatively high D of 287.35 $\mu m^2/s$ has been measured by FRAP for insulin in solution. This might rely on the method of measurement. When calculating the apparent D as in the model introduced by Lustig and Peppas (1988) for the diffusion of solutes in hydrogels, a resulting value is 146.86 $\mu m^2/s$ (for ξ = 11.4 nm, r_s = 2.4 nm, and Q = 3.3). This is value is also higher than the observed D for labelled insulin in the composite membrane. Reasons for the abbreviation of D might be that the hydrogel polymers cannot reach a state of relaxed equilibrium within the pores of the membrane. To find an approximation of the polymer network state, the stiffness of the hydrogels in an unswollen condition has been investigated and found to deliver a “softer“ gel which might explain the divergence of D. Further reasons might be that the calculation of the diffusion characteristics from FRAP is based on the assumption that the diffusing molecules can diffuse freely in all directions. However, the macroporous structure of the ePTFE might interfere with these movements. Further FRAP experiments will have to be performed to solidify these results. A further method to estimate the diffusion of insulin over the composite membrane were experiments applying a diffusion chamber setup as applied for the permeability estimation of IgG. However, surface adsorption effects interfered with the reproducibility of this data.

At the time of this study the vascularisation properties of the hydrogel *in vivo* has only been briefly investigated. The implantation of the cell-cleavable version of the heparin-starPEG hydrogels revealed at a later date, that the material causes haemorrhage when the hydrogels degrade over time. In this study a different version of the hydrogel chemistry namely with non-cleavable linkers with a different crosslinking chemistry (amide bond via EDC-NHS chemistry rather than a thiol-maleimide reaction) was used, which doesn’t degrade as easily through cell-secreted enzymes. Still, for increased safety we propose to apply the desulfated version of the heparin component (Atallah et al., 2018) and repeat the investigated methods. The desulfated heparin has less charges and has been shown to have a higher and prolonged release, compared to the normal heparin.

For the application of the developed composite membrane further work has to be done to investigate the sterilisability of the membrane. This might be possible for example by γ-radiation. Furthermore the applicability of the heparin component has to be investigated. Since heparin applied in this study is derived from porcine mucosa this might be a hurdle in the translation into a good manufacturing practice (GMP) conform production process for a clinical setting.

The final membrane membrane surface shall have the correct immunoisolating properties in combination with a good biocompatibility. Both are presumingly possible with application of

heparin-starPEG hydrogels, which will be investigated further in the proposed animal experiment. The application of MSC on the membrane which can attach via their integrin receptors to RGD-cell attachment sites, are expected to have a superior effect on the integration at the implant site via their immunomodulatory role and vascularisation stimulating effects. This has been shown for instance in the Theracyte™ device (Wang et al., 2015) or the induction of vascularisation in a chicken embryo CAM assay by growth factor release from heparin-starPEG hydrogels (Zieris et al., 2011).

5.4.1 Concept for *in vivo* biocompatibility assessment and vascularisation properties of the composite membrane

The vascularisation and biocompatibility of the surface of the implant is key to a proper function of the encapsulated cells. The closer capillaries are formed in proximity to the membrane the faster molecules, especially oxygen, can diffuse towards the encapsulated cells. Former studies have shown that heparin-starPEG hydrogels have a positive effect on angiogenesis and wound healing (Freudenberg et al., 2015; Lohmann et al., 2017; Schirmer et al., 2020). Therefore a concept for the *in vivo* evaluation of heparin-starPEG hydrogels in different combinations with the membrane has been developed.

Heparin-starPEG hydrogels can be produced via different crosslinking chemistries and with or without cell-cleavable linkers. For the immunoisolating function of the composite membrane a hydrogel with NHS-EDC chemistry without cleavable linkers has been chosen (blue layer, Figure 50 a). This ‘basic’ version of the immunoisolating membrane has been optimised in the previous subsections for its pore size, selectivity, permeability and biocompatibility. In the following experiment, the immunoisolating membrane will be supplemented with additional growth factors, cell-cleavable hydrogel layers and/or mesenchymal stromal cells in various combinations to create an optimal microenvironment for vascularisation on the immunoisolating membrane.

Cell-cleavable heparin-starPEG hydrogels of medium stiffness (1.0 to 2.5 kPa) loaded with various growth factors have been shown to have the highest potential to create a vascularisation-stimulating environment (Schirmer et al., 2020), though the specific optimal stiffness and growth factor load have not been determined. To find the optimal conditions of these parameters, an experimental design based on DOE (chapter 4) has been developed. In more detail, to find the optimal conditions a response surface (response surface methodology) is determined. Here, based on the measurement of a set of combinations of the chosen variables, a ‘heatmap’ is created depicting the optimal combination of the variables.

The implant with modified surface characteristics shall be implanted in Wistar rats to find the optimal vascularizing hydrogel parameters. The application for an animal license requires an

estimation of the sample size to reach a certain power and confidence interval and needs to be assumed based on the mean and standard deviations derived from previously attained data. For this optimisation experiment, two factors have been considered for to reach an optimal vascularisation response: the growth-factor load and the stiffness of the hydrogel. These are varied each over three levels and span the matrix of the to-be-estimated response surface (heatmap), each taking up one dimension. A full factorial design of this response surface therefore consists of 3^2= 9 combinations (figure). This design consist of a centre point (0), corner points (c) and star points (s).

Data evaluating the vessel density based on these two variables have been published by Schirmer et al. (2020), Figure 6b. The variance of this data relates to the square of the mean of the readout variable vessel density, e.g. a four-fold increase of the mean brings along a 16-fold increase of the variance. Therefore, a log transformation of the readout parameters has been performed to stabilise the variance. Based on this data and with support from the 'Institut für medizinische Biometrie' at the University Hospital Carl Gustav Carus, various combinations of repetitive sampling have been analysed to calculate the confidence interval and the maximal standard deviation of the prospective response surface. In more detail, the sample number of centre points (0), corner points (c) and star points (s) has been varied (Appendix 10.2). Furthermore, an indifference margin δ of 20% has been assumed. On the log-scale this transforms to log(1.2) = 1.8 and the simple width of a (90% or 95%) confidence interval for predicting the expected readout value should not exceed this value anywhere in the range studied.

A further parameter to be defined in the application of the hydrogel as a vascularising environment for the proposed animal experiment is the thickness of the hydrogel applied on top of the immunoisolating membrane. Prokoph et al., (2012) investigated the migration of endothelial progenitor cells (EPCs) isolated from human blood into cell-cleavable heparin-starPEG hydrogels and showed that EPCs migrate 40 µm over 72h (13.3 µm per day). For the application on the membrane, a thickness of around 100 µm will be chosen, which should be repopulated over a time frame of 7 days.

The readout parameter for the evaluation of the vascularisation on the implant surface is going to be the CD31 positive (endothelial cells) stained area. Further parameters investigated will be the abundance of immune cells and the developed fibrotic layer.

After establishing the optimal hydrogel parameters as explained above, a second set of experiments is planned. The hydrogel layer optimised for vascularisation as determined in the above first set of experiments will be evaluated against other variants of the immunoisolating membrane. These are:

1) A native ePTFE membrane without any coating. This material has been proven to be a good vascularizing material in studies executed by Baxter Healthcare (Papas et al., 2019) for the development of the Theracyte™ encapsulation device (Figure 50 a) .
2) An ePTFE membrane impregnated with high mannuronic (HM) acid alginate at 6% (w/v) under vacuum and crosslinked by 30mM $BrCl_2$ as applied in the BetaAir encapsulation device by $BetaO_2$ Technologies (Figure 50 b).
3) An ePTFE membrane impregnated by desulfated heparin-starPEG hydrogel based on the gel parameters as described in this chapter (Figure 50 c).
4) A membrane as described in 3) in combination with a cell-cleavable hydrogel without growth factors. Growth factors might pose difficulties in the process of admission of approval. Therefore this data are of interest (Figure 50 d).
5) A membrane as described in 3) doped with growth factors at the concentration determined in the first set of experiments (Figure 50 e).
6) A membrane as described in 3) with the optimised cell-cleavable hydrogel with growth factors as determined in the first set of experiments (Figure 50 f).

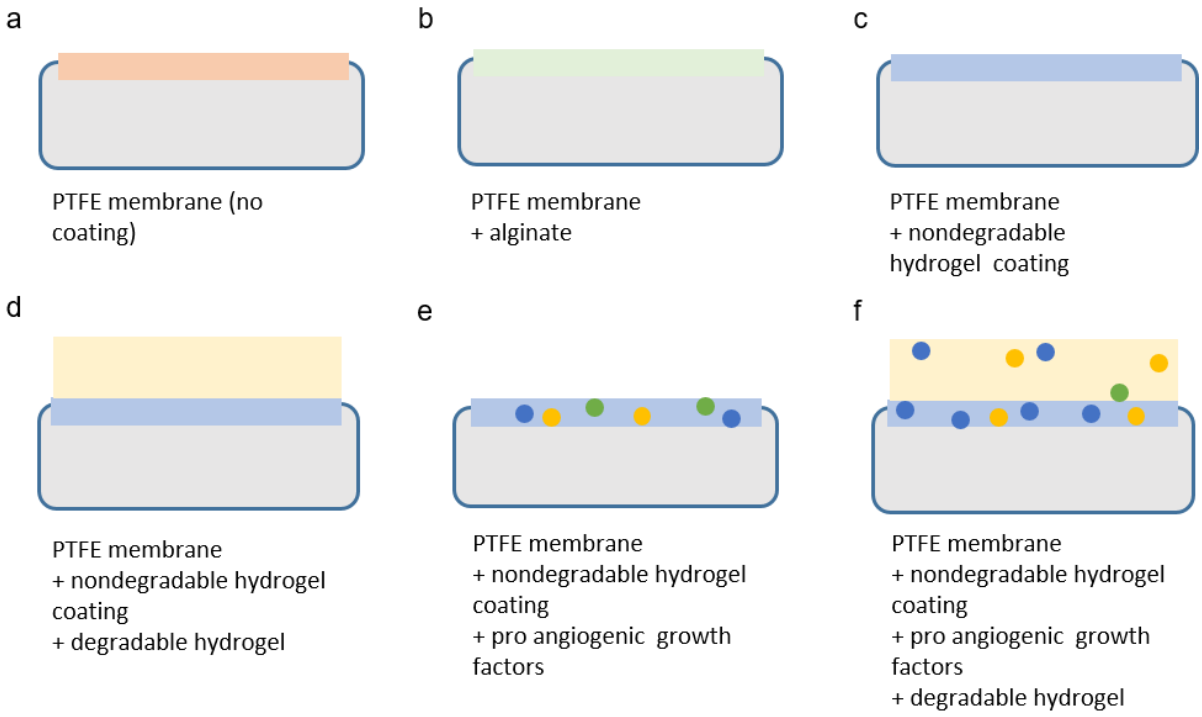

Figure 50. Preparation of variants of the immunoisolating membrane for in vivo biocompatibility and vascularisation analysis.

MSCs have been shown repetitively to have an immune modulatory effect on their environment and support vascularisation processes. Therefore in a third set of experiments in combination with syngeneic derived MSCs the variants 3) - 6)will be implanted (Figure 51).

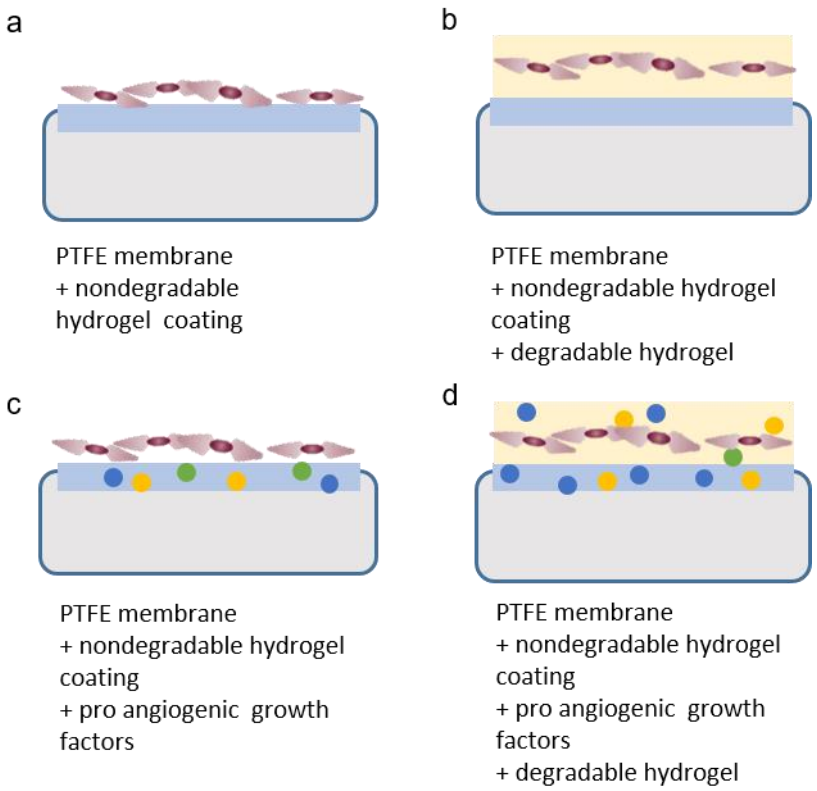

Figure 51. Preparation of variants of the immunoisolating membrane for in vivo biocompatibility and vascularisation analysis in combination with mesenchymal stem cells.

In summary, three sets of experiments have been designed to determine an optimal vascularisation environment around the implant. The first experiment studies the parameters stiffness and growth factor loading of cell-cleavable heparin-starPEG hydrogels and determines a response surface to choose the optimal parameters of these factors. The second set compares this optimised variant against other versions of the immunoisolating membrane. The third set of experiments combines the vascularizing gels with MSCs to use their immune-modulatory and vascularisation-stimulating effect to improve the environment around the implant.

5.5 Acknowledgements

Parts of the experimental work described in this chapter (measurement of swelling degree, rheology, IgG permeability) were executed by Annika Möller in the framework of her Bachelor's thesis (Berufsakademie Riesa, Germany).

6 Islet oxygenation during early post transplantation phase

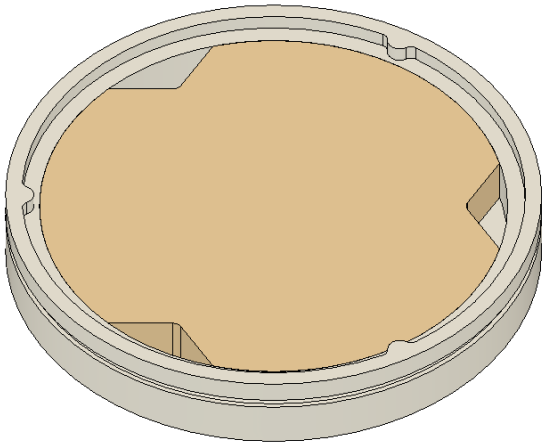

6.1 Introduction

For a successful transplantation of encapsulated islets it is crucial that the islets continuously have sufficient oxygen available. Particularly during the early post transplantation phase a lack of oxygen is critical. During the islet isolation process, the islets have lost their vascularisation and are then encapsulated to deny access of the immune system. The immunoisolating barrier on purpose prevents the possibility of a revascularisation of the islets. At physiological tissue oxygen pressure, the oxygen diffusion from the capillaries in the surroundings hypothetically can keep up the oxygen supply of the cells as the islets within the device are arranged accordingly (chapter 4). However, in the early post transplantation phase, the tissue surrounding the implant is compromised due to the tissue damage from the surgery. Until a physiologic oxygen condition is reached again, capillaries need to develop in close proximity to the implant.

Various approaches have been made to overcome this initial lack of oxygen, for example, by prevascularisation of the encapsulation device as realised in the Defymed device (Defymed, 2021). This device is implanted for several weeks before the islets are filled into the device via a port system.

In the here proposed encapsulation device, the islets are arranged in a pre-defined regular array, which prohibits the filling via a portsystem at a later stage. Therefore, other means of initial oxygen supply were explored.

In the field of tissue engineering, oxygen-releasing biomaterials have been described which release oxygen for a limited time induced via a chemical reaction with water. Such system might bridge the initial critical phase early after implantation when a proper revascularisation has not yet been established. In chapter 4, an experiment to determine the optimal partial oxygen pressure supporting islet integrity has been described as 1.8 mg/l (40 mmHg). This reflects also the concentration, that must be provided by an oxygen generating material for at least the first few weeks after implantation. However, the oxygen should also not exceed a certain concentration. As indicated by *in vitro* experiments, oxygen concentrations of 24.1 mg/l and 30.5 mg/l may induce toxic effects on the islets (Komatsu et al., 2017).

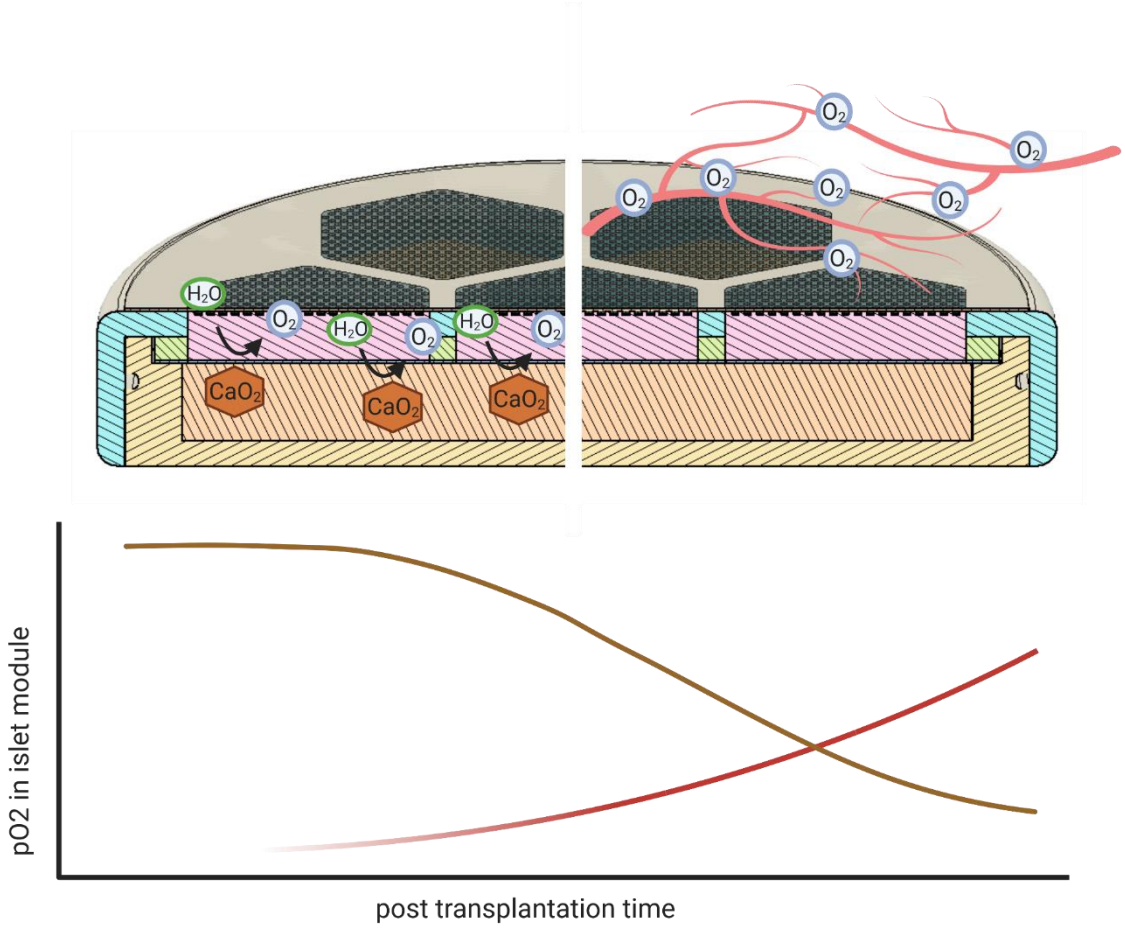

Figure 52. Continuous oxygen supply to the encapsulated islets directly after implantation and during long-term engraftment of the implant. *During the initial time of implantation, oxygen is provided from the oxygen module via a degradation process of the integrated calcium peroxide. After some time the implant surface is vascularised from the host tissue and oxygen is provided via diffusion from the capillary, when the oxygen reservoir from the oxygen module is exhausted.*

6.1.1 Oxygen provision by oxygen-generating materials

Oxygen-generating materials release oxygen via a chemical reaction. The oxygen is chemically bound and set free by a decomposition reaction. Most applied materials are solids. In contrast to oxygen gas, these can be included into a tissue scaffold in a condensed format and the oxygen is available directly at the site where it is needed.

These oxygen-delivering molecules belong to the group of the peroxides and are characterised by a peroxo group (R-O-O-R) with the oxidation status of -1. This is a metastable configuration as the free electron pairs of the oxygen are interacting with each other. The solid peroxides Calcium peroxide (CaO_2), Magnesium peroxide (MgO_2) and sodium percarbonate ($(NaCO_3)_2 \cdot H_2O_2$) are the most studied ones for oxygen production in tissue-engineering applications.

MgO_2 has a decomposition temperature of 88°C and a solubility with an equilibrium coefficient of $9.8 * 10^{-9}$ (Waite et al., 1999). CaO_2 is a pale yellowish powder and has the highest decomposition temperature of the mentioned peroxides of 275°C and a low solubility with an equilibrium coefficient of $1.8 * 10^{-11}$ (Waite et al., 1999). $(Na_2CO_3)_2 \cdot 3\ H_2O_2$, in contrast, is well dissolvable in water with an equilibrium coefficient of $1 * 10^{-5}$. The latter two are commercially available at higher purities (Gholipourmalekabadi et al., 2016). Solid peroxides are used in a variety of applications such as in soil decontamination to deliver oxygen for microorganisms or as a bleaching agent in laundry detergents or tooth paste.

When getting in contact with water, solid peroxides decompose into hydrogen peroxide (H_2O_2) and a hydroxide or sodium carbonate as shown in the reactions below:

$$CaO_2(s) + 2H_2O \rightarrow Ca(OH)_2(s) + H_2O_2 \quad (1)$$

$$MgO_2(s) + 2H_2O \rightarrow Mg(OH)_2(s) + H_2O_2 \quad (2)$$

$$(Na_2CO_3)_2 \cdot 3\ H_2O_2 \rightarrow 4Na^+ + 2CO_3^{2-} + 3H_2O_2 \quad (3)$$

As the first step of this reaction is dependent on water, the release of oxygen can be controlled by the access of water to the peroxide. The highest release rate of oxygen has been observed for $(Na_2CO_3)_2 \cdot 3\ H_2O_2$ at 132 mg $* L^{-1} * h^{-1}$. CaO_2 and MgO_2 have lower release rates of 22.06±3.3 $mg*L^{-1}*h^{-1}$ and 3.22±0.7 $mg*L^{-1}*h^{-1}$ as expected from their equilibrium constants in water (Waite et al., 1999). Other environmental factors that can influence the reaction aretemperature and pH. By inhibiting the chemical reaction, the release of oxygen can potentially be prolonged. In a second reaction step, the H_2O_2 is spontaneously reacting forming oxygen. This reaction, though, is rather slow and needs to be induced by a catalyst such as catalase, peroxidases, manganese dioxide, iron and others (Ward et al., 2013).

High levels of H_2O_2 may react into reactive oxygen species by taking up an electron as described by Ma et al. (2007). The decomposition of CaO2 has been proposed to have intermediate states of reactive oxygen species:

$$CaO_2(s) + 2H_2O \rightarrow Ca(OH)_2(s) + H_2O_2 \quad (4)$$

$$H_2O_2 + e^- \rightarrow \bullet OH + OH^- \quad (5)$$

$$\bullet OH + H_2O_2 \rightarrow H2O + HO_2\bullet \quad (6)$$

$$HO_2\bullet \rightarrow \bullet O_2^- \quad (7)$$

The above reactive oxygen species have a short lifetime (e.g. •OH, ~10^{-6} s; •O2−, ~0.1 s) and readily convert into water and oxygen (Ma et al., 2007).

$$HO_2\bullet + \bullet OH \rightarrow H_2O + O_2 \quad (8)$$

$$\bullet O_2^- \rightarrow O_2 + e^- \quad (9)$$

The human body has developed many defensive mechanisms against reactive oxygen species in the form of various enzymes and molecules such as glutathione peroxidase, superoxide dismutase and catalase (Pigeolet et al., 1990). H_2O_2 is furthermore an important molecule for cell signalling, but also has harmful effects when abundant in excessive concentrations. Hence the human body itself presumably has the highest levels of catalase in the animal kingdom to prevent cell damage (Veal et al., 2007).

In conclusion, the rate of oxygen release can be controlled by the access of water, while catalysts can control the production of ROS. Ideally, a prolonged and controlled decomposition time of the oxygen-releasing material is needed for supporting survival of the islets in the early post transplantation phase.

6.1.2 Carrier materials for oxygen-generating materials

The oxygen production by oxygen-generating materials is strongly dependent on the availability of water. The incorporation of these oxygen-generating materials into additional materials can increase their applicability by controlling their release characteristics. Furthermore, these additional materials can be used to limit the release of reactive oxygen species.

Various materials have been applied as carrier material such as poly(lactic-co-glycolic acid) (PLGA), polyvinylpyrrolidone (PVP), poly(methyl mathacrylate) (PMMA) or PDMS. Since CaO_2 and MgO_2 have a low solubility in water, they have often been combined with hydrophilic polymers to get incorporated into tissue constructs. H_2O_2 itself is a liquid and therefore often coupled to polymers. Montazeri et al. (2016) created microparticles by coacervation of

PVP/H_2O_2 with PLGA. After hardening the microparticles, catalase was incorporated onto the outer shell. In this construct, the hydrophobic PLGA acted as a transient shield to lower the release of H_2O_2, which was then catalysed by the catalase at the surface of the microparticle. The particles produced oxygen for a period of 14 days and showed increased survival of MIN6 cells under hypoxic conditions. Furthermore, islets were encapsulated with the oxygen releasing microparticles in collagen/heparin/VEGF hydrogels and showed improved engraftment and intraperitoneal glucose tolerance test (ipGTT). Other microparticle systems employed PLGA as the H_2O_2 containing matrix via a double emulsion solvent evaporation method and coated with alginate containing immobilised catalase (Abdi et al., 2011). The rate of oxygen release was controlled by the percentage of alginate used for the outer shell, which showed a slower release for a higher percentage of alginate. From the solid peroxides, CaO_2 has been employed in combination with different polymers. For example, Oh et al. (2009) incorporated CaO_2 into 3D PLGA scaffolds and could measure a slight increase of oxygen tension in the media for a period of 10 days under hypoxic conditions.

The longest oxygen release of an oxygen-generating material combined with a polymer was achieved by mixing CaO_2 with PDMS (Figure 53). At hypoxic conditions this material delivered oxygen at above-physiological tissue concentrations (about 80 µmol/L or 57 mmHg) for 40 days (Pedraza et al., 2012). PDMS as a hydrophobic polymer can sufficiently delay the access of water by acting as a diffusion barrier. Then again, PDMS provides a high diffusivity of oxygen, which facilitates the fast removal of oxygen driving the reaction of H_2O_2 to O_2 forward and thereby reducing the possibility of reactive oxygen species intermediates production in the process. Furthermore, this material does not require any additional catalase. Though the authors of the paper do not mention the catalytic agent, we hypothesise that the reaction of

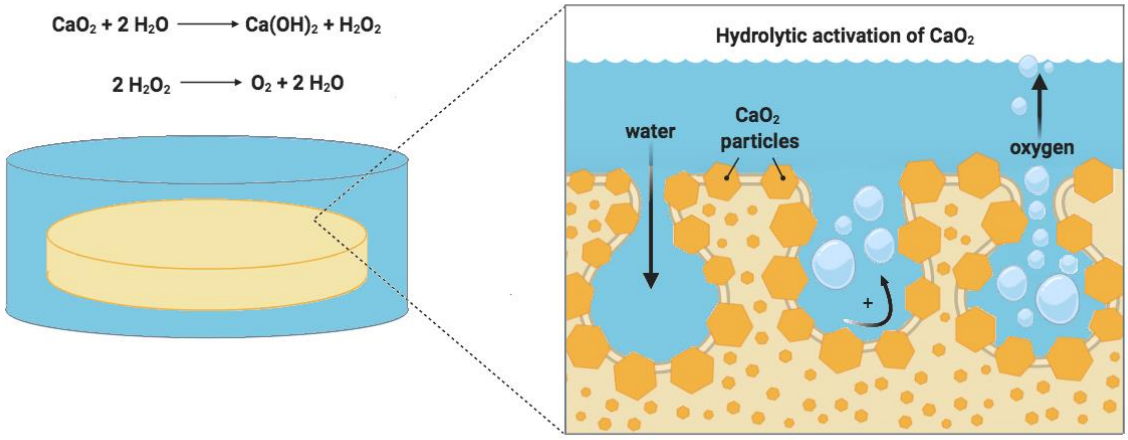

***Figure 53. Oxygen generation by CaO_2 embedded is silicone disks. W**ater can only slowly penetrate between the hydrophobic polymers and activate the degradation of CaO_2.*

H_2O_2 to O_2 is catalysed by platinum, a component of the PDMS needed for crosslinking the PDMS. The material has been used in 2D cell cultures for islets and maintained islet function under hypoxic conditions. Moreover, islet cultures with CaO_2 –PDMS disks were assessed with LDH cytotoxicity assays showing decreased levels of cytotoxicity (Pedraza et al., 2012). The pH was measured over five consecutive days of oxygen disk incubation in CMRL media and remained stable around pH 7.5. However, low levels of H_2O_2 of about 50 µM were detected in the media. Islets precultured with these oxygen scaffolds under hypoxic conditions were still able to lower blood glucose levels of diabetic animals upon implantation (Coronel et al., 2017). As published by the Stabler group, the scaffold was further investigated as a basis for a macroencapsulation scaffold. Isolated islets were encapsulated in mouse-scaled devices with agarose around the oxygen-generating scaffold and then implanted into the abdominal cavity. All animals implanted with oxygen-generating disks became normoglycemic in contrast to only 50% of the animals in the control group with PDMS disk without CaO_2. After 30 days, the devices were removed and the viability of the encapsulated islets subsequently assessed. In devices with oxygen-generating disks, the islets proved viable throughout the entire thickness of the device. In the control groups only islets close to the implant's surface were shown viable. Microscopical images documented the viability of islet clusters until about 200µm into the scaffold (Coronel et al., 2019b).

From the material combinations described above, CaO_2 incorporated into PDMS as described by Pedraza et al., 2012, Coronel et al., 2017 and Coronel et al., 2019 seemed to be the most promising material for incorporation into the proposed encapsulation device. Therefore the proposed oxygen release scaffold was further investigated for application in the proposed device.

6.2 Methods

6.2.1 Preparation of oxygen-generating disks fitted to device geometry

Moulds were designed by CAD software to create oxygen-generating disks that exactly fit into the device geometry and then 3D printed by an Asiga MAX 385 UV™ printer with R11 Resin (EnvisionTEC). The structures were washed twice for five minutes with isopropanol in an ultrasound bath and subsequently hardened under an UV lamp in glycerol for 30 minutes per side.

Medical-grade Silicone MED-6015 (NuSil) suitable for implantation was mixed at a ratio of 10:1 (Part A : Part B). CaO_2 was added at 25 % (wt/wt) and the mixture was degassed for 20 minutes in a small aluminum bowl. Afterwards the mixture was filled into the printed moulds and cured over night at 60°C. Control disk were produced the same way without CaO_2.

6.2.2 Measurement of released oxygen from oxygen-generating disks

For measurement of the oxygen release from the oxygen-generating disk an oxygen sensor spot SP-PSt3-YAU (PreSens, Germany) in combination with an OXY-4 mini oxygen meter (PreSens) was used (Figure 54). The setup was placed inside an incubator with an oxygen control unit, allowing tight control the oxygen environment. Each sensor spot was calibrated in accordance with the instruction manual. For the first calibration point at 0 % oxygen the glass vessels were filled with 1 % Na_2SO_3 in PBS, for the second calibration point at 100 % oxygen saturation, PBS was oxygenated for 20 minutes and then filled into the chambers. The calibration process was performed at 37°C and an air pressure of 1013 hPa.

The following measurement was also performed at 37 °C in a controlled 0.1 % oxygen atmosphere. The oxygen-generating disks were placed into 15 ml PBS and the oxygen concentration of the medium was recorded every 15 sec. For each experiment, a control disk without CaO_2 was taken along to record fluctuations due to opening of the incubator for observations and the adjustment of the sensor position.

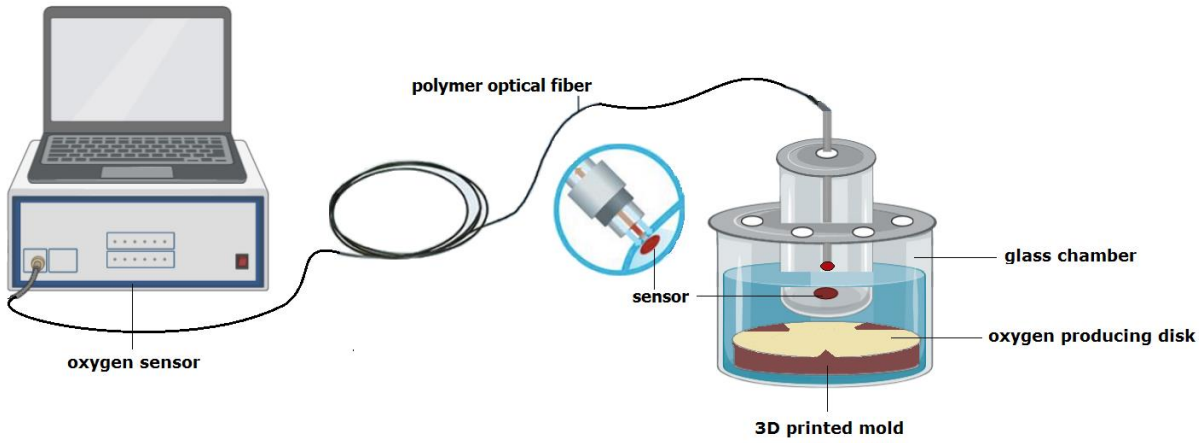

Figure 54. Oxygen measurement setup to quantify the released oxygen of oxygen-generating disks.

6.3 Results

6.3.1 Release kinetics of oxygen disk in device prototype

Upon implantation of the encapsulation device, the surrounding environment is insufficiently vascularised. During the surgical implantation procedure the microvasculature has been disrupted and cannot sufficiently support the tissue with oxygen. After approximately two weeks the biomolecular cues provided by the hydrogel-modified surface of the encapsulation device (chapter 5) capillaries are expected to have regrown in the implant environment. A transiently oxygen-generating scaffold is intended to bridge this initial hypoxic phase and guarantee for proper oxygenation throughout.

Oxygen-generating disks (OGD) have been produced from CaO_2 and medical-grade silicone fitted to the size of the implant. These OGDs have been placed into an encapsulation device skeleton and incubated in PBS for 3 to 4 weeks at 37°C in an oxygen-controlled environment at 0.1 % oxygen to recapitulate the hypoxic transplantation environment. Upon contact with water the OGDs started to release oxygen. The oxygen released into the surrounding media has been recorded with temporal resolution of 15 sec (figure).

Two sets of OGDs have been tested (Figure 55). Each set contained two different thicknesses of oxygen-generating disks with a height of either 1 mm or 3 mm. The water-exposed surface for both OGD types was 6.28 cm^2. The control silicone disk did not contain CaO2 and could therefore not release oxygen. It therefore gave an indication on whether the incubator has been opened for control measures, which poses an increase in the air oxygen concentration and dissolved oxygen in the measurement chamber. During the first set of experiments, technical problems with oxygen measurements were encountered and therefore only data starting from the sixth day after incubation have been plotted.

The oxygen release for both types of disk thicknesses was higher than 6.7 mg/l for all except one OGD. This compares to the oxygen concentration in air (depicted by the red dashed line in Figure 55) over the whole period of measurement of at least three weeks. This oxygen concentration is 3.7 times higher than tissue oxygen levels in the pancreas of about 8 mg/l or 40 mmHg. Furthermore, the long-term release of oxygen by the OGD is indicated by gas bubbles that can be observed at the OGD surface during the whole experiment. The observed fluctuations of the oxygen release profiles (figure 5) can be explained by gas bubbles releasing from the disks at irregular time intervals. In both sets of experiments, the oxygen profiles for disks of different thicknesses do not deviate. Therefore, it can be concluded that the oxygen release from the disks is primarily dependent on the water exposed surface of the disks.

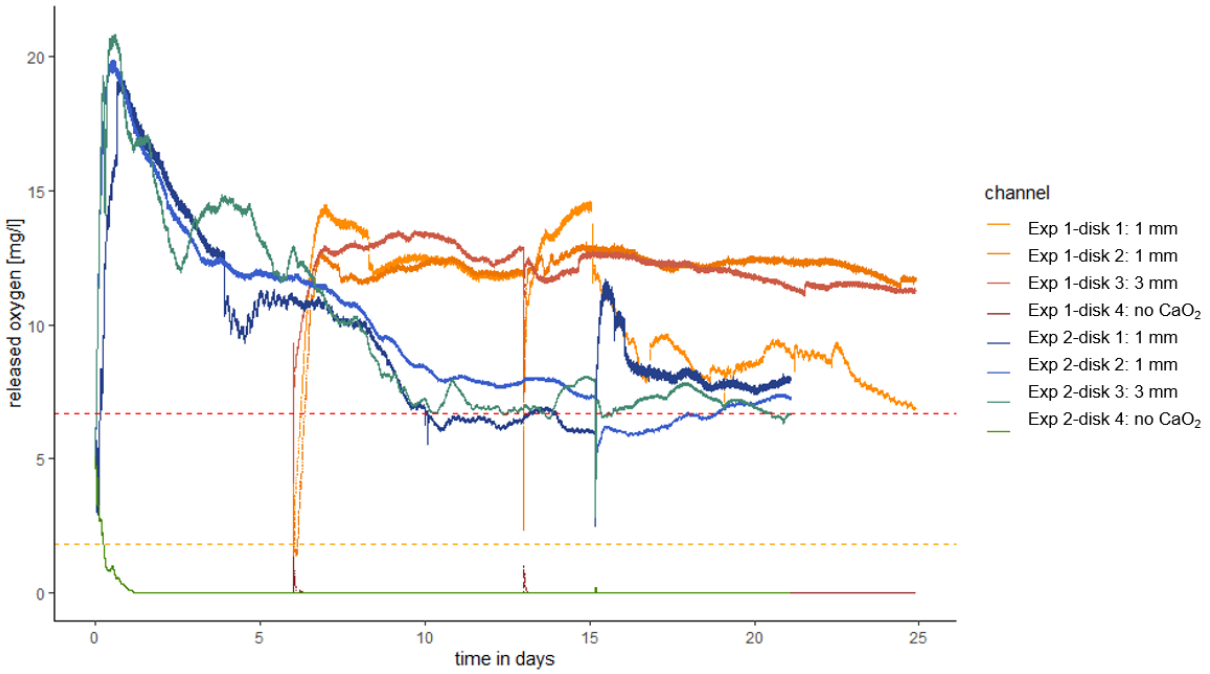

Figure 55. Oxygen release of oxygen-generating disk. *Red dashed horizontal line: 6.7 mg/l oxygen ≙ 20,9 % oxygen saturation ≙ 149,30 mmHg (oxygen concentration in air). Orange horizontal line: 1.8 mg/l oxygen ≙ 5,6 % oxygen saturation ≙ 40 mmHg (physiologic tissue oxygen concentration).*

In the first set of experiments, the oxygen concentration readings plateaued at about 12 mg/l. For the second set of experiments, the oxygen concentration decreased over the first 10 days and then plateaued at around 6.7 mg/l. The difference in the readings of both sets of experiments may be explained as follows: In the current oxygen-measurement setup, the sensor cannot be adjusted at the exact same height above the disk. The oxygen concentration gradient above the disk might have been measured at different levels, which explains the different levels of oxygen readings between different disks in the same set of experiments. Second, some of the disks started floating out of the skeleton holders as for example observed for all disks in the second experiment and for disk 2 in the first set of experiments. This exposes the lower surface of the OGD and results in faster exhaustion of the OGD material.

In the encapsulation device the OGD is overlaid by the islet holder filled with agarose microwells. This layer might have an influence on the release characteristics of the OGD. A preliminary experiment has been executed by overlaying the OGD with a layer of 2 % agarose. The oxygen release for this disk showed a more flat curve compared to the bluntly exposed disk, but at a comparable oxygen concentration level (Figure 56).

Next, to test how the oxygen release could be further modulated, an additional layer of silicone was prepared on top of the OGD. Silicone has the characteristics of a low permeability for water, while it has a high permeability for oxygen. This layer can therefore reduce the amount of water penetrating towards the CaO_2, while allowing the free egress of gas oxygen.

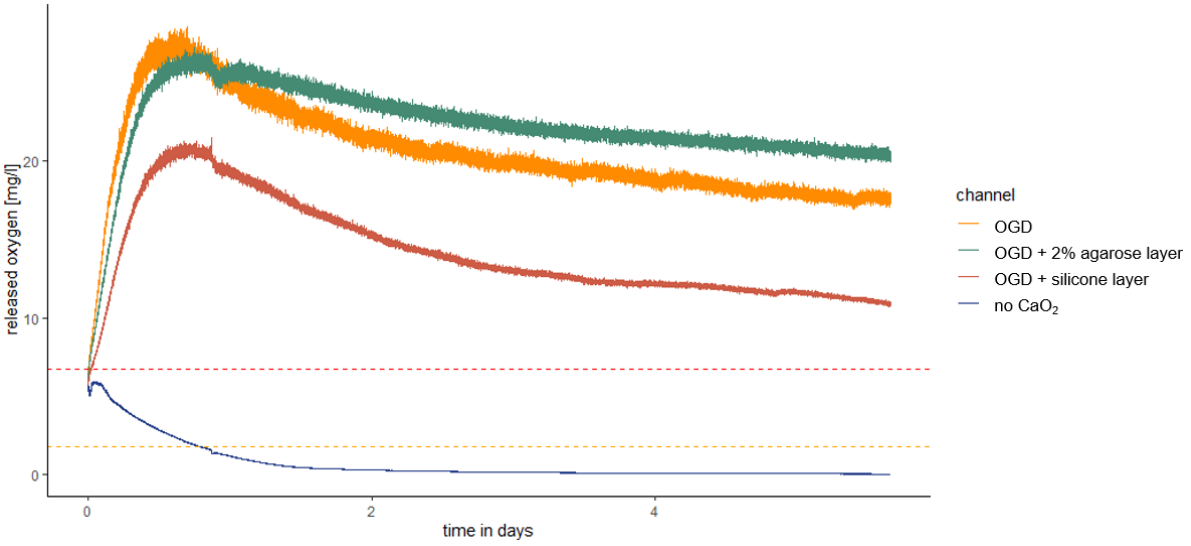

Figure 56. Oxygen release of oxygen-generating disk in combination with a buffer layer of either silicone or agarose. *Red dashed horizontal line: 6.7 mg/l oxygen ≙ 20,9 % oxygen saturation ≙ 149,30 mmHg (oxygen concentration in air). Orange horizontal line: 1.8 mg/l oxygen ≙ 5,6 % oxygen saturation ≙ 40 mmHg (physiologic tissue oxygen concentration).*

In conclusion, oxygen can be provided to the encapsulated cells at more than 6.7 mg/l for four weeks by CaO_2-silicone disks. This oxygen concentration corresponds to the oxygen levels in air and is 3.7 times higher than physiologic tissue oxygen levels. This concentration correlates with the optimally desired oxygen concentration to support the encapsulated islets throughout the early post transplantation period.

6.4 Conclusion and outlook

With the proposed oxygen-generating disk, proper oxygenation of the islets during the initial three weeks, can be achieved as a minimum. The disk consists of two components - CaO_2 and silicone. The decomposition reaction of CaO_2 into oxygen is controlled by the availability of H_2O. Hydrophobic nature of silicone slows this decomposition reaction, thereby accomplishing long release times.

With the current oxygen measurement setup, the relative distance of the sensor to the disk cannot be precisely controlled, provoking divergences between different measurement series. We therefore aim to improve the setup with a micromanipulator to adjust height of the sensor above the disk more precisely.

Modulation of the release could be achieved by adjusting the silicone stiffness to vary the ingress of water into the disk. The concentration of CaO_2 can also be adapted to modulate the oxygen release. So far, the oxygen measurements have only been performed in the skeleton

module. Further experiments will include the measurement of the oxygen release in combination with the islet holder and membrane module. A proof of principle will include survival of the islets inside the device for more than three weeks at a surrounding physiological oxygen concentration of 40 mm Hg, mimicking the transplantation environment.

6.5 Acknowledgements

Parts of the experimental work described in this chapter (preparation method of oxygen-generating disk) were executed by Victoria Sarangova in the framework of her Master's thesis (TU Dresden, Germany).

7 Device assembly, cell insertion & clinical translation

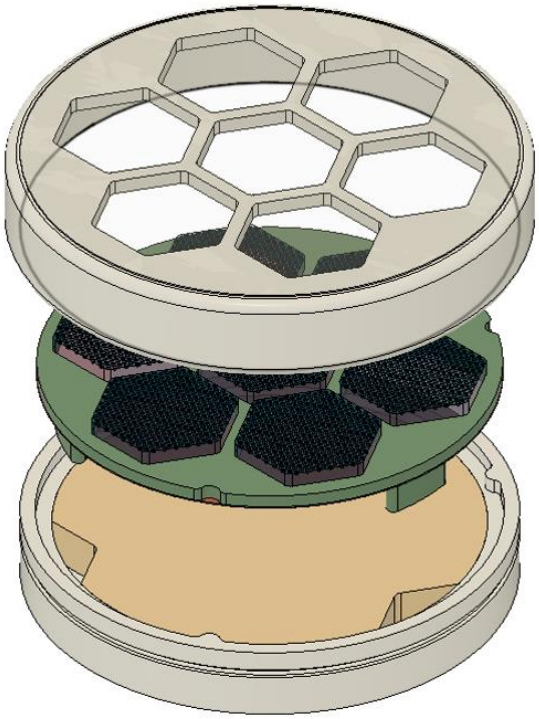

7.1 Introduction

In Chapter 3 the requirements regarding the geometry of the encapsulation device in order to ensure its proper function were discussed taking into account the physical limitations of diffusion especially in regard to oxygen. A concept subdividing the encapsulation device into different functional modules was developed. In this chapter the previously described single functional modules are combined to a first version of the encapsulation device in a high fidelity prototype and aspects of translation of the encapsulation device into the clinic are discussed:

The prototyping process supported by additive manufacturing techniques is explained and medium and large scale series production methods are investigated. Suitable material components for the different modules of the encapsulation device and their assembly are discussed and the post processing and assembly process of the final overall design variant are explained. Moreover, the up-scaling of the device is considered. It is shown, how the design can be easily adapted for larger species requiring a larger islet mass, including humans. Finally, a concept for the preclinical evaluation of the presented encapsulation device is described.

7.2 Prototyping of the encapsulation device design by additive manufacturing

As a first step towards manufacturing the encapsulation device additive manufacturing techniques such as 3D printing were applied in the design process. Single components of the overall design were printed in a short period of time, which enabled rapid prototyping for a realistic proof of concept and fast optimisation cycles. After validating the assembly process and the practicability of the single components of the prototypes, these concepts were advanced into a high fidelity prototype. A selection of prototype structures is shown in Figure 57.

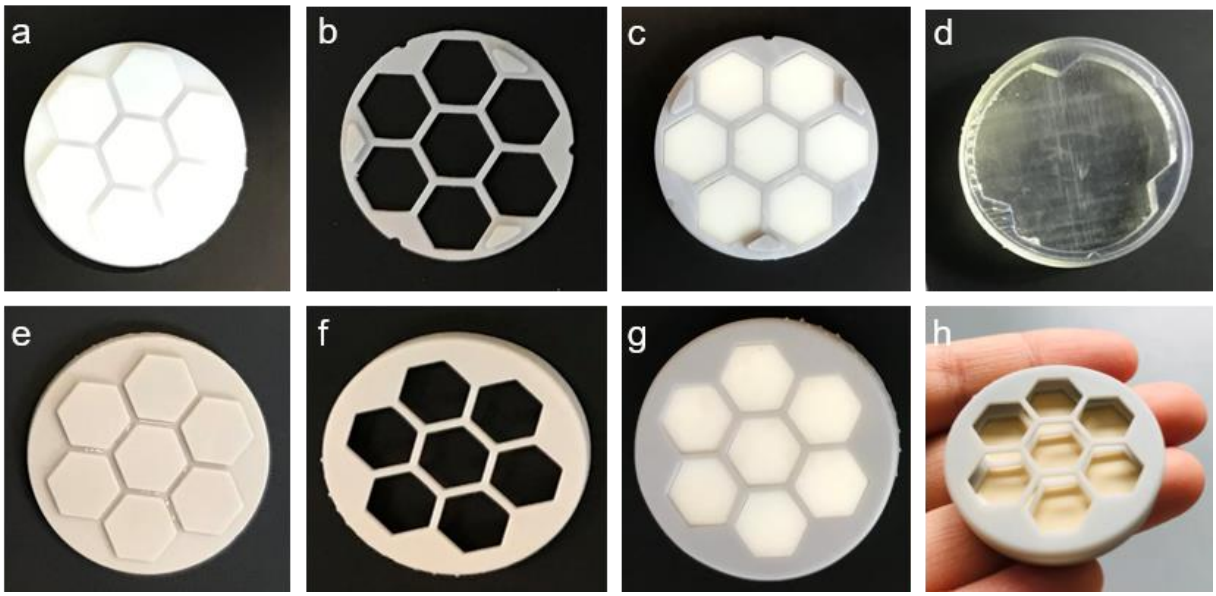

Figure 57. Prototyping of encapsulation device components. *a Insert for islet holder.* ***b*** *Islet holder.* ***c*** *Fitting of islet holder on insert to test tolerances.* ***d*** *Skeleton* ***e*** *Insert for membrane holder.* ***f*** *Membrane holder.* ***g*** *Membrane holder fitted with insert.* ***h*** *Assembly of whole setup with oxygen disk.*

For the prototyping process of the proposed encapsulation device high resolution SLA printing was applied. In this technique the structures are created by repetitive photopolymerisation of resin layers on top of each other. In more detail, a build platform is lowered into a photo-crosslinkable resin bath and the first layer is exposed onto the platform by using an LED screen. For the next layer, the build platform is moved upwards and lowered again to allow the resin to flow under the build platform again. The next layer is exposed onto the first layer. This process is repeated until the full height of the structure is reached.

3D printing is a fast accessible way to create structures, though harbors problems of toxicity for cells, especially as for commercial available resins the ingredients are often not stated. Furthermore, unreacted precursors might leach out of the structures if crosslinking is not complete. As well many materials are not stable against standard sterilisation techniques such

as autoclaving. A few materials exist, which are already applied in SLA in a medical context such as for example for hearing aids or temporary teeth, but these materials are not credited for long-term implantation.

3D printing was applied for different workflows in the design process of the proposed encapsulation device such as the platform for moulding agarose replicas (Chapter 4), moulds for the production of oxygen disks (Chapter 6), holders for gluing membranes (Chapter 7), pillar microstructures and microwells (Chapter 4) and last but not least the prototypes of the design variants and the high fidelity prototype (Chapter 7). These 3D printed parts were of great advantage to specify the detailed design of the high fidelity prototype implant, which is described in the next section.

7.3 Specification of detailed design features of the device geometry

The high fidelity design prototype was revised with some detailed features for a proper functioning device, which are explained in the section below.

First, for the proper alignment of the different modules with each other, alignment structures have been integrated into the geometry (Figure 58 a). The heart of the device, the islet module, needs to fit exactly into the hexagons of the membrane holder. The crucial detail here is that the hydrogels are extruding out of the islet holder to lift the islets placed at the top of the hydrogel directly under the membrane. The hydrogels are extruding 1 mm out of the islet holder to lift the islets in the microwells directly under the membrane. To have a proper alignment of these two elements a set of struts was included. Furthermore, the islet holder is standing on three triangular pillars, which are designed to place the islet holder at the correct height relative to the base of the device as the oxygen module lying below is prone to small variations in thickness due to its production process. The pillars though depending on the chosen production process can be produced with a higher accuracy.

For the implementation for a later on serial scale production process the designed structure needed some additional modifications. A method for medium scale production of parts in medical grade material is CNC-drilling (Chapter 7.5). The drills needed for this technique are round and cannot generate angular transitions. This had to be taken into account in the design of the structures. Therefore, the framing of hexagons and other transitions have round transitions at edges in the X-Y production surface of the structure (Figure 58 b). The framing hexagons have a radius of 0.5 mm. Furthermore, the drilling process requires a certain minimal wall thickness. Accordingly all wall thicknesses were kept at a minimum of 1 mm.

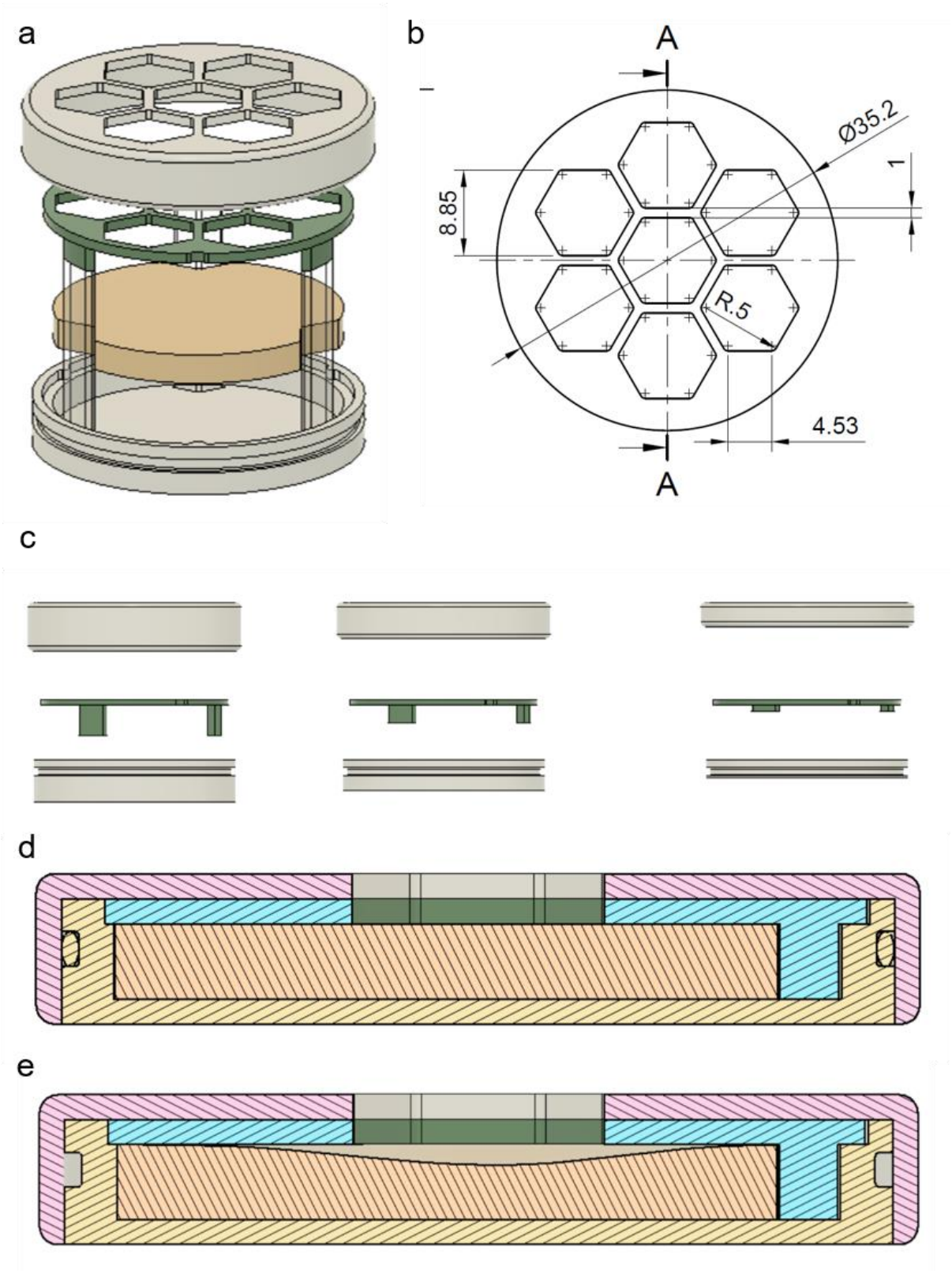

Figure 58. Detailed design features of the encapsulation device. a *Alignment structures have been developed, which place the islets at the exact height under the membrane.* ***b*** *Technical drawing (top view) indicating the corner roundness for CNC milling.* ***c*** *Design variants of the device for different volumes of oxygen disks.* ***d*** *Cross section of the assembled device components indicating the position of the O-ring.* ***e*** *Cross section with aberrant oxygen-generating disk highlighting the requirement of the height positioning stands of the islet holder.*

The total height of the implant was designed in a way that the height could be adapted according to the needs required for the oxygen module (Figure 58 c). Different thicknesses of oxygen disks can produce oxygen over a various timescale and levels of oxygen. According to the later on specified need depending on the time required for the establishment of a vascularizing network around the device the required disk volume and device size can be chosen.

For proper immunoisolation the inside of the device needs to be separated from the outside environment except for the membrane area. The filling process requires a completely accessible islet module. To seal the lid after the filling a sealing mechanism by an O-ring was chosen. An O-ring is a commonly used seal to tightly separate different compartments. The O-ring groove was designed according to the specified lists for the used sealing ring inner diameter and cross section (Figure 58 d). To be able to apply a shelf sold O-ring the device circumference had to be designed accordingly. This allows to have a single axial straight sealing line which can be fulfilled by an O-ring.

7.4 Assembly process for modular macroencapsulation device

An overview of the assembly and post processing of the device modules is given in the Figure 59 and are described in detail in the following subsection.

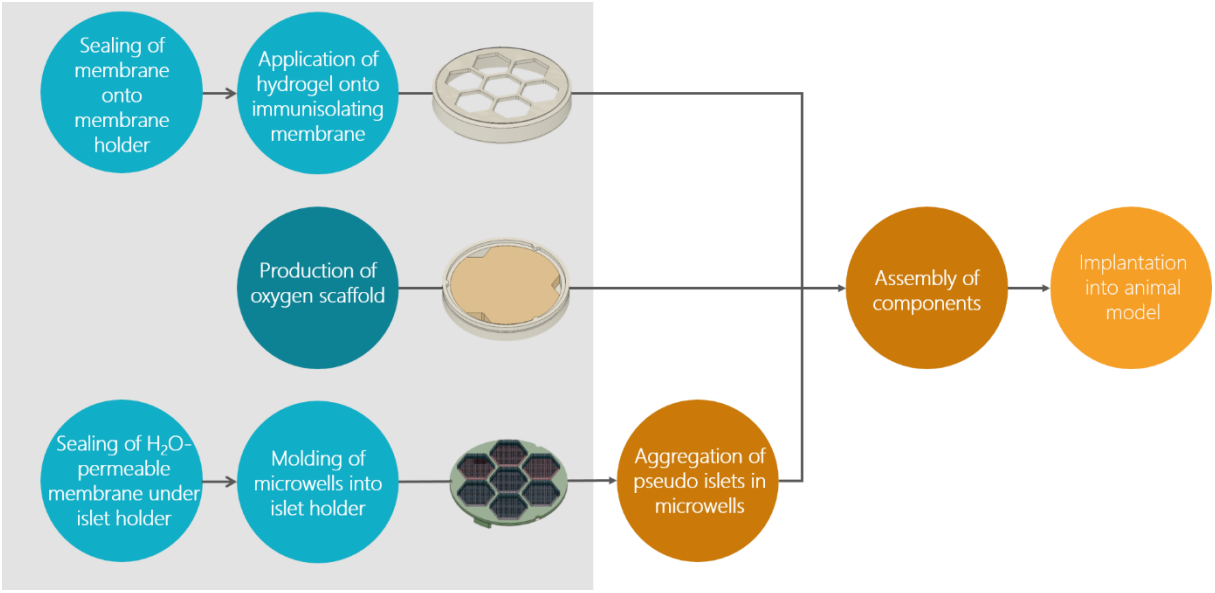

Figure 59. Overview of the post processing and assembly steps of the encapsulation device.

7.4.1 Membrane holder

The membrane holder is finalised by two spin coating steps. First, a fitting negative structure is placed behind the grid and silicone glue is distributed on the plane surface (Figure 60 a). To yield a homogenous and thin distribution of the glue layer the module is spin coated. For this process the combined component is fixed onto a plate by a vacuum. The glue is roughly distributed on top of the combined component. When the plate is rotated, the glue is homogenously distributed and excess glue is tossed off because of the centrifugal force. During this process it has to be taken care that the handling time does not exceed the curing time of the glue. After the spin coating process, the negative is removed and a membrane punched to the diameter of the membrane holder is fixed on top of the membrane holder and left for the silicone glue to cure.

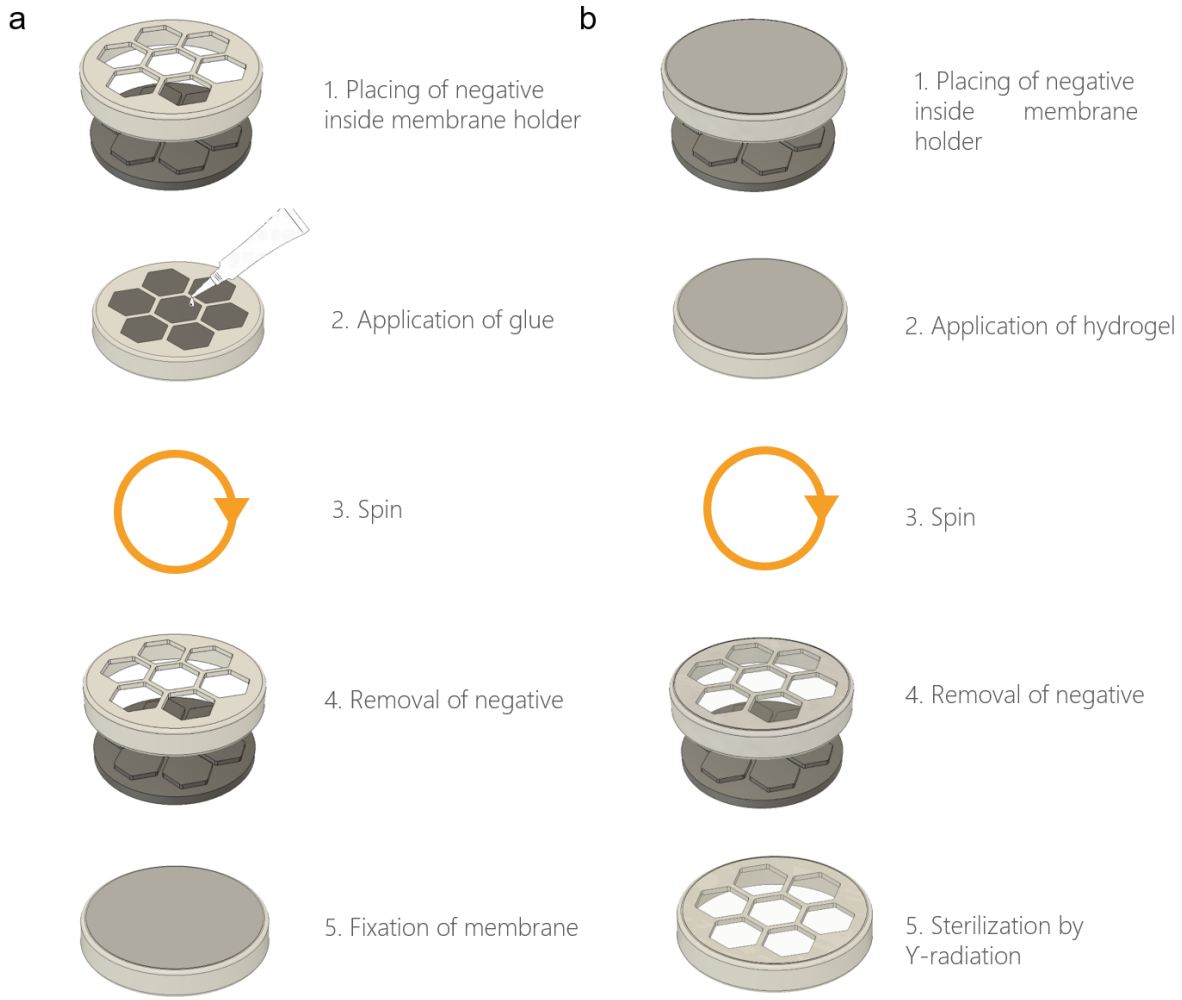

Figure 60. Post processing of the membrane holder. a *A negative insert is placed behind the hexagon structure and glue is distributed by a spin coater. The negative is removed, the membrane is positioned on the hexagon struts and the left for curing.* ***b*** *A clean negative is placed behind the membrane and the hydrogel layer is distributed by a second spin coating step. After curing of the hydrogel the negative is removed and the complete membrane holder can be sterilised.*

For the second spin coating step a clean negative is placed behind the membrane again and a liquid hydrogel precursor solution is placed on top (Figure 60 b). After spinning the membrane is left in a humidified container to allow the polymer ankers establish their links to form a layer within the pores of the membrane. Residual side products are removed by multiple washing steps in a physiological buffer. Further layers and signalling molecules for improved vascularisation can be applied in a next step and finally, the fixed composite hydrogel membranes need to be sterilised for implantation by Y-radiation.

7.4.2 Oxygen-generating disk and skeleton

The oxygen-generating CaO_2-silicone disk (oxygen-generating disk) needs to have an exact geometry to fit into the skeleton of the encapsulation device. The oxygen-generating scaffold is prepared by filling medical grade silicone premixed with CaO_2 into a mould. After a heat vulcanisation process, the CaO_2 disk is removed from the mould and placed into the skeleton (Figure 61). The detailed production process is described in chapter 6.2. An O-ring is placed at the groove of the skeleton for later sealing of the device. A photograph of the assembly is shown in Figure 62 below.

Figure 61. Production process of the oxygen module. *The curing mould with triangular extrusions is filled with medical grade silicone premixed with CaO_2. After curing of the silicone, the oxygen-generating disk is removed and placed in the skeleton of the encapsulation device.*

Figure 62. Photograph of the combined oxygen module*. The skeleton (produced by CNC-drilling from PEEK) combined with an oxygen-generating disk and an O-ring.*

7.4.3 Islet holder

In the islet holder the pseudo islets are aggregated and cultured. As a post processing step an oxygen-permeable membrane has to be fixed at the bottom of the islet holder to prevent the microwell hydrogel arrays from falling through the grid. For this, in the same way as described for the fixation of the immunoisolating membrane to the membrane holder, a negative structure is placed in between the grid. Glue is distributed at the back side and spin coated to form a homogenous layer. The negative is removed, an oxygen-permeable membrane is fixed on top and the glue is left to polymerise (Figure 63 a).

Multiple microwell hydrogel arrays are produced from a replica mould as described in chapter 4. A funnel is placed on top of the islet holder and the microwell hydrogel arrays are placed into the compartments at the top. This combined module is now used for the preparation and microstructured arrangement of the pseudo islets (Figure 63 c, d). For this process the combined islet module is first placed into a 6-well cell culture plate and a single islet cell suspension is seeded into the hexagon compartments. The islet module is placed into a humidified CO_2 incubator at 37°C for several days. The single islet cells now reaggregate into pseudo islet clusters. As described in chapter 4 the size and arrangement of these clusters is optimised for sufficient nutrient supply by diffusion over the immunoisolating membrane. After the pseudo islets have formed the funnel is removed and the final implant can be assembled.

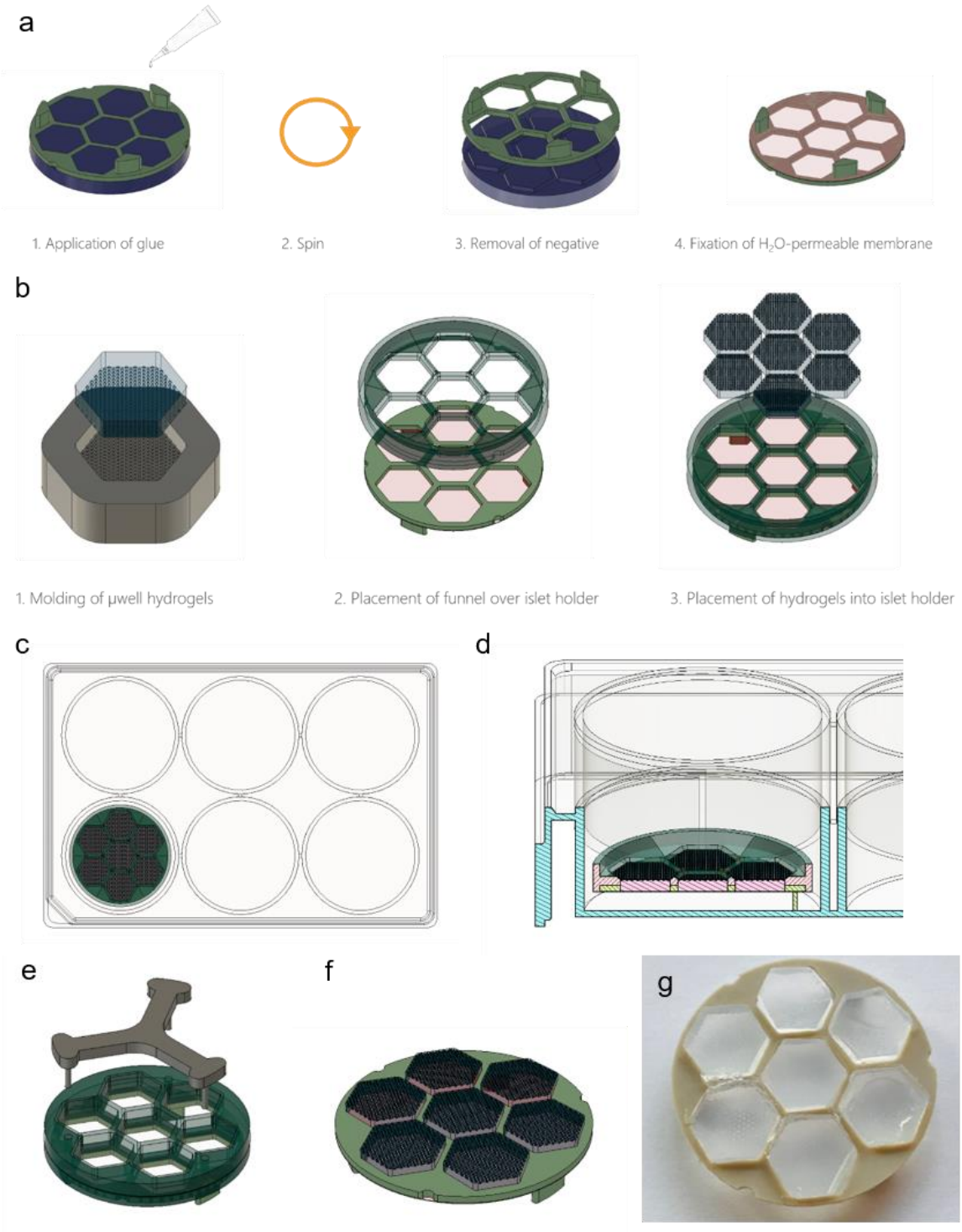

Figure 63. Post processing and filling of the islet module. a *A negative is placed in the islet holder and medical grade glue is distributed by a spin coating process. The negative is removed and an oxygen-permeable membrane to prevent the hydrogel arrays to fall through the islet holder is fixed on the bottom of the islet holder.* ***b*** *Microwell hydrogel arrays are produced and placed together with a funnel on the islet holder* ***c, d*** *The combined islet holder placed in cell culture dish and single islet cells are seeded on top and incubated for aggregation of the pseudo islets.* ***e*** *The funnel is removed from the islet holder with a removing.* ***f*** *Schematic of complete islet holder with microwell hydrogel arrays****. g*** *Photograph of fully assembled islet holder with microwell hydrogel arrays.*

As a proof of principle, the seeding of the cells into the device has been tested with an INS-1 cell line. An islet holder was set up with a funnel and hydrogel microwell arrays (five with microwells of 150 µm width and 150 µm distance and two hydrogel microwell arrays of 300 µm width and 300 µm distance) and placed in a 6-well plate. 2.24 x 10^6 INS-1 cells were seeded in 1ml of cell culture medium and the plate was spinned for 300 x g for 1 min. After 24 hours the aggregation of the cell clusters have aggregated into clusters within the wells (Figure 65) and were viable as indicated by an FDA staining (Figure 66).

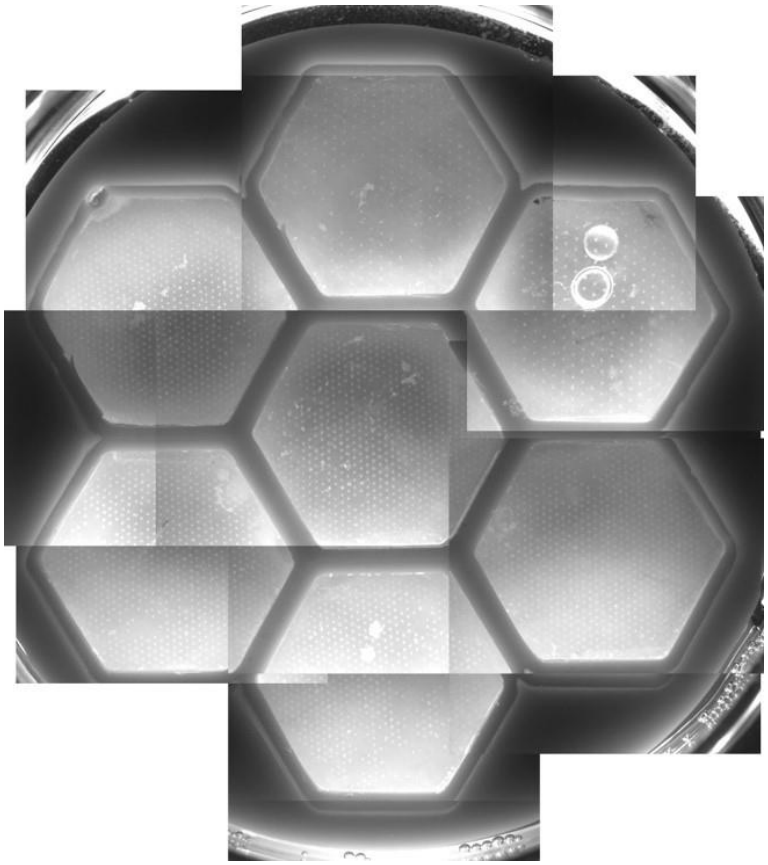

Figure 64. Islet holder seeded with 400 INS-1 cells per microwell. *Aggregated INS-1 clusters after one day of culture in hydrogel microwell arrays of 150 µm width and 150 µm distance or 150 µm width and 300 µm distance (upper and upper right hexagon).*

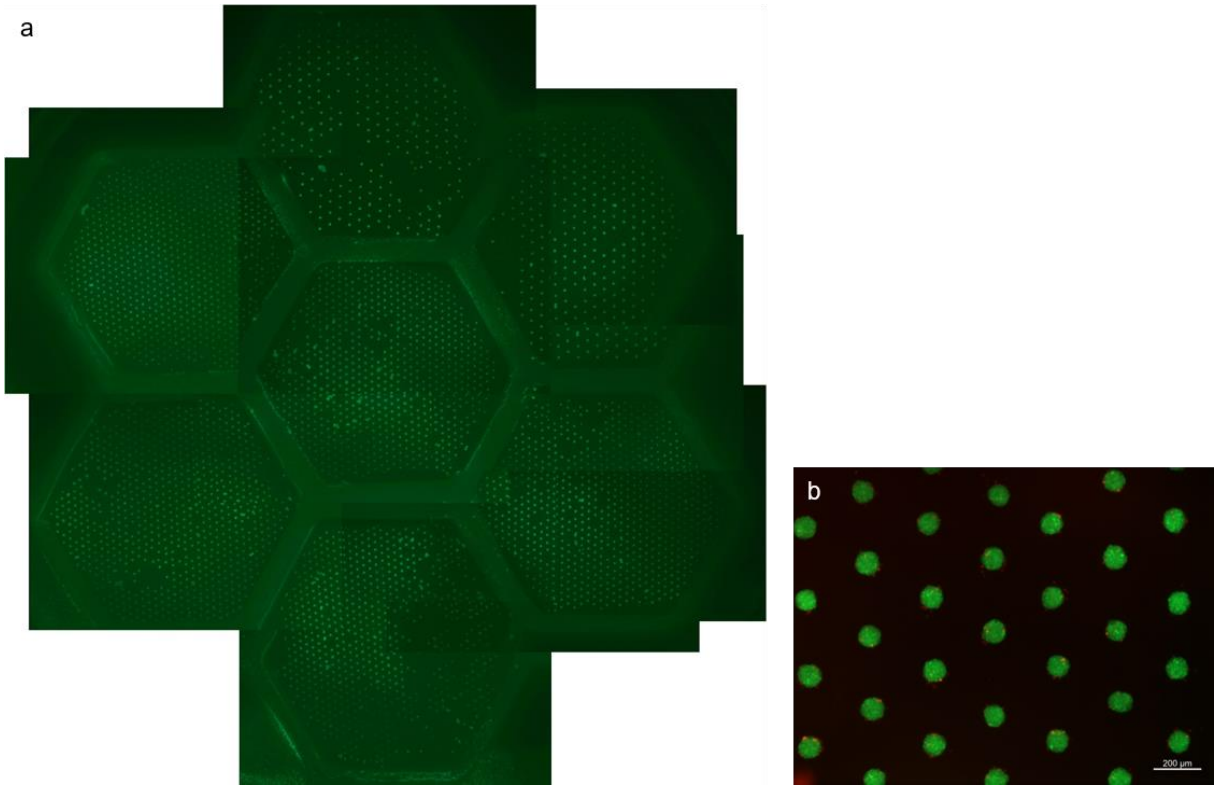

Figure 65. Islet holder seeded with 400 INS-1 cells per microwell and stained for viability by fluorescein diacetate and propidium iodide. *Aggregated INS-1 clusters after one day of culture in hydrogel microwell arrays of 150 µm width and 150 µm distance or 150 µm width and 300 µm distance (upper and upper right hexagon).* ***a*** *Seven hexagon islet holder.* ***b*** *Magnification of clusters.*

7.4.4 Final assembly of the novel encapsulation device

After all single modules have been processed, they are combined into a complete implantable device as follows: The skeleton with the oxygen-generating disk is the base. Inside, the islet module is placed with the struts fitting the triangular holes of the disk. Finally, the membrane module is placed on top (Figure 66). The inside is sealed in between the membrane holder and skeleton via the O-ring. In this way passage of (macro)molecules is only possible via the immunoisolating membrane. The unique feature of this constructional set up is that the islets are placed directly under the membrane in a single layer and have an optimal distance to each other as depicted in the Figure 66 c.

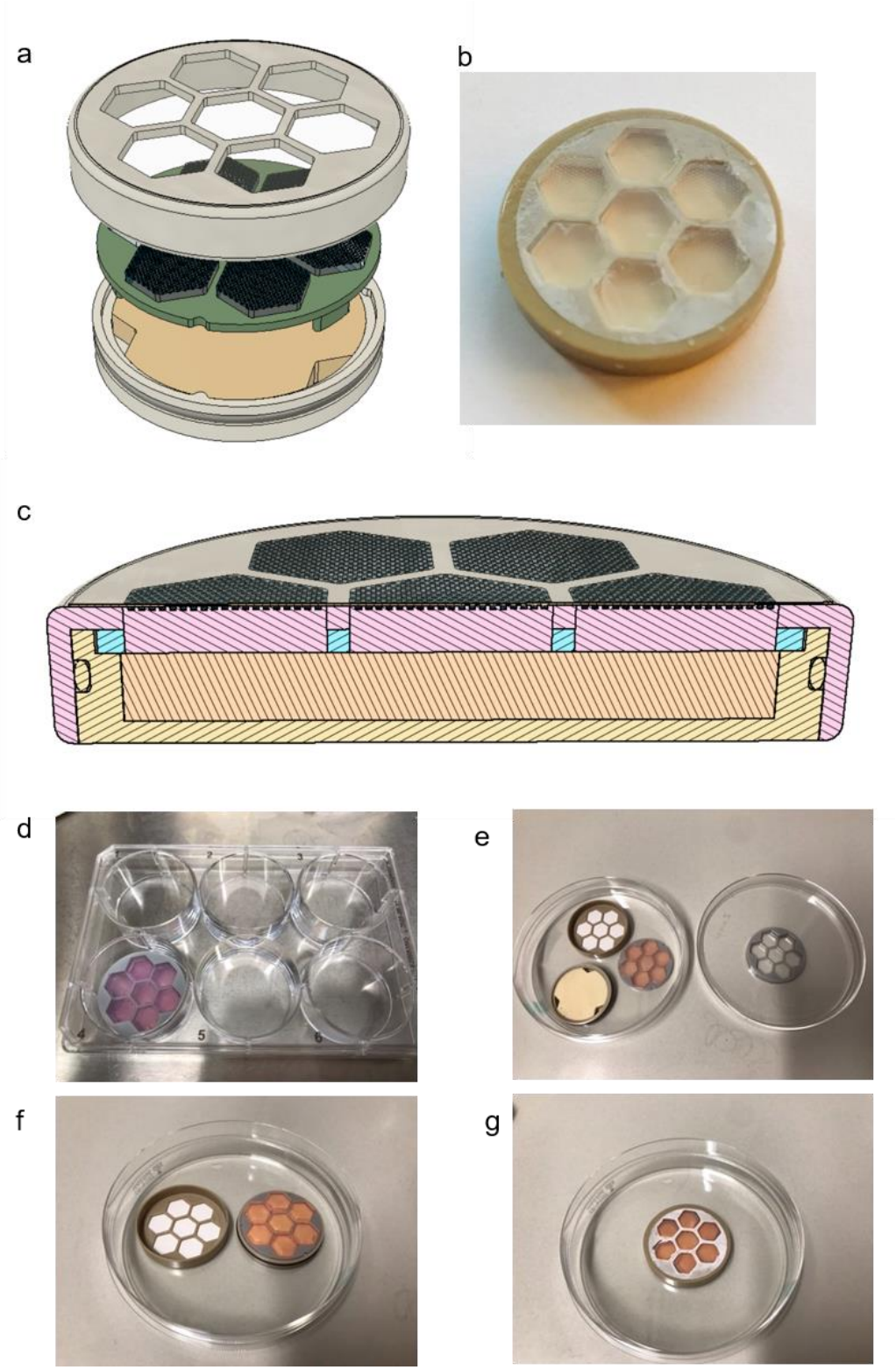

Figure 66. Final assembly of the encapsulation device modules for implantation. ***a*** *Exploded view of assembled device components****. b*** *Photograph of high fidelity prototype manufactured by CNC milling in PEEK****. c*** *Cross section of completely assembled device depicting the placement of the islets directly under the immunoisolating membrane.* ***d*** *Islet holder filled with hydrogel microwell arrays and funnel in 6-well plate to allow islet aggregation****. e*** *Single device modules before assembly.* ***f*** *Islet holder placed on skeleton.* ***g*** *Closing of device with membrane module.*

7.5 Production techniques and materials for serial scale production

To be able to bring the novel designed encapsulation into clinical practice great care has been taken on its scalability for a larger islet mass. The following section describes available production methods and for which stages of the preclinical and clinical application these are useful. Furthermore, an overview of the applied materials in the high fidelity prototype is given and the possibility of their application for a clinically scalable device are discussed.

7.5.1 Available industrial methods for small and large scale production

Two applicable techniques for the recreation of the proposed implant in industrial scale manufacturing techniques are CNC milling and injection moulding. In contrast to additive manufacturing techniques as for example 3D printing with photo-crosslinkable materials these methods enable the production with well-established biocompatible materials already used for medical devices and implants for long-term implantation in humans.

CNC milling uses a cutting tool on a rotating spindle for selective removal of material from a work piece. The raw material is mounted on a table with a vice and the material is removed layer by layer. The table and the rotating spindle can move in several axes to each other to be able to take away the material from different angles. The manufacturing instructions for this process are entered into a computer using a CAD program. This data is then converted into a machine readable format and exported to the CNC machine. After it is equipped with the appropriate tools, the milling process can start to recreate the desired shape from the material. For the construction of parts for production by CNC milling the design needs to respect certain limitations of the drilling process based on discussions with the workshop facility at IPF Dresden. For example inner vertical edges need to have an inner radius of at least 1/3 of the depth of the cavity and a minimum wall thickness for plastics of 1 mm has to be taken into account. Standard tolerances for CNC milling are ± 0.125 mm. The costs for parts produced by means of CNC milling are affected by the machining time and the complexity of the processing steps. For the manufacturing of the proposed encapsulation device this technique offers manufacturing of components from biocompatible material for smaller scale series production.

For injection moulding a tool in form of a hollow metal block needs to be fabricated first. Components are produced by injection of molten material into the metal mould. After the piece has cooled down the mould block is opened again and the moulded component is released. The up-front costs for this process are high due to the design of the mould block, testing and tooling requirements and the production of the mould tool block is also going along with long lead times. After the high initial setup cost the price per unit is low, making injection moulding

a suitable method for large series production. Furthermore, it is easier to produce complex shapes and thinner structures in contrast to CNC milling. Also the components are more regular. This is especially interesting for the production of the proposed encapsulation device as the function is strongly dependent on the micrometer-exact placement of the islets within the device.

For the preclinical evaluation of the proposed encapsulation device CNC milling is the preferred method, though the walls of the design have to be thicker. In detail this means that the bridges between the hexagons need to be designed thicker due to the required wall thickness. For a clinical scale version for application in humans a moulding tool for injection moulding can be designed. In this way, the structures can be designed lighter for large scale production.

7.5.2 Medical grade device materials and state for application

For the choice of materials certain criteria have to be fulfilled such as the stability against sterilisation, durability and their biocompatibility. For the later on application in human implantation a focus has been laid on to choose materials that are already used in medical device fabrication. An overview of the used materials is provided in Table 6.

Table 6. Materials applied in the high fidelity prototype of the proposed encapsulation device.

Part of the device	**Material**	**Product name, manufacturer**	**Current application**
Skeleton	polyetheretherketone (PEEK)	PEEK-OPTIMA™, invibio Zeniva® PEEK, solvay	medical grade product, used for surgical implant applications
O-ring on skeleton	Ethylene propylene diene monomer rubber (EPDM)	O-ring 30x1, C. Otto Gehrckens GmbH & Co. KG	FDA; USP Klasse VI; 3-A Sanitary Standard
Membrane	Hydrophilised expanded polytetrafluoroethylene (ePTFE)	Biopore Membrane Filter roll, hydrophilic PTFE, Merck Millipore	applied in macroencapsulation devices (medical implants), e.g. Theracyte™ device, βAir device
Membrane	Silicone Adhesive	MED-1137, NuSil™	medical grade product
Membrane	Heparin	heparin sodium salt from porcine intestinal mucosa, Merck	BioReagent, used for cell culture, available as medical drug
Membrane	starPEG	starPEG-NH_2, JemKem Technology	used in cell culture grade for *in vitro* experiments
Islet module	Agarose	Agarose, Sigma-Aldrich, USA	BioReagent
Oxygen module	Silicone (“PDMS”)	MED-6015, NuSil™	medical grade product
Oxygen module	Calcium peroxide	CaO_2, Sigma Aldrich, USA	used as food additive

The main components of the encapsulation device are manufactured in polyetheretherketone (PEEK). It is a semi-crystalline, high-performance thermoplastic, which has strong mechanical properties, resistance to fatigue and stress-cracking and a good structure for bearing, wear and structural applications. Furthermore, it can be manufactured by CNC milling and injection moulding. The material has extensively been used in biomedical applications and sold from different manufacturers as a medical grade material (e.g. PEEK-OPTIMA™ (invibio), Zeniva® PEEK (solvay)) as raw material rods, blocks or pellets. Especially important is its compatibility for sterilisation and its chemical resistance. It is a radiolucent material and thus not visible under X-ray, MRI or CT.

The O-ring is produced from ethylene propylene diene monomer rubber (EPDM). EPDM is a synthetic rubber that can be autoclaved as it is heat resistant till 150 °C.

The basis for the membrane used for this device (oxygen-permeable membrane and immunoisolating membrane) is an ePTFE membrane that has been applied in multiple other encapsulation devices as for example in the βAir device from BetaO_2 technologies or the Theracyte™ device (Chapter 2.4). In the previous applications it has repetitively been reported to provide good vascularisation properties (Papas et al., 2019). The production process of the membrane includes the pulling of the material under heat, which gives rise to the pores in it. Raw PTFE is hydrophobic, therefore in a further processing step it is hydrophilised. In the encapsulation device it serves a mechanical barrier with a filtration limit of 400 µm. A finer filtration mesh is obtained by filling the pores with a hydrogel network consisting of heparin and starPEG with a mesh size in the range of several tens of nm. So far, heparin-starPEG gels have been applied in animal experiments (Lohmann et al., 2017; Schirmer et al., 2020). Both single components have been regularly applied in drugs for therapeutic use. Though for the experiments polymers for laboratory use have been applied, there are medical grade products available on the market. For the application under cGMP conditions these products have to be carefully reselected as the heparin is produced from porcine mucosa and might be difficult to be approved by regulatory boards as it is derived from animal origin.

The glue to fix the membrane on the membrane holder is obtained as a medical grade silicone from NuSil™. Here it is important to use a non-slump silicone, which does not pull into the pores of the membrane. Figure 67 a shows the gluing of the membrane with a self-leveling glue, in contrast in Figure 67 b a non-slump glue is applied, which did not pull into the membrane and clock the pores. As the skeleton, produced from PEEK and the ePTFE membrane are both thermoplastic materials, the gluing step can later in an advanced manufacturing setting be replaced by a heating step, which anneals the membrane. This makes the production and faster.

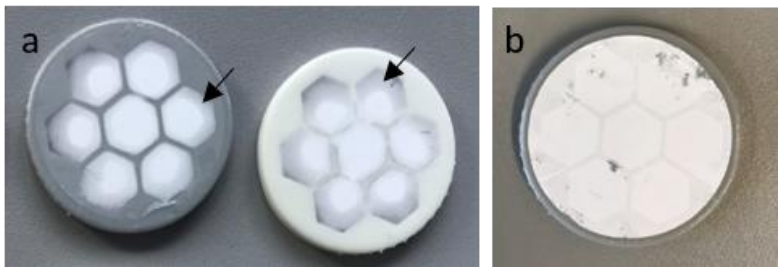

Figure 67. Islet holder produced by additive manufacturing with glued membrane with silicone adhesives with different rheological properties. a *Flowable / self levelling silicone adhesive pulls into the membrane and clocks the pores as indicated by arrows* ***b*** *Thixotropic / non-slump silicone adhesive stays at the supporting structures of the membrane holder and does not clock the membrane.*

The hydrogel microwell arrays in the islet module are produced from agarose. It is a polymer originally purified from algae, which is a widely applied polymer in the biomedical field. For the production of the microwell array it is used due to its easy applicable gelation and moulding process by a simple heating and cooling process. Furthermore, as a hydrogel it allows the free penetration of water from the implant environment to the oxygen module to activate the production of oxygen.

The oxygen scaffold is produced by mixing two components: silicone and CaO_2. The silicone is obtained from NuSil™ as a medical grade material. For the setup and testing series so far MED-6015 has been used, which is applicable for implantation in human for less than 29 days. For later on long-term applications MED-6415, which is the same medical grade material, but applicable for implantation longer than 29 days. CaO_2 is obtained from Sigma-Aldrich (USA), here further investigations have to be made whether the purity of the material from this supplier can be used for implantation.

7.6 Scalability of the macroencapsulation device for clinical application

7.6.1 Scaling of dimensions

For the design of the encapsulation device a repetitive unit of hexagons has been chosen. This gives the possibility to scale the device depending on the organism the device is applied to. This furthermore gives a tremendous advantage for the preclinical evaluation of the device. A typical small animal model in diabetes research for example is the rat, but also larger animals like rhesus macaques, pigs or dogs are models used in diabetes research and need to be used to test the function of the encapsulation device. However, these organisms have a different requirement of islet number depending on their mass, which requires a larger container to encapsulate them.

As sketched in Figure 68, encapsulation devices can be manufactured by arranging a manifold of the hexagon units, each housing a microwell hydrogel array. The size of the device can be adapted by placing 1, 3, 7, 19, 37 or 61 hexagon units together. From increasing the number of hexagon units from 7 to 19 another row of hexagons is added around the 7 hexagon unit. In the same manner the number of the hexagon units can be increased to 37 and 61 for larger designed devices. The outer layout has consciously been kept round to be able to apply an O-ring sealing mechanism. For 1, 3, 7, 19, 37 or 61 hexagon units respectively 996, 2988, 6972, 18924, 36852 or 60756 cIEQ fit into one macroencapsulation device, whereby the device diameter ranges from 14.06 mm to 94.31 mm. For estimation of the number of IEQ that fit into the devices a theoretically optimised islet density of 996 cIEQ/microwell hydrogel array (hexagon unit) is assumed as derived in chapter 4.

The islet load of the proposed encapsulation device design can furthermore be doubled by repeating the hexagons at the other side of the implant (figure). This is especially important for implantation of the encapsulation device in larger organisms, which require a much higher number of transplanted islets.

An overview of the key data for the respective device sizes with single- and double-sided placement of hexagon units is given in the Table 7.

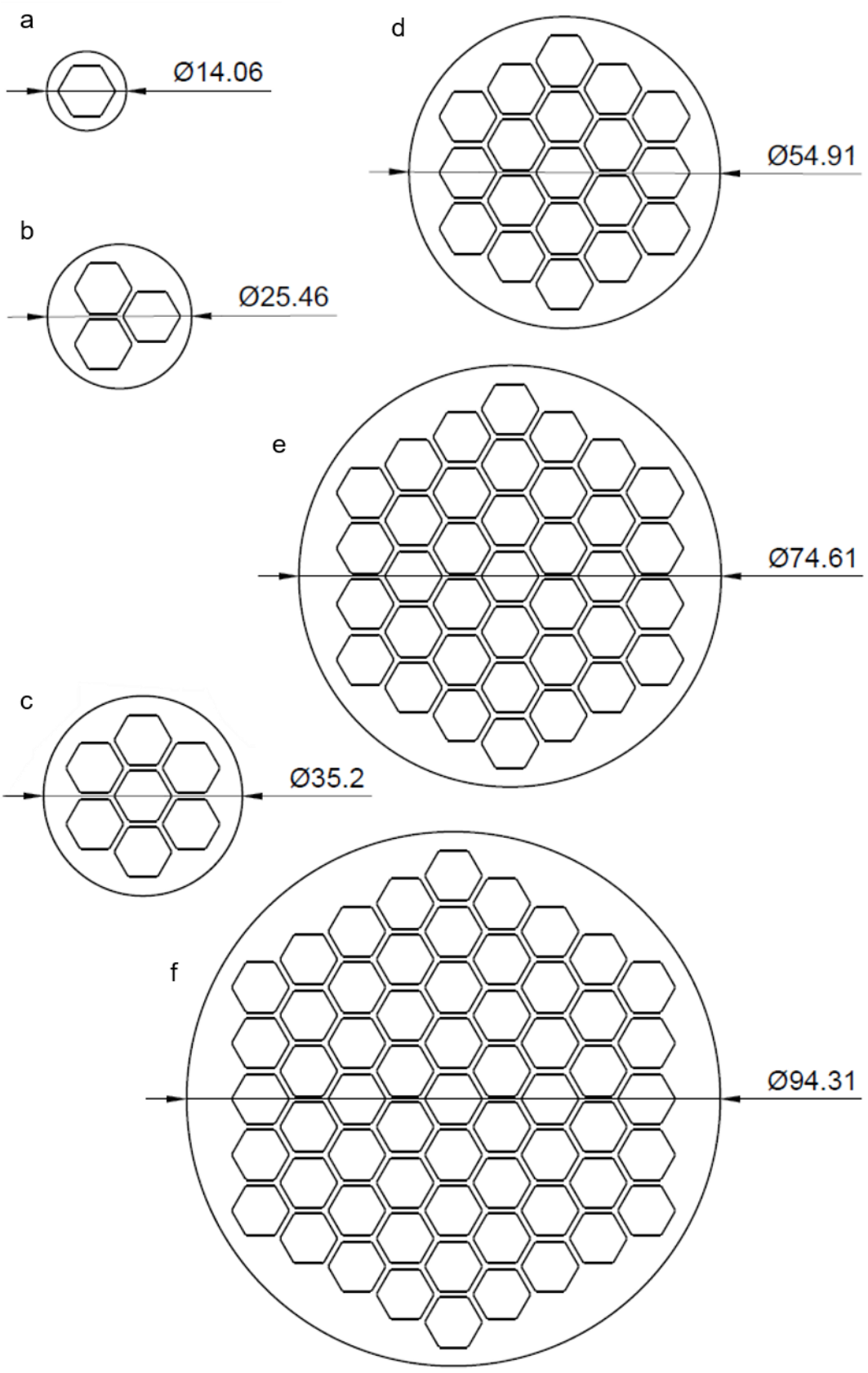

***Figure 68. Scaling of the device by arrangement of repetitive hexagon units (microwell hydrogel arrays). a** 1, **b** 3, **c** 7, **d** 19, **e** 37, **f** 61 hexagon units. Diameters in mm.*

Table 7. Analysis of dimensions and islet loading capacity of differently scaled devices.

# hexagons single-sided device	*# hexagons double-sided device*	*total surface area per side [mm²]*	*device diameter [mm]*	*cIEQ at theoretically optimised density for single-sided device (996 cIEQ/ hexagon)*	*cIEQ at theoretically optimised density for double-sided device (996 cIEQ/ hexagon)*	*possible model animal*
1	2	154.973	14.056	996	1992	rat
3	6	510.678	25.458	2988	5976	rabbit
7	14	973.136	35.2	6972	13944	sausage dog & Rhesus Macaque
19	38	2368.012	54.91	18924	37848	black wallaroo
37	74	4371.732	74.08	36852	73704	minipig
61	122	6984.936	92.306	60756	121512	human

7.6.2 Estimation of islet loading capacity and optimal islet density

In the sketched designs the device surface covered by hexagons and thus by islets is just a fraction of the whole surface. This is due to the technique chosen for the production of the holder, by CNC milling, which only allows for a minimal wall thickness of the struts of 1 mm. However, for an *in vivo* applicable device, the size is aimed to be limited to a minimum. Relative comparison of the surface area exposed to the host tissue with underlying islets (diffusion open/directly under membrane surfaces) in comparison to the total surface area ranges from 39 % to 59 % (Figure 69).

Thus, another huge advantage of the presented encapsulation device is its easy scalability. Only the skeleton structure has to be changed and the respective number of microwell hydrogel arrays has to be produced and placed into the device. This greatly reduces the production cost and time for the microwells in the large hexagon units, which are manufactured by photo and soft lithography techniques.

However, for larger scale production for a clinical setting other methods of production such as injection moulding, which allows to fabricate thinner features, must be considered as preferred manufacturing method (chapter 7.5). Thereby the dead space in between the islet-containing hexagons can be further reduced.

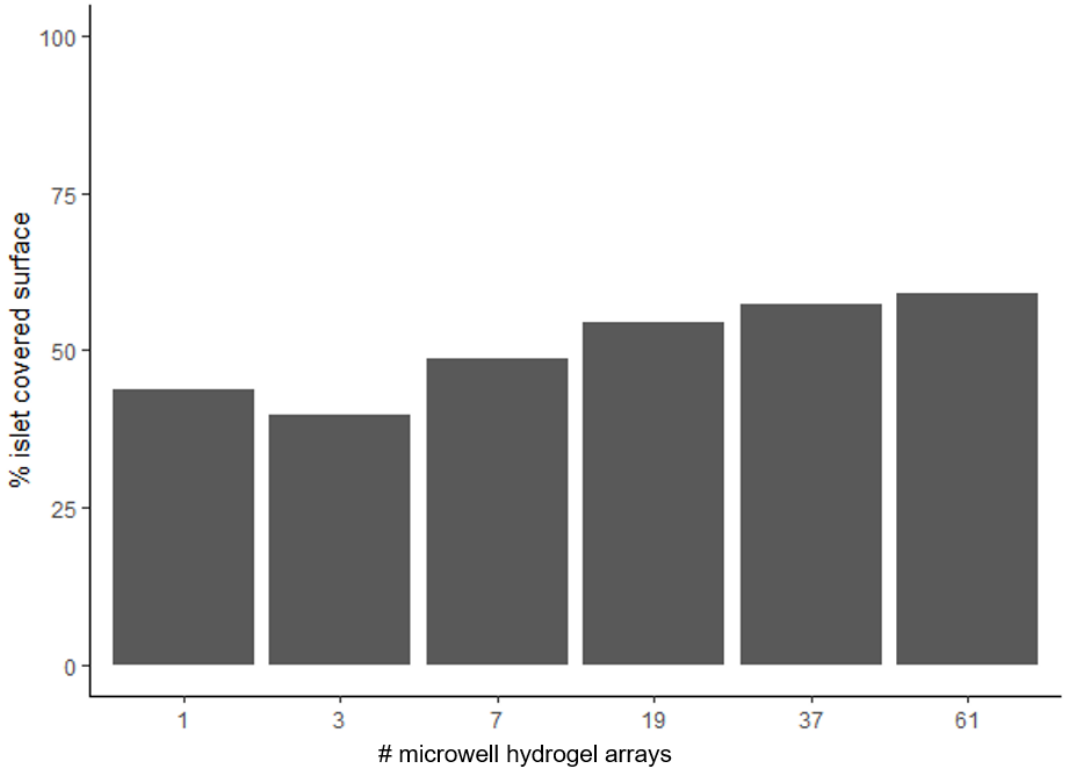

Figure 69. Relative surface area covered with islets (area of hydrogel microwell area/total surface area) for differently scaled devices produced by CNC milling.

For a single-sided CNC-fabricated device theoretically 996 to 60756 cIEQ can be encapsulated and for a double-sided device 1 992 to 121 512 cIEQ. With this amount of encapsulated islets we assume to be able to supply animals with a weight of 400 g to 24.3 kg with the single-sided device and those with a weight between 800 g and 48.6 kg with a double-sided device (Figure 70). For this calculation we assume an islet transplantation mass of 2500 IEQ/kg as proposed by Sörenby et al. (2008). This is feasible as in this novel device the islets are supplied with oxygen all the time (e.g. arrangement of islets → chapter 4; oxygen module → chapter 6) and only a minimal islet loss is assumed. With injection moulding we assume to be able to design an encapsulation device where only 15 % of the surface needs to be used for structural support. If the same size of devices is designed, the islet volume that can be encapsulated ranges from 1 939 to 87 375 IEQ for single-sided devices and 3 877 to 174 750 IEQ for a double-sided devices (Figure 71 a). These higher islet loading numbers are reflected in the organism´s mass that could be supported. For an optimised device produced by injection moulding in a single-sided set up the maximum mass is 35 kg and it is 69.9 kg for a double-sided device with a diameter of 92.3 mm (Figure 71 b).

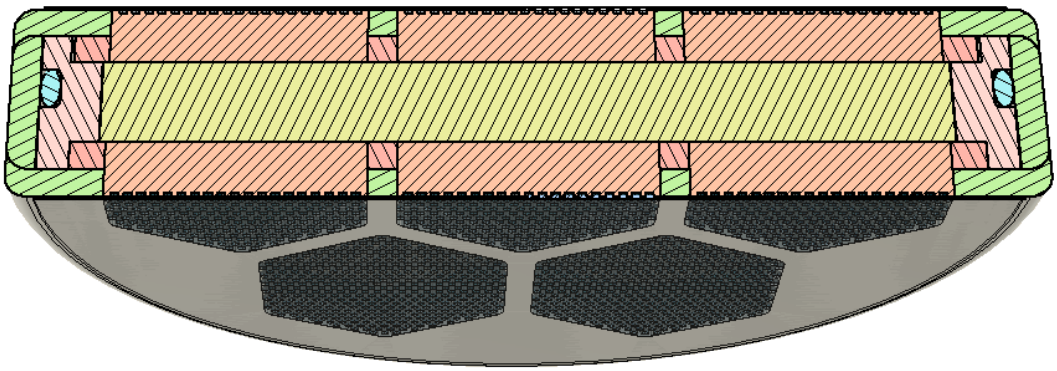

Figure 70. Schematic cross sectional view of double-sided device design.

In conclusion, the device has been designed in a way that is easily scalable for different organism sizes in preclinical testing. The proposed encapsulation device can easily be produced to fit the amount of islets needed for a rat of about 230 g by using one large hexagon microwell unit and in the same way a pig could be transplanted. A device of 2 times 61 hexagon units in a double-sided device loaded with 121512 IEQ in total can be used to transplant an adult Göttingen minipig with about 40 kg. For a scale up to clinical application injection moulding can be used, which allows a lighter design of the supporting skeleton structures and therefore the same device size can be used to encapsulated 174 750 IEQ enough for a 70 kg human patient.

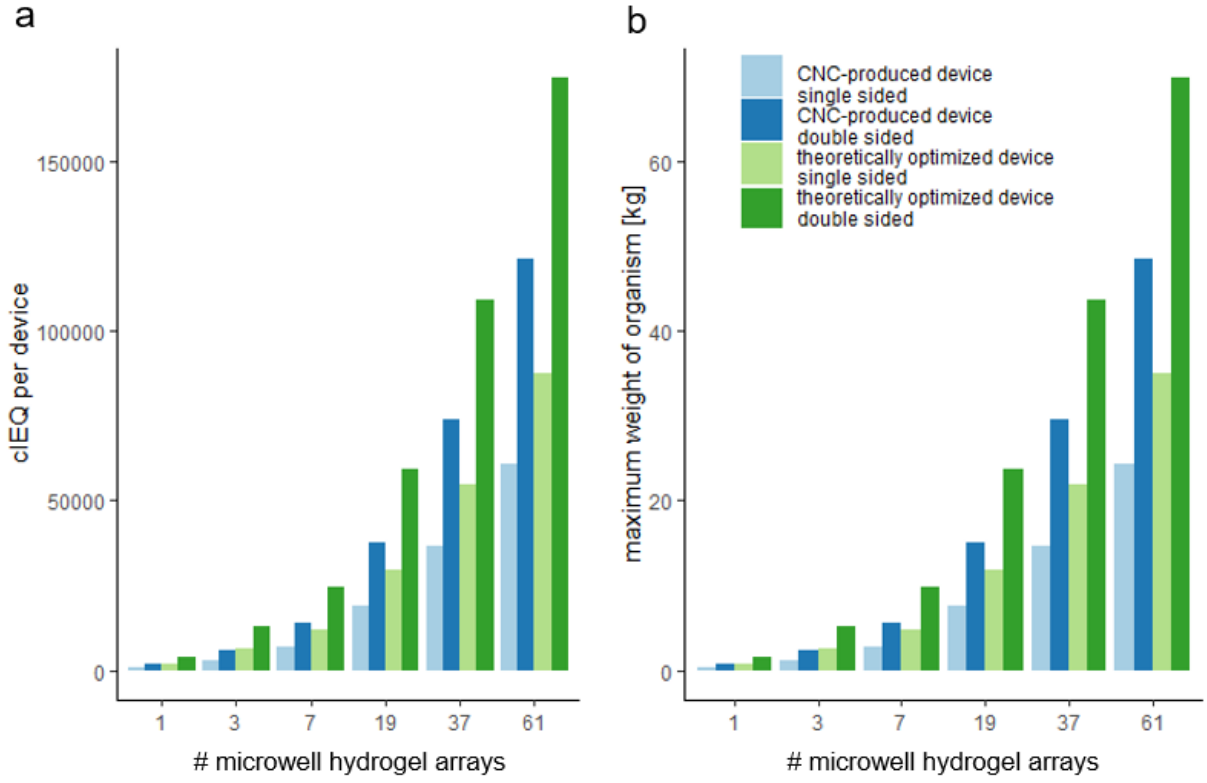

Figure 71. Properties of differently scaled single- and double-sided devices. a *Islet capacity of differently sized encapsulation device sizes.* ***b*** *Theoretical weight of organism, which can be controlled by differently sized devices.*

7.7 Concept for the preclinical evaluation of the implant

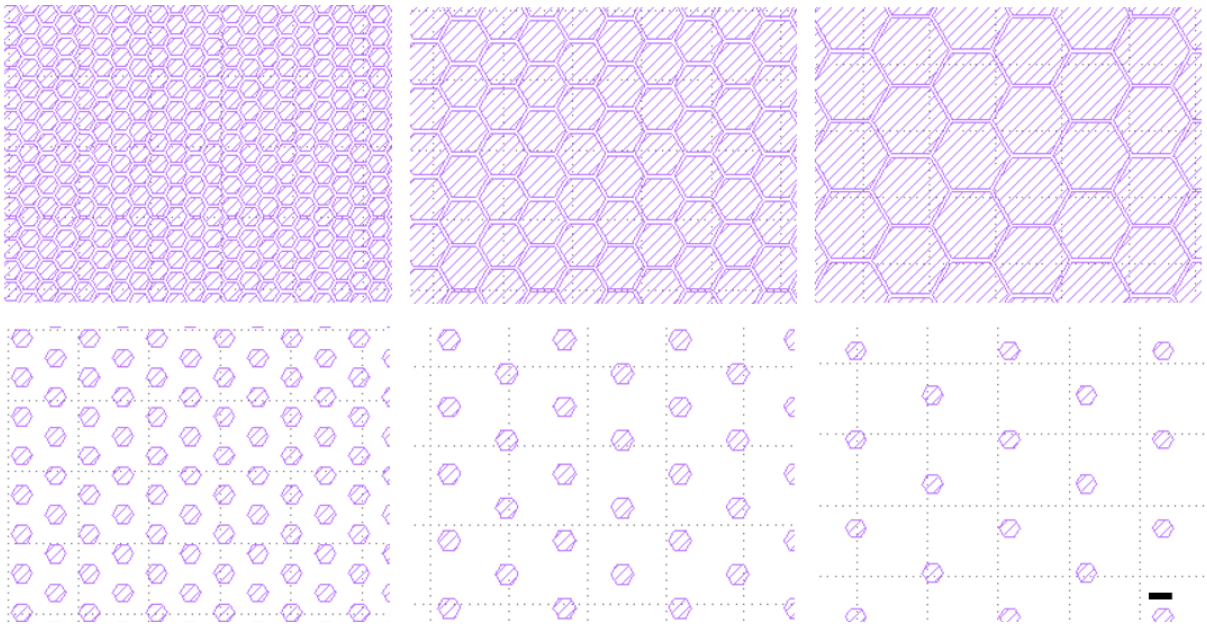

Figure 72. Hydrogel microwell array arrangements. *For the preclinical evaluation of the encapsulation device the optimal pseudo islets density is investigated by placing microwell hydrogel scaffolds filled with pseudo islets of different size and distance into the encapsulation devices. Scale bar 100 µm.*

The preclinical evaluation of the developed encapsulation device is the most critical step before scaling the device to clinical application. This chapter describes a protocol for a first evaluation of the encapsulation device in a rat model. The islets within the hexagonal hydrogel microwells arrays have been optimised in size and distance to each other in order to support their viability and function under physiologic conditions. In chapter 4 an experiment was explained, whereby pseudo islets aggregate in arrays of microwells with different width and distance to each other. Islets were cultured at 40 mm Hg oxygen (5 % oxygen concentration) to mimic the physiological transplantation environment. However, the real physiological conditions might deviate from the artificially created environment, therefore a set of different islet arrangements with 1000 IEQ each needs to be tested *in vivo (*Figure 73*)*. The criteria for the function of the implants are the reversal of the diabetes mellitus and an intraperitoneal glucose tolerance test. After explantation of the implant the pseudo islets in the hydrogels are carefully investigated for their viability and function. A detailed protocol of the procedure is described below. A second part of the animal experiment to evaluate the biocompatibility and vascularisation potential is described in chapter 4.5.

In the planned animal trial, female Sprague-Dawley rats aged 9 weeks are used. The body weight of these Sprague-Dawley rats is approximately 200 - 220 g. Sprague-Dawley rats are breeding animals with a high degree of standardisation and high genetic homogeneity while still maintaining individual diversity. These characteristics are necessary for the experiment to

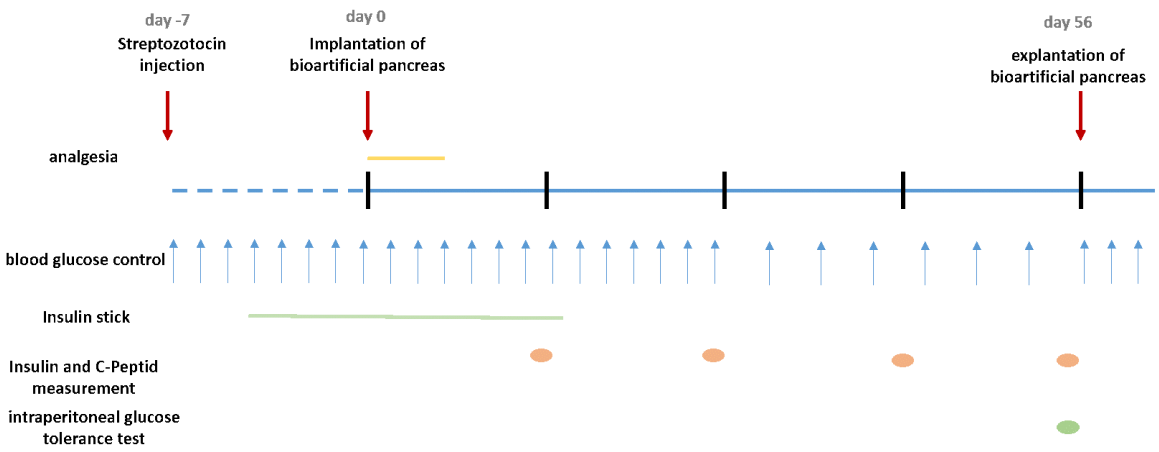

Figure 73. Timeline for implantation of the novel encapsulation device for preclinical evaluation in a rat animal model.

be successful. The animals are transplanted at the age of 9 weeks, which roughly corresponds to the human teenage age, the most critical phase of the disease, where the patients show a high vulnerability and adequate or inadequate therapy becomes highly evident and has the most critical consequences. In addition, at 9 weeks of age, the animals are already of a size that makes transplantation of the implant technically feasible.

Diabetes induction are achieved by a single intraperitoneal injection of streptozotocin at a dose of 85 mg/kg body weight (Akbarzadeh et al., 2007; Ludwig et al., 2012). This substance is a beta cell specific toxin that leads to insulin deficiency diabetes through targeted destruction of insulin-producing cells. Streptozotocin injection is the worldwide standard for diabetes induction in small animals (Akbarzadeh et al., 2007). Prior to injection, animals are kept overnight fasting, access to water remains *ad libitum*. The response to streptozotocin treatment is monitored by blood glucose. If diabetic metabolic status (blood glucose above 25 mmol/l) is not achieved within three days of injection, the animals must be classified as treatment failures and euthanised. Diabetic animals are injected with an insulin implant, which temporarily supplies the animals with insulin. The implant are removed 7 days after implantation of the encapsulation device. Glucose monitoring is carried out initially daily and subsequently 3 times a week via a tail vein and with the aid of a conventional glucometer.

For the preparation of the implant islets are isolated from rat pancreata to fill the implants. After cultivation of the islets for 24h, the islets are dissociated and seeded as single cells into the corresponding microwell array hexagons. After the islets are aggregated into pseudo-islets, the scaffolds are encapsulated in the implants.

For implantation, the diabetic animals are anaesthetised with ketamine/xylazine. The back of the animals is shaved and disinfected with ethanol and betaisodona. Using a blunt dissection technique, a pocket is prepared dorso-laterally under the skin and an implant is inserted in the pocket. The skin is then closed with absorbable suture material (Vicryl Rapide 5-0 suture

material) using a continuous suture technique. The operation takes less than 15 minutes. After completion of the procedure, the animals are clinically monitored, i.e. vigilance and mobility are checked and documented hourly for the first three hours. Prophylactically, the animals receive analgesia (0.03 mg/kg buprenorphine) and metamizole (1g/l) via drinking water at the end of the procedure. Starting on the first postoperative day, the morning blood glucose is measured daily for the first week, then 3 times a week by lancet puncture of a tail vein using a conventional glucometer.

The function of the implants is further checked by an intraperitoneal glucose tolerance test. In addition to the blood glucose profile measurements, this is an important functional test to control the insulin reserve of the animals and the insulin secretion kinetics. Before diabetes induction with streptozotocin, a total of 6 animals are subjected to an ipGTT. These test results serve as control values. All animals included in the experimental project will again be subjected to an ipGTT 1 week and 4 weeks after capsule implantation. For this purpose, the animals are fasted overnight (fluid *ad libitum*) and then a glucose solution is applied intraperitoneally at a dose of 3 g/kg body weight. Blood glucose is determined at time 0 (before glucose administration), after 15 min, 30 min, 60 min, 90 min, 120 min and 180 min.

At the end of the observation period of eight weeks, the subcutaneous capsule is surgically removed and histologically processed. Prior to this, 20 minutes before the capsules are removed, the animals are given a marker for blood vessels (biotinylated tomato lectin) intravenously (Robertson et al., 2014; Cohrs et al., 2017). This makes the analysis of the data more accurate, as all blood vessels are stained equally by this method. The blood glucose level of the animals is monitored for three more days to document the return to a diabetic metabolic state and thus confirm the function of the graft. The pseudo islets are removed from the graft and examined for function and viability.

The stress to the animals in this protocol is low in relation to the purpose of the investigation, namely the preclinical testing of a concept for curing patients with type 1 diabetes mellitus. It is limited to a surgical intervention under anaesthesia, which is conducted as atraumatically as possible for the animals through postoperative close monitoring and sufficient analgesia. In case of treatment failure or complications, the animals are euthanised immediately.

7.8 Discussion and outlook

A novel islet macroencapsulation device was designed by applying rapid prototyping using stereo lithography 3D printing in the design process. Especially to design features that relate to the applicability in the assembly process it was of great advantage to print the single components and evaluate the assembly by having short design cycles and without large production costs. Great care has been taken for the geometric scalability of the device for preclinical testing in variously sized animal models by applying a modular geometry of hexagon units carrying the islets, which allows to easily create encapsulation devices with customised islet encapsulation capacity. The device geometry was designed as such, that it can be produced by CNC milling. In this way devices can be fabricated fast and at a considerable cost for medium scale series production. This method has the drawback that it requires a minimal wall thickness of 1 mm, which needs a relative large fraction of 39 % to 59 % of the surface area of the implant. This surface fraction cannot be used to place islets, while it is important to keep the implant at a considerable size for the feasibility of transplantation. For clinical application injection moulding is suggested, which requires less minimal walls thickness, though has the drawback of long setup times and high initial cost, while large series scale production costs are low. For the major structure of the encapsulation device PEEK is chosen as a versatile biocompatible material routinely applied for medical implants, which is further suitable for both production methods - CNC milling and injection moulding. The various encapsulation devices with different sizes produced by CNC milling can be filled with a single hydrogel hexagon unit in a single-sided device up to two times 61 hydrogel hexagon units and thus can carry 996 cIEQ up to 121 512 cIEQ. These islet volumes are theoretically enough to regulate the blood glucose of organisms ranging from 400 g to 48.6 kg. Furthermore, we assume that a device of reasonable size for human application can be produced by an injection moulding technique thereby reducing support structures that are required at a minimal size for CNC milling. Finally, a protocol for the preclinical evaluation in rats is suggested to validate the optimised density of islets in the hexagons.

The calculations of the suitable device size for the mass of different organism is based on the hypothesis that an islet transplantation volume of 2500 IEQ/kg is enough to regulate blood glucose in an organism. In contrast, in human islet transplantation a minimal threshold for transplantation is set at 5 000 IEQ/kg body weight. Further larger metadata analyses report, that a minimal mass of 10 000 IEQ/kg body weight is required to bring a patient to a stable metabolic state (Shapiro et al., 2006; Mccall and Shapiro, 2012). It has been reported that about 60 % of the islets die during the early post transplantation period (Biarnés et al., 2002). In clinical islet transplantation the islets are transplanted without an immunoisolating barrier and are thus attacked by the immune system. Furthermore, the islet are subjected to a lack of

sufficient oxygenation as the sufficient vascularisation from the host tissue requires some time. Especially large islet clusters, which substantially contribute to the transplanted islet volume are developing a necrotic core and are lost. Theoretical calculations have predicted encapsulation devices of unacceptable size when an approach is used as for example in the Theracyte™ device, when islets are transplanted inside the device without taking care of any enhanced initial oxygenation (Papas et al., 2019). Though it has also been shown that islet mass can be reduced to 2500 IEQ/kg in a mouse model in the Theracyte™ device, when the device was initially transplanted without islets for prevascularisation (Sörenby et al., 2008). Accordingly, it is assumed that in the novel encapsulation device 2500 IEQ/kg is enough islet mass as extra care has been taken for sufficient oxygenation of the islets from the beginning on after transplantation. The oxygenation is achieved as the islet size is limited to a size at which a hypoxic core cannot occur and the islets stay functional. In addition, in the critical early post transplantation phase, when no capillaries are yet available on the surface of the implant, the oxygenation is provided by a transient internal oxygen source (chapter 6).

The novel encapsulation device is modular in design, which allows to place the islets exactly under the membrane and provides early on oxygenation. The constructional setup though shall prove that by respecting the physical limitations of oxygen diffusion islet transplantation within an encapsulation device is feasible. For this approach a rather rudimentary design has been chosen, but which offers the great advantage of easy production from biocompatible material and easy scalability. In future other manufacturing techniques must be considered that allow are lighter design and greater patient comfort as for example ultrasonic welding. As well great improvements of additive manufacturing techniques and materials are expected. These could be for example materials with biocompatibility that allow to use printed constructs for long-term implantation or other material classes such as for example printable PTFE (3M, 2021).

8 Concluding considerations and outlook

The design idea of the proposed encapsulation device is derived from a number of highly advanced techniques of various disciplines, involving micromoulding, the formation of pseudo islets, novel semi-synthetic biomaterials and advanced manufacturing techniques. Additive manufacturing techniques like 3D printing in particular tremendously progressed prototype development by shortening prototyping cycles.

The developed encapsulation device relies on a novel filling strategy that has to our knowledge, not yet been applied. The filling strategy utilises the intrinsic self-assembly properties of pancreatic islets which allow them to reaggregate into pseudo islet clusters after their dissociation. This reaggregation takes place in a hydrogel microwell array, which allows for precise positioning of the pseudo islets, facilitating an adequate oxygen supply, solely depending on diffusion through the immunoisolating membrane. Therefore, the microwell arrangement with maximally reduced distance between islets and minimal implant surface area is crucial for a potential clinical applicability. Besides placing the islets at an optimal distance, the pseudo islet approach also allows for tuned and optimal islet sizes. It is well described that islet size is a crucial determinant for hypoxia mediated cell death (Lehmann et al., 2007b).

Alongside the novel filling strategy, the encapsulation system features a readily customisable and scalable design for different islet filling volumes. The hydrogel microwell array carrying the islets is hexagonally shaped to allow upscaling of a single unit in a plane. While structuring of the microwell pattern is time consuming, replica moulding of the single hexagon unit of a microwell master structure greatly enhances the efficiency of the process. A multitude of the hexagonal shaped microwell units are thereby used to fill a plane. At last, the proposed device geometry features a modular setup composed of a membrane module, a skeleton module and an oxygen module. The properties of each module can be advanced separately.

While islet size and distribution inside an optimally dimensioned encapsulation device are of vital importance, the choice of a suitable transplantation site decides over the final functionality of the apparatus in the human body. An environment with a high vascularisation and an accordingly high oxygen tension in the tissue is desired. Due to the relatively large size of the device, implantation is restricted to certain locations in the human body. These are either the subcutaneous site, the omental pouch, intra-peritoneal, or pre-peritoneal. The subcutaneous space has the great advantage of easy access for implantation, retrieval and biopsy, but provides only poor vascularisation. In preclinical studies, this site often led to failure of an implantation device when translated to larger animal models. Moreover, the insulin drainage of this site is less physiologic when compared to the native situation in the pancreas. In this regard, omentum or preperitoneum offer superior characteristics. Both are highly vascularised

and provide a more physiologic insulin delivery. The membrane used for coverage of the device is doped with vascularising and trophic growth factors, allowing a gradual release over time. In this way, a gradient is established towards the device that attracts endothelial cells and enhances a vascularising network in close proximity to the membrane. The correct transplantation site in combination with the delivery of growth factors shall therefore ensure adequate delivery of oxygen to the encapsulated cells and the drainage of insulin into the capillaries.

Alongside the enhancement of the islet arrangement, respecting nature's physical laws for the clinical application, a microwell arrangement by pseudo islet formation has a further advantage. The encapsulated islet volume can be precisely determined by the cell seeding number of the pseudo islets and is highly reproducible. In contrast, the general procedure of islet volume estimation is highly dependent on the researcher counting the islets as these are mostly counted and measured manually with the help of a microscope. The pseudo islet method allows establishment of a more explicit standard operating procedures for GMP applications. Additional arrays of islets could be produced during the encapsulation procedure as well, which could be used for quality control measures.

The developed concept for an encapsulation device allows the individual adaptation or advancement of single modules. Possible future changes arising e.g. from preclinical evaluation may include a further increased oxygen supply to the islets. To improve oxygen diffusion, the microwell hydrogel array might be supplemented with additional oxygen carriers such as perfluorcarbons and haemoglobin. These improve the oxygen diffusivity through the matrix and thereby oxygen availability (Johnson et al., 2009). Currently, oxygen is supplied via a degradation reaction of CaO_2 via H_2O_2 to O_2 during the initial post transplantation phase. For further advancement, additional protection of the islets could be achieved by adding catalase to the matrix of the hydrogel microwell array. Coating with ECM components is another approach to potentially increase islet functionality (Hadavi et al., 2019). Similar principles could be applied to the microwell hydrogel array by e.g. coating the microwells with collagen and laminins. Also, the shape of the islets could be modified for further enhancement of the islet loading volume. The current microwell approach supports the formation of round islets. Through the microstructuring approach however, other formats are technically feasible such as large circular flat islets. This format could then be supported by the aforementioned ECM approach. Furthermore, we have shown that a co-culture of pseudo islets in combination with MSCs can further increase the long-term functionality and integrity of the islets (see Appendix 10.3 Functional enhancement of pseudo islets by co-culture with MSCs).

The current first prototype of the device is designed to fit about 7000 IEQ. For the planned animal experiment a rat model will be chosen, which does not require such a large islet mass.

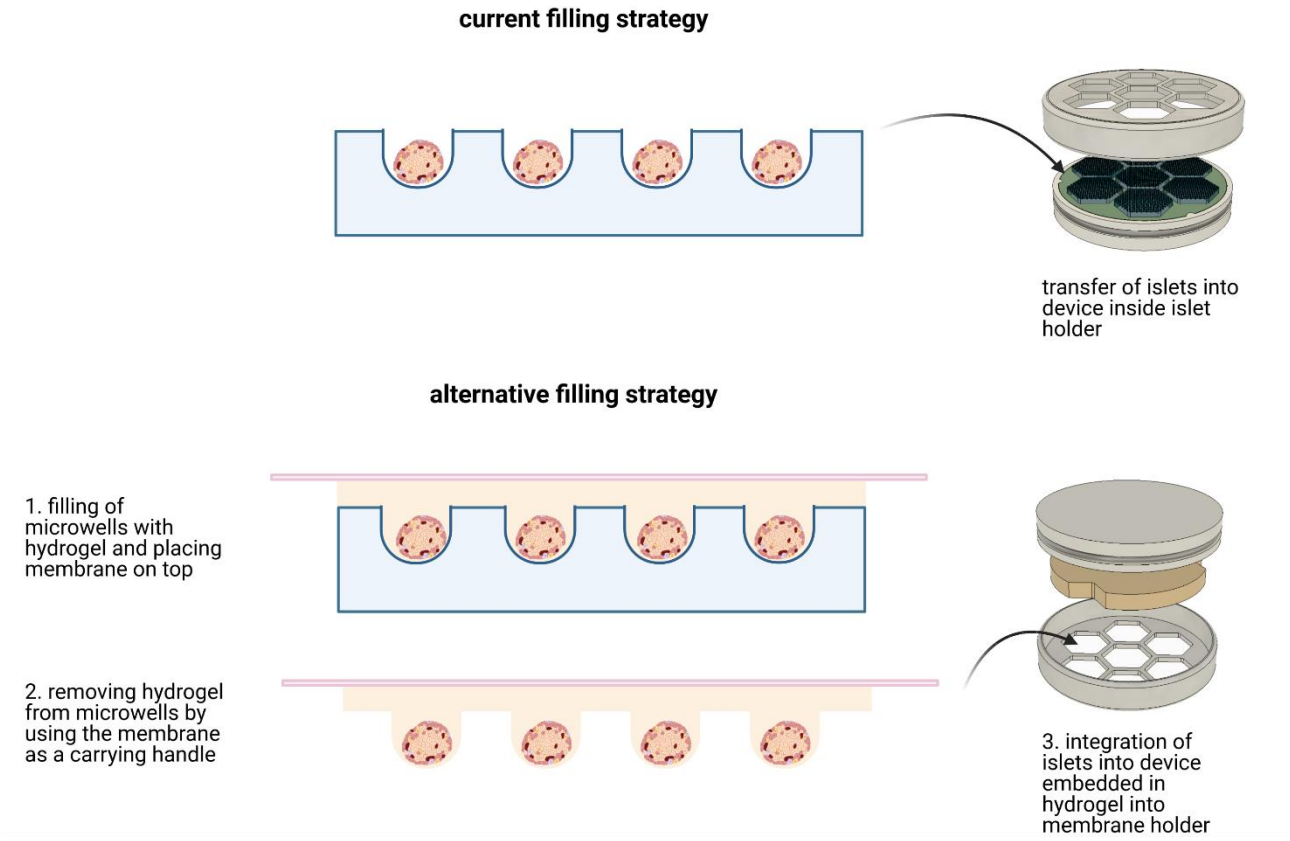

Figure 74. Current and alternative filling strategy of the novel encapsulation device.

Therefore, a prototype will be manufactured with the reduced number of three hexagonal units. Furthermore, the results of our oxygen release experiments show that the thickness of oxygen-producing disk plays a minor role for the duration of oxygen production. This allows further reduction of the device' dimensions and therefore advantages with regard to the implantation procedure.

With regard to clinical scalability, a flattening of the device could be achieved by embedding the islets in hydrogel and placing them inside the encapsulation device (Figure 74). For the application of this method in the assembly process of the device, the pseudo islets could be assembled in the described hydrogel microwell arrays. After reaggregation of the islets, an *in situ* polymerising hydrogel precursor solution can be applied on the arranged pseudo islets in combination with a membrane which could be used as a handle. These thin hydrogel sheets could then be transferred onto the inside of the membrane holder and fixed in position by a redesigned oxygen-generating disk in combination with the enclosing skeleton.

Encapsulation technology will play an important role in tomorrow's treatment of diabetes and other endocrine diseases. The method of islet encapsulation will extend the horizon of possible beta cell sources to stem cell derived beta-like cells and xenogeneic islets. This provides a much higher availability of tissue sources as these are not dependent on the limited pool of

tissue derived from deceased donors. Furthermore, the required immunosuppression associated with major comorbidities will not longer be necessary and therefore widen the indication and the eligible cohort of patients for beta cell replacement.

9 References

3M. 2021. Hochleistungspolymere und -werkstoffe - Additive Fertigung mit PTFE. [accessed: 02/02/2021] URL: https://www.3mdeutschland.de/3M/de_DE/entwicklungs-und-spezialmaterialien/3d-druck/.

Aamodt KI, Powers AC. 2017. Signals in the pancreatic islet microenvironment influence β-cell proliferation. Diabetes, Obes Metab, 19(Suppl 1):124–136 DOI: 10.1111/dom.13031.

Abdi SIH, Ng SM, Lim JO. 2011. An enzyme-modulated oxygen-producing micro-system for regenerative therapeutics. Int J Pharm, 409(1–2):203–205 DOI: 10.1016/j.ijpharm.2011.02.041.

Achilli TM, Meyer J, Morgan JR. 2012. Advances in the formation, use and understanding of multi-cellular spheroids. Expert Opin Biol Ther, 12(10):1347–1360 DOI: 10.1517/14712598.2012.707181.

Akbarzadeh A, Norouzian D, Mehrabi M, Jamshidi S, Farhangi A, Allah Verdi A, Mofidian S, Lame Rad B, Akbarzadeh Azim. 2007. Induction of Diabetes by Streptozotocin in rats.

Anon. PhysiologyWeb. [accessed: 06/01/2021] URL: https://www.physiologyweb.com/calculators/diffusion_time_calculator.html.

Aoun RB, Sigrist S, Sproll S. 2013. US20160310541A1 - A chamber for encapsulating secreting cells.

Artimo P, Jonnalagedda M, Arnold K, Baratin D, Csardi G, De Castro E, Duvaud S, Flegel V, Fortier A, Gasteiger E, Grosdidier A, Hernandez C, Ioannidis V, Kuznetsov D, Liechti R, Moretti S, Mostaguir K, Redaschi N, Rossier G, Xenarios I, Stockinger H. 2012. ExPASy: SIB bioinformatics resource portal. Nucleic Acids Res, 40(W1) DOI: 10.1093/nar/gks400.

Aso Y, Yoshiioka S, Kojima S. 1998. Determination of the Diffusion Coefficient of Insulin an Lysozyme in Crosslinked Dextran Hydrogels by Pulsed- Field- Gradient NMR. [accessed: 06/01/2021] URL: http://www.mendeley.com/research/geology-volcanic-history-eruptive-style-yakedake-volcano-group-central-japan/.

Atallah P, Schirmer L, Tsurkan M, Putra Limasale YD, Zimmermann R, Werner C, Freudenberg U. 2018. In situ-forming, cell-instructive hydrogels based on glycosaminoglycans with varied sulfation patterns. Biomaterials, 181:227–239 DOI: 10.1016/j.biomaterials.2018.07.056.

Barkai U, Rotem A, de Vos P. 2016. Survival of encapsulated islets: More than a membrane story. World J Transplant, 6(1):69–90 DOI: 10.5500/wjt.v6.i1.69.

Barkai U, Weir GC, Colton CK, Ludwig B, Bornstein SR, Brendel MD, Neufeld T, Bremer C, Leon A, Evron Y, Yavriyants K, Azarov D, Zimermann B, Maimon S, Shabtay N, Balyura M, Rozenshtein T, Vardi P, Bloch K, De Vos P, Rotem A. 2013. Enhanced Oxygen Supply Improves Islet Viability in a New Bioartificial Pancreas. Cell Transplant, 22(8):1463–1476 DOI: 10.3727/096368912X657341.

Barrett KE, Boitano S, Barman SM BH (2009-07-22). 2010. Ganong's review of medical physiology.

Biarnés M, Montolio M, Nacher V, Raurell M, Soler J, Montanya E. 2002. β-cell death and mass in syngeneically transplanted islets exposed to short- and long-term hyperglycemia. Diabetes, 51(1):66–72 DOI: 10.2337/diabetes.51.1.66.

Bosco D, Meda P, Halban PA, Rouiller DG. 2000. Importance of cell-matrix interactions in rat islet β-cell secretion in vitro: Role of α6β1 integrin. Diabetes, 49(2):233–243 DOI: 10.2337/diabetes.49.2.233.

Bouchoux A, Roux-De Balmann H, Lutin F. 2005. Nanofiltration of glucose and sodium lactate solutions: Variations of retention between single- and mixed-solute solutions. J Memb Sci, 258(1–2):123–132 DOI: 10.1016/j.memsci.2005.03.002.

Bray LJ, Binner M, Holzheu A, Friedrichs J, Freudenberg U, Hutmacher DW, Werner C. 2015. Multi-parametric hydrogels support 3D invitro bioengineered microenvironment models of tumour angiogenesis. Biomaterials, 53(June):609–620 DOI: 10.1016/j.biomaterials.2015.02.124.

Buchwald P, Wang X, Khan A, Bernal A, Fraker C, Inverardi L, Ricordi C. 2009. Quantitative Assessment of Islet Cell Products: Estimating the Accuracy of the Existing Protocol and Accounting for Islet Size Distribution. Cell Transplant, 18:1223–1235 DOI: 10.3727/096368909X476968.

Carlsson PO, Espes D, Sedigh A, Rotem A, Zimerman B, Grinberg H, Goldman T, Barkai U, Avni Y, Westermark GT, Carlbom L, Ahlström H, Eriksson O, Olerud J, Korsgren O. 2018. Transplantation of macroencapsulated human islets within the bioartificial pancreas βAir to patients with type 1 diabetes mellitus. Am J Transplant DOI: 10.1111/ajt.14642.

Charles A Janeway J, Travers P, Walport M, Shlomchik MJ. 2001. The structure of a typical antibody molecule. [accessed: 31/01/2021] URL: https://www.ncbi.nlm.nih.gov/books/NBK27144/.

Chwalek K, Tsurkan M V., Freudenberg U, Werner C. 2014. Glycosaminoglycan-based hydrogels to modulate heterocellular communication in in vitro angiogenesis models. Sci

Rep, 4:4–11 DOI: 10.1038/srep04414.

Cohrs CM, Chen C, Jahn SR, Stertmann J, Chmelova H, Weitz J, Bähr A, Klymiuk N, Steffen A, Ludwig B, Kamvissi V, Wolf E, Bornstein SR, Solimena M, Speier S. 2017. Vessel network architecture of adult human islets promotes distinct cell-cell interactions in situ and is altered after transplantation. Endocrinology, 158(5):1373–1385 DOI: 10.1210/en.2016-1184.

Colton CK. 2014. Oxygen supply to encapsulated therapeutic cells. Adv Drug Deliv Rev, 67–68:93–110 DOI: 10.1016/J.ADDR.2014.02.007.

Cooper DKC, Good AH, Koren E, Oriol R, Malcolm AJ, Ippolito RM, Neethling FA, Ye Y, Romano E, Zuhdi N. 1993. Identification of α-galactosyl and other carbohydrate epitopes that are bound by human anti-pig antibodies: relevance to discordant xenografting in man. Transpl Immunol, 1(3):198–205 DOI: 10.1016/0966-3274(93)90047-C.

Coronel MM, Geusz R, Stabler CL. 2017. Mitigating hypoxic stress on pancreatic islets via in situ oxygen generating biomaterial. Biomaterials, 129:139–151 DOI: 10.1016/J.BIOMATERIALS.2017.03.018.

Coronel MM, Liang J-P, Li Y, Stabler CL. 2019a. Oxygen generating biomaterial improves the function and efficacy of beta cells within a macroencapsulation device. Biomaterials, 210:1–11 DOI: 10.1016/j.biomaterials.2019.04.017.

Coronel MM, Liang J-P, Li Y, Stabler CL. 2019b. Oxygen generating biomaterial improves the function and efficacy of beta cells within a macroencapsulation device. Biomaterials, 210:1–11 DOI: 10.1016/J.BIOMATERIALS.2019.04.017.

Decembrini S, Hoehnel S, Brandenberg N, Arsenijevic Y, Lutolf MP. 2020. Hydrogel-based milliwell arrays for standardized and scalable retinal organoid cultures. Sci Rep, 10(1):1–10 DOI: 10.1038/s41598-020-67012-7.

Defymed. 2021. Defymed webpage. URL: https://defymed.com/mailpan/.

Deutsche Diabetes Gesellschaft. 2018. S3-Leitlinie Therapie des Typ-1-Diabetes, 2. Auflage. [accessed: 06/02/2021] URL: www.awmf.org/leitlinien/detail/ll/057-013.html.

Dionne KE, Colton CK, Yarmush ML. 1993. Effect of hypoxia on insulin secretion by isolated rat and canine islets of Langerhans. Diabetes, 42(1):12–21 DOI: 10.2337/diab.42.1.12.

Elliott RB, Escobar L, Tan PLJ, Muzina M, Zwain S, Buchanan C. 2007. Live encapsulated porcine islets from a type 1 diabetic patient 9.5 yr after xenotransplantation. Xenotransplantation, 14(2):157–161 DOI: 10.1111/j.1399-3089.2007.00384.x.

Evron Y, Colton CK, Ludwig B, Weir GC, Zimermann B, Maimon S, Neufeld T, Shalev N, Goldman T, Leon A, Yavriyants K, Shabtay N, Rozenshtein T, Azarov D, Diienno AR, Steffen A, De Vos P, Bornstein SR, Barkai U, Rotem A. 2018. Long-term viability and function of transplanted islets macroencapsulated at high density are achieved by enhanced oxygen supply OPEN. , 8:6508 DOI: 10.1038/s41598-018-23862-w.

Feldhusen J, Grote K-H (eds). 2013. Pahl/Beitz Konstruktionslehre. Springer Berlin Heidelberg DOI: 10.1007/978-3-642-29569-0.

Fischer S, Schmidt-Göhrich K, Verlohren M, Schulze J. 2004. Diagnostik und Therapie des Diabetes mellitus Typ 2. Ärzteblatt Sachsen Orig, 12:561–574.

Freudenberg U, Hermann A, Welzel PB, Stirl K, Schwarz SC, Grimmer M, Zieris A, Panyanuwat W, Zschoche S, Meinhold D, Storch A, Werner C. 2009. A star-PEG–heparin hydrogel platform to aid cell replacement therapies for neurodegenerative diseases. Biomaterials, 30(28):5049–5060 DOI: 10.1016/j.biomaterials.2009.06.002.

Freudenberg U, Zieris A, Chwalek K, Tsurkan M V., Maitz MF, Atallah P, Levental KR, Eming SA, Werner C. 2015. Heparin desulfation modulates VEGF release and angiogenesis in diabetic wounds. J Control Release, 220:79–88 DOI: 10.1016/J.JCONREL.2015.10.028.

Gagnon P, Nian R, Leong D, Hoi A. 2015. Transient conformational modification of immunoglobulin G during purification by protein A affinity chromatography. J Chromatogr A, 1395:136–142 DOI: 10.1016/j.chroma.2015.03.080.

Geller RL, Loudovaris T, Neuenfeldt S, Johnson RC, Brauker JH. 2006. Use of an Immunoisolation Device for Cell Transplantation and Tumor Immunotherapy. Ann N Y Acad Sci, 831(1):438–451 DOI: 10.1111/j.1749-6632.1997.tb52216.x.

Gholipourmalekabadi M, Zhao S, Harrison BS, Mozafari M, Seifalian AM. 2016. Oxygen-Generating Biomaterials: A New, Viable Paradigm for Tissue Engineering? Trends Biotechnol, 34(12):1010–1021 DOI: 10.1016/j.tibtech.2016.05.012.

Giraldo JA, Weaver JD, Stabler CL. 2010. Enhancing Clinical Islet Transplantation through Tissue Engineeering Strategies. [accessed: 26/01/2021] URL: www.journalofdst.org.

Groth CG, Tibell A, Tollemar J, Bolinder J, Östman J, Möller E, Reinholt FP, Korsgren O, Hellerström C, Andersson A. 1994. Transplantation of porcine fetal pancreas to diabetic patients. Lancet, 344(8934):1402–1404 DOI: 10.1016/S0140-6736(94)90570-3.

Hadavi E, Leijten J, Engelse M, De Koning E, Jonkheijm P, Karperien M, Van Apeldoorn A. 2019. Microwell scaffolds using collagen-IV and laminin-111 lead to improved insulin secretion of human islets. Tissue Eng - Part C Methods, 25(2):71–81 DOI:

10.1089/ten.tec.2018.0336.

Heinz HP. 1989. Biological functions of C1q expressed by conformational changes. Behring Inst Mitt, (84):20—31 URL: http://europepmc.org/abstract/MED/2478117.

Henderson JR, Moss MC. 1985. A MORPHOMETRIC STUDY OF THE ENDOCRINE AND EXOCRINE CAPILLARIES OF THE PANCREAS. Q J Exp Physiol, 70(3):347–356 DOI: 10.1113/expphysiol.1985.sp002920.

Hilderink J, Spijker S, Carlotti F, Lange L, Engelse M, van Blitterswijk C, de Koning E, Karperien M, van Apeldoorn A. 2015. Controlled aggregation of primary human pancreatic islet cells leads to glucose-responsive pseudoislets comparable to native islets. J Cell Mol Med, 19(8):1836–1846 DOI: 10.1111/jcmm.12555.

Hoffman AS. 2012. Hydrogels for biomedical applications. Adv Drug Deliv Rev, 64:18–23 DOI: 10.1016/J.ADDR.2012.09.010.

Hogrebe NJ, Augsornworawat P, Maxwell KG, Velazco-Cruz L, Millman JR. 2020. Targeting the cytoskeleton to direct pancreatic differentiation of human pluripotent stem cells. Nat Biotechnol, 38(4):460–470 DOI: 10.1038/s41587-020-0430-6.

Ichihara Y, Utoh R, Yamada M, Shimizu T, Uchigata Y. 2016. Size effect of engineered islets prepared using microfabricated wells on islet cell function and arrangement. Heliyon, 2(6) DOI: 10.1016/j.heliyon.2016.e00129.

In't Veld P, Marichal M. 2010. Microscopic anatomy of the human islet of Langerhans. Adv Exp Med Biol, 654:1–19 DOI: 10.1007/978-90-481-3271-3_1.

International Diabetes Foundation. 2019. No Title. IDF Diabetes Atlas URL: https://www.diabetesatlas.org/en.

Jensen SS, Jensen H, Cornett C, Møller EH, Østergaard J. 2014. Insulin diffusion and self-association characterized by real-time UV imaging and Taylor dispersion analysis. J Pharm Biomed Anal, 92:203–210 DOI: 10.1016/j.jpba.2014.01.022.

Jesser C, Kessler L, Lambert A, Belcourt A, Pinget M. 1996. Pancreatic Islet Macroencapsulation: A New Device for the Evaluation of Artificial Membrane. Artif Organs, 20(9):997–1007 DOI: 10.1111/j.1525-1594.1996.tb04587.x.

Johnson AS, Fisher RJ, Weir GC, Colton CK. 2009. Oxygen consumption and diffusion in assemblages of respiring spheres: Performance enhancement of a bioartificial pancreas. Chem Eng Sci, 64(22):4470–4487 DOI: 10.1016/J.CES.2009.06.028.

Jun Y, Kang AR, Lee JS, Park SJ, Lee DY, Moon SH, Lee SH. 2014. Microchip-based

engineering of super-pancreatic islets supported by adipose-derived stem cells. Biomaterials, 35(17):4815–4826 DOI: 10.1016/j.biomaterials.2014.02.045.

Kaido T, Yebra M, Cirulli V, Montgomery AM. 2004. Regulation of human β-cell adhesion, motility, and insulin secretion by collagen IV and its receptor α1β1. J Biol Chem, 279(51):53762–53769 DOI: 10.1074/jbc.M411202200.

Kobel S, Limacher M, Gobaa S, Laroche T, Lutolf MP. 2009. Micropatterning of hydrogels by soft embossing. Langmuir, 25(15):8774–8779 DOI: 10.1021/la9002115.

Komatsu H, Cook C, Wang C-H, Medrano L, Lin H, Kandeel F, Tai Y-C, Mullen Y. 2017. Oxygen environment and islet size are the primary limiting factors of isolated pancreatic islet survival. In: Bencharit S (ed) PLoS One, 12(8):e0183780 DOI: 10.1371/journal.pone.0183780.

Koulouras G, Panagopoulos A, Rapsomaniki MA, Giakoumakis NN, Taraviras S, Lygerou Z. 2018. EasyFRAP-web: A web-based tool for the analysis of fluorescence recovery after photobleaching data. Nucleic Acids Res, 46(W1):W467–W472 DOI: 10.1093/nar/gky508.

Kroon E, Martinson LA, Kadoya K, Bang AG, Kelly OG, Eliazer S, Young H, Richardson M, Smart NG, Cunningham J, Agulnick AD, D'Amour KA, Carpenter MK, Baetge EE. 2008. Pancreatic endoderm derived from human embryonic stem cells generates glucose-responsive insulin-secreting cells in vivo. Nat Biotechnol, 26(4):443–452 DOI: 10.1038/nbt1393.

Lee GH, Lee JS, Oh HJ, Lee SH. 2016. Reproducible construction of surface tension-mediated honeycomb concave microwell arrays for engineering of 3D microtissues with minimal cell loss. PLoS One, 11(8) DOI: 10.1371/journal.pone.0161026.

Lehmann R, Zuellig RA, Kugelmeier P, Baenninger PB, Moritz W, Perren A, Clavien PA, Weber M, Spinas GA. 2007a. Superiority of small islets in human islet transplantation. Diabetes, 56(3):594–603 DOI: 10.2337/db06-0779.

Lehmann R, Zuellig RA, Kugelmeier P, Baenninger PB, Moritz W, Perren A, Clavien PA, Weber M, Spinas GA. 2007b. Superiority of small islets in human islet transplantation. Diabetes, 56(3):594–603 DOI: 10.2337/db06-0779.

Limasale YDP, Atallah P, Werner C, Freudenberg U, Zimmermann R. 2020. Tuning the Local Availability of VEGF within Glycosaminoglycan- Based Hydrogels to Modulate Vascular Endothelial Cell Morphogenesis. Adv Funct Mater:2000068 DOI: 10.1002/adfm.202000068.

Livingstone SJ, Levin D, Looker HC, Lindsay RS, Wild SH, Joss N, Leese G, Leslie P,

McCrimmon RJ, Metcalfe W, McKnight JA, Morris AD, Pearson DWM, Petrie JR, Philip S, Sattar NA, Traynor JP, Colhoun HM. 2015. Estimated life expectancy in a scottish cohort with type 1 diabetes, 2008-2010. JAMA - J Am Med Assoc, 313(1):37–44 DOI: 10.1001/jama.2014.16425.

Lohmann N, Schirmer L, Atallah P, Wandel E, Ferrer RA, Werner C, Simon JC, Franz S, Freudenberg U. 2017. Glycosaminoglycan-based hydrogels capture inflammatory chemokines and rescue defective wound healing in mice. Sci Transl Med, 9(386):eaai9044 DOI: 10.1126/scitranslmed.aai9044.

Ludwig B, Ludwig S, Steffen A, Knauf Y, Zimerman B, Heinke S, Lehmann S, Schubert U, Schmid J, Bleyer M, Schönmann U, Colton CK, Bonifacio E, Solimena M, Reichel A, Schally A V., Rotem A, Barkai U, Grinberg-Rashi H, Kaup F-J, Avni Y, Jones P, Bornstein SR. 2017. Favorable outcome of experimental islet xenotransplantation without immunosuppression in a nonhuman primate model of diabetes. Proc Natl Acad Sci:201708420 DOI: 10.1073/pnas.1708420114.

Ludwig B, Reichel A, Steffen A, Zimerman B, Schally A V, Block NL, Colton CK, Ludwig S, Kersting S, Bonifacio E, Solimena M, Gendler Z, Rotem A, Barkai U, Bornstein SR. 2013. Transplantation of human islets without immunosuppression. Proc Natl Acad Sci U S A, 110(47):19054–8 DOI: 10.1073/pnas.1317561110.

Ludwig B, Rotem A, Schmid J, Weir GC, Colton CK, Brendel MD, Neufeld T, Block NL, Yavriyants K, Steffen A, Ludwig S, Chavakis T, Reichel A, Azarov D, Zimermann B, Maimon S, Balyura M, Rozenshtein T, Shabtay N, Vardi P, Bloch K, de Vos P, Schally A V, Bornstein SR, Barkai U. 2012. Improvement of islet function in a bioartificial pancreas by enhanced oxygen supply and growth hormone releasing hormone agonist. Proc Natl Acad Sci U S A, 109(13):5022–7 DOI: 10.1073/pnas.1201868109.

Ludwig B, Zimerman B, Steffen A, Yavriants K, Azarov D, Reichel A, Vardi P, German T, Shabtay N, Rotem A, Evron Y, Neufeld T, Mimon S, Ludwig S, Brendel M, Bornstein S, Barkai U. 2010. A Novel Device for Islet Transplantation Providing Immune Protection and Oxygen Supply. Horm Metab Res, 42(13):918–922 DOI: 10.1055/s-0030-1267916.

Lustig SR, Peppas NA. 1988. Solute diffusion in swollen membranes. IX. Scaling laws for solute diffusion in gels. J Appl Polym Sci, 36(4):735–747 DOI: 10.1002/app.1988.070360401.

Ma Y, Zhang B-T, Zhao L, Guo G, Lin J-M. 2007. Study on the generation mechanism of reactive oxygen species on calcium peroxide by chemiluminescence and UV-visible spectra. Luminescence, 22(6):575–580 DOI: 10.1002/bio.1003.

Mccall M, Shapiro AMJ. 2012. Update on Islet Transplantation. Cold Spring Harb Perspect Med, 2(7)::a007823 DOI: 10.1101/cshperspect.a007823.

Meisinger C, Wölke G, Brasche S, Strube G, Heinrich J. 2006. Postload Plasma Glucose and 30-Year Mortality Among Nondiabetic Middle-Aged Men From the General Population: The ERFORT Study. Ann Epidemiol, 16:534–539 DOI: 10.1016/j.annepidem.2005.10.008.

Millman JR, Xie C, Van Dervort A, Gürtler M, Pagliuca FW, Melton DA. 2016. Generation of stem cell-derived β-cells from patients with type 1 diabetes. Nat Commun, 7 DOI: 10.1038/ncomms11463.

Min BH, Shin JS, Kim JM, Kang SJ, Kim HJ, Yoon IH, Park SK, Choi JW, Lee MS, Park CG. 2018. Delayed revascularization of islets after transplantation by IL-6 blockade in pig to non-human primate islet xenotransplantation model. Xenotransplantation, 25(1) DOI: 10.1111/xen.12374.

Mirab F, Kang YJ, Majd S. 2019. Preparation and characterization of size-controlled glioma spheroids using agarose hydrogel microwells. PLoS One, 14(1) DOI: 10.1371/journal.pone.0211078.

Mödinger Y, Teixeira GQ, Neidlinger-Wilke C, Ignatius A. 2018. Role of the complement system in the response to orthopedic biomaterials. Int J Mol Sci, 19(11) DOI: 10.3390/ijms19113367.

Montazeri L, Hojjati-Emami S, Bonakdar S, Tahamtani Y, Hajizadeh-Saffar E, Noori-Keshtkar M, Najar-Asl M, Ashtiani MK, Baharvand H. 2016. Improvement of islet engrafts by enhanced angiogenesis and microparticle-mediated oxygenation. Biomaterials, 89:157–165 DOI: 10.1016/j.biomaterials.2016.02.043.

Müller E, Pompe T, Freudenberg U, Werner C. 2017. Solvent-Assisted Micromolding of Biohybrid Hydrogels to Maintain Human Hematopoietic Stem and Progenitor Cells Ex Vivo. Adv Mater, 29(42):1703489 DOI: 10.1002/adma.201703489.

Nair GG, Liu JS, Russ HA, Tran S, Saxton MS, Chen R, Juang C, Li M lan, Nguyen VQ, Giacometti S, Puri S, Xing Y, Wang Y, Szot GL, Oberholzer J, Bhushan A, Hebrok M. 2019. Recapitulating endocrine cell clustering in culture promotes maturation of human stem-cell-derived β cells. Nat Cell Biol, 21(2):263–274 DOI: 10.1038/s41556-018-0271-4.

Nair GG, Tzanakakis ES, Hebrok M. 2020. Emerging routes to the generation of functional β-cells for diabetes mellitus cell therapy. Nat Rev Endocrinol, 16(9):506–518 DOI:

10.1038/s41574-020-0375-3.

Neufeld T, Ludwig B, Barkai U, Weir GC, Colton CK, Evron Y, Balyura M, Yavriyants K, Zimermann B, Azarov D, Maimon S, Shabtay N, Rozenshtein T, Lorber D, Steffen A, Willenz U, Bloch K, Vardi P, Taube R, de Vos P, Lewis EC, Bornstein SR, Rotem A. 2013. The Efficacy of an Immunoisolating Membrane System for Islet Xenotransplantation in Minipigs. PLoS One, 8(8) DOI: 10.1371/journal.pone.0070150.

Niclauss N, Meier R, Bédat B, Berishvili E, Berney T. 2016. Beta-cell replacement: Pancreas and islet cell transplantation. Endocr Dev, 31:146–162 DOI: 10.1159/000439412.

Oh SH, Ward CL, Atala A, Yoo JJ, Harrison BS. 2009. Oxygen generating scaffolds for enhancing engineered tissue survival. Biomaterials, 30(5):757–762 DOI: 10.1016/j.biomaterials.2008.09.065.

Pagliuca FW, Millman JR, Gürtler M, Segel M, Van Dervort A, Ryu JH, Peterson QP, Greiner D, Melton DA. 2014. Generation of functional human pancreatic β cells in vitro. Cell, 159(2):428–439 DOI: 10.1016/j.cell.2014.09.040.

Papas KK, De Leon H, Suszynski TM, Johnson RC. 2019. Oxygenation strategies for encapsulated islet and beta cell transplants. DOI: 10.1016/j.addr.2019.05.002.

Park JH, Park K. 2019. Development of micropatterns on curved surfaces using two-step ultrasonic forming. Micromachines, 10(10) DOI: 10.3390/mi10100654.

Pedraza E, Coronel MM, Fraker CA, Ricordi C, Stabler CL. 2012. Preventing hypoxia-induced cell death in beta cells and islets via hydrolytically activated, oxygen-generating biomaterials. Proc Natl Acad Sci, 109(11):4245–4250 DOI: 10.1073/pnas.1113560109.

Pigeolet E, Corbisier P, Houbion A, Lambert D, Michiels C, Raes M, Zachary MD, Remacle J. 1990. Glutathione peroxidase, superoxide dismutase, and catalase inactivation by peroxides and oxygen derived free radicals. Mech Ageing Dev, 51(3):283–297 DOI: 10.1016/0047-6374(90)90078-T.

Prin C, Bene MC, Gobert B, Montagne P, Faure GC. 1995. Isoelectric restriction of human immunoglobulin isotypes. Biochim Biophys Acta, 1243:287–290.

Prokoph S, Chavakis E, Levental KR, Zieris A, Freudenberg U, Dimmeler S, Werner C. 2012. Sustained delivery of SDF-1α from heparin-based hydrogels to attract circulating pro-angiogenic cells. Biomaterials, 33(19):4792–4800 DOI: 10.1016/j.biomaterials.2012.03.039.

Qin D, Xia Y, Whitesides GM. 2010. Soft lithography for micro- and nanoscale patterning. Nat Protoc, 5(3):491–502 DOI: 10.1038/nprot.2009.234.

Rezania A, Bruin JE, Arora P, Rubin A, Batushansky I, Asadi A, O'Dwyer S, Quiskamp N, Mojibian M, Albrecht T, Yang YHC, Johnson JD, Kieffer TJ. 2014. Reversal of diabetes with insulin-producing cells derived in vitro from human pluripotent stem cells. Nat Biotechnol, 32(11):1121–1133 DOI: 10.1038/nbt.3033.

Ricordi C, Gray D, Hering BJ, Kaufman DB, Warnock GL, Kneteman NM, Lake S, London NJM, Soccp C, Alejandro R, Zeng Y, Scharp DW, Viviani G, Falquil L, Tzakis A, Bretzel RG, Federlin K, Pozza G, James RFL, Pajotte R V, Di Carlo' V, Morris PJ, Sutherland DER, Starzl TE, Mintz DH, Lacy PE. 1990. Islet Isolation and Assessment in Man and Large Animals. Acta Diabetol, 27:185–195.

Robertson RT, Levine ST, Haynes SM, Gutierrez P, Baratta JL, Tan Z, Longmuir KJ. 2014. Use of labeled tomato lectin for imaging vasculature structures. Histochem Cell Biol, 143(2):225–234 DOI: 10.1007/s00418-014-1301-3.

Rojas-Canales DM, Waibel M, Forget A, Penko D, Nitschke J, Harding FJ, Delalat B, Blencowe A, Loudovaris T, Grey ST, Thomas HE, Kay TWH, Drogemuller CJ, Voelcker NH, Coates PT. 2018. Oxygen-permeable microwell device maintains islet mass and integrity during shipping. Endocr Connect, 7(3):490–503 DOI: 10.1530/EC-17-0349.

Rosén A, Ek K, Åman P. 1979. Agarose isoelectric focusing of native human immunoglobulin M and α2-macroglobulin. J Immunol Methods, 28(1–2):1–11 DOI: 10.1016/0022-1759(79)90322-3.

Rosenbauer J, Neu A, Rothe U, Seufert J, Holl RW. 2019. Types of diabetes are not limited to age groups: type 1 diabetes in adults and type 2 diabetes in children and adolescents. J Heal Monit, 4(2) DOI: 10.25646/5987.

Rubinstein M, Colby RH. 2003. Polymer Physics. Oxforf university press, Oxford, New York.

Schirmer L, Chwalek K, Tsurkan M V., Freudenberg U, Werner C. 2020. Glycosaminoglycan-based hydrogels with programmable host reactions. Biomaterials, 228:119557 DOI: 10.1016/j.biomaterials.2019.119557.

Scott DA, Fisher AM. 1935. Crystalline insulin. Biochem J, 29(5):1048–1054 DOI: 10.1042/bj0291048.

SES Analytical Systems GmbH. Side - Bi - Side Cells. [accessed: 12/01/2021] URL: http://www.ses-analysesysteme.de/SES-Franz_Cell_side_bi_side_uk.htm.

Shapiro AMJ, Lakey JRT, Ryan EA, Korbutt GS, Toth E, Warnock GL, Kneteman NM, Rajotte R V. 2000. Islet Transplantation in Seven Patients with Type 1 Diabetes Mellitus Using a Glucocorticoid-Free Immunosuppressive Regimen. N Engl J Med, 343(4):230–238 DOI:

10.1056/nejm200007273430401.

Shapiro AMJ, Ricordi C, Hering BJ, Auchincloss H, Lindblad R, Robertson RP, Secchi A, Brendel MD, Berney T, Brennan DC, Cagliero E, Alejandro R, Ryan EA, DiMercurio B, Morel P, Polonsky KS, Reems J-A, Bretzel RG, Bertuzzi F, Froud T, Kandaswamy R, Sutherland DER, Eisenbarth G, Segal M, Preiksaitis J, Korbutt GS, Barton FB, Viviano L, Seyfert-Margolis V, Bluestone J, Lakey JRT. 2006. International Trial of the Edmonton Protocol for Islet Transplantation. N Engl J Med, 355(13):1318–1330 DOI: 10.1056/NEJMoa061267.

Shin JS, Kim JM, Kim JS, Min BH, Kim YH, Kim HJ, Jang JY, Yoon IH, Kang HJ, Kim J, Hwang ES, Lim DG, Lee WW, Ha J, Jung KC, Park SH, Kim SJ, Park CG. 2015. Long-term control of diabetes in immunosuppressed nonhuman primates (NHP) by the transplantation of adult porcine islets. Am J Transplant, 15(11):2837–2850 DOI: 10.1111/ajt.13345.

Shorten PR, McMahon CD, Soboleva TK. 2007. Insulin transport within skeletal muscle transverse tubule networks. Biophys J, 93(9):3001–3007 DOI: 10.1529/biophysj.107.107888.

Skrzypek K, Curcio E, Stamatialis D. 2020. Modelling of mass transport and insulin secretion of a membrane-based encapsulation device of pancreatic islets. Chem Eng Res Des, 153:496–506 DOI: 10.1016/j.cherd.2019.11.020.

Sörenby AK, Kumagai-Braesch M, Sharma A, Hultenby KR, Wernerson AM, Tibell AB. 2008. Preimplantation of an Immunoprotective Device Can Lower the Curative Dose of Islets to That of Free Islet Transplantation—Studies in a Rodent Model. Transplantation, 86(2):364–366 DOI: 10.1097/TP.0b013e31817efc78.

Stibler H, Jaeken J. 1990. Carbohydrate deficient serum transferrin in a new systemic hereditary syndrome. Arch Dis Child, 65(1):107–111 DOI: 10.1136/adc.65.1.107.

Suszynski TM, Wilhelm JJ, Radosevich DM, Balamurugan AN, Sutherland DER, Beilman GJ, Dunn TB, Chinnakotla S, Pruett TL, Vickers SM, Hering BJ, Papas KK, Bellin MD. 2014. Islet size index as a predictor of outcomes in clinical islet autotransplantation. Transplantation, 97(12):1286–1291 DOI: 10.1097/01.TP.0000441873.35383.1e.

Taplin C, Barker J. 2008. Autoantibodies in type 1 diabetes. Autoimmunity, 41(1):11–18 DOI: 10.1080/08916930701619169.

TEDDY Study Group. 2008. The Environmental Determinants of Diabetes in the Young. Ann N Y Acad Sci, 1150:1–13 DOI: 10.1196/annals.1447.062.

Thomas M, Moriyama K, Ledebo I. 2011. AN69: Evolution of the World's First High Permeability Membrane. In: Contributions to Nephrology. Karger Publishers, pp. 119–129 DOI: 10.1159/000328961.

Tönnies T, Röckl S, Hoyer A, Heidemann C, Baumert J, Du Y, Scheidt-Nave C, Brinks R. 2019. Projected number of people with diagnosed Type 2 diabetes in Germany in 2040. Diabet Med, 36(10):1217–1225 DOI: 10.1111/dme.13902.

Tsurkan M V., Chwalek K, Prokoph S, Zieris A, Levental KR, Freudenberg U, Werner C. 2013. Defined polymer-peptide conjugates to form cell-instructive starpeg-heparin matrices in situ. Adv Mater, 25(18):2606–2610 DOI: 10.1002/adma.201300691.

Veal EA, Day AM, Morgan BA. 2007. Hydrogen Peroxide Sensing and Signaling. Mol Cell, 26(1):1–14 DOI: 10.1016/j.molcel.2007.03.016.

ViaCyte. 2021. ViaCyte. URL: https://viacyte.com/pipeline/.

Waite AJ, Bonner JS, Autenrieth R. 1999. Kinetics and Stoichiometry of Oxygen Release from Solid Peroxides. [accessed: 16/12/2020] URL: www.liebertpub.com.

Wang K, Yu L-Y, Jiang L-Y, Wang H-B, Wang C-Y, Luo Y. 2015. The paracrine effects of adipose-derived stem cells on neovascularization and biocompatibility of a macroencapsulation device. Acta Biomater, 15:65–76 DOI: 10.1016/j.actbio.2014.12.025.

Ward KR, Huvard GS, McHugh M, Mallepally RR, Imbruce R. 2013. Chemical oxygen generation. In: Respiratory Care. Respiratory Care, pp. 184–194 DOI: 10.4187/respcare.01983.

Wassmer CH, Bellofatto K, Perez L, Lavallard V, Cottet-Dumoulin D, Ljubicic S, Parnaud G, Bosco D, Berishvili E, Lebreton F. 2020. Engineering of Primary Pancreatic Islet Cell Spheroids for Three-dimensional Culture or Transplantation: A Methodological Comparative Study. Cell Transplant, 29:1–8 DOI: 10.1177/0963689720937292.

Wassmer CH, Lebreton F, Bellofatto K, Bosco D, Berney T, Berishvili E. 2020. Generation of insulin-secreting organoids: a step toward engineering and transplanting the bioartificial pancreas. Transpl Int, 33(12):1577–1588 DOI: 10.1111/tri.13721.

Welzel PB, Prokoph S, Zieris A, Grimmer M, Zschoche S, Freudenberg U, Werner C. 2011. Modulating Biofunctional starPEG Heparin Hydrogels by Varying Size and Ratio of the Constituents. Polymers (Basel), 3(1):602–620 DOI: 10.3390/polym3010602.

Zieris A, Chwalek K, Prokoph S, Levental KR, Welzel PB, Freudenberg U, Werner C. 2011. Dual independent delivery of pro-angiogenic growth factors from starPEG-heparin hydrogels. J Control Release, 156(1):28–36 DOI: 10.1016/J.JCONREL.2011.06.042.

Zieris A, Prokoph S, Levental KR, Welzel PB, Grimmer M, Freudenberg U, Werner C. 2010. FGF-2 and VEGF functionalization of starPEG–heparin hydrogels to modulate biomolecular and physical cues of angiogenesis. Biomaterials, 31(31):7985–7994 DOI: 10.1016/J.BIOMATERIALS.2010.07.021.

10 Appendix

10.1 Microscale thermoresis

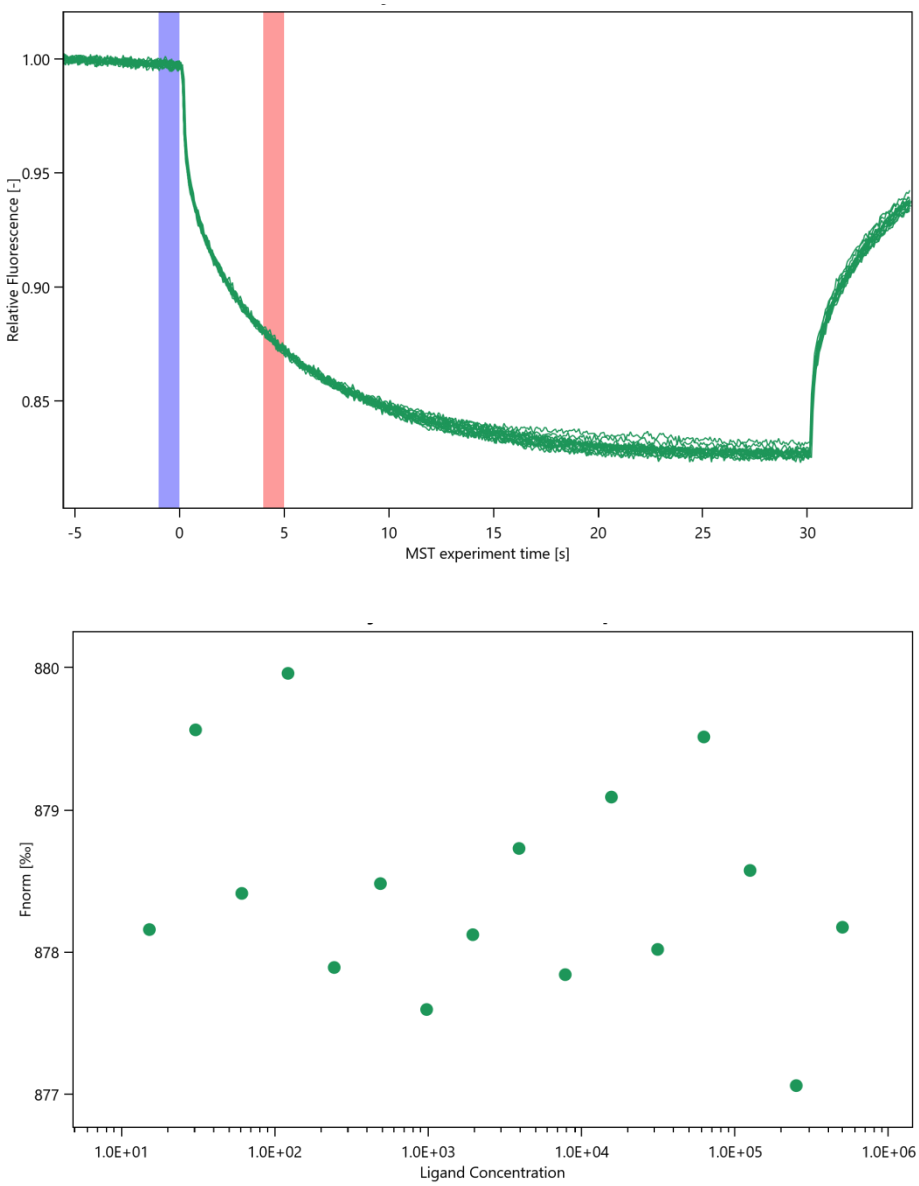

Thermophoretic movement of Dylight488-labeled insulin in various concentrations of heparin. Insulin diffusion is not affected by interactions with heparin.

10.2 Sample size calculation of the response surface for parameter optimisation of the vascularizing hydrogel

- Sample size calculations were performed by Matthias Kuhn at the ‘Institut für medizinische Informatik und Biometrie’ at the Universitätsklinikum Carl Gustav Carus Dresden

- Full factorial design of 3^2 =9 combinations, 1 central point, 4 corner points, 4 star points
- based on the data from figure 6b by (Schirmer et al., 2020)
- n = sample size per combination
- N = total sample size
- n_0 = number of samples for centre point
- n_c = number of samples per corner point
- n_s = number of samples per star point
- se_max = maximum standard error
- ci90_half = half confidence interval of 90 %
- ci95_half = half confidence interval of 95 %

N: Gesamtzahl der untersuchten Implantate, n_0, n_c, n_s: Replikate des zentralen Punkts, der 4 Eckpunkte und der 4 Stern-Punkte im Design.

n_0	n_c	n_s	N	se_max	ci90_half	ci95_half
10	20	20	170	0.093	0.152	0.181
10	20	15	150	0.098	0.162	0.193
5	20	20	165	0.102	0.168	0.200
10	20	12	138	0.103	0.170	0.203
10	15	20	150	0.104	0.171	0.204
5	15	20	145	0.105	0.172	0.205
10	15	15	130	0.107	0.175	0.209
10	20	10	130	0.108	0.177	0.211
10	15	12	118	0.108	0.178	0.213
10	15	10	110	0.110	0.180	0.215
5	20	15	145	0.111	0.183	0.218
5	15	15	125	0.113	0.187	0.222
10	12	20	138	0.114	0.188	0.223
5	12	20	133	0.115	0.189	0.225
10	12	15	118	0.117	0.192	0.229
5	12	15	113	0.118	0.193	0.230
10	12	12	106	0.119	0.196	0.233
5	20	12	133	0.119	0.196	0.233
10	12	10	98	0.121	0.199	0.237
5	15	12	113	0.121	0.199	0.237
5	12	12	101	0.122	0.201	0.240
10	10	20	130	0.122	0.201	0.240
5	10	20	125	0.123	0.203	0.242
5	20	10	125	0.126	0.206	0.246
10	10	15	110	0.126	0.207	0.247
5	10	15	105	0.127	0.208	0.248
5	15	10	105	0.127	0.209	0.249
5	12	10	93	0.128	0.211	0.252
10	10	12	98	0.128	0.211	0.252
5	10	12	93	0.129	0.212	0.253
10	10	10	90	0.130	0.214	0.255
10	20	5	110	0.130	0.214	0.255
5	10	10	85	0.131	0.215	0.257
10	15	5	90	0.133	0.219	0.261
10	12	5	78	0.136	0.223	0.266
10	10	5	70	0.138	0.227	0.271

10.3 Functional enhancement of pseudo islets by co-culture with MSCs

Islets are highly specified cell clusters with only a small proportion (1-2%) of stromal cells. This means they barely have the capacity to produce extracellular matrix factors. Especially islets, which are exposed to collagenase during the isolation process, have only little endogenous extracellular matrix components. Mesenchymal stromal cells (MSCs) have been shown to improve islet function in cocultures and can provide extracellular matrix factors. We therefore have mixed single islet cells with MSCs and seeded them together in microwell scaffolds (Figure 1).

Figure 2 shows the reaggregation of single islet cells and single islet cells with MSCs into pseudo islets and pseudo MSC islet composites. MSC pseudo islet composites aggregate faster compared to pseudo islets (already after 1 day). After 2 – 3 days, MSC and islets separate again and the MSC migrate to the outside of islet clusters and gradually disappear. Comparing control and MSC-supported pseudo islets, we observed islet of similar cluster size. However, MSC islet composites appear more compacted and stable. Control islets show a wider range of islet diameter (Figure 3).

Pseudo islets and pseudo MSC composite islets remain functional *in vitro* for up to 14 days (Figure 4). Islets were cultured as native control islets, pseudo islets or MSC pseudo islet composites in microwells for 3 or 14 days and a glucose stimulated insulin secretion assay was performed by picking triplets of islets and incubating them at either basal (2 mM) or stimulating (20 mM) glucose concentration. At 3 days of culture basal insulin secretion was lower for islets cocultured with MSC. This might indicate a nursing function of MSCs repairing leaky insulin secretion of islets damaged after isolation. In this experiment control islets have a higher stimulated insulin secretion than both other groups. This can be explained by the larger islet size of control islets (Figure 2). After 14 days of culture in microwells islets have reached a comparable level of basal insulin secretion and MSC pseudo islet composites have the highest stimulated insulin secretion. This is a promising result, although a way has to be found to calibrate for different islet size in control and pseudo islets.

To test the effect of the soft microwell culturing format, control islets were cultured in either in petri dishes or alginate microwells (Figure 5). After 4 days of culture islets cultured in microwells have triple the amount of stimulated insulin secretion over islets cultured in dishes indicated benefit of the microwell culture environment.

The increased functionality of control islets and MSC pseudo islet composites can further be observed in their structural integrity in electron microscopy pictures. These have a smooth and round surface compared to islets directly after isolation and pseudo islets (Figure 6).

Immunohistochemistry stainings indicate that MSCs deposit collagen within the islet cluster in MSC pseudo islet composites (Figure 7).

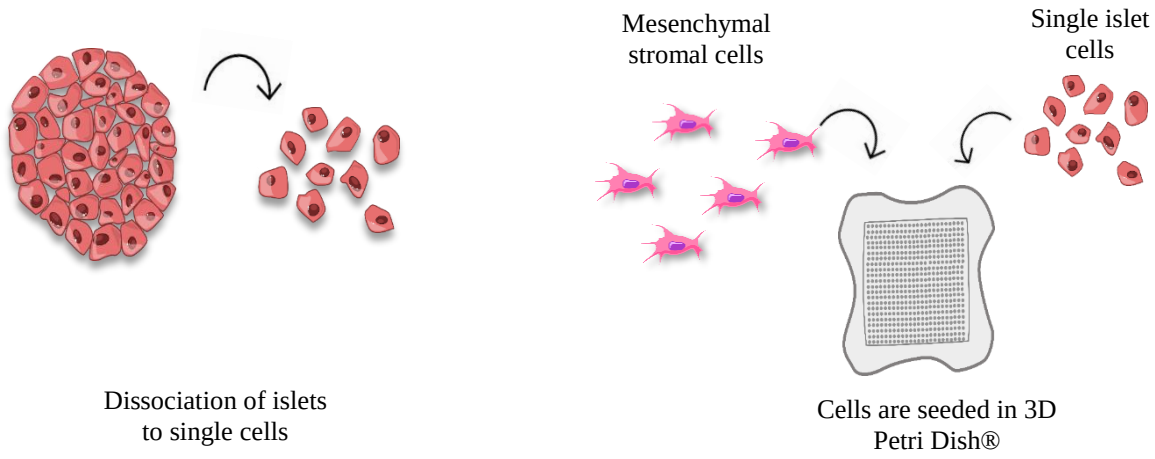

Figure 1. Preparation of pseudo islets and pseudo MSC composites.

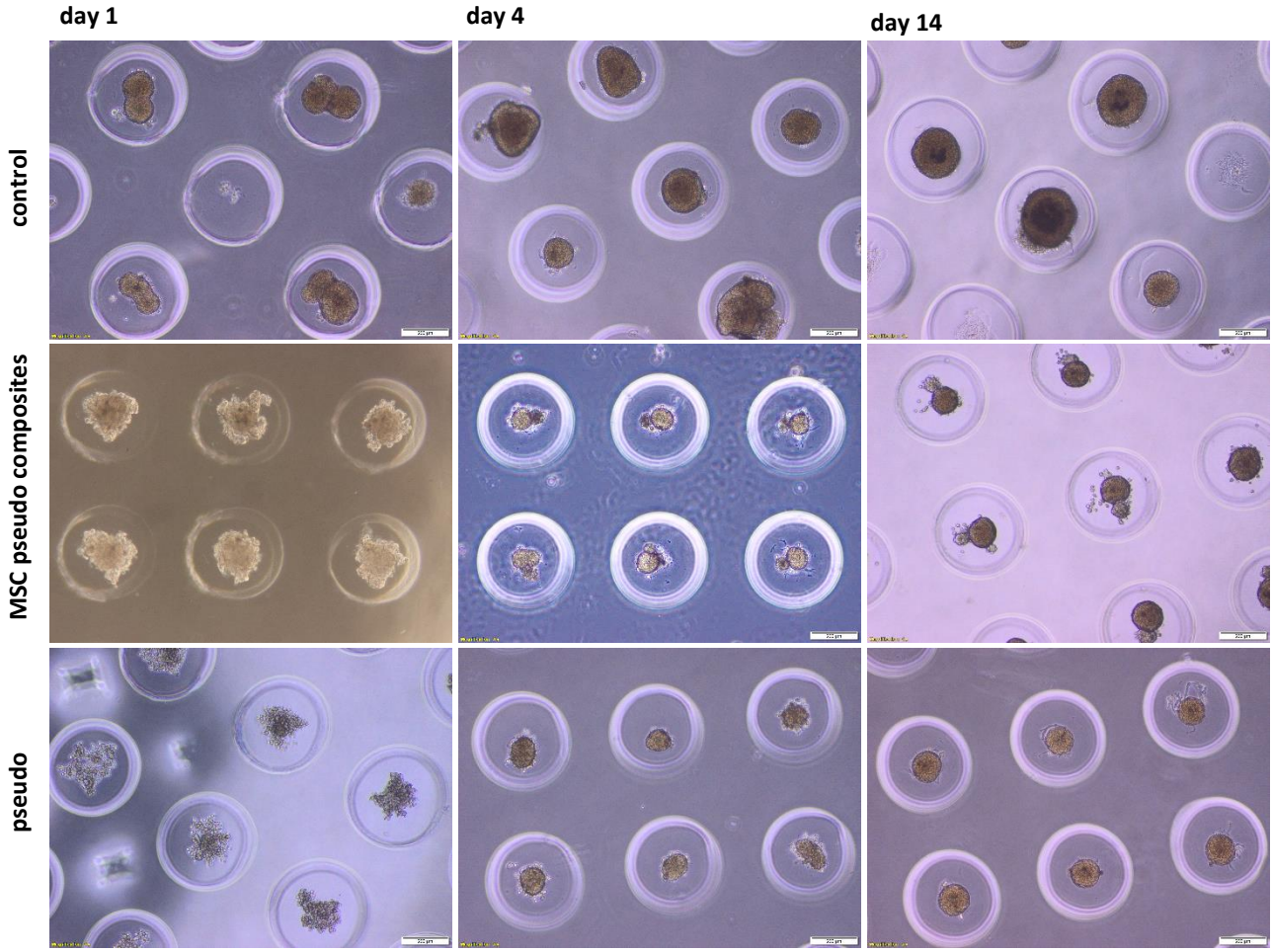

Figure 2. Morphology of islets, MSC pseudo islet composites and pseudo islets on day 1, 4 and 14 days in alginate microwells.

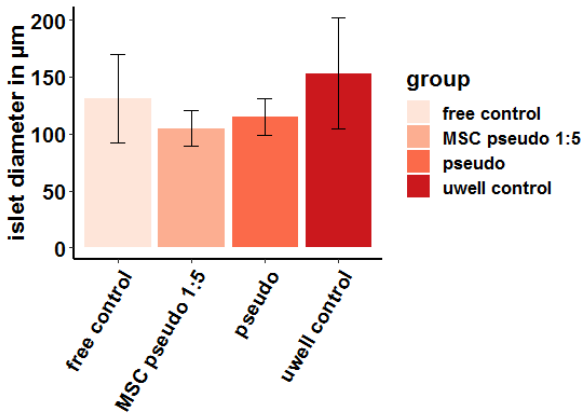

Figure 3. Size of islets grown in microwells after 4 days.

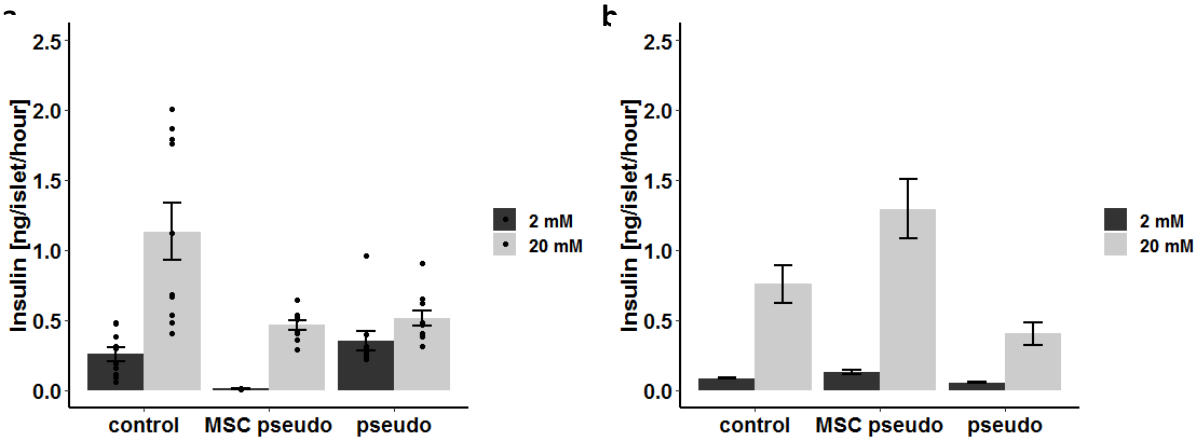

Figure 4. Glucose stimulated insulin release after short and long-term incubation. Mouse islets, pseudo islets or MSC pseudo composites (1:1) were cultivated for a) 3 and b) 14 days in alginate microwells.

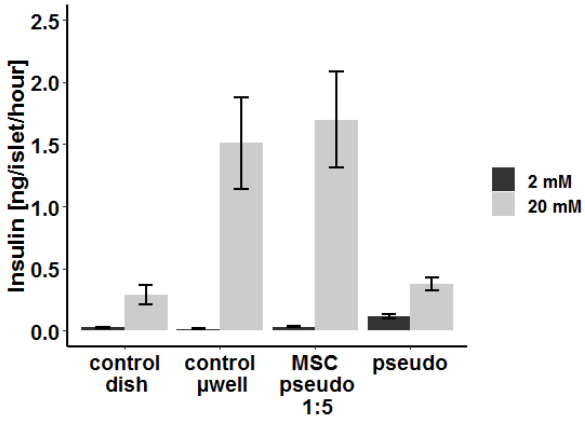

Figure 5. Glucose stimulated insulin release after short term incubation in microwells or petri dishes for 4 days. Control islets, pseudo islets or MSC pseudo islet composites (1:5) were cultivated in microwells for days. For a second control islets were cultivated in petri dishes.

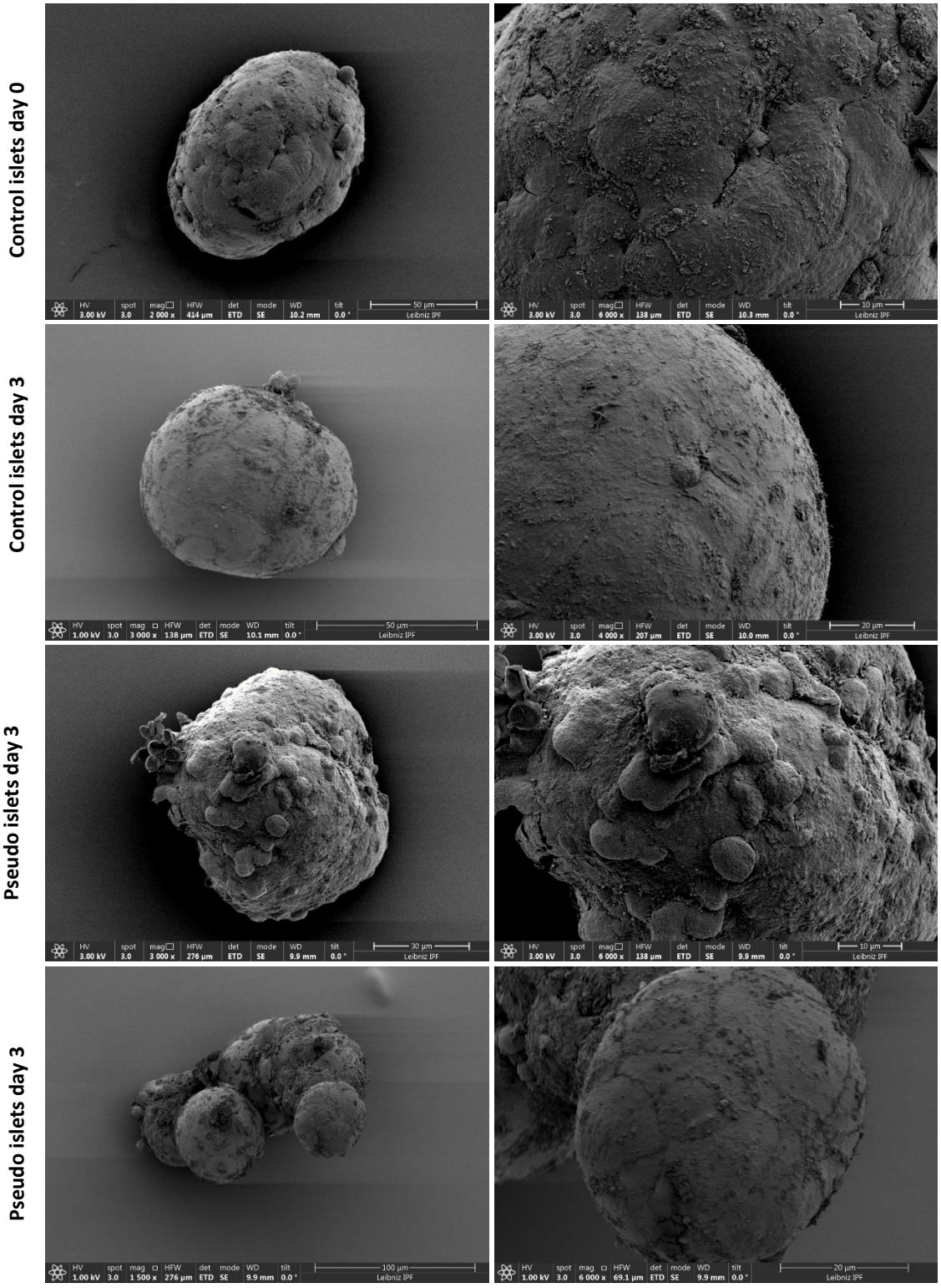

Figure 6. Surface electron microscopy of mouse islets. Directly after isolation, after 3 days culture in microwells as complete islet, reassociated islets (pseudo islet) and reassociated pseudo islet MSC composites.

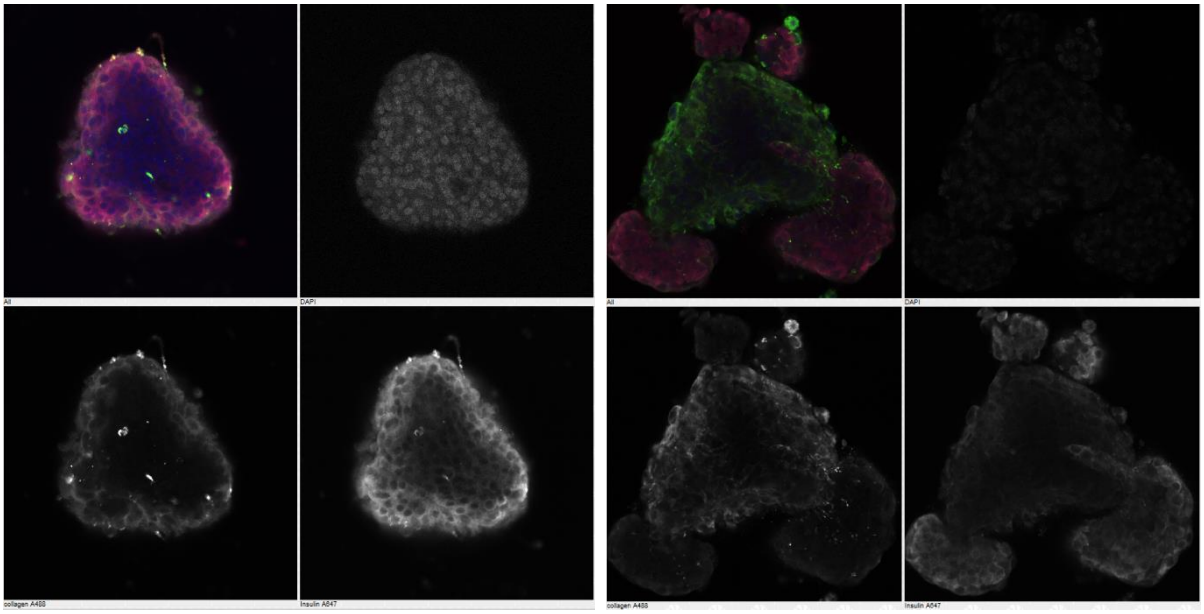

Figure 7. Immuohistochemistry of islets grown in microwells. 3 days culture in microwells as a) complete islet and b) pseudo islet MSC composites. Stained for insulin (pink) and collagen 4 (green) and nuclei (blue).

10.4 Attachments 1 & 2

Technische Universität Dresden Medizinische Fakultät Carl Gustav Carus Promotionsordnung vom 24. Juli 2011

Erklärungen zur Eröffnung des Promotionsverfahrens

1. Hiermit versichere ich, dass ich die vorliegende Arbeit ohne unzulässige Hilfe Dritter und ohne Benutzung anderer als der angegebenen Hilfsmittel angefertigt habe; die aus fremden Quellen direkt oder indirekt übernommenen Gedanken sind als solche kenntlich gemacht.

2. Bei der Auswahl und Auswertung des Materials sowie bei der Herstellung des Manuskripts habe ich Unterstützungsleistungen von folgenden Personen erhalten:

3. Weitere Personen waren an der geistigen Herstellung der vorliegenden Arbeit nicht beteiligt. Insbesondere habe ich nicht die Hilfe eines kommerziellen Promotionsberaters in Anspruch genommen. Dritte haben von mir weder unmittelbar noch mittelbar geldwerte Leistungen für Arbeiten erhalten, die im Zusammenhang mit dem Inhalt der vorgelegten Dissertation stehen.

4. Die Arbeit wurde bisher weder im Inland noch im Ausland in gleicher oder ähnlicher Form einer anderen Prüfungsbehörde vorgelegt.

5. Die Inhalte dieser Dissertation wurden in folgender Form veröffentlicht:

6. Ich bestätige, dass es keine zurückliegenden erfolglosen Promotionsverfahren gab.

7. Ich bestätige, dass ich die Promotionsordnung der Medizinischen Fakultät der Technischen Universität Dresden anerkenne.

8. Ich habe die Zitierrichtlinien für Dissertationen an der Medizinischen Fakultät der Technischen Universität Dresden zur Kenntnis genommen und befolgt.

Ort, Datum

Unterschrift des Doktoranden

Hiermit bestätige ich die Einhaltung der folgenden aktuellen gesetzlichen Vorgaben im Rahmen meiner Dissertation

- das zustimmende Votum der Ethikkommission bei Klinischen Studien, epidemiologischen Untersuchungen mit Personenbezug oder Sachverhalten, die das Medizinproduktegesetz betreffen
  Aktenzeichen der zuständigen Ethikkommission

- die Einhaltung der Bestimmungen des Tierschutzgesetzes *Aktenzeichen der Genehmigungsbehörde zum Vorhaben/zur Mitwirkung*

- die Einhaltung des Gentechnikgesetzes
  Projektnummer

- die Einhaltung von Datenschutzbestimmungen der Medizinischen Fakultät und des Universitätsklinikums Carl Gustav Carus.

Ort, Datum

Unterschrift des Doktoranden